

TECHNISCHE UNIVERSITÄT MÜNCHEN

WACKER-Lehrstuhl für Makromolekulare Chemie

---

# Two-dimensional Hybrid Nanomaterials: Functionalization and Characterization of Photoluminescent Silicon Nanosheets

---

**Tobias Helbich**

Vollständiger Abdruck der von der Fakultät für Chemie der Technischen Universität München zur Erlangung des akademischen Grades eines

**Doktors der Naturwissenschaften**

genehmigten Dissertation.

Vorsitzender:

Univ.-Prof. Dr. Richard Fischer

Prüfer der Dissertation:

1. Univ.-Prof. Dr. Dr. h.c. Bernhard Rieger

2. Univ.-Prof. Dr. Tom Nilges

3. apl. Prof. Dr. Wolfgang Eisenreich (mündliche Prüfung)

Prof. Mita Dasog, PhD, Dalhousie University, Halifax,

Kanada (schriftliche Beurteilung)

Die Dissertation wurde am 13. Juni 2017 bei der Technischen Universität München eingereicht und durch die Fakultät für Chemie am 10. August 2017 angenommen.

*“There is a single light of science,  
and to brighten it anywhere is to brighten it everywhere.”*

Isaac Asimov

## - Danksagung -

Mein besonderer Dank gilt *Prof. Dr. Dr. h.c. Bernhard Rieger* für die Aufnahme an seinem Lehrstuhl und die Möglichkeit meine Promotion auf einem so interessanten Thema durchführen zu dürfen. Die Erforschung neuer Materialien im Rahmen der Alberta Technical University of Munich Graduate School for Functional Hybrid Materials schaffte das für mich perfekte Umfeld.

*Prof. Dr. Jonathan G. C. Veinot* danke ich für seine fachliche Unterstützung, die freundschaftliche Aufnahme in seinen Arbeitskreis, die vielen außerfachlichen Gespräche und die lustigen gemeinsamen Momente in Kanada.

Bedanken möchte ich mich auch bei *Dr. Carsten Troll* für die konstante Unterstützung und den unermüdlichen Einsatz alles am Laufen zu halten, so wie *Katia Rodewald*, Frau *Bauer* und Frau *Saul-Hubrich* für die organisatorische Hilfe.

Mein Dank gilt allen Mitgliedern des WACKER-Lehrstuhls. Insbesondere danke ich *Philipp Marx*, *Marco Decker*, *Marc Kloberg* und *Philipp Holzmüller*, deren Arbeit während ihrer Zeit als Masteranden beträchtlich zu meiner Doktorarbeit beigetragen hat. Es war eine super Zeit mit euch.

Vielen Dank, *Alina Lyuleeva* für die gute Zusammenarbeit und die unzähligen lustigen gemeinsamen Momente während unseres Studiums. Wenn du springst, springe ich auch!

Des Weiteren möchte ich meine Kollegen *Arzu Angi*, *Ignaz Höhle*, *Julian Kehrle*, *Theresa Ludwig*, *Maximilian Knaus*, *Raphael Grötsch*, *Markus Pschenitza* und *Marco Giuman* für die vielen wertvollen fachlichen und außerfachlichen Diskussionen und die schöne gemeinsame Zeit danken.

*Jan Schwämmlein* danke ich für die Hilfestellungen bei all meinen elektrochemischen Herausforderungen, *Frank Deubel* für die Unterstützung als Mentor und *Lavinia Scherf* für mein Ausgangsmaterial.

Dem gesamten Arbeitskreis von Prof. Veinot danke ich für die Hilfsbereitschaft und die freundliche Aufnahme während meiner Zeit in Edmonton. *Regina Sinelnikov* und *Alyx Aarbo* für die gemeinsamen Ausflüge und die interessante Zeit in Saskatoon. *Tapas Purkait* und *Haoyang (Emmett) Yu* möchte ich für die Kooperation in Kanada und München danken.

Vielen Dank *Benni Rehl* für das gemeinsame Pumpen im Gym und die grandiose Zeit zusammen. *Hias Michael David Roy* danke ich für die lustigen Stunden in den diversen Pubs Edmontons und Münchens und *Dagmar* für die lustige Zeit in Tschechien. *Sarah Parke* danke ich für die anstrengende Zeit an der Kletterwand.

Allen Mitgliedern von *ATUMS* danke ich für die interessante Zeit in München, Raitenhaslach und Kanada.

Der *Studienstiftung des Deutschen Volkes*, die meine Promotion großzügig über das Promotionsstipendium unterstützt hat, bin ich sehr verbunden.

Ganz besonders möchte ich mich bei meinen Eltern *Gabriele* und *Peter* sowie meiner Schwester *Cornelia*, meinen Opas *Wastl* und *Ernst* und dem Rest der *Familie* für ihre fortwährende Unterstützung während meiner Promotion, meines Studiums und den nicht unbedeutenderen Jahren davor bedanken. Ihr seid die Besten!

# Content

Table of Abbreviations.....	1
1. Introduction.....	2
2. Silicon Nanosheets.....	4
2.1 Synthesis of Silicon Nanosheets.....	4
2.1.1 Silicenes.....	4
2.1.2 Silicanes.....	6
2.2 Surface Functionalization of Silicanes.....	8
2.3 Properties of Silicon Nanosheets.....	9
2.3.1 Properties of Silicenes.....	9
2.3.2 Properties of Silicanes.....	12
2.3.2.1 Hydride Terminated Silicanes.....	12
2.3.2.2 Functionalized Silicanes.....	14
2.4 Applications.....	16
2.4.1 Silicenes.....	16
2.4.2 Silicanes.....	18
3. Aim of this Work.....	21
4. Radical Induced Hydrosilylation Reactions for the Functionalization of Two-Dimensional Hydride Terminated Silicon Nanosheets.....	24
5. One-Step Synthesis of Photoluminescent Covalent Polymeric Nanocomposites from 2D Silicon Nanosheets.....	43
6. <i>Lewis</i> Acid Induced Functionalization of Photoluminescent Two-Dimensional Silicon Nanosheets for Enhanced P3HT Based Solution Gated Field Effect Transistor Fabrication.....	68
7. Diaryl Iodonium Salts as Hydrosilylation Initiators for the Surface Functionalization of Silicon Nanomaterials and their Collaborative Effect as Ring Opening Polymerization Initiator.....	87
8. Silicon Nanosheets as Initiators for Diaryliodonium Induced Radical and Cationic Polymerization....	110
9. Summary and Outlook.....	111
10. Zusammenfassung und Ausblick.....	115
11. Publications Beyond the Scope of this Thesis.....	120
11.1 Diazonium Salts as Grafting Agents and Efficient Radical-Hydrosilylation Initiators for Free Standing Photoluminescent Silicon Nanocrystals.....	121
11.2 Thermoresponsive and Photoluminescent Hybrid Silicon Nanoparticles by Surface-Initiated Group Transfer Polymerization of Diethyl Vinylphosphonate.....	122
11.3 Polymer–Silicon Nanosheet Composites: Bridging the Way to Practical (Opto)electronic Applications.....	123
11.4 In-situ Infrared Spectroscopy as Tool for Monitoring the Radical Hydrosilylation Process on Silicon Nanocrystal Surfaces.....	124
12. Bibliography.....	125

13. Appendix.....	134
13.1 Silicon Nanosheets as Initiators for Diaryliodonium Induced Radical and Cationic Polymerization .....	134
13.2 Supplementary Information .....	139
13.3 Licenses for Copyrighted Content.....	152

## Table of Abbreviations

TMD	Transition metal dichalcogenide
0D	Zero-dimensional
1D	One-dimensional
2D	Two-dimensional
3D	Three-dimensional
AA	Acrylic acid
AFM	Atomic force microscopy
AIBN	Azobisisobutyronitrile
ARPES	Angle-resolved photoemission spectroscopy
CVD	Chemical vapor deposition
Cz	Carbazolylmethylamino
DFT	Density functional theory
$E_g$	Band gap
FET	Field effect transistor
FTIR	Fourier transform infrared
HAADF-STEM	High-angle annular dark field scanning transmission electron microscopy
HR	High resolution
MMA	Methyl methacrylate
NMR	Nuclear magnetic resonance
Np	Naphthylmethyl
P3HT	Poly(3-hexylthiophene)
PAA	Poly(acrylic acid)
Ph	Phenyl
PL	Photoluminescence
PMMA	Polymethyl methacrylate
PS	Polystyrene
SEM	Scanning electron microscopy
SiNC	Silicon Nanocrystal
SiNS	Silicon Nanosheet
SiNS-PAA@PAA	Polyacrylic acid functionalized SiNSs in polyacrylic acid matrix
SiNS-PMMA@PMMA	Polymethyl methacrylate functionalized SiNSs in polymethyl methacrylate matrix
SiNS-PS@PS	Polystyrene functionalized SiNSs in polystyrene matrix
STEM-EDX	Scanning transmission electron microscopy-energy-dispersive X-ray spectroscopy
STM	Scanning tunneling microscopy
STS	Scanning tunneling spectroscopy
TEM	Transmission electron microscopy
UV/VIS	Ultraviolet/visible
XANES	X-ray absorption near edge structure
XEOL	X-ray excited optical luminescence
XPS	X-ray photoelectron spectroscopy
XRD	X-ray diffraction
$\lambda_{ex}$	Excitation wavelength
$\lambda_{max}$	Emission maximum

# 1. Introduction

## - Two-dimensionality -

In his 2010 Nobel Lecture “Graphene: Materials in the Flatland,” Kostya S. Novoselov described: “Intuitively, one can easily discern the difference between two- and three-dimensional objects: restrict the size or motion of an object to its width and length and forget (or reduce to zero) its height, and you will arrive in “flatland”. The consequences of subtracting one (or more) dimensions from our 3D world are often severe and dramatic.”<sup>[1]</sup> These severe and dramatic changes lead to a multitude of outstanding and unique properties of two-dimensional (2D) nanomaterials that scientists of different disciplines around the world strive to understand and exploit. As such, ever since the discovery of graphene, ultrathin 2D nanomaterials represent a key class material in condensed matter physics, material science and chemistry.<sup>[2]</sup> For example transition metal dichalcogenides (TMDs, e.g.,  $\text{MX}_2$ ; M = transition metal; X = chalcogen; e.g., M = Mo, W and X = S, Se, Te),<sup>[3]</sup> layered metal oxides,<sup>[4]</sup> layered double hydroxides,<sup>[5]</sup> hexagonal and graphitic boron nitrides,<sup>[6,7]</sup> metal organic-<sup>[8–10]</sup> and covalent organic frameworks,<sup>[11,12]</sup> MXenes,<sup>[13]</sup> and phosphorenes<sup>[14]</sup> extend the scope of layered 2D nanomaterials. Their versatile properties lead to many applications in for example biomedicine,<sup>[15]</sup> and electronics.<sup>[2,14,16]</sup>

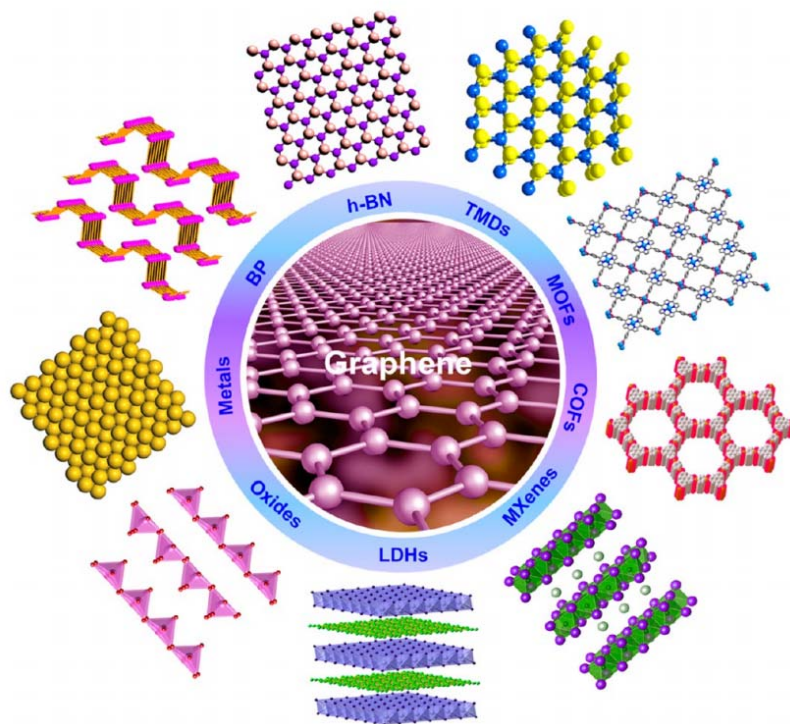


**Figure 1.** Schematic illustration of different typical 2D nanomaterials taken under an ACS AuthorChoice License from Ref [2].

Due to their monolayered structure, 2D nanomaterials can combine maximal mechanical strength and flexibility with optical transparency.<sup>[17]</sup> They exhibit outstanding and tunable (opto)electronic

characteristics such as band gap<sup>[18–20]</sup> and conductivity properties.<sup>[21–24]</sup> Furthermore, they are very promising candidates for surface active applications due to their ultra-high surface area.<sup>[2,24,25]</sup> Additionally, these nanomaterials are very susceptible to external influences such as strain<sup>[26]</sup> or interacting molecules, which opens the possibility for e.g., (bio)sensing applications.<sup>[7,27–29]</sup> Furthermore the high surface area leads to increased reactivities and enables surface modifications, which can be used to tailor their properties.<sup>[30–32]</sup>

As silicon is purported non-toxic,<sup>[33,34]</sup> abundantly found in the earth's crust and represents the basis of current information technology, one of the important aims of recent "flatland" science is to explore 2D silicon materials to a similar extent as their carbon or TMD counterparts. Silicon nanosheets (SiNSs) could contribute the unique and tunable properties of 2D nanomaterials without the need to change the current silicon -based status quo<sup>[35]</sup> and might thus boost the field of nanoelectronics.

Within the last few years, great efforts have been made to explore the synthesis, characterization and applications of SiNSs and to determine if the many theoretical predictions could be met at an experimental level. Still, as they are very new and sensitive materials, many challenges remain. A first aim of current research is to tackle their sensitivity at ambient conditions that arises due to the strong oxophilicity of silicon. As this shortcoming can be tackled by introducing stabilizing surface modifications, the exploration of the surface chemistry most likely represents the basis of any further research on SiNSs and should enable the determination of their manifold properties and their use in further applications.

## 2. Silicon Nanosheets

Similar to their carbon homologue, silicon can appear in different hybridization states. The two-dimensional,  $sp^2$  hybridized carbon modification graphene is well examined and understood and of great importance in the scientific community.<sup>[36]</sup> By terminating the monolayer with hydrogen and thus changing the hybridization state of the carbon atoms, graphane is formed,<sup>[37]</sup> which also results in a drastic change of properties.<sup>[2]</sup>

As the heavier homologue of carbon, similar structural differences and structure dependent properties can be observed for silicon. Two-dimensional silicon monolayers can be differentiated in its  $sp^2$  hybridized form, silicene, as well as the  $sp^3$  hybridized silicon layer, silicane.<sup>[38]</sup> Both modifications exhibit a great potential for future applications in diverse fields (see below; e.g., field effect transistors (FET),<sup>[39]</sup> lithium ion batteries,<sup>[40–44]</sup> water splitting,<sup>[45]</sup> photocatalysis<sup>[45]</sup> hydrogen storage,<sup>[46]</sup> etc.), but differ strongly in their properties and syntheses.

### 2.1 Synthesis of Silicon Nanosheets

Many syntheses exist to produce nanomaterials of different consistency and forms, but they can all be assigned to two different categories: bottom-up and top-down.<sup>[47]</sup> In bottom-up approaches smaller units are assembled into bigger and more complex systems. In nanotechnology these syntheses often start from molecular precursors that can self-assemble, or are brought to a reaction by different initiation methods<sup>[48–50]</sup> (e.g., laser, heat, etc.). In top-down procedures larger starting systems are used and separated into smaller (nanodimensional) components/segments. This is mostly done with conventional, mechanical methods such as grinding or attrition.<sup>[47]</sup>

For SiNSs, several synthesis procedures have been published. Yu *et al.* reported the synthesis of silicon nanosheets by direct current (DC) arc discharge in an argon/hydrogen atmosphere and analyzed their electrochemical properties towards the suitability as Li-ion battery material.<sup>[51]</sup> Further publications describe the synthesis of SiNSs by magnesiothermic reduction of sand<sup>[52]</sup> or chemical vapor deposition (CVD).<sup>[53,54]</sup> In 2014 Kim *et al.* synthesized SiNSs of various thicknesses (1 – 13 nm) *via* dendritic growth and demonstrated a thickness dependent photoluminescence (1.6 – 3.2 eV).<sup>[55]</sup> However, in this work the emphasis lies on a different synthesis approach which will be discussed in the following in further detail.

#### 2.1.1 Silicenes

Silicene does not exist in nature due to its instability in ambient conditions,<sup>[56]</sup> but as the silicon analogue of graphene, it awoke the interest of many scientists. Although first theoretical calculations demonstrated, that silicenes should be stable and gave the first insights into their potential structural

characteristics,<sup>[57]</sup> a successful preparative synthesis took another decade. In 2005 Léandri *et al.* reported the growth of Si nanostructures upon deposition of Si from a direct current heated silicon wafer (flashed at  $\sim 1250$  °C) under ultra-high vacuum conditions on Ag(110).<sup>[58]</sup> This was the first step towards the successful synthesis of silicene. But only further experimental and theoretical elucidation in 2007 confirmed the effective synthesis of graphene-like honeycomb silicenes (in early works referred to as silicon nanoribbons) of  $\sim 1.7$  nm width and varying lengths (1 nm – tens of nm).<sup>[59]</sup> Scanning tunneling microscopy (STM) measurements of these nanoribbons showed a Si–Si-distance of  $2.24$  Å<sup>[60]</sup> and thus confirmed DFT calculations showing that Si can exhibit stable, 2D, low buckled, honeycomb structures similar to graphene.<sup>[61–63]</sup> Further studies were performed on Ag(110),<sup>[64–69]</sup> which led to the first evidence of local silicene-like  $sp^2$  character.<sup>[66,67]</sup> In 2010 Aufray and co-workers presented silicene layers epitaxially grown on a Ag(111) single crystal *via* direct condensation of a silicon atomic flux onto the substrate.<sup>[70]</sup> In 2012 Vogt *et al.* then synthesized a one atom thick two-dimensional silicon layer on Ag(111) with an extended width of 100 - 150 nm and a height of  $\sim 0.1$  nm, giving experimental evidence for larger, graphene-like 2D silicon.<sup>[71]</sup> Ag(111) with its 6-fold symmetry is expected to favor the formation of the honeycomb silicon layer.<sup>[72]</sup> **Figure 2** shows the STM image of the silicene surface on the substrate (**Figure 2b**) and the model of the arrangement of the silicon atoms (**Figure 2c**). Further morphological characterizations of the silicon layers show that the corrugated silicene domains grow with different preferential orientations and tend to cover the surface in patchwork-like patterns.<sup>[72]</sup> Temperature dependent examinations combined with calculations indicate that with increasing substrate temperatures, the silicon atoms on the substrate form some metastable structures (i.e., self-assembled honeycomb building block, incomplete silicene films), which eventually evolve into the most stable phase (i.e., monolayer or bilayer silicene films).<sup>[73]</sup>

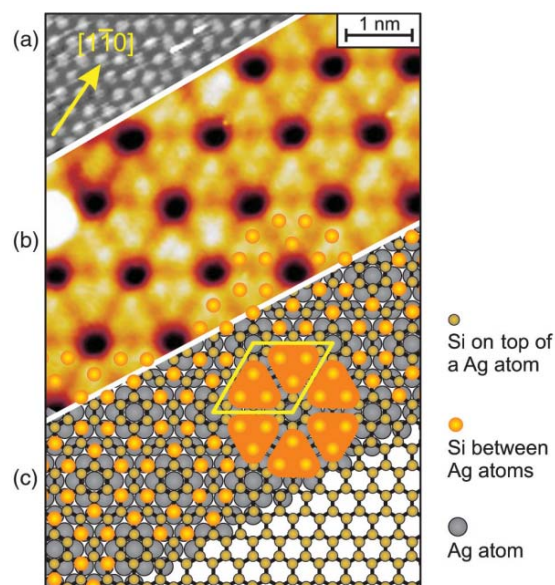


**Figure 2** Construction of the atomic structure model for the 2D Si adlayer. Filled-states STM images of (a) the initial clean Ag(111) surface, (b) the silicene sheet and (c) the model of silicene on Ag(111). Si atoms sitting on top of Ag atoms are highlighted as larger orange circles, resembling the measured STM image. Bottom right corner: the ball-and-stick model for the freestanding silicene layer is shown with a Si-Si distance of  $0.22$  nm.<sup>[71]</sup> Reprinted with permission from P. Vogt, P. De Padova, C. Quaresima, J. Avila, E. Frantzeskakis, M. C. Asensio, A. Resta, B. Ealet, G. Le Lay, *Phys. Rev. Lett.*, 108, 155501, 2012; copyright (2012) by the American Physical Society.

The synthesis of silicene-like structures is not confined to Ag surfaces. In 2012 the formation and characterization of silicene on  $\text{ZrBr}_2$ <sup>[74]</sup> was reported, to which in 2013  $\text{Ir}(111)$ <sup>[75]</sup> and  $\text{Au}(110)$ <sup>[76]</sup> were added. Le Lay and co-workers also reported the synthesis of aligned multilayer silicene nanoribbons with a pyramidal cross section and their electronic properties.<sup>[77]</sup>

Additionally, DFT calculations suggest 2D hexagonal boron nitride (h-BN) monolayer on a  $\text{Cu}(111)$  substrate<sup>[78]</sup> or solid  $\text{Ar}(111)$ <sup>[79]</sup> as a potential platform for silicene. In this case, due to the weak substrate-sample-interactions an influence of the substrate on the electronic properties of silicene should be minimized and detachment of silicene from the substrate should be possible. In another approach, first-principle works show that the separation of the silicon layer from the support can be chemically executed by e.g., hydrogenation or calcium intercalation, resulting in the desired monolayer.<sup>[80]</sup> Furthermore, Houssa *et al.* suggested the stabilization of silicene in a graphite-like nanolattice, maintaining its gapless-semiconducting character.<sup>[81]</sup> Such a stabilization approach was then executed experimentally, when silicene layers were successfully stabilized by encapsulation in  $\text{Al}_2\text{O}_3$ .<sup>[82,83]</sup> This encapsulation enables the detachment from the substrate, but does not render free standing silicenes. In contrast, for silicanes, no stabilizing substrate is needed and the free standing materials are stable for a limited time without encapsulation or modification.

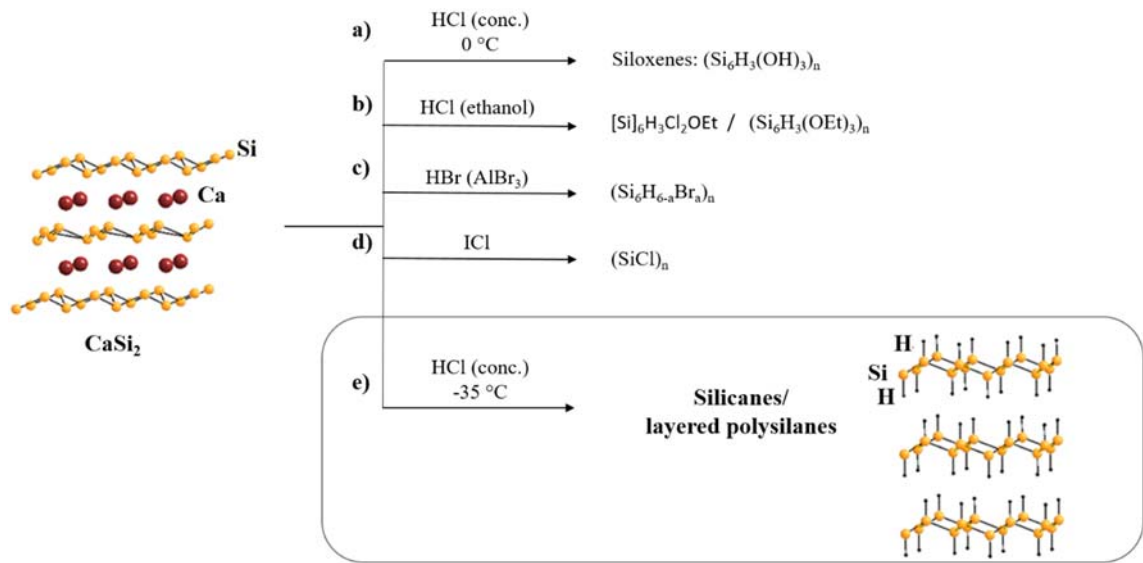
## 2.1.2 Silicanes

Silicanes<sup>a</sup> are  $\text{sp}^3$  hybridized SiNSs and can be synthesized by a top-down approach from calcium disilicide  $\text{CaSi}_2$ . This Zintl disilicide contains anionic puckered silicon layers  $(\text{Si}^-)_n$  which consist of interconnected  $\text{Si}_6$  rings. The layers are stabilized by a planar cationic monolayer of  $\text{Ca}^{2+}$  ions (**Scheme 1**) which can be deintercalated, leading to the exfoliation of the silicon layers. The single layers tend to stack and form a silicon based graphite analogue, which, in literature, is mostly referred to as layered polysilane.<sup>[84]</sup>

This approach was first shown in 1863, when Wöhler described the synthesis of siloxenes<sup>[85]</sup> by the treatment of  $\text{CaSi}_2$  with hydrochloric acid (**Scheme 1a**). Based on the work of Wöhler, in the 1920s Kautsky *et al.* described the synthesis and properties of these siloxenes in more detail.<sup>[86,87]</sup>

---

<sup>a</sup> In some theoretical publications the authors refer to silicanes as hydrogenated silicenes. Other publications refer to the material as hydride terminated SiNSs or when stacked as layered polysilanes.



**Scheme 1.** Schematic of the possible deintercalation reactions of  $\text{Ca}^{2+}$  from  $\text{CaSi}_2$ . a) Reactions with HCl at moderate temperatures lead to siloxenes<sup>[85]</sup>, while b) deintercalations in ethanol render siloxene derivatives with chlorine, ethoxy surfaces; or alkoxyated siloxenes<sup>[88,89]</sup> c) the treatment of  $\text{CaSi}_2$  with HBr in molten  $\text{AlBr}_3$  is believed to render hydride/bromide terminated SiNSs<sup>[88]</sup> and d) reactions with iodo monochloride ICl were reported to yield the less well characterized  $(\text{SiCl})_n$ .<sup>[90]</sup> e) Reactions with concentrated HCl at low temperatures render silicenes.<sup>[91]</sup>

Although the publications did not get much attention, this deintercalation approach was further developed by Schott and Hengge. In 1957 Schott *et al.* reported the reaction of  $\text{CaSi}_2$  with HCl in anhydrous ethanol, leading to the siloxene derivatives  $[\text{Si}]_6\text{H}_3\text{Cl}_2\text{OEt}$ .<sup>[92]</sup> For similar reaction conditions Weiss *et al.* reported the formation of alkoxyated siloxene derivatives (**Scheme 1b**).<sup>[89]</sup> In the same year the authors reacted  $\text{CaSi}_2$  in molten  $\text{AlBr}_3$  with HBr and found that the silicon layers were partially substituted with H and Br atoms respectively (**Scheme 1c**).<sup>[88]</sup> In the 1970s, Hengge used iodine monochloride ICl to synthesize  $(\text{SiCl})_n$  layers<sup>[90]</sup> (**Scheme 1d**), which can be reacted further with  $\text{SbF}_3$  to render  $(\text{SiF})_n$  or with  $\text{LiAlH}_4$  to synthesize  $(\text{SiH})_n$ <sup>[93]</sup> layers respectively. For halogen substituted SiNSs  $(\text{SiX})_n$ , the more electronegative halogen substituents lead to absorptions in the regime of shorter wavelengths and thus colored products.<sup>[94]</sup> Hengge did not observe any PL for his  $(\text{SiX})_n$  ( $\text{X} = \text{Cl}, \text{Br}, \text{I}, \text{F}, \text{H}$ ) silicon layers,<sup>[93]</sup> while for the siloxenes described by Wöhler and Kautsky, new experimental studies were published<sup>[89,95]</sup> in which e.g., PL properties were described.<sup>[96]</sup>

The synthesis of hydrogen terminated silicenes required different reaction conditions. In 1993 Dahn *et al.*<sup>[84]</sup> reported a new approach to synthesize free standing hydride terminated silicon monolayers from  $\text{CaSi}_2$  via chemical exfoliation at very low temperatures ( $< -30$  °C), which was improved in 1996 by Yamanaka *et al.* (**Scheme 1e**).<sup>[91]</sup>

Based on this procedure, Nakano *et al.* synthesized SiNSs from Mg doped  $\text{CaSi}_2$ . The incorporation of Mg should facilitate the exfoliation of the nanosheets due to a decrease in negative charge on the silicon layers and the resulting weakening of the Ca-Si-interactions.<sup>[97]</sup>

While for silicenes no large scale syntheses were reported so far, as the  $\text{sp}^2$ -hybridized materials need stabilization from the (semi)metallic support, silicenes can be synthesized in the gram scale.

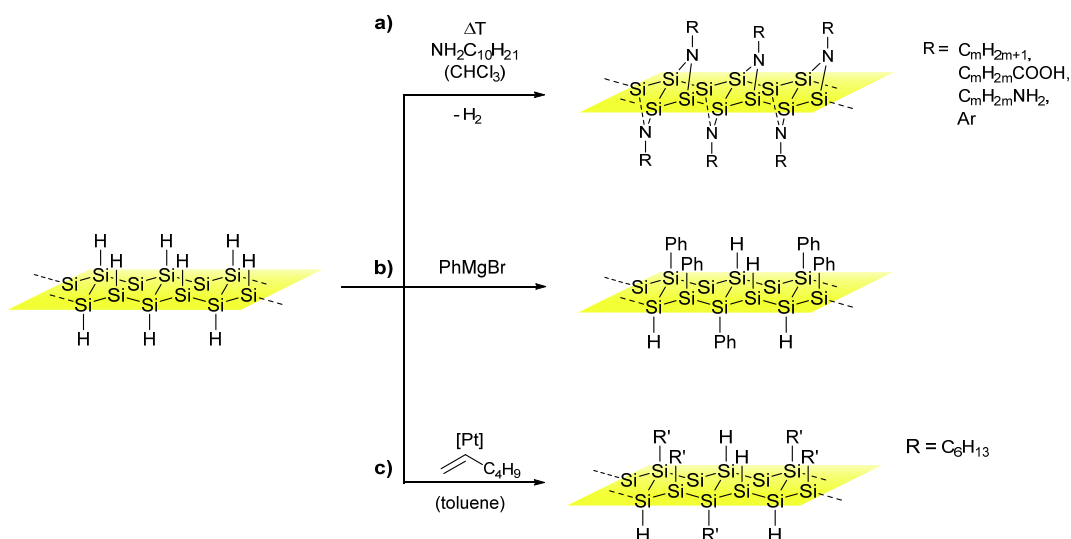
Additionally, for silicon the  $sp^3$  character is energetically favored,<sup>[56]</sup> leading to a higher stability of silicenes and many possibilities to alter their properties e.g., *via* surface functionalization.

## 2.2 Surface Functionalization of Silicenes

Due to the strong oxophilicity of silicon, hydride terminated silicon materials are merely metastable at ambient conditions and as such prone to oxidize. This results in a change of their properties, but can be suppressed by functionalization of the silicon surface,<sup>[98]</sup> as known for other silicon based nanomaterials (e.g., silicon nanocrystals,<sup>[99,100]</sup> porous silicon<sup>[101]</sup>). In addition to stabilization, functionalization influences the dispersibility of the nanomaterial<sup>[102–104]</sup> and might affect its (opto)electronic properties.<sup>[105,106]</sup> Silicenes tend to stack due to their 2D structure. Thus, surface modifications are also expected to promote the exfoliation of the single layers<sup>[107]</sup> and prevent them from stacking.

Compared to silicon nanocrystals (SiNCs) or porous silicon (pSi), little is known about the surface chemistry of SiNSs. For silicenes Okamoto *et al.* reported the synthesis of amine functionalized SiNSs with *N*-decylamine (**Scheme 2a**).<sup>[108]</sup> In further studies the authors attached aromatic amines<sup>[109]</sup> and functional substrates (i.e., diamines and carboxylic acids)<sup>[110]</sup> to the SiNSs surface.

In order to stabilize the sensitive Si surface, formation of stable Si-C bonds is desirable. This can be achieved through the reaction of SiNSs-H with the Grignard reagent PhMgBr<sup>[98]</sup> or *via* Pt catalyzed hydrosilylation with 1-hexene as published by Nakano *et al.*<sup>[111]</sup> When diluted in  $CHCl_3$ , the products of the reaction render clear dispersions.



**Scheme 2.** Functionalization of hydride terminated SiNSs a) through nucleophilic substitution with decylamine ( $m = 2,3,6,12$ ; Ar = Ph, Np, Cz),<sup>[108–110]</sup> b) through reaction with the Grignard reagent PhMgBr<sup>[98]</sup> and c) through platinum catalyzed hydrosilylation reaction with 1-hexene.<sup>[111]</sup>

Aside from the vast, potential chemistry of SiNSs, the only further reactivity besides surface functionalizations that has been examined experimentally, is mechanochemical lithiation.<sup>[112]</sup> In

theoretical publications functionalization of hydride terminated SiNSs with aldehydes is suggested.<sup>[113]</sup>

As known for nanomaterials, the nature (i.e., modification) of the SiNS surface has a strong influence on the properties due to their large surface area. This underlines the importance of the above described works, and also emphasizes the potential of further studies on surface functionalization.

## 2.3 Properties of Silicon Nanosheets

2D nanostructures exhibit layer thicknesses in the nano regime and lateral sizes on the microscale. This anisotropic structural property is an important attribute in nanodevice fabrication<sup>[114]</sup> and one of the few characteristics that silicenes and silicenes have in common. Besides that, their properties (i.e., optic, electronic, magnetic, etc.) differ strongly from each other.

### 2.3.1 Properties of Silicenes

Silicene is often referred to as the silicon based graphene. However, in terms of stability, structure and properties, the materials exhibit many differences.<sup>[115]</sup> Some of its properties (i.e., stability) represent challenges that the scientific community needs to tackle before device fabrication is possible. Others offer reaction routes and possibilities, different from the ones explored with graphene or other 2D nanomaterials. Thus, silicene is regarded as a new and promising material for existing as well as unique future applications.

#### *Theoretically Determined Properties*

First principle calculations predicted the stability of silicene, its structural characteristics as well as its size- and orientation dependent magnetic and electronic properties such as the semi metallic character with crossing of the  $\pi$  and  $\pi^*$  bands at the Fermi level.<sup>[63]</sup> Additionally, silicene exhibits very high intrinsic carrier mobilities<sup>[116,117]</sup> with charge carriers behaving like massless Dirac fermions.<sup>[63]</sup> Silicene was also determined to exhibit a giant magnetoresistance,<sup>[118]</sup> various exotic field-dependent states<sup>[119]</sup> and be able to realize the quantum spin Hall effect<sup>[119,120]</sup> whose significance can differ upon application of hydrostatic strain due to a change in gap size.<sup>[120]</sup>

When grown on Ag(111) **substrates**, silicene exhibits a metallic character; thus it does not possess the Dirac cone electronic structure, characteristic of freestanding silicene or graphene. This theoretical change of properties emphasizes the need for experimental studies on this material, but also demonstrates that the band structure of SiNSs can be altered by external influences. As such, the Ag(111) support is not only predicted to stabilize silicene<sup>[121,122]</sup> but also changes its properties<sup>[121,123,124]</sup> due to the strong interactions with the silicon monolayers. When “inert” supports

are used that merely interact with silicenes *via* weak van-der-Waals-interactions (e.g., MoS<sub>2</sub>,<sup>[125,126]</sup> *h*-BN,<sup>[121,127]</sup> SiC(0001),<sup>[127]</sup> hydrogen-passivated Si(111) and Ge(111) substrates<sup>[128]</sup> or silicane<sup>[129–131]</sup>), only minor influences on the silicene band structure occur.

Besides the substrate, **external influences**, such as electrical fields can be used to tune the bandgap of silicene.<sup>[119,132,133]</sup> DFT calculations also reveal, that silicene, just like nanoribbons shows a strong size and geometry dependent electronic and magnetic behavior,<sup>[63]</sup> that can also be altered by introduction of defects.<sup>[134–136]</sup> Furthermore, chemical modifications can significantly alter the band structure characteristics (i.e., direct/indirect band gap, metallic/semiconducting features) of silicene. As such, the functionalization of the surface (e.g., halogenation,<sup>[137–139]</sup> hydrogenation<sup>[140]</sup>) can be used to alter the electronic properties (e.g., opening of the band gap<sup>[141]</sup>) and the physical properties (e.g., adsorption energy of hydrogen chemisorption,<sup>[142]</sup> optical absorption,<sup>[141]</sup> magnetic properties<sup>[63]</sup>) of silicene. Additionally, seemingly minor influences like the arrangement of the hydrogenated surfaces<sup>[140,143]</sup> and the crystallinity of the substrate<sup>[144]</sup> can have an effect on the band structure. Further studies show the band gap opening due small, electron donating molecules (e.g., tetrathiafulvalene) that interact with silicene, but do not covalently functionalize it.<sup>[145]</sup> This behavior indicates potential in sensing applications. However the behavior is also dependent on the interacting molecules themselves. For example, the adsorption of the ionic liquid choline benzoate does not affect the electronic properties of silicenes. On the other hand, a strong change in the HOMO/LUMO of the adsorbed molecules was observed, which could be valuable for the use of silicene as catalyst material.<sup>[146]</sup>

Further calculations show that the formation of silicene **bi- or multilayers** is possible (e.g., by exploiting self-organization in confined systems),<sup>[147,148]</sup> wherein the interlayer distance influences their properties.<sup>[149,150]</sup> Silicene bilayers were found to exhibit a graphene-like semi metallic character<sup>[148]</sup> and were strongly affected by external influences (e.g., Ag support<sup>[151–153]</sup>). Despite the fact that monolayered silicene in some properties is similar to graphene, silicene multilayers strongly differ in geometry and electronic properties from graphene multilayers (e.g., stronger interlayer covalent bonds).<sup>[154]</sup>

In summary, a vast number of theoretical works (in part based on different models) deal with the outstanding and often unique properties of silicene, as the material exhibits the potential to compete with or even overtake graphene, the key player in nanotechnology. Some of the results are very specific to each system (e.g., symmetry, conformation, considered number of atoms, used substrate, multilayer system, etc.) and may thus have (partly) different results from each other (e.g., metallic<sup>[155]</sup> vs. semiconducting<sup>[63]</sup> behavior). However, all publications underline the great potential of 2D silicon monolayers and some results have even been confirmed on an experimental level (*vide infra*). Thus, the calculations provide a good starting point for experimental scientists to further explore the silicon counterpart of graphene.

*Experimentally Determined Properties*

Silicene-like nanoribbons of 1.6 nm width on **Ag(110)** show the expected honeycomb geometry<sup>[60]</sup> and the metallic,  $sp^2$ -like character of the silicon orbitals.<sup>[67]</sup> The growth is mediated and influenced by the silver substrate. Angle-resolved photoemission spectroscopy (APRES) demonstrates one dimensional quantum confined electronic states and suggests a Dirac cone-like band structure, similar to graphene on different substrates.<sup>[60]</sup> Interestingly, these silicene stripes exhibit a stronger chemical stability than graphene (with its edge reactivity), whereby the oxidation process starts at the extremities in a “burning match” mechanism.<sup>[156]</sup>

On **Ag(111)** silicene exhibits an unambiguously strong buckling of the honeycomb layer, as shown by the combination of non-contact AFM and STM measurements.<sup>[157]</sup> APRES measurements point toward the existence of Dirac fermions in the silicene band, similar to that in graphene,<sup>[71]</sup> with a Fermi velocity of  $1.3 \cdot 10^6 \text{ ms}^{-1}$ . For freestanding silicene a zero band gap is expected, while the Ag(111) substrate for the here-mentioned material is thought to induce the measured band gap.<sup>[71]</sup> This likely occurs due to the hybridization of the interfacing Si  $p_z$  orbital and the Ag d orbitals.<sup>[158]</sup> The samples exhibit a massive Dirac cone state with a large band gap between the  $\pi$  and  $\pi^*$  bands at the K point.<sup>[71,73,159]</sup> However, the combination of experimental data (e.g., APRES) and DFT calculations also show that the substrate substantially influences the electronic structure of silicene, leading to different properties (e.g., absence of  $\pi$  and  $\pi^*$  bands, loss of Dirac fermion characteristics, etc.).<sup>[123,124,160,161]</sup> Silicene multilayers were grown on the same Ag(111) substrate and the process was examined.<sup>[162]</sup> For few-layer-systems synchrotron radiation photoelectron spectroscopy shows a cone-like dispersion at the Brillouin zone center due to band folding and gapless Dirac fermions can be detected.<sup>[163]</sup> Scanning tunneling spectroscopy (STS) studies furthermore demonstrate that for small voltages the system is in the direct tunneling regime, while the Fowler-Nordheim regime can be reached for tip voltages  $V_{\text{tip}} > 1.3 \text{ V}$ .<sup>[72]</sup> Interestingly this is consistent with data collected on silicene type SiNSs (see 2.3.2.1).<sup>[164]</sup>

Molle *et al.* studied the **oxidation stability** of silicene on Ag(111) and found, that the short term exposure of the material to small concentrations of pure oxygen (1 s at  $10^{-6}$  Torr) does not lead to strong oxidations, coinciding with publications on Ag(110) substrates, stating the low reactivity.<sup>[165]</sup> When the system is exposed to air (here for 3 min), XPS data shows that the Si(0) signals decline clearly, while strong signals in the Si(IV) region appear. After one day the silicene monolayer is completely oxidized.<sup>[83]</sup> To tackle this problem, encapsulation in a stabilizing cover of Al or  $\text{Al}_2\text{O}_3$  can be used independent of the support, leading to stable, atomically sharp, chemically intact metal/silicene interfaces that allow the characterization of the system as well as its use for device fabrication.<sup>[83]</sup>

Additionally, silicene was grown on **ZrBr<sub>2</sub>**, for which epitaxial strain was found to influence the electronic properties,<sup>[74]</sup> as confirmed by the combination of DFT calculations and Raman measurements that reflect the multihybridized nature of the nanoribbons, which is caused by the substrate induced strain and the resulting buckled/distorted lattice.<sup>[166]</sup>

While monolayered silicene was found to be highly unstable, multilayer silicene exhibits inert characteristics, even in the presence of oxygen. With a growing number of silicene layers, the **silicene stacks** are decoupled from the substrate<sup>[167]</sup> and an ultra-thin native oxide film is formed on the exposed surface region. This layer protects the silicene stack for  $\geq 24$  h at ambient conditions.<sup>[168]</sup>

CaSi<sub>2</sub>, the starting material for silicene synthesis, can also be regarded as **calcium intercalated multilayer silicene**, as is the case for the heavier alkaline earth metal Sr in SrSi<sub>2</sub>.<sup>[169]</sup> High-resolution APRES studies of CaSi<sub>2</sub> show massless Dirac cone  $\mu$ -electron dispersions at the K(H) point in the Brillouin zone.<sup>[170]</sup> Nakano and co-workers further used CaSi<sub>2</sub> and reacted it with the BF<sub>4</sub><sup>-</sup>-based ionic liquid (1-butyl-3-methylimidazolium tetrafluoroborate) to observe the diffusion of F<sup>-</sup> ions into the Zintl salt and the subsequent formation of silicene bilayers with different symmetries.<sup>[44]</sup> The obtained material consists of silicene bilayers alternating with planar crystals of CaSi<sub>2</sub> and/or CaF<sub>2</sub> as observed with high-angle annular dark field scanning transmission electron microscopy (HAADF-STEM) and STEM-energy-dispersive X-ray spectroscopy (STEM-EDX). Calculations suggest the formation of a new silicene allotrope with four-, five-, and six-membered sp<sup>3</sup> silicon rings and the opening of the indirect band gap to 1.08 eV.

As the measurements also show a substantial charge transfer from the Ca atoms to the anionic “silicene” layers, as well as the substantial influence of the support of grown silicene layers (e.g., on Ag surfaces), further studies of uninfluenced, free standing silicenes would be of interest, but currently present a challenge for the scientific community.

## 2.3.2 Properties of Silicanes

### 2.3.2.1 *Hydride Terminated Silicanes*

#### *Theoretically Determined Properties*

As mentioned before, many theoretical publications deal with the difference between silicenes and silicanes as well as the transformation of one material into the other.

For the conducting graphene, e.g., doping and the introduction of defects are used to disturb the conjugated sp<sup>2</sup> system and thus induce an electronic band gap for semiconductor applications.<sup>[171,172]</sup> Due to their sp<sup>3</sup>-character, silicanes are semiconducting by default and hence their **electronic properties** are of particular interest. Thus, calculations deal with the influence of the conformation,<sup>[129]</sup> the size and orientation dependency (also on magnetic properties)<sup>[63,173]</sup> and predict the band gap properties of silicanes. These range from indirect band gaps of 2.19 eV<sup>[141]</sup> or 2.2 eV<sup>[174]</sup> to almost direct band gaps of 2.75 eV<sup>[175]</sup> and direct band gaps,<sup>[173]</sup> depending on the used model and applied conditions. When looking at bilayers of (non-functionalized) silicanes, the band gap properties are influenced by the interactions with the second layer (almost direct band gap of 2.75 eV).<sup>[175]</sup> When looking at functionalized SiNSs the influence is strongly reduced.<sup>[176]</sup> Few-layer systems of hydride

terminated silicenes show increasing band gaps as well as formation energies with the reduction of the layer size, indicating a lower structural stability with fewer layers. This can be explained with the high surface/volume ratio of the SiNSs.<sup>[177]</sup>

In further first-principle calculations silicenes were found to exhibit non-**magnetic** semiconducting **behavior**. This differs from “half-hydrogenated” silicenes, where only one side is terminated by Si–H groups, which exhibit localized, unpaired electrons of the silicon atoms, thus showing ferromagnetic semiconducting properties.<sup>[178]</sup> Time dependent DFT calculations show the fundamental potential of SiNSs for exploring the characteristics of excitons in confined dimensions due to the easy formation of self-trapped electron-hole pairs.<sup>[179]</sup>

Other calculations show that silicenes are semiconductors whose indirect band gap can be influenced by **physical strain**, leading to an indirect-to-direct gap transition. Different models show that asymmetrical strain leads to direct-to-indirect transitions in (100) SiNSs, while symmetrical strain retains the indirect band gap characteristic.<sup>[180]</sup> Further DFT calculations confirm the sensitivity of the band gap of silicenes towards strain by looking at the Si–H- and Si–Si-bond lengths.<sup>[149]</sup> Thus, unstrained silicenes exhibit a considerably lower electron mobility (464 cm<sup>2</sup>/Vs) than silicon (1450 cm<sup>2</sup>/Vs), but when strain is applied, the band gap becomes direct and the mobility rises drastically (8551 cm<sup>2</sup>/Vs).<sup>[149]</sup>

As determined for silicenes, silicenes also exhibit a strong dependency of their (opto)electronic properties on external influences (e.g., electric field, strain) and internal conditions (e.g., functionalization, zigzag vs. armchair configuration), leading to, in part drastic changes (e.g., direct vs. indirect band gap),<sup>[181]</sup> which demands for the experimental determination of their properties to understand which material is feasible and which properties accessible.

### *Experimentally Determined Properties*

The **structural properties** of silicene are defined by its sp<sup>3</sup> hybridized silicon atoms, forming honeycomb, buckled silicon layers mainly based on the Si(111) lattice.<sup>[38]</sup> The single layers show a stacking behavior similar to the anionic silicon sheets in the starting material CaSi<sub>2</sub>, but with much weaker van-der-Waals force-based interlayer bonding,<sup>[38]</sup> thus forming a graphite analogue structure with hexagonal layers with an in-plane lattice constant of 3.38 Å and a layer spacing of 5.4 Å.<sup>[84]</sup>

The previously described **Mg doped SiNSs** were extracted from the supernatant over an insoluble, black, metallic solid. The oxygen capped SiNSs were found to have thicknesses of 0.37 nm and lateral sizes of 200-500 nm and exhibited blue PL ( $\lambda_{\text{max}} = 434$  nm at excitation wavelengths of  $\lambda_{\text{ex}} = 350$  nm).<sup>[97]</sup> Electron diffraction patterns show that the material is single crystalline. Absorption measurements show a peak at 268 nm (4.8 eV) corresponding to the L→L critical point of the silicon band structure.

Optical absorption measurements of **hydride terminated SiNSs** were executed by diffuse scattering method and show an absorption edge of ca. 2.4 eV,<sup>[91]</sup> which is similar to the almost direct band gap of 2.75 eV<sup>[175]</sup> and in accordance with the direct band gap (2.41 eV) of the boat like conformation<sup>[140]</sup> that density functional theory (DFT) calculations reported.

Little is said about the **origin of the PL** of SiNSs: For CVD<sup>b</sup> grown SiNSs,<sup>[54,55]</sup> an enhanced direct band was found to be a potential reason for its occurrence.<sup>[54]</sup> 2D nanostructures are under compressive strain,<sup>[182]</sup> which is known to induce an indirect-direct band gap transition in Si materials.<sup>[183,184]</sup> Furthermore the PL of different silicon nanostructures was proposed to originate from excitonic recombination (i.e., exciton formation by recombination of electrons and holes) or charge carrier trapping at the surface and their subsequent recombination (i.e., recombination of surface state trapped electrons and holes).<sup>[55,185]</sup> Only in the former case, the size of Si nanostructures influences the wavelengths of the emissions, thus offering a good basis for further exploration.<sup>c</sup>

### 2.3.2.2 Functionalized Silicanes

#### *Theoretically Determined Properties*

First principle calculations show that the surface **functionalization has a strong** influence on the properties of the SiNSs. Hence, bromination influences the magnetic properties<sup>[178]</sup> and fluorination (or hydrogenation) of silicene was found to remove the conductivity at the Dirac point, causing band gap opening.<sup>[138,141]</sup> Band gaps of F-silicanes relative to H-silicene are reduced by at least 50%.<sup>[181]</sup> Other calculations show that the fluorination of silicene opens up a band gap whose values can be continuously tuned by physical strain.<sup>[186]</sup> Furthermore, external electric fields can induce a special separation in the electron and hole states and even render silicene self-doped.<sup>[181]</sup> Calculations starting from layered polysilanes show that the formerly indirect band gap turns direct upon fluorination, whereby the fluorine coverage determines the band gap width.<sup>[187]</sup> A study comparing the influence of the different halogen atoms F, Cl, Br and I on the silicanes, based on the DFT screened exchange local density approximation method, show a non-monotonic change of the material's electronic features with increasing periodic number of the halogen atoms (**Figure 3**).<sup>[137]</sup>

---

<sup>b</sup> The publication refers to silicon nanosheets; the termination of the SiNSs is not further examined.

<sup>c</sup> Experimental work on the origin of the PL of non- as well as functionalized silicanes is currently in progress and will be published soon.

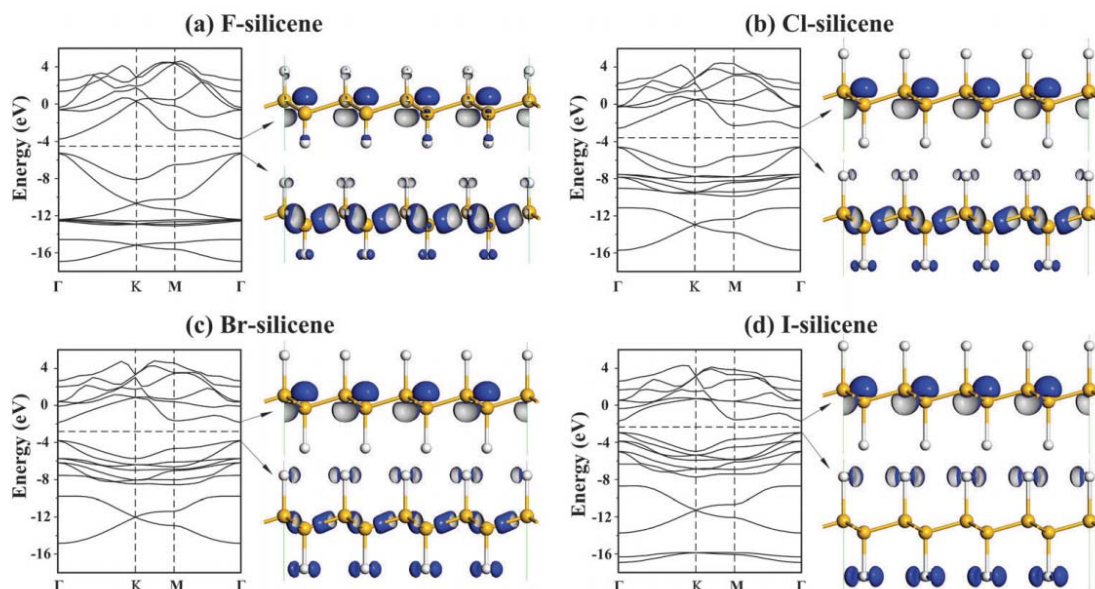


**Figure 3.** Electronic band structures (left) and charge density distributions of the conduction band maximum (right top) and the valence band maximum (right bottom) states at the  $\Gamma$  point for differently halogenated silicene. The dashed line indicates the Fermi level. Reproduced from Ref.<sup>[137]</sup> with permission of the PCCP Owner Societies.

Theoretical works on the properties of **phenyl-functionalized** SiNSs demonstrate the potential of surface functionalization to tune the electronic properties of SiNSs. Modified SiNSs were found to exhibit a direct band gap of 1.92 eV. Additionally the calculations show, that the phenyl groups do not interact strongly on the surface, thus allowing reorientation.<sup>[188]</sup> The organic groups prevent individual layers from interacting strongly with each other, so that stacked layers can still be regarded as individual layers.

DFT calculations for **hexyl-terminated** SiNSs show that a uniform distribution (periodicity of 7.17 Å) of the hexyl-groups on both sides of the silicon layers lead to the most stable structure, most likely due to electrostatic repulsion.<sup>[189]</sup> The authors additionally showed that the length of the alkyl group does not influence the direct band gap, but that physical strain can be used to tune the band gap continuously.<sup>[176]</sup>

#### *Experimentally Determined Properties*

Since the successful synthesis of silicene, Nakano and co-workers developed three different methods to modify the surface of SiNSs and were thus able to provide a first experimental glimpse into the outstanding properties of this new material.

**Amine-functionalized** SiNSs consist of 7.5 nm thick layers that stack with interlayer distances of 2.98 nm and exhibit blue PL ( $\lambda_{\text{max}} = 350$  nm).<sup>[108]</sup> When the solvent is slowly evaporated from a dispersion in toluene, the hybrid material turns into a gel, while the slow evaporation of a solvent mixture of toluene/chloroform leads to a sponge like material. The material was further examined by

looking at the electron transport properties perpendicular to the sheets by conductive atomic force microscopy (cAFM).<sup>[164]</sup> At voltages  $< 0.54$  V, direct tunneling could be observed, while for voltages  $> 0.54$  V Fowler-Nordheim tunneling was found to be dominant. These findings indicate that the tunneling barrier of the sheets are smaller than those of the organic molecules on the surface and introduce cAFM as a promising method for the electronic characterization of SiNSs, e.g., with different functionalities.

**Aryl-functionalized SiNSs** synthesized by the treatment of SiNSs-H with phenylmagnesium bromide were found to exhibit layer thicknesses of 1 nm and a PL emission maximum of  $\lambda_{\text{max}} = 350$  nm.<sup>[98]</sup> When the hybrid material was deposited on a three-electrode-photochemical cell, photocurrents could be measured under direct irradiation with a xenon lamp for wavelengths  $< 420$  nm<sup>[98]</sup> indicating, that the photocurrent forms *via* direct band gap transition. When aromatic groups were attached to the surface *via* Si-N-bonds, the PL emission maximum was  $\lambda_{\text{max}} = 370$  nm ( $\lambda_{\text{ex}} = 250$  nm) or 433 nm ( $\lambda_{\text{ex}} = 350$  nm) and photocurrents could be measured when the hybrid material was illuminated with a Xe-lamp.<sup>[109]</sup> According to the authors, photocurrent generation cannot be observed with alkyl functionalized SiNSs.

**Hexyl-functionalized SiNSs** rendered clear dispersions in chloroform and a layer thickness of ca. 3 nm.<sup>[111]</sup> The authors do not make any statement about PL properties, but published absorption associated band gap transitions at 4.2 eV.

The functionalization of SiNSs was found to stabilize the SiNSs and facilitates the dispersibility of the inorganic materials in organic solvents and is therefore the starting point for the use of SiNSs in any of the various potential applications that could make use of the outstanding properties of SiNSs.

## 2.4 Applications

### 2.4.1 Silicenes

#### *Potential Applications based on Theoretical Calculations*

Currently, FET technology is approaching its performance limits as the miniaturization of the silicon based integrated circuitry reaches its limits (e.g., in lithography).<sup>[190]</sup> However, FETs with a thin channel region are supposed to suppress short channel effects, enabling the fabrication of FETs with very short gate lengths.<sup>[191]</sup> SiNSs with a monoatomic layer represent the thinnest channel possible and thus exhibit a great potential for information technology.<sup>[137]</sup> The electronic properties of silicene (i.e., Dirac fermion character of the charge carriers resulting in high carrier mobilities, tunable band gap, etc.) make it an ideal FET material.<sup>[63,137]</sup>

As mentioned before, surface adsorption or functionalization of silicenes can be used to tune their band gap. Ni *et al.* showed that a sizeable band gap can be opened at the Dirac point of silicene without degrading the electronic properties. On the basis of Cu, Ag, Au, Ir and Pt adsorption the materials can

be doped and used for the fabrication of a p-i-n-tunneling FET with an on/off ratio of  $10^3$ , a small threshold swing of  $77 \text{ mV dec}^{-1}$  and a large state current of  $1 \text{ mA } \mu\text{m}$  under a supply voltage of  $1.7 \text{ V}$ .<sup>[39]</sup>

Van-der-Waal corrected DFT calculations suggest strong potential of silicane/silicene bilayers in FET technology. The hydride terminated silicanes represent an ideal substrate, that opens the band gap of silicene. The properties of the bilayer can be modulated by strain or applying a bias voltage, making the material a good candidate for high-performance room temperature operating FETs.<sup>[131]</sup>

Pristine silicene is impermeable to helium due to a high penetration energy barrier ( $1.66 \text{ eV}$ ), demonstrating its potential as a **gas purification** material.<sup>[192]</sup> Upon introduction of defects, the material becomes permeable for He, thus for example Ne or Ar can be separated from it due to the different atomic radii. These defects can also be used to separate  $\text{H}_2$  gas from common gaseous molecules (i.e.,  $\text{N}_2$ ,  $\text{CO}$ ,  $\text{CO}_2$ ,  $\text{CH}_4$ ,  $\text{H}_2\text{O}$ ), showing a potential application of porous silicene in gas separation and filtering applications,<sup>[193]</sup> e.g., in the chemical industries. First principle calculations show that metalized (i.e., K decorated) silicenes and silicanes can additionally act as a high capacity  **$\text{H}_2$  storage** medium with capacities of  $6.13 \text{ wt\%}$ .<sup>[46]</sup>

Furthermore, silicene shows potential for **Na- or Li-ion batteries**. First principle studies show that defects, which are more likely to occur for silicene than for graphene, lead to high Li-ion mobilities on the surface and low diffusion barriers. The layered structure of 2D materials, the large surface area, the short diffusion length and the space in between the layers should facilitate Li storage, as seen in the conventionally used graphite anodes.<sup>[194–196]</sup> Additionally, silicene exhibits large Li adsorption energies,<sup>[197]</sup> even when compared to graphene,<sup>[195]</sup> which may prevent the formation of lithium clusters.<sup>[194,195,198]</sup> Calculations on the Li-ion diffusion defines its pathways.<sup>[196,199]</sup> Together with adsorption energies of free standing mono- and bilayer silicenes, these calculations conclude that no structural changes should arise during the (de)lithiation. These studies could prove beneficial for the production of high energy density batteries with improved lifetimes.<sup>[198]</sup>

Some gases, such as  $\text{NH}_3$ ,  $\text{NO}$  and  $\text{NO}_2$  were determined to adsorb on the surface of silicene *via* strong chemical bonds, thus changing the band structure and opening the band gap at the Dirac point of silicene. This demonstrates the potential of silicene as sensitive molecule **sensors**.<sup>[200]</sup>

#### *Potential Applications based on Experimental Work*

For the synthesis of silicene a support is necessary to stabilize the material, which simultaneously induces the band gap. This is essential for, for example, FET applications. In 2015 Alkinwande and co-workers reported the first silicene based transistor, operating at room temperature.<sup>[82]</sup> For the fabrication, the authors developed the “silicene encapsulated delamination with native electrodes” process (**Figure 4**). Here the silicene layer was first encapsulated in between a layer of  $\text{Al}_2\text{O}_3$  and the  $\text{Ag}(111)$ /mica support. The  $\text{Al}_2\text{O}_3$ /silicene/Ag layers were then detached from the mica support and

the Ag film used as contact electrode material. The silicene based FET exhibits a transport behavior similar that of graphene based devices due to the analogous Dirac band structures. However, it possesses a lower residual carrier density and higher gate modulations, which suggests a small bandgap opening in the experimental devices. Alkinwande and co-workers additionally fabricated silicene multilayer based FETs, which were found to exhibit characteristic ambipolar charge carrier transport behavior.<sup>[162]</sup>

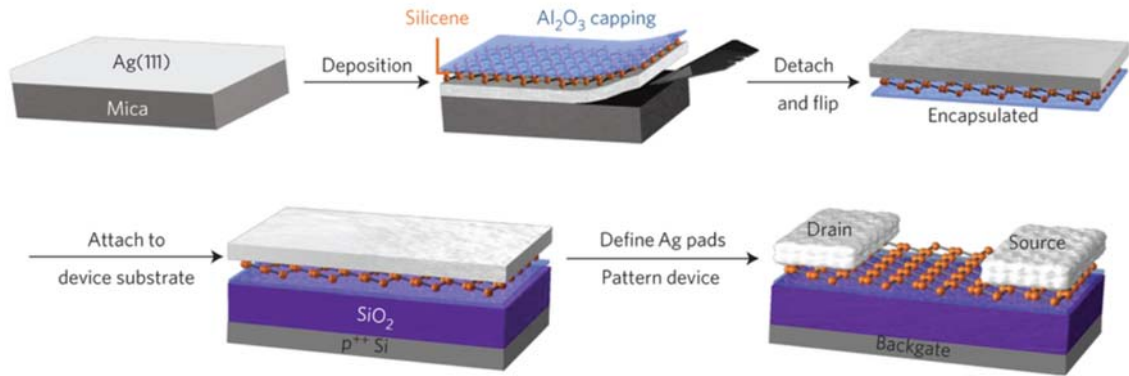


**Figure 4.** Process of silicene encapsulated delamination with native electrode. Key steps herein are: epitaxial growth of silicene on crystallized Ag(111) thin film, *in situ* Al<sub>2</sub>O<sub>3</sub> capping, encapsulated delamination transfer of silicene, and native contact electrode formation to enable back-gated silicene transistors.<sup>[82]</sup> Adapted by permission from Macmillan Publishers Ltd: Nature Nanotechnology Ref [82], copyright 2015.

Despite the many theoretical applications of silicene, only its suitability in FETs was examined experimentally. The more the material is understood, the easier it will be to implement it in further devices and applications and thus evaluate its potential. One essential aim remains the stabilization of silicene on its support and the detachment of the monolayers from it.

## 2.4.2 Silicanes

Due to the different synthesis route, no detachment of the silicon layers is necessary for silicanes in order to examine their properties and function in different applications. As such a variety of possibilities have been determined theoretically and first experimental results are available as well.

### *Potential Applications based on Theoretical Work*

Together with the sp<sup>3</sup>-hybridization of the silicon atoms, a band gap is expected to be induced in silicane, relative to silicene. Thus the semiconducting silicanes exhibits a large potential for **FET** applications, as 2D single silicon layers represent the thinnest possible channel. For example F- and I-terminated SiNSs were suggested as possible channel materials for FETs as the material is stabilized strongly by negative formation energy values.<sup>[137]</sup>

Furthermore, hybrid DFT calculations show that the SiH/TiO<sub>2</sub> heterojunction of a combination of silicane with anatase TiO<sub>2</sub>(101) composite exhibits great potential as a visible light excited **photocatalyst**.<sup>[201]</sup> It possesses an ideal band gap of 2.08 eV, a favorable band alignment and a facilitated carrier separation at the interface region. The direct band gap makes the material a promising candidate for **optoelectronic devices** as it enables efficient light emission/absorption.<sup>[173]</sup>

Additionally, DFT calculations show that the Na diffusion into silicane stacks is much higher than for bulk silicon, in which Na diffusion is energetically unfavorable.<sup>[202]</sup> Improved binding energies and the difference in activation energy for Na diffusion arise due to the large surface area and interlayer spaces. Thus silicane demonstrates potential as **alkali-ion battery** anode material.

#### *Potential Applications based on Experimental Work*

Nakano and co-workers investigated the potential of layered silicane as anode material in **lithium ion battery applications**.<sup>[203,204]</sup> Silicon with the highest theoretical capacity (3579 mA h g<sup>-1</sup> for Li<sub>15</sub>Si<sub>4</sub>),<sup>[42]</sup> is a much more promising material than the conventionally used carbon based anodes (372 mA h g<sup>-1</sup>), but in its bulk form increases its volume up to 300% when charged with lithium. This drastic change represents an up-to-now unmet challenge in the production of batteries with Si based anodes, as it leads to the degradation of the anode, loss of contact and thus a drop in performance of the battery after few cycles.<sup>[203,204]</sup> A layered structure with spaces might act as pathways for Li-ions<sup>[42]</sup> and buffer the potential change in volume. Layered polysilanes with their graphite-like structure thus possess ideal physical and structural properties for lithium ion battery applications.

Nakano and co-workers tested silicane multilayers (i.e., layered polysilanes) as anode materials and found first charge capacities of 1677 mAhg<sup>-1</sup> (as compared to a Si powder electrode 910 mAhg<sup>-1</sup>), a volumetric capacity of 2730 AhL<sup>-1</sup> (graphite: 820 AhL<sup>-1</sup>) and apparent chemical diffusion coefficients of Li<sup>+</sup> of 2.3·10<sup>-9</sup> cm<sup>2</sup>s<sup>-1</sup> (Si powder: 4.9·10<sup>-10</sup> cm<sup>2</sup>s<sup>-1</sup>). With the absorption of the Li-ions, amorphous Li<sub>x</sub>Si was formed and the volume increased by 150%. As a consequence, the capacity after the 10<sup>th</sup> cycle dropped to 817 mAhg<sup>-1</sup>.<sup>[42]</sup> To stabilize the SiNSs and increase the cycling performance, carbon/SiNSs composite materials were used as anode materials and characterized. They demonstrate a higher capacity retention than non-coated stacks of SiNSs and a higher conductivity than SiNSs/carbon powder mixtures.<sup>[40,41]</sup> Nakano *et al.* further fabricated a so called BF<sub>4</sub> anion rocking-chair-type secondary battery from the SiNSs based material [Si<sub>10</sub>H<sub>8</sub>(OCH<sub>2</sub>CH<sub>2</sub>NH(CH<sub>3</sub>)<sub>2</sub>)<sub>2</sub>](BF<sub>4</sub>)<sub>2</sub> in which SiNSs are functionalized with 2-(dimethylamino)ethanol.<sup>[43]</sup> Upon protonation to alkylammonium groups, the counter ion BF<sub>4</sub><sup>-</sup> can be brought into the system. The anode material was found to be stable for repeated electrochemical reduction-oxidation steps. Additionally, in contrast to conventional Li-ion batteries that do not work at low temperatures, the here described battery exhibited energy densities of 40 Whg<sup>-1</sup> at a current density of 100 mA g<sup>-1</sup> at operating temperatures of -30 °C.

Another work that deals with SiNSs as anode material for Li-ion batteries, uses SiNSs synthesized *via* magnesiothermic reduction of sand.<sup>[52]</sup> The electrochemical properties of an anode based on this type

of SiNSs are similar to commercial Si nanopowder. But when encapsulated with reduced graphene oxide, the electrode shows high-reversible capacity and excellent rate capability.

Despite the vast possibility of potential applications for SiNSs, only their suitability for Li-ion batteries has been examined due to the novelty of the material. This leaves a big field of yet undiscovered reactivities, properties and applications for SiNSs and identifies the material as a playground for scientists of different disciplines.

### 3. Aim of this Work

The discovery of graphene opened a new era in nanotechnology and emphasized the vast potential of 2D nanomaterials in future technologies. Since then, the scientific community has started to explore a variety of new two-dimensional materials. Amongst them silicon nanosheets play an important role for theoretical chemists and physicists, as in its 2D form, the carbon homologue silicon might exhibit similar potential as graphene. Although the performed theoretical work promises many outstanding properties and possible applications, for silicon nanosheets, not much experimental work has been published so far.

The 0D counterparts of SiNSs, SiNCs are better studied and understood. Also in our group we built up expertise in this field. Thus, since we started to work with SiNCs in 2013 we could develop new methods for their surface functionalization. As such diazonium salt initiators were shown to offer mild and straight forward means of surface modifications<sup>[102]</sup> and alkylsilylchloride terminated, electrophilic core shell particles could be synthesized that were susceptible to nucleophilic compounds.<sup>[205]</sup> Additionally, organolithium reagents were demonstrated to enable the direct attachment of aromatic and conjugated systems on the nanocrystal, hence representing a stabilizing surface functionalization method that does not isolate the SiNCs, but instead guarantees access to their electronic properties.<sup>[206,207]</sup> Furthermore, the controlled polymerization of functional polymers from silicon nanocrystals was shown to lead to a stabilization of the SiNCs and combined properties of both materials (e.g., photoluminescent temperature responsive hybrid materials).<sup>[208,209]</sup>

At the start of this thesis stood thus the question if the hydride terminated, 2D silicenes are also susceptible to such a rich surface chemistry and if their unique optic and electronic properties could be maintained by surface functionalization. The control over the surface chemistry of these new and promising materials depicts the first step towards a better understanding of their properties and potentials and should open possibilities in a broad field of applications. Additionally the combination of their properties with those of other materials (e.g., functional polymers), as shown for SiNCs, could open up new fields of application and might lead to first silicene-based devices. Therefore it is necessary to firstly investigate the characteristics and reactivity of the used SiNSs to determine if the materials keep up with their purported superiority over graphene.

One research aim hence is, to **characterize the materials** and their properties and to determine their potential applications. In order to facilitate characterization, the SiNSs need to be modified, as surface functionalization of silicon nanomaterials protects the material against external influences and can additionally be used to tune their properties (e.g., dispersibility,<sup>[102-104]</sup> band gap,<sup>[105,106]</sup> etc.). Every method has its advantages and disadvantages (e.g., reaction conditions, influence on PL properties, substrate scope, etc.) and only little experimental data has been collected for SiNSs.<sup>[98,108,111]</sup> Thus, **new surface modification pathways are needed** that guarantee mild, broadly applicable and easy to execute conditions. Although one cannot easily suggest the same properties for (silicon) materials, when the dimensions are reduced to the nanoregime, a good basis for this work lies in the published

modification methods for SiNCs. Thermal reactions are the most common functionalization methods for silicon (nano)materials and thus represent first potential initiation conditions (see chapter 4). Furthermore Lewis acid catalyzed surface functionalization for SiNCs was shown to proceed fast and without any side product impurities<sup>[210]</sup> (see chapter 6). A further, commonly used method to functionalize bulk and nanostructured silicon surfaces is UV induced hydrosilylation, which might also be applicable for SiNSs (see chapter 5). The great functional group tolerance of diazonium salts and the straight forward reaction procedure underlines the potential of these compounds for SiNM surface modifications. Hence diazonium compounds could be examined for their applicability for SiNSs as well (see chapter 4), as they were shown to successfully initiate functionalization of pSi<sup>[211]</sup> and SiNCs<sup>[102]</sup> and can be used for electroreductive grafting on bulk silicon.<sup>[212]</sup> Although only one publication deals with the grafting of diaryliodonium salts on silicon surfaces,<sup>[213]</sup> these compounds might in this context be very promising materials as well and could potentially be used for grafting onto the SiNS surface or as hydrosilylation initiator for other substrates, similar to diazonium compounds (see chapter 7).

Another research aim arises from the fact that nanomaterials are commonly used as a filler material in polymer composites. The resulting hybrid materials often combine the properties of both components,<sup>[209,214]</sup> or can drastically improve their properties (e.g., mechanical and electrical properties<sup>[215–217]</sup>), as was also shown for SiNCs. The **combination of SiNSs and common polymers in nanocomposites** might lead to new and interesting features (see chapter 5), which can contribute to the implementation of SiNSs in different nanoelectronic devices (see chapter 11.3). Hence the synthesis and characterization of a SiNSs based nanocomposite might be a rewarding aim. An important aspect of nanocomposite materials is the consistency of the filler material. As such, one distinguishes between covalent (i.e., the nanomaterial is functionalized) and non-covalent (i.e., a blend of filler and matrix) nanocomposites, which in the case of SiNSs might play an important role, as non-functionalized SiNSs might not be stable, even in the polymer matrix. Investigations into this matter may be interesting and helpful for further applications.

Due to the outstanding properties of SiNSs, functionalized SiNS as well as the nanocomposite hybrids could be used for the **fabrication and characterization of devices**, which is another attractive target that needs to be tackled once the SiNSs and their properties are better understood (see chapter 6). Their semiconducting character and the tunable band gap<sup>[180]</sup> make them very promising targets for nanoelectronic, and especially field effect transistor applications. Functionalized SiNSs as well as SiNSs blends with semiconducting polymers might represent good materials for this purpose. Similar FET applications were for example shown for carbon nanotubes.<sup>[218]</sup> Additionally, with phenyl-functionalized SiNSs, photocurrents could be measured. This observation depicts their potential in applications as photonic sensors due to the photosensitive behavior and is another desirable aim for this thesis (see chapter 11.3).

As some 2D nanomaterials (e.g., graphene) were found to be catalytically active,<sup>[219]</sup> and theoretical works suggests the same for silicon nanomaterials,<sup>[45]</sup> a further appealing aspect would be to **examine**

**the role of SiNSs as catalysts or reaction initiators** (see chapter 7 and chapter 8). If SiNSs were found to activate compounds, the big surface area of the nanomaterial could additionally enhance the reaction. The above mentioned applications in photocatalysis could be a starting point for examinations into “chemical applications” of SiNSs. Furthermore molecular silanes are commonly used as reduction reagents, which means, if applicable, SiNSs could reductively activate other molecules.

In conclusion, the aim of this work is to investigate the surface reactivity of silicane type SiNSs, their functionalization under different reaction conditions and their use as catalytic material. Another aspect is the characterization of their unique properties and their application as functional filler materials in nanocomposites as well as first nanoelectronic devices.

## 4. Radical Induced Hydrosilylation Reactions for the Functionalization of Two-Dimensional Hydride Terminated Silicon Nanosheets

<b>Status</b>	Published online March 15, 2016
<b>Journal</b>	Chemistry – A European Journal, 2016, Volume 22, 6194 - 6198
<b>Publisher</b>	Wiley-VCH
<b>DOI</b>	10.1002/chem.201505134
<b>Authors</b>	Tobias Helbich, Alina Lyuleeva, Ignaz M. H. Höhle, Philipp Marx, Lavinia M. Scherf, Julian Kehrle, Thomas F. Fässler, Paolo Lugli, Bernhard Rieger <sup>d</sup>

Reproduced by permission of John Wiley and Sons (license number 4078160391640).

### Content:

On various 3D and 0D silicon materials high temperatures as well as diazonium salts have been used to initiate surface functionalizations. Due to the novelty of 2D silicon nanomaterials, these methods have not yet been explored for SiNSs. The communication deals with this matter. Both methods have been shown to efficiently functionalize the surface of hydride terminated SiNSs with a broad variety of substrates. While diazonium salts could not be used for protic substrates on SiNCs, for SiNSs unsaturated acids as well as alcohols could be used, thus emphasizing the different reactivity of SiNCs and SiNSs. The diazonium salt initiated hydrosilylation is executed at room temperature and thus represents a very mild way of surface functionalization, rendering photoluminescent, two-dimensional silicon nanomaterials.

© 2016 Wiley-VCH Verlag GmbH & Co. KGaA, Weinheim

---

<sup>d</sup> T. Helbich planned and executed all experiments and wrote the manuscript; A. Lyuleeva contributed with AFM measurements; L. Scherf performed XRD measurements and synthesized the starting material  $\text{CaSi}_2$ ; I. Höhle, J. Kehrle and P. Marx contributed with mental input. All work was performed under the supervision of T. Fässler, P. Lugli and B. Rieger.

Surface Chemistry

# Radical-Induced Hydrosilylation Reactions for the Functionalization of Two-Dimensional Hydride Terminated Silicon Nanosheets

Tobias Helbich,<sup>[a]</sup> Alina Lyuleeva,<sup>[b]</sup> Ignaz M. D. Höhlein,<sup>[a]</sup> Philipp Marx,<sup>[a]</sup> Lavinia M. Scherf,<sup>[c]</sup> Julian Kehrle,<sup>[a]</sup> Thomas F. Fässler,<sup>[c]</sup> Paolo Lugli,<sup>[b]</sup> and Bernhard Rieger<sup>\*[a]</sup>

**Abstract:** Herein we present the functionalization of free-standing silicon nanosheets (SiNSs) by radical-induced hydrosilylation reactions. An efficient hydrosilylation of Si–H terminated SiNSs can be achieved by thermal initiation or the addition of diazonium salts with a variety of alkene or alkyne derivatives. The radical-induced hydrosilylation is applicable for a wide variety of substrates with different functionalities, improving the stability and dispersibility of the functional SiNSs in organic solvents and potentially opening up new fields of application for these hybrid materials.

Silicon nanosheets (SiNSs) are two-dimensional semiconducting materials with a layer thickness in the nano-regime and sheet sizes up to the micro-scale.<sup>[1]</sup> Like graphene they combine outstanding structural and electronic characteristics. As the electronic properties of these two materials differ from each other, SiNSs should hence expand the field of applications for 2D nanomaterials.

According to theoretical and experimental studies the band gap of SiNSs is tunable by physical strain,<sup>[2]</sup> the degree of hydrogenation, termination with heteroatoms,<sup>[3,4]</sup> and surface functionalization with different substrates.<sup>[5,6]</sup> Additionally, SiNSs exhibit unique optical properties such as a layer-thickness-dependent absorption edge<sup>[7]</sup> and photoluminescence (PL) emission arising from an enhanced direct band gap transition.<sup>[8,9]</sup> Hence SiNSs are promising candidates for microelectronics such as novel field effect transistors (FET)<sup>[5,10]</sup> and pho-

tovoltaic solar cells<sup>[9]</sup> and have already been proven to exhibit potential for lithium ion battery application.<sup>[11–13]</sup>

Several routes have been reported for the production of SiNSs. They can be synthesized by magnesiothermic reduction of SiO<sub>2</sub><sup>[14,15]</sup> or grown on supports such as Ag and Si by chemical vapor deposition.<sup>[8,16,17]</sup> Another straightforward and easily scalable route is chemical exfoliation from CaSi<sub>2</sub>.<sup>[18,19]</sup> The Zintl salt CaSi<sub>2</sub> consists of interconnected Si<sub>6</sub> rings which form puckered two dimensional, anionic silicon sheets and planar monolayers of Ca<sup>2+</sup> ions. Through treatment with hydrochloric acid the Ca<sup>2+</sup> ions can be deintercalated giving exfoliated hydride terminated SiNSs (Figure 1).

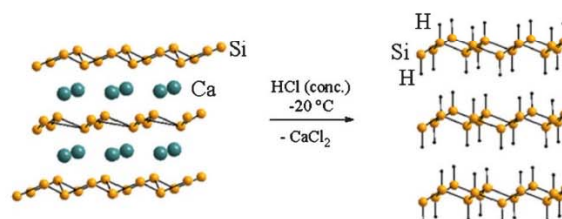


Figure 1. Synthesis of layered polysilanes by chemical exfoliation from CaSi<sub>2</sub>.

Due to their structural properties (i.e., sp<sup>3</sup> character), hydride terminated SiNSs are also referred to as layered polysilanes.<sup>[20]</sup> They are prone to oxidation under ambient conditions and must therefore be functionalized to be of further use. Additionally functionalization breaks up the stacked structure of non-functionalized SiNSs, rendering freestanding monolayers. Functionalized SiNSs are dispersible in organic solvents which facilitates their handling and characterization.

So far only three different methods have been published in which the functionalization of hydride terminated SiNSs with organic compounds is described. The reaction with *n*-alkylamines leads to stable Si–N–Si derivatives which exhibit blue PL,<sup>[21,22]</sup> while the conversion of SiNSs with the Grignard compound PhMgBr renders (Si<sub>6</sub>H<sub>4</sub>Ph<sub>2</sub>)<sub>n</sub> layers.<sup>[11]</sup> Additionally Pt-catalyzed hydrosilylation with 1-hexene enables the functionalization of SiNSs and yields stable colloidal dispersions in chloroform.<sup>[23]</sup>

Hydrosilylation reactions can be used to react molecular and surface Si–H groups with various unsaturated substrates. The reaction does not take place spontaneously, but needs initia-

[a] T. Helbich, Dr. I. M. D. Höhlein, P. Marx, J. Kehrle, Prof. Dr. B. Rieger  
Wacker-Lehrstuhl für Makromolekulare Chemie  
Technische Universität München, Lichtenbergstrasse 4  
85747 Garching (Germany)  
E-mail: rieger@tum.de

[b] A. Lyuleeva, Prof. Dr. P. Lugli  
Institute for Nanoelectronics, Technische Universität München  
Arcisstrasse 21, 80333 Munich (Germany)

[c] L. M. Scherf, Prof. Dr. T. F. Fässler  
Lehrstuhl für Anorganische Chemie mit Schwerpunkt Neue Materialien  
Technische Universität München, Lichtenbergstrasse 4  
85747 Garching (Germany)

Supporting information for this article is available on the WWW under <http://dx.doi.org/10.1002/chem.201505134>.

tion. On the molecular level it can be mediated by a catalyst, while on surfaces, thermally or initiator-induced radical reactions are also possible.<sup>[24–26]</sup> The latter are easily feasible, cost-efficient and tolerant towards a broad variety of functional groups. Another advantage is that radical-induced hydrosilylation is conducted without the introduction of transition metal impurities which are known to alter the PL properties of silicon nanomaterials<sup>[27,28]</sup> and lead to increased surface oxidation.<sup>[29]</sup> Despite their advantages, radical-induced hydrosilylation reactions have not yet been examined for the surface functionalization of SiNSs.

In this work the reactivity of SiNSs towards unsaturated compounds with different functionalities was examined (Scheme 1). The reactions were conducted in the absence of a catalyst under thermal initiation (130 °C) or by the addition of a diazonium salt as radical initiators with a variety of functional substrates. The resulting hybrid materials were fully characterized by FTIR, NMR spectroscopy, AFM, TGA, XRD and PL measurements.

The hydride-terminated SiNSs used in this work were synthesized following a literature known procedure.<sup>[19]</sup> CaSi<sub>2</sub> was chemically exfoliated with HCl (conc.) at –20 °C for 7 days. To remove residual oxide the obtained SiNSs were then etched with hydrofluoric acid and extracted with dichloromethane. As can be seen from the Si–H stretching- ( $\approx 2100\text{ cm}^{-1}$ ), scissoring- ( $\approx 900\text{ cm}^{-1}$ ) and wagging bands ( $\approx 860\text{ cm}^{-1}$ ) in FTIR spectra of the freshly etched SiNSs, the resulting silicon sheets are hydride-terminated with only slight traces of Si–O ( $\approx 1100\text{ cm}^{-1}$ ) and no Si–OH (Figure 2a).

To understand the reactivity of the SiNSs towards unsaturated carbon compounds, control experiments were conducted without a radical initiator at room temperature in the dark. Therefore the HF treated SiNSs (15 mg) were dispersed in a mixture of dry toluene (2 mL) and 1-dodecene (3 mmol), degassed by three freeze-thaw-pump cycles and subsequently stirred overnight under argon in the dark.

Neither molecular silanes<sup>[30,31]</sup> (see the Supporting Information) nor hydride terminated silicon surfaces of bulk silicon<sup>[32]</sup> or nanostructured silicon<sup>[33]</sup> show functionalization under these conditions. Therefore we were surprised to observe a significant amount of dodecyl groups on the SiNSs in FTIR measurements (Figure 2c) and TGA (Figure S7 in the Supporting Information). However this functionalization method is not sufficient to fully

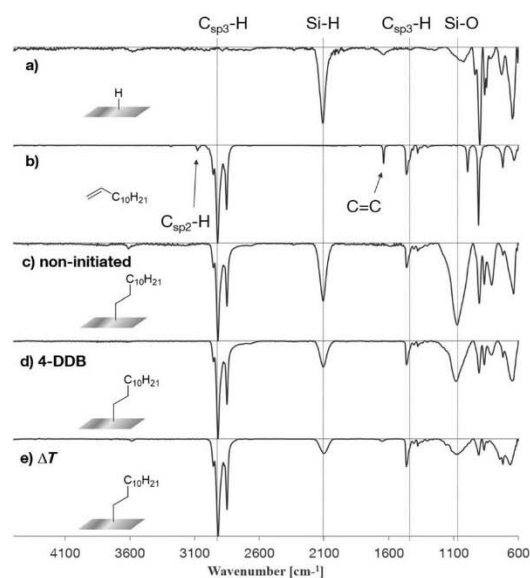


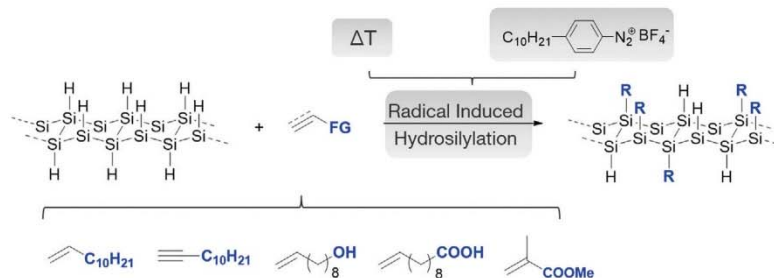
**Figure 2.** FTIR spectra of: a) freshly etched SiNSs, b) 1-dodecene and 1-dodecene-functionalized SiNSs, c) without the addition of an initiator, d) with 4-DDB, and e)  $\Delta T$ -induced hydrosilylation.

prevent stacking of the SiNSs (Figure S8 in the Supporting Information). Additionally, after the workup strong Si–O and residual Si–H bands, visible in IR spectra indicate, that the functionalization only takes place to a minor extent.

The cause for this unprecedented reactivity is not fully understood and remains part of the ongoing research in our group. Potential explanations are the very high surface area and energy which results in a higher reactivity of the nanomaterial<sup>[34]</sup> or the surface activation by traces of oxygen which were shown to initiate hydrosilylations on SiNCs.<sup>[35]</sup>

To achieve a higher degree of surface functionalization, the SiNSs were subsequently treated with 1-dodecene under radical initiation conditions (Scheme 1).

Diazonium salts are known to be mild radical initiators for hydrosilylation reactions on nanostructured silicon.<sup>[36]</sup> Especially 4-decylbenzene diazonium tetrafluoroborate (4-DDB) is suitable due to its solubility in nonpolar solvents.<sup>[26]</sup> Additionally elevated temperatures can initiate hydrosilylation.<sup>[35]</sup>



**Scheme 1.** Schematic overview of the executed functionalization methods: Thermal and diazonium salt induced hydrosilylations are applicable on a broad variety of substrates.

Exfoliated SiNSs (15 mg) were etched with HF (48%), extracted and dispersed in a mixture of dry toluene (2 mL) with 1-dodecene (3 mmol). After degassing, 4-DDB (15  $\mu$ mol) was added and the reaction mixture was stirred at room temperature, overnight. For thermal functionalization Si–H-terminated SiNSs were dispersed in 1-dodecene (1 mL), degassed and subsequently stirred at 130  $^{\circ}$ C, overnight.

The mechanism for both initiation conditions is proposed to proceed by the formation of silyl-radicals.<sup>[37]</sup> The 4-DDB-induced functionalization occurs through reduction of the diazonium compound, release of nitrogen and hence the formation of an aryl radical. After deprotonation a silyl surface radical is formed which then reacts with the unsaturated compound, leading to the Si–C bond and a carbon centered radical. Abstraction of a neighboring hydrogen radical again forms a silicon surface radical and the hydrosilylation proceeds as a radical chain reaction (Scheme 2a).<sup>[26,38]</sup>

Thermally induced hydrosilylation is stated to be dependent on the reaction temperature. While temperatures  $\geq 150$   $^{\circ}$ C provide enough energy to homolytically cleave Si–H bonds and thus induce the radical chain propagation (Scheme 2b), for temperatures between 80–150  $^{\circ}$ C traces of oxygen are proposed to accelerate hydrogen abstraction (Scheme 2c).<sup>[35]</sup>

After the reaction, the FTIR spectra of the functionalized SiNSs (Figure 2d and e) show strong  $C_{sp^3}$ –H bands ( $\approx 2920$   $cm^{-1}$ ,  $\approx 1460$   $cm^{-1}$ ) while only weak bands of residual Si–H ( $\approx 2100$   $cm^{-1}$ ) and Si–O ( $\approx 1100$   $cm^{-1}$ ) are present. This indicates a higher coverage of the SiNSs with dodecyl groups in contrast to functionalization without radical initiation, which is also supported by differences in the weight loss of the differently functionalized material in TGA measurements (Figure S7 in the Supporting Information).

Additionally we confirmed the 4-DDB and thermally induced functionalization with  $^1H$  NMR experiments in solution (Figure 3). Due to the restricted freedom of movement of the organic substrates attached to the Si surface the spectra can only qualitatively be used to show the successful functionalization and purification. The peaks of the double bond (A:  $\delta = 5.82$  ppm; B + C:  $\delta = 4.96$  ppm) and the methylene group next to it (D:  $\delta = 2.04$  ppm) have vanished and the spectra still show the peaks of the terminal  $CH_3$  group (F:  $\delta = 0.85$  ppm) and of the  $-CH_2$  groups (E:  $\delta = 1.25$  ppm) of the alkyl chain.

Atomic force microscope (AFM) images of the 1-dodecene-functionalized SiNSs show freestanding monolayers with a thickness of about 2.0 nm (Figure 4) which is similar to the

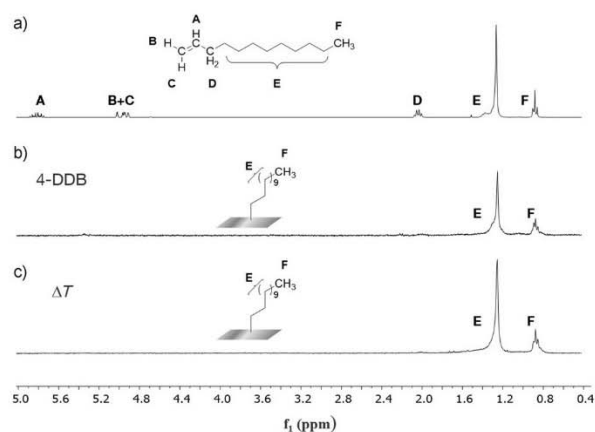
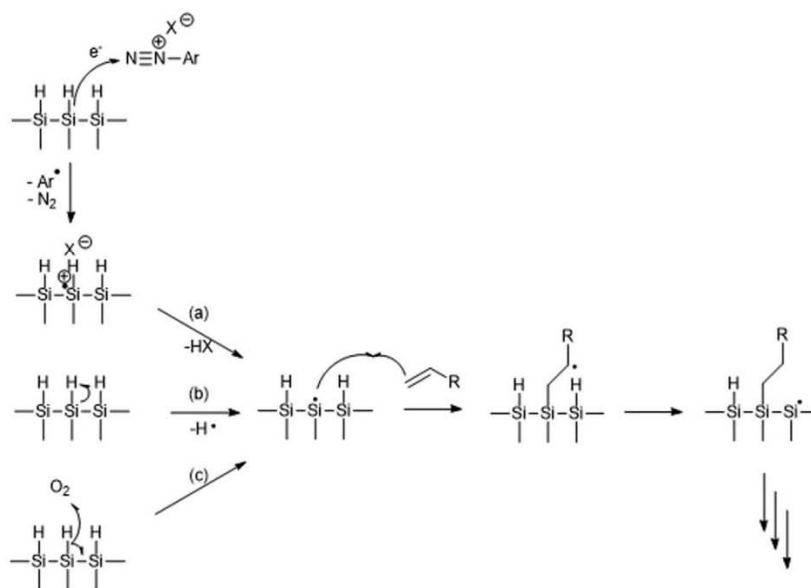


**Figure 3.** NMR spectra of: a) 1-dodecene, 1-dodecene-functionalized SiNSs with b) 4-DDB, and c)  $\Delta T$ -induced hydrosilylation.



**Scheme 2.** Proposed mechanism for the: a) diazonium-compound induced mechanism and thermally induced hydrosilylation at temperatures between b) 80–150  $^{\circ}$ C, and c)  $\geq 150$   $^{\circ}$ C.<sup>[25,35,39]</sup>

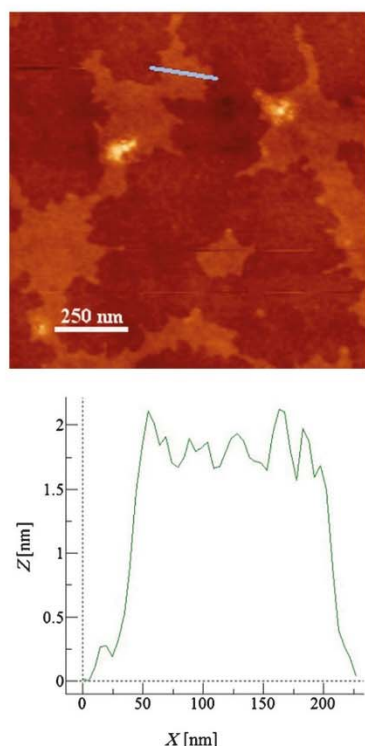


**Figure 4.** Non-contact mode AFM image of 4-DDB-induced 1-dodecene-functionalized SiNSs (top) and their line profile (bottom) taken along the line in the left image.

thickness of the 1-hexene-functionalized SiNSs reported by Nakano et al.<sup>[23]</sup>

XRD patterns recorded from the non-functionalized and 1-dodecene-functionalized SiNSs show that the characteristic re-

flections of the stacked, non-functionalized sheets decrease significantly in intensity when the SiNSs are functionalized without the initiator and even further with radical initiation (Figure S8 in the Supporting Information). The long dodecyl chains on the surface seem to stabilize the monolayers and hinder the SiNSs from stacking, resulting in a less ordered material.

Besides the model substrate 1-dodecene, functional substrates are promising candidates for further applications of the hybrid nanomaterials. Hence, to demonstrate the broad applicability of thermally and diazonium salt-induced hydrosilylations with hydride terminated SiNSs, a number of functional alkenes and alkynes were used. In this context we explored the functionalization with 10-undecenoic acid, 1-dodecyne, 9-decen-1-ol and *tert*-butyl methacrylate (tBuMA). In the case of tBuMA thermal hydrosilylation leads to a vast excess of polymerized alkene. No such side reaction could be observed in the 4-DDB-induced functionalization of the SiNSs, demonstrating the advantage of this mild method.

FTIR spectra of the functionalized SiNSs (4-DDB: Figure 5;  $\Delta T$ : Figure S9 in the Supporting Information) with the different substrates confirm the successful reaction exhibiting the expected bands such as  $C_{sp^3}-H$  ( $\approx 2920\text{ cm}^{-1}$ ),  $C=C$  ( $\approx 1640\text{ cm}^{-1}$ ),  $C=O$  ( $\approx 1700\text{ cm}^{-1}$ ),  $OH$  ( $\approx 2920\text{ cm}^{-1}$ ),  $C-O$  ( $\approx 1150\text{ cm}^{-1}$ ) while only traces of  $Si-H$  ( $\approx 2100\text{ cm}^{-1}$ ), and  $Si-O$  ( $\approx 1100\text{ cm}^{-1}$ ) can be detected. SiNS- $C_{10}H_{20}OH$  and SiNS- $C_{10}H_{20}COOH$  are dispersible in protic solvents such as ethanol and methanol while for SiNS- $C_{12}H_{25}$  and SiNS- $CHCH-C_{10}H_{21}$  nonpolar hydrocarbons such as toluene and benzene are the solvents of choice. Further reactions are possible with the thus introduced functionalities on the SiNSs surface. This approach is currently under investigation and should open up new fields of applications.

The hybrid materials exhibit similar photoluminescence properties to the non-functionalized materials, namely an emis-

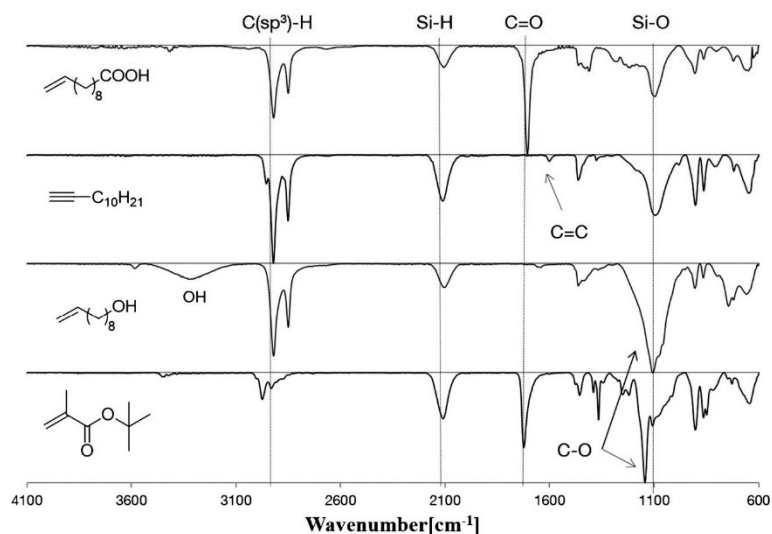


**Figure 5.** FTIR spectra of functionalized SiNSs by 4-DDB-induced hydrosilylation.

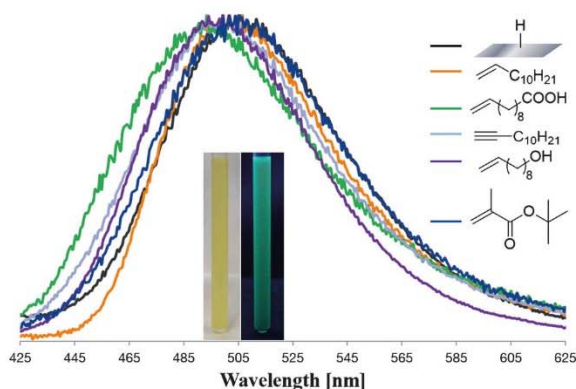


Figure 6. PL spectra of freshly etched and functionalized SiNSs by 4-DDB-induced hydrosilylation.

sion at  $\lambda_{\max} \approx 500$  nm (Figure 6, Figure S10 in the Supporting Information). This is in accord with the functionalized SiNCs which show similar PL for Si–H– and Si–C–capped SiNCs.<sup>[26]</sup>

In summary we present the first radical-induced hydrosilylation approach for the efficient functionalization of hydride terminated SiNSs. High temperatures (130 °C) or the addition of diazonium compounds successfully initiate the reaction. With this method SiNSs are functionalized with (non-)functional alkenes and alkynes, introducing alkyl, hydroxyl-, carboxy- and ester groups which improve the dispersibility properties. The free-standing SiNSs were found to have a thickness of about 2 nm and exhibit PL ( $\approx 500$  nm). Additionally, we demonstrate that NMR experiments in solution can be used to show the successful functionalization of the SiNSs. The obtained functional hybrid materials should be valuable for subsequent reactions and open up possibilities for new applications, for example, in electronics or optoelectronic devices.

### Acknowledgements

M. Knaus, R. Csiki, M. Kloberg and K. Melzer are thanked for their support as well as TUM Graduate School and IGSSSE. The authors thank the DFG for financial support of Alberta/Technische Universität München Graduate School for Functional Hybrid Materials ATUMS (IRTG2022). T.H. and L.M.S. are thankful for their fellowship from Studienstiftung des deutschen Volkes. I.M.D.H. and L.M.S. gratefully acknowledge the funding from Fonds der Chemischen Industrie.

**Keywords:** hydrosilylation · layered polysilane · nanotechnology · silicon nanosheets · surface chemistry

- [1] Y. Sugiyama, H. Okamoto, T. Mitsuoka, T. Morikawa, K. Nakanishi, T. Ohta, H. Nakano, *J. Am. Chem. Soc.* **2010**, *132*, 5946–5947.  
 [2] F. Li, R. Lu, Q. Yao, E. Kan, Y. Liu, H. Wu, Y. Yuan, C. Xiao, K. Deng, *J. Phys. Chem. C* **2013**, *117*, 13283–13288.  
 [3] T. H. Osborn, A. a. Farajian, O. V. Pupyshva, R. S. Aga, L. C. Lew Yan Voon, *Chem. Phys. Lett.* **2011**, *511*, 101–105.

- [4] F. Zheng, C. Zhang, *Nanoscale Res. Lett.* **2012**, *7*, 422.  
 [5] N. Gao, W. T. Zheng, Q. Jiang, *Phys. Chem. Chem. Phys.* **2012**, *14*, 257.  
 [6] Y. Ding, Y. Wang, *Appl. Phys. Lett.* **2012**, *100*, 083102.  
 [7] Y. Liu, H. Shu, P. Liang, D. Cao, X. Chen, W. Lu, *J. Appl. Phys.* **2013**, *114*, 094308.  
 [8] U. Kim, I. Kim, Y. Park, K.-Y. Lee, S.-Y. Yim, J.-G. G. Park, H.-G. G. Ahn, S.-H. H. Park, H.-J. J. Choi, *ACS Nano* **2011**, *5*, 2176–2181.  
 [9] H. Okamoto, Y. Sugiyama, H. Nakano, *Chem. Eur. J.* **2011**, *17*, 9864–9887.  
 [10] O. D. Restrepo, R. Mishra, J. E. Goldberger, W. Windl, *J. Appl. Phys.* **2014**, *115*, 033711.  
 [11] Y. Kumai, S. Shirai, E. Sudo, J. Seki, H. Okamoto, Y. Sugiyama, H. Nakano, *J. Power Sources* **2011**, *196*, 1503–1507.  
 [12] Y. Kumai, H. Kadoura, E. Sudo, M. Iwaki, H. Okamoto, Y. Sugiyama, H. Nakano, *J. Mater. Chem.* **2011**, *21*, 11941.  
 [13] Y. Kumai, H. Nakano, *Jpn. J. Appl. Phys.* **2015**, *54*, 035201.  
 [14] W.-S. Kim, Y. Hwa, J.-H. Shin, M. Yang, H.-J. Sohn, S.-H. Hong, *Nanoscale* **2014**, *6*, 4297–4302.  
 [15] Z. Lu, J. Zhu, D. Sim, W. Zhou, W. Shi, H. H. Hng, Q. Yan, *Chem. Mater.* **2011**, *23*, 5293–5295.  
 [16] B. Lalmi, H. Oughaddou, H. Enriquez, A. Kara, S. Vizzini, B. Ealet, B. Aufray, *Appl. Phys. Lett.* **2010**, *97*, 223109.  
 [17] P. Vogt, P. De Padova, C. Quaresima, J. Avila, E. Frantzeskakis, M. C. Asensio, A. Resta, B. Ealet, G. Le Lay, *Phys. Rev. Lett.* **2012**, *108*, 155501.  
 [18] O. Böhm, J. Hassel, *Z. Anorg. Allg. Chem.* **1927**, *160*, 152; Hassel, *Z. Anorg. Allg. Chem.* **1927**, *160*, 152.  
 [19] S. Yamanaka, H. Matsu-ura, M. Ishikawa, *Mater. Res. Bull.* **1996**, *31*, 307–316.  
 [20] H. Nakano, T. Mitsuoka, M. Harada, K. Horibuchi, H. Nozaki, N. Takahashi, T. Nonaka, Y. Seno, H. Nakamura, *Angew. Chem. Int. Ed.* **2006**, *118*, 6451–6454; *Angew. Chem.* **2006**, *118*, 6451–6454.  
 [21] H. Okamoto, Y. Kumai, Y. Sugiyama, T. Mitsuoka, K. Nakanishi, T. Ohta, H. Nozaki, S. Yamaguchi, S. Shirai, H. Nakano, *J. Am. Chem. Soc.* **2010**, *132*, 2710–2718.  
 [22] H. Okamoto, Y. Sugiyama, K. Nakanishi, T. Ohta, T. Mitsuoka, H. Nakano, *Chem. Mater.* **2015**, *27*, 1292–1298.  
 [23] H. Nakano, M. Nakano, K. Nakanishi, D. Tanaka, Y. Sugiyama, T. Ikuno, H. Okamoto, T. Ohta, *J. Am. Chem. Soc.* **2012**, *134*, 5452–5455.  
 [24] J. G. C. Veinot, *Chem. Commun.* **2006**, 4160–4168.  
 [25] J. M. Buriak, *Chem. Commun.* **1999**, 1051–1060.  
 [26] I. M. D. Höhle, J. Kehrle, T. Helbich, Z. Yang, J. G. C. Veinot, B. Rieger, *Chem. Eur. J.* **2014**, *20*, 4212–4216.  
 [27] D. Andsager, J. Hilliard, J. M. Hetrick, L. H. AbuHassan, M. Plisch, M. H. Nayfeh, *J. Appl. Phys.* **1993**, *74*, 4783.  
 [28] S. Li, I. N. Germanenko, M. S. El-Shall, *J. Phys. Chem. B* **1998**, *102*, 7319–7322.  
 [29] J. M. Holland, M. P. Stewart, M. J. Allen, J. M. Buriak, *J. Solid State Chem.* **1999**, *147*, 251–258.  
 [30] I. Ojima, N. Clos, R. Donovan, P. Ingallina, *Organometallics* **1990**, *9*, 3127–3133.  
 [31] B. Marciniak, in *Comprehensive Handbook on Hydrosilylation* (Ed.: B. Marciniak), Pergamon, Amsterdam, **1992**.  
 [32] R. L. Cicero, M. R. Linford, C. E. D. Chidsey, *Langmuir* **2000**, *16*, 5688–5695.  
 [33] Y. Yu, C. M. Hessel, T. D. Bogart, M. G. Panthani, M. R. Rasch, B. A. Korgel, *Langmuir* **2013**, *29*, 1533–1540.  
 [34] E. Roduner, *Chem. Soc. Rev.* **2006**, *35*, 583–592.  
 [35] Z. Yang, M. Iqbal, A. R. Dobbie, J. G. C. Veinot, *J. Am. Chem. Soc.* **2013**, *135*, 17595–17601.  
 [36] D. Wang, J. M. Buriak, *Langmuir* **2006**, *22*, 6214–6221.  
 [37] M. Woods, S. Carlsson, Q. Hong, S. N. Patole, L. H. Lie, A. Houlton, B. R. Horrocks, *J. Phys. Chem. B* **2005**, *109*, 24035–24045.  
 [38] J. M. Buriak, *Chem. Rev.* **2002**, *102*, 1271–1308.  
 [39] I. M. D. Höhle, J. Kehrle, T. K. Purkait, J. G. C. Veinot, B. Rieger, *Nanoscale* **2015**, *7*, 914–918.

Received: December 22, 2015

Published online on March 15, 2016

# CHEMISTRY

## A **European** Journal

### Supporting Information

#### **Radical-Induced Hydrosilylation Reactions for the Functionalization of Two-Dimensional Hydride Terminated Silicon Nanosheets**

Tobias Helbich,<sup>[a]</sup> Alina Lyuleeva,<sup>[b]</sup> Ignaz M. D. Höhle,<sup>[a]</sup> Philipp Marx,<sup>[a]</sup> Lavinia M. Scherf,<sup>[c]</sup> Julian Kehrlé,<sup>[a]</sup> Thomas F. Fässler,<sup>[c]</sup> Paolo Lugli,<sup>[b]</sup> and Bernhard Rieger<sup>\*[a]</sup>

chem\_201505134\_sm\_miscellaneous\_information.pdf

**Contents**

General Information.....	2
Syntheses and Procedures .....	2
Synthesis of CaSi <sub>2</sub> .....	2
Synthesis of Layered Polysilanes <i>via</i> Chemical Exfoliation.....	3
Etching of Silicon Nanosheets .....	3
Functionalization of Silicon Nanosheets Without Initiators.....	3
4-Decylbenzene Diazonium Tetrafluoroborate-Induced Functionalization.....	4
Thermal Induced Functionalization.....	4
Hydrosilylation Reactivity of Molecular Silanes .....	5
Figures .....	9
TGA Comparison of the Different Initiation Methods.....	9
XRD Patterns.....	9
FTIR Spectra of Functionalized Silicon Nanosheets.....	10
PL Spectra .....	10
TGA Measurements.....	11

## General Information

All reactants and reagents were purchased from *Sigma-Aldrich* and used without further purification if not stated otherwise. *Tert*-butylmethacrylate was distilled under reduced pressure and stored over molecular sieve. Toluene was dried prior to use with a *MBraun* solvent purification system *MB SPS-800* whereby argon 5.0 (99.9990 %, *Westfalen AG*) was used as inert gas. Acetone was dried over molecular sieve, degassed via 3 freeze-pump-thaw cycles and stored under argon. For storage of the exfoliated SiNSs a *LABmaster 130 (MBraun)* glove box was used with argon 4.8 (99.998 %, *Westfalen AG*). Air or water sensitive reactions were executed under standard Schlenk techniques.

For **NMR** measurements the functionalized SiNSs were freeze dried from benzene. The spectra were measured on an *ARX-300* from *Bruker* at 300 K. The chemical shifts ( $\delta$ ) are given in ppm and are calibrated to the rest proton signal of the deuterated solvent. **FTIR** spectra were measured with a *Bruker Vertex 70 FTIR* using a *Platinum ATR* from *Bruker*. **PL** spectra were taken with an *AVA-Spec 2048* from *Avantes* using a *Prismatrix (LED Current controller)* as light source in toluene or ethanol. **TGA** measurements were executed with a *Netzsch TG 209 F 1 Libra* with heating rates of 10 K/min and argon flow rates of 20 mL/min under argon 4.8 (99.998 %, *Westfalen AG*). For **AFM** measurements (contact mode, *Asylum Research MFP-3D AFM* with an *ARC Controller*) thin films of SiNS-C<sub>12</sub>H<sub>25</sub> (15 mg of exfoliated sheets in 2 mL of toluene) were spin coated (90 seconds, 1000 RPM) on Si/SiO<sub>2</sub> substrates. For **Powder X-ray Diffraction Analysis** powder diffraction patterns were recorded using a *Stoe STADI P* diffractometer equipped with a *Ge(111)* monochromator for Cu K $\alpha$  radiation ( $\lambda = 1.54056 \text{ \AA}$ ) and a *Dectris MYTHEN DCS 1K* solid-state detector. Samples were ground in an agate mortar and filled into 0.5 mm glass capillaries which were then sealed. The samples were measured within a  $2\theta$ -range of 5–89° (PSD steps, 0.075°; time/step, 41 s).

## Syntheses and Procedures

### Synthesis of CaSi<sub>2</sub>

A stoichiometric mixture of calcium (Alfa Aesar, 99.5 %) and silicon (Wacker, 99.99 %) was pressed to a pellet and subsequently melted together in an arc furnace installed in an argon-filled glovebox. To ensure homogenization, the resulting silver colored, metallic regulus was melted from both sides, ground thoroughly in an agate mortar, pressed to a pellet, melted from both sides in the arc furnace and ground to a powder again. A powder diffraction pattern of the resulting product shows that phase-pure CaSi<sub>2</sub> could be obtained.

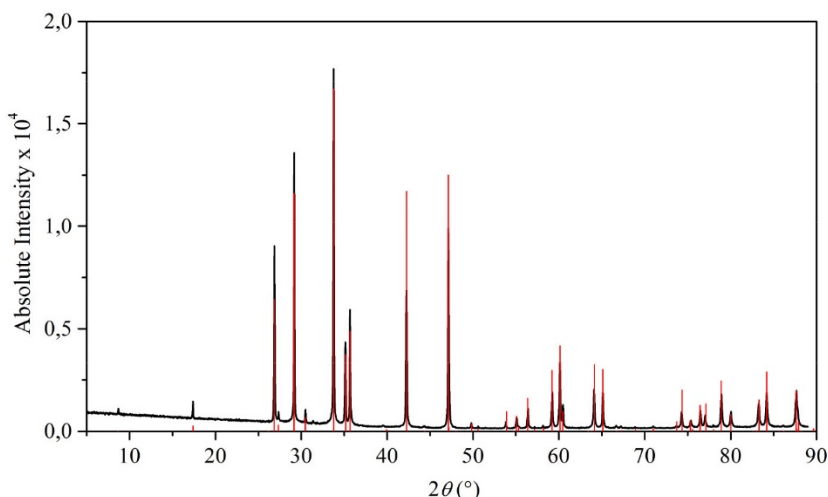
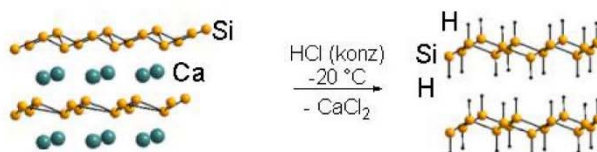


**Figure S1.** Experimental (black) and theoretical (red) powder diffraction patterns of CaSi<sub>2</sub>.

### Synthesis of Layered Polysilanes *via* Chemical Exfoliation



100 mL of HCl (conc.) in a schlenk flask were cooled to  $-30\text{ }^{\circ}\text{C}$  and 1.00 g of  $\text{CaSi}_2$  was added under argon and stirred at  $-20\text{ }^{\circ}\text{C}$  for 7 d. Then the reaction mixture was transferred into another schlenk flask *via* cannula and subsequently filtered off with a glass frit. The yellow filter cake was then washed with dry, degassed acetone and dried under vacuum. The thus obtained exfoliated  $(\text{Si}_6\text{H}_6)_n$  was stored under argon in a glove box.

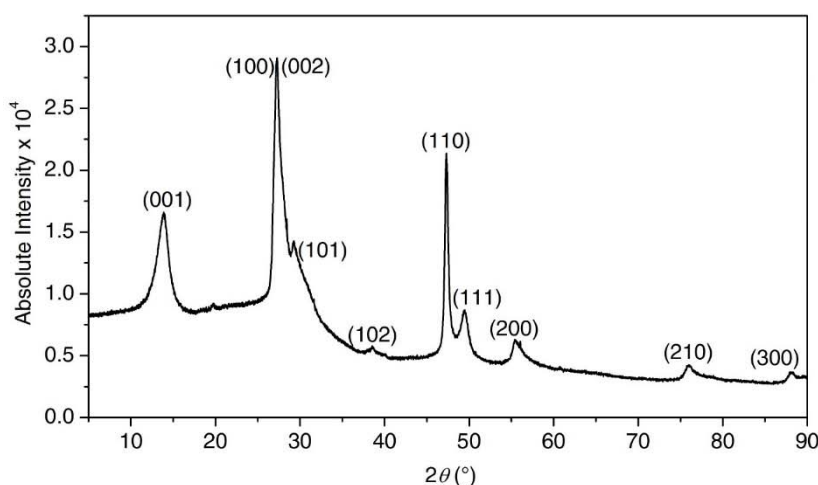
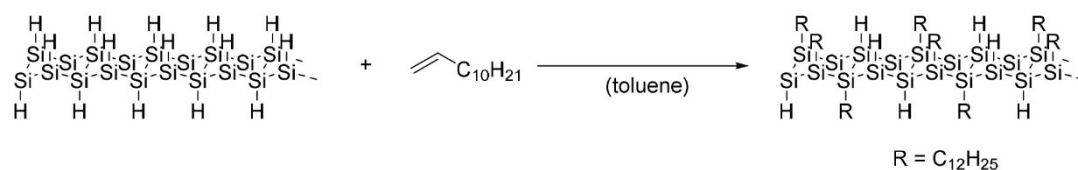


**Figure S2.** Powder diffraction patterns of as-synthesized SiNSs. The reflections of the regularly stacked sheets can be indexed by a hexagonal unit cell with  $a = 3.8331\text{ }\text{\AA}$  and  $c = 6.3751\text{ }\text{\AA}$ .

### Etching of Silicon Nanosheets

60.0 mg of the yellow  $(\text{Si}_6\text{H}_6)_n$  sheets were dispersed in  $\text{EtOH}/\text{H}_2\text{O}/\text{HF}$  (conc.) (1 mL/1 mL/1 mL) (*Caution: HF is highly dangerous and must be handled with extreme care*) and immediately extracted with  $3 \times 5\text{ mL}$  dichloromethane into PTFE centrifugation tubes. To the dispersion were then added 40 mL of toluene and the SiNSs isolated by centrifugation (9000 rpm/5 min). The supernatant was discarded and the SiNSs redispersed in 2 mL of dry toluene to remove residual traces of water. After centrifugation the SiNSs corresponding to 15 mg were dispersed in 2 mL of dry toluene (for DDB-induced functionalization) or in 1 mL of the substrate (for thermal-induced functionalization).

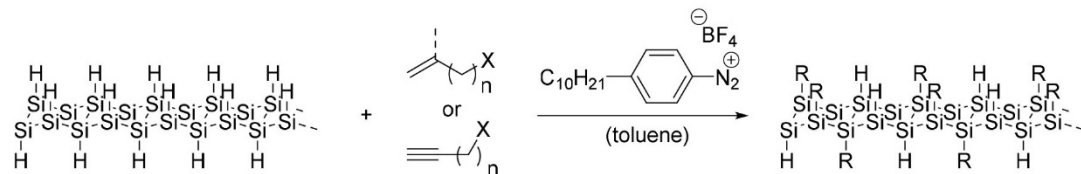
### Functionalization of Silicon Nanosheets Without Initiator



2 mL of the dispersion of hydride-terminated SiNSs in dry, degassed toluene (corresponds to 15 mg exfoliated  $(\text{Si}_6\text{H}_6)_n$ ) are transferred into a baked out schlenk tube covered with aluminum foil and 3 mmol of 1-dodecene are added. Then the reaction mixture is degassed *via* three freeze-thaw-pump cycles in the dark. After stirring over night at room temperature in the dark, the mixture is transferred into a centrifuge tube, mixed with 3 mL of ethanol and centrifuged (9000 rpm/4 min). Afterwards

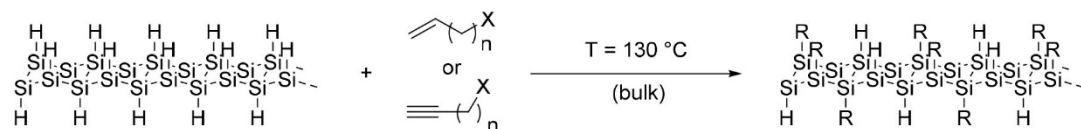
the residue is twice redispersed in a minimal amount of toluene and centrifuged with 1 mL of methanol. The SiNSs were then freeze dried from benzene for further analytics.

#### 4-Decylbenzene Diazonium Tetrafluoroborate-Induced Functionalization



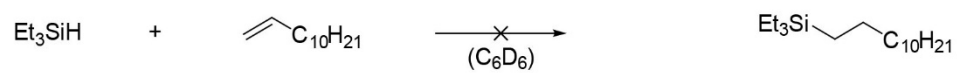
2 mL of the dispersion of hydride-terminated SiNSs in dry, degassed toluene (corresponds to 15 mg exfoliated  $(\text{Si}_6\text{H}_6)_n$ ) were transferred into a baked out schlenk tube and 3.00 mmol of the substrate were added. Then the reaction mixture was degassed *via* three freeze-thaw-pump cycles and 5.00 mg of 4-DDB was added under argon. After stirring overnight at rt the mixture was transferred into a centrifuge tube, mixed with 3 mL of methanol (for dodecene, dodecyne, <sup>t</sup>BuMA) or pentane (for undeceneic acid, decenol) respectively and centrifuged (9000 rpm/4 min). Afterwards the residue was twice redispersed in a minimal amount of toluene (or ethanol respectively) and centrifuged with 2 mL of the corresponding anti-solvent. The SiNSs were then redispersed in toluene (or ethanol) for further use.

#### Thermal Induced Functionalization



After dispersion of 15.0 mg of the hydride-terminated SiNSs in 1 mL of the substrate the reaction mixture was transferred into a baked out schlenk tube and degassed *via* three freeze-thaw-pump cycles, filled with argon and stirred at 130 °C over night. Afterwards the mixture was transferred into a PTFE centrifuge tube, mixed with 3 mL of ethanol (for dodecene, dodecyne) or pentane respectively (for undeceneic acid, decenol) and centrifuged (9000 rpm/5 min). Then the residue was twice redispersed in a minimal amount of toluene (or ethanol respectively) and centrifuged with 2 mL of the respective anti solvent. The SiNSs were then redispersed in toluene (or ethanol) for further use.

**Hydrosilylation Reactivity of Molecular Silanes**



100  $\mu\text{L}$  (546  $\mu\text{mol}$ , 1 eq) of  $\text{Et}_3\text{SiH}$  and 655  $\mu\text{mol}$  (1.2 eq) of the 1-dodecene are stirred in 1.5 mL of deuterated benzene in the glove box. After the given time an aliquot is taken for immediate  $^1\text{H}$ -NMR analysis.

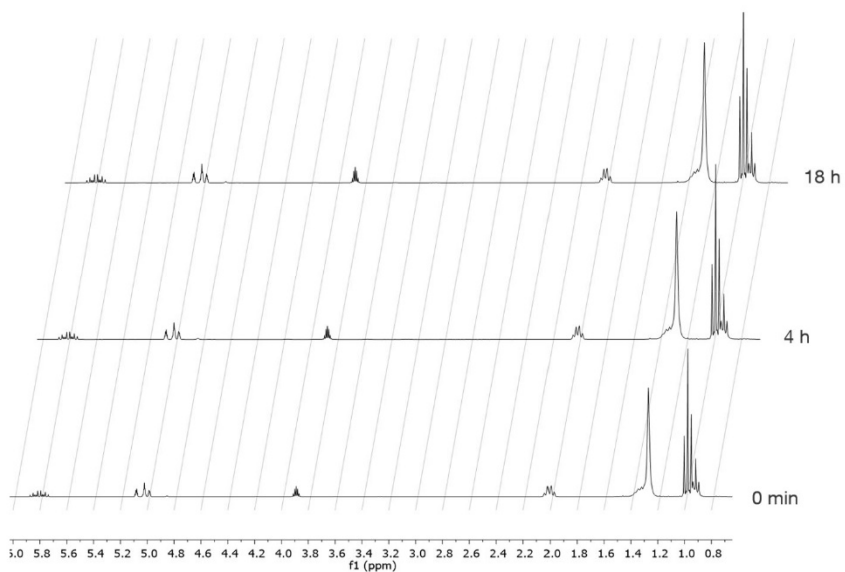
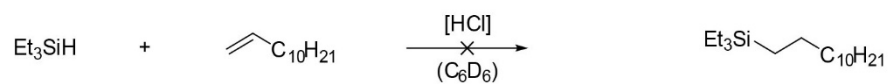


**Figure S3.** NMR spectra of the reaction mixture of triethylsilane with 1-dodecene after 0 min, 4 h and 18 h.

## Radical Induced Hydrosilylation Reactions for the Functionalization of Two-Dimensional Hydride Terminated Silicon Nanosheets



100  $\mu\text{L}$  (546  $\mu\text{mol}$ , 1 eq) of  $\text{Et}_3\text{SiH}$  and 655  $\mu\text{mol}$  (1.2 eq) of the 1-dodecene are stirred in 1.5 mL of deuterated benzene in the glove box and 20.0  $\mu\text{L}$  HCl (2.0 M in diethylether) were added. After the given time an aliquot is taken for immediate  $^1\text{H-NMR}$  analysis.

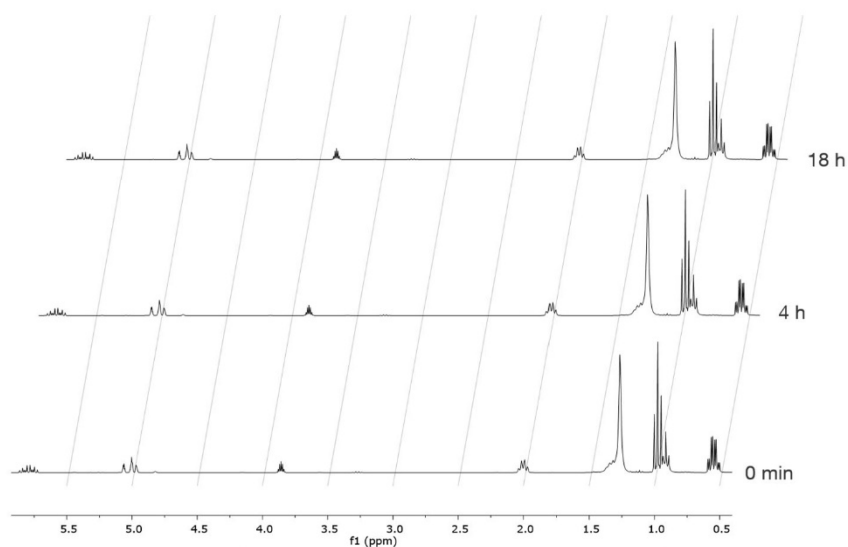
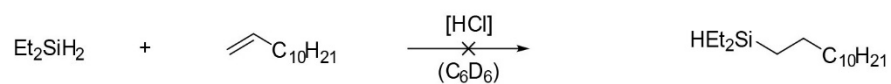


**Figure S4.** NMR spectra of the reaction mixture of triethylsilane with 1-dodecene and catalytic amounts of HCl after 0 min, 4 h and 18 h.

## Radical Induced Hydrosilylation Reactions for the Functionalization of Two-Dimensional Hydride Terminated Silicon Nanosheets



58  $\mu\text{L}$  (450  $\mu\text{mol}$ , 1eq)  $\text{Et}_2\text{SiH}_2$  and 100  $\mu\text{L}$  (1 eq) of the 1-dodecene are stirred in 1.5 mL of deuterated benzene in the glove box. After the given time an aliquot is taken for immediate  $^1\text{H-NMR}$  analysis.

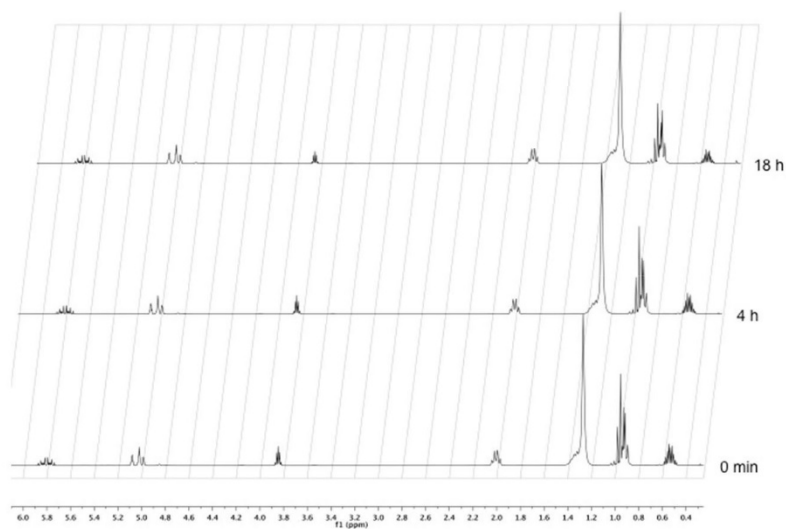
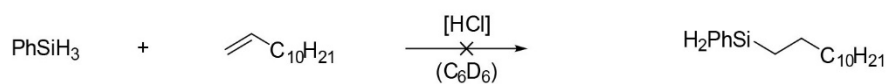


**Figure S5.** NMR spectra of the reaction mixture of diethylsilane with 1-dodecene after 0 min, 4 h and 18 h.

## Radical Induced Hydrosilylation Reactions for the Functionalization of Two-Dimensional Hydride Terminated Silicon Nanosheets



55  $\mu\text{L}$  (450  $\mu\text{mol}$ , 1eq)  $\text{PhSiH}_3$  and 100  $\mu\text{L}$  (1 eq) of the 1-dodecene are stirred in 1.5 mL of deuterated benzene in the glove box. After the given time an aliquot is taken for immediate  $^1\text{H}$ -NMR analysis.

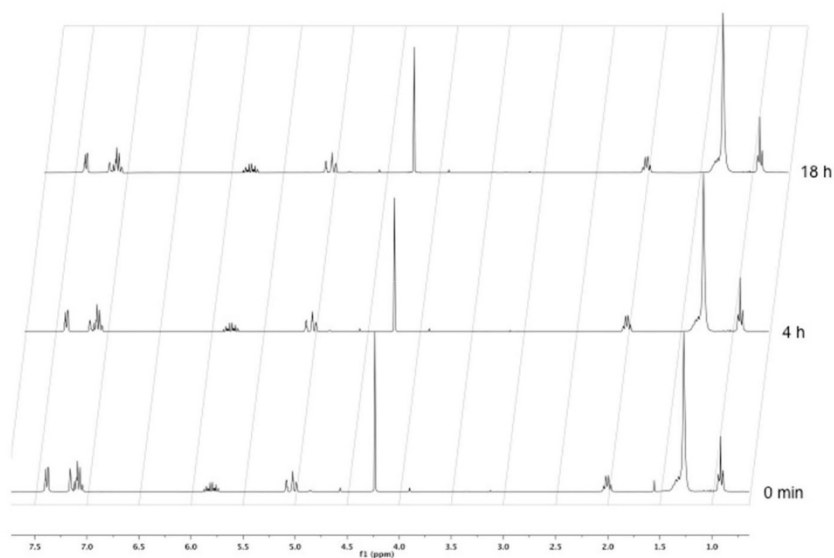


**Figure S6.** NMR spectra of the reaction mixture of phenylsilane with 1-dodecene after 0 min, 4 h and 18 h.

Molecular silanes cannot be reacted with 1-dodecene in the dark at room temperature (in the presence or absence of HCl) without any activation.

## Figures

TGA Comparison of the Different Initiation Methods

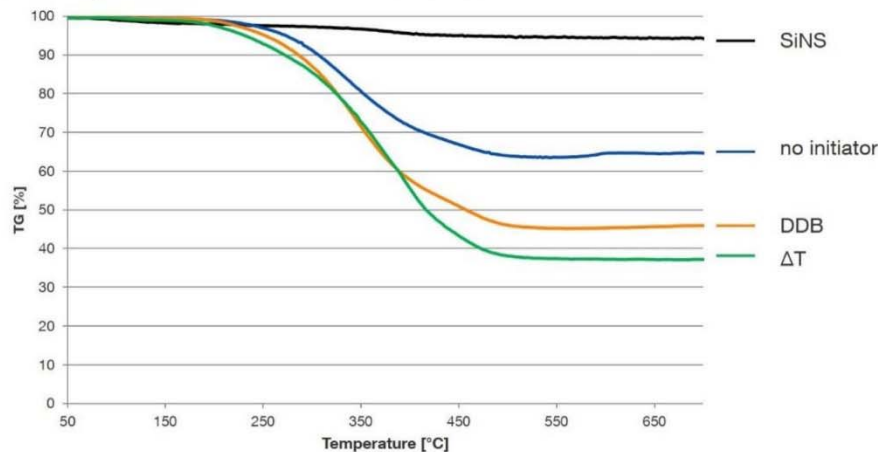


Figure S7. TGA measurements of unfunctionalized and 1-dodecene functionalized SiNSs.

## XRD Patterns

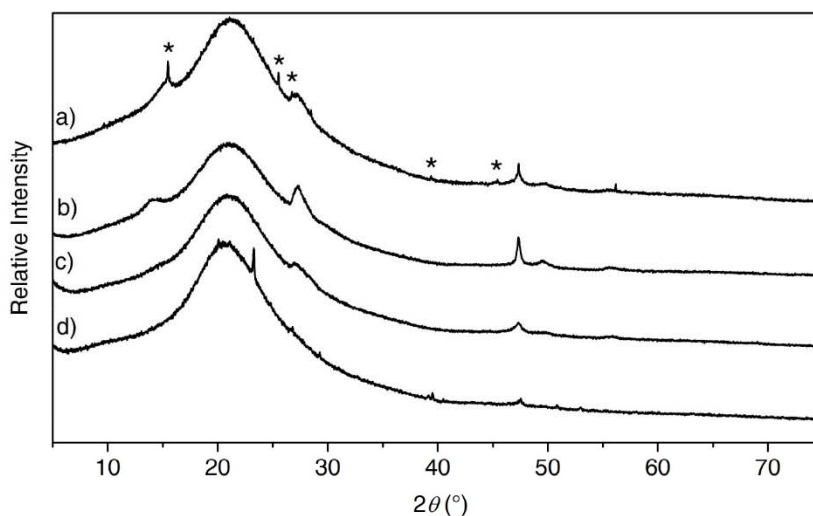


Figure S8. Powder diffraction patterns of (a) HF-etched SiNS-H, 1-dodecene functionalized SiNSs (b) without the addition of initiator (c) *via* DDB and (d) thermal initiation. Reflections marked with \* correspond to traces of  $\text{CaSiF}_6 \cdot 2 \text{H}_2\text{O}$  (PDF 44-0751). The increased background signal centered around  $21^\circ 2\theta$  is caused by the silica capillaries employed.

XRD patterns recorded from the non-functionalized and 1-dodecene functionalized SiNSs show that the characteristic reflections of stacked sheets decrease significantly in intensity with the increasing content of organic material. The surface functionalization hinders the SiNSs from stacking, resulting in a less ordered material.

FTIR Spectra of Functionalized Silicon Nanosheets

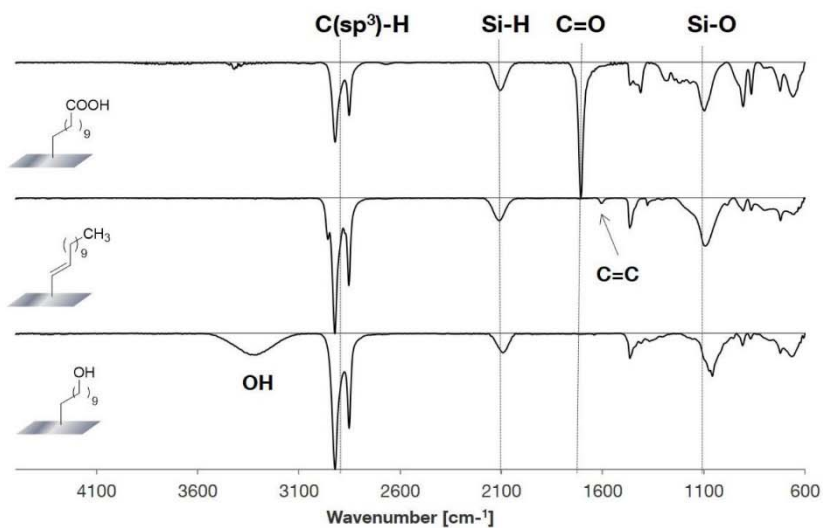


Figure S9. FTIR spectra of functionalized SiNSs *via* thermal-induced hydrosilylation.

PL Spectra

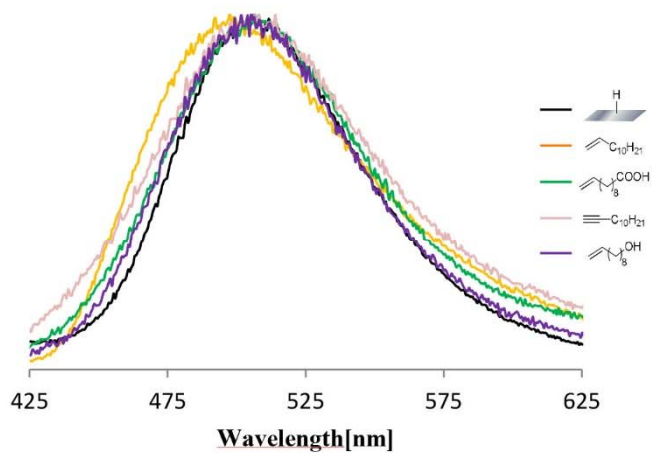


Figure S10. PL spectra of freshly etched and functionalized SiNSs *via* thermal-induced hydrosilylation. Excitation wavelength 365 nm.

### TGA Measurements

TGA measurements were executed with the unfunctionalized SiNSs. Unfunctionalized SiNSs lose 5% of their mass as can be seen in Fig. S6. This indicates the pyrolysis of the silicon monolayers at elevated temperatures and is different from TGA measurements with silicon nanocrystals for example, which do not show any loss.<sup>5</sup> Additionally it can be seen that the functionalization of the sheets with organic compounds is successful and that the stability of the functionalized SiNSs is dependent on the substrates (see also Fig. S8).

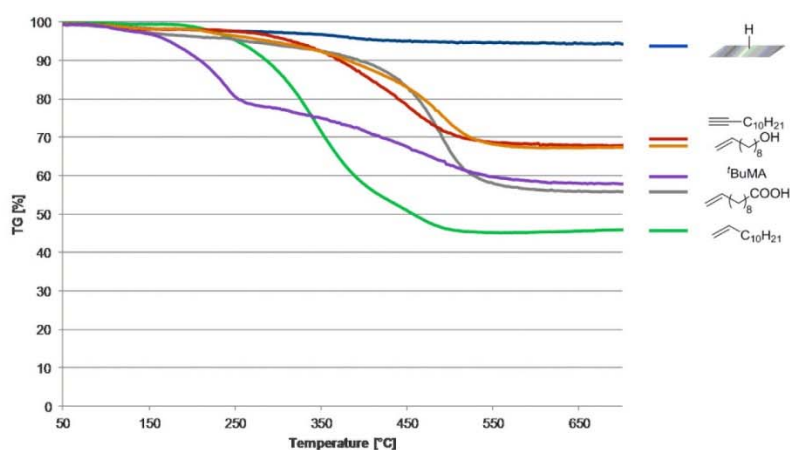


Figure S11. TGA measurements of unfunctionalized and functionalized SiNSs (4-DDB induced).

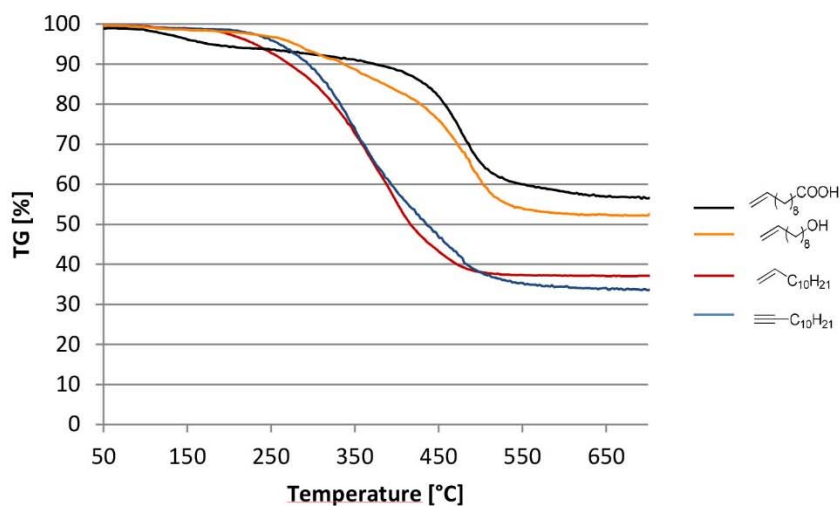


Figure S12 TGA measurements of thermally-induced functionalized SiNSs.

**Table S1** TG data from functionalized SiNSs.

reagent	initiation method	weigh tloss [%]	molecular weight [g/mol]	weight loss/molecular weight
dodecene	4-DDB	54,06	169,33	0,32
	$\Delta T$	62,88	169,33	0,37
undecenoic acid	4-DDB	44,30	185,28	0,24
	$\Delta T$	43,48	185,28	0,23
dodecyne	4-DDB	32,08	167,31	0,19
	$\Delta T$	47,38	167,31	0,28
decenol	4-DDB	32,71	157,27	0,21
	$\Delta T$	47,80	157,27	0,30
tBuMA	4-DDB	42,17	143,2	0,29

Table S1 shows the ratio of weight loss/molecular weight of the attached organic substrates in order to get comparable values of how many molecules are on the surface. For the thermal initiation, higher weight loss is observed compared to 4-DDB. On silicon nanocrystals thermal initiation is known to lead to oligomerization of the substrates on the silicon surface.<sup>6</sup> This can be the case as well for SiNSs and as such explain the different weight loss ratios.

- (1) Yu, Y.; Hessel, C. M.; Bogart, T. D.; Panthani, M. G.; Rasch, M. R.; Korgel, B. A. *Langmuir* **2013**, *29*, 1533.
- (2) Cicero, R. L.; Linford, M. R.; Chidsey, C. E. D. *Langmuir* **2000**, *16*, 5688.
- (3) Roduner, E. *Chem. Soc. Rev.* **2006**, *35*, 583.
- (4) Pavesi, L.; Turan, R. *Silicon Nanocrystals*; Pavesi, L., Turan, R., Eds.; Wiley-VCH Verlag GmbH & Co. KGaA: Weinheim, Germany, 2010.
- (5) Kehrle, J.; Höhle, I. M. D.; Yang, Z.; Jochem, A.; Helbich, T.; Kraus, T.; Veinot, J. G. C.; Rieger, B. *Angew. Chemie Int. Ed.* **2014**, *53*, 12494.
- (6) Yang, Z.; Iqbal, M.; Dobbie, A. R.; Veinot, J. G. C. *J. Am. Chem. Soc.* **2013**, *135*, 17595.

## 5. One-Step Synthesis of Photoluminescent Covalent Polymeric Nanocomposites from 2D Silicon Nanosheets

<b>Status</b>	Published online July 28 <sup>th</sup> , 2016
<b>Journal</b>	Advanced Functional Materials, 2016, Volume 26, 6711 – 6718.
<b>Publisher</b>	Wiley-VCH
<b>DOI</b>	10.1002/adfm.201602137
<b>Authors</b>	Tobias Helbich, Alina Lyuleeva, Theresa Ludwig, Lavinia M. Scherf, Thomas F. Fässler, Paolo Lugli, Bernhard Rieger <sup>e</sup>

Reproduced by permission of John Wiley and Sons (license number 4078160049566).

### Content:

In our previous work we could show, that radical induced hydrosilylation is an efficient way to functionalize the surface of SiNSs. In this publication we report the use of the classical radical polymerization initiator azobisisobutyronitrile for surface functionalization with different functional substrates. Additionally, the publication deals with UV light induced decomposition of SiNSs, which was observed during the studies on the radical induced surface functionalization of SiNSs, as UV light is another commonly used initiation method. While UV-induced hydrosilylations are broadly used to functionalize pSi or SiNCs,<sup>[220,221]</sup> the here used monolayered SiNSs decompose upon irradiation, most likely due to homolytic Si–Si-bond cleavage. This sensitivity against UV light needs to be tackled if SiNSs should find their way into further applications. Thus, we next reported the synthesis of SiNS based nanocomposites. The nanocomposite is synthesized in one step by radical polymerization of different monomers and the simultaneous radical induced surface functionalization of SiNSs. We could demonstrate this covalent character of the nanocomposite by the combination of different work-up procedures with GPC measurements. Lastly, we look into the properties of the SiNSs nanocomposites and demonstrate that they combine the processing properties of the organic polymer matrix with the (opto)electronic properties of the inorganic SiNSs. Additionally, the polymer matrix successfully contributes to the desired stabilization of the SiNSs against external influences such as UV light and bases.

© 2016 WILEY-VCH Verlag GmbH & Co. KGaA, Weinheim

---

<sup>e</sup> T. Helbich planned and executed all experiments and wrote the manuscript; A. Lyuleeva contributed with AFM measurements; T. Ludwig supported the work with polymer processing techniques; L. Scherf synthesized the starting material CaSi<sub>2</sub>. All work was performed under the supervision of T. Fässler, P. Lugli and B. Rieger.

Vol. 26 • No. 37 • October 4 • 2016

www.afm-journal.de

# ADVANCED FUNCTIONAL MATERIALS

SILICON  
NANOSHEETS  
NANOCOMPOSITE  
POLYMER  
MATRIX  
STYRENE  
ACRYLIC ACID  
OPTOELECTRONIC  
BASE  
MATERIAL  
HYBRID  
NANO  
UV-LIGHT  
FT-IR  
EXFOLIATION  
ULTRASOUND  
NANOCRYSTAL  
SILANE  
AIBN  
EDX  
FILTRATION  
RADICAL  
DECOMPOSITION  
MONOLAYER  
FUNCTION  
ORGANIC  
SUBSTRATE  
STABILITY  
SiNS@PAA

WILEY-VCH

# One-Step Synthesis of Photoluminescent Covalent Polymeric Nanocomposites from 2D Silicon Nanosheets

Tobias Helbich, Alina Lyuleeva, Theresa Ludwig, Lavinia M. Scherf, Thomas F. Fässler, Paolo Lugli, and Bernhard Rieger\*

Herein, the synthesis and characterization of the first polymeric nanocomposite based on silicon nanosheets (SiNSs) are reported. In a one-step reaction, the formation of the polymeric matrix material and simultaneous functionalization of the SiNSs with polymers occur via radical polymerization of organic monomers such as styrene, methyl methacrylate, and acrylic acid. Depending on the purification method used, a covalently linked nanocomposite or the functionalized SiNSs are obtained. SiNSs decompose when exposed to basic conditions or to UV light. The UV-light-based decomposition is briefly investigated. In the nanocomposite, the stability of the 2D nanomaterial enhances significantly against these external influences, while the optoelectronic properties (e.g., photoluminescence) of the SiNSs and the processing characteristics of the polymeric matrix are preserved.

## 1. Introduction

Hybrid organic–inorganic composites consisting of a polymeric matrix and inorganic nanomaterials have gathered much attention in recent literature. Such hybrid materials often combine the properties of both components<sup>[1]</sup> or even show improved features compared to those of either single substance (e.g., mechanical and electronic properties).<sup>[2–4]</sup> The use of nanomaterial-based fillers not only leads to homogeneous systems<sup>[2]</sup> but also to unexpected and improved characteristics (“nano effect”) in many cases.<sup>[5]</sup> Graphene–polystyrene nanocomposites, for example, have been observed to exhibit a percolation threshold of 0.1 vol% for room-temperature electrical conductivity and a conductivity of  $\approx 0.1 \text{ S m}^{-1}$  (1 wt% graphene).<sup>[6]</sup> The 2D character of carbon nanosheets, in particular, leads to interesting

properties because of the anisotropic character of the monolayers.<sup>[7]</sup>

Hydrogenated silicon nanosheets (SiNSs), also referred to as layered polysilanes<sup>[8]</sup> or silicanes,<sup>[9]</sup> exhibit a layer thickness in the nano regime and sheet sizes up to the microscale.<sup>[10]</sup> Based on theoretical calculations, SiNSs possess outstanding (opto)electronic properties,<sup>[11–13]</sup> some of which have already been demonstrated experimentally.<sup>[10]</sup> They exhibit photoluminescence<sup>[14]</sup> and are expected to generate highly localized excitons.<sup>[12]</sup> In addition, calculations have shown that their band gap can be tuned by physical strain,<sup>[15]</sup> external electric fields,<sup>[16]</sup> the influence of the underlying substrate,<sup>[17]</sup>

and different surface functionalizations.<sup>[13,18–20]</sup> Thus, SiNSs are promising materials for microelectronic applications such as novel silicon-based field-effect transistors,<sup>[19,21]</sup> photovoltaic solar cells,<sup>[8]</sup> and photodetectors.<sup>[22]</sup> Another promising field of application is lithium-ion batteries.<sup>[23–25]</sup> Silicon exhibits very high lithium storage capacities,<sup>[26]</sup> making it a seemingly ideal anode material. Silicon cannot be used in its bulk form because of the decomposition of the silicon anode triggered by the immense increase in anode volume when  $\text{Li}^+$  ions are inserted into the silicon lattice, leading to the formation of  $\text{Li}_{15}\text{Si}_4$ . This decomposition results in very short battery lifetimes.<sup>[26]</sup> Compared to silicon powder, silicon monolayers exhibit a significantly smaller change in volume and faster  $\text{Li}^+$  diffusion.<sup>[23]</sup> These properties should thus enable SiNSs to overcome the drawback of bulk silicon and compete with the current carbon-based systems. Nakano and Kumai used carbon-coated SiNSs to demonstrate their promising properties as anode materials.<sup>[25]</sup> In this case, the inorganic, conductive carbon coating protects the SiNSs from external influences; in contrast, a tailored flexible polymeric matrix might additionally buffer the smaller change in volume induced by lithium adsorption, highlighting the potential of SiNS-based polymer nanocomposites.

We have recently demonstrated that SiNSs can be functionalized via radical-induced hydrosilylation reactions with unsaturated compounds.<sup>[27]</sup> In the present work, we use azobisisobutyronitrile (AIBN) to initiate a radical polymerization of small, polymerizable molecules (i.e., styrene, methyl methacrylate, and acrylic acid) in the presence of SiNSs. Thus, in one step, the hydride-terminated SiNSs are covalently functionalized with organic monomers, and free polymer is formed in solution. As a result, after workup, the hybrid nanocomposite still

T. Helbich, T. Ludwig, Prof. B. Rieger  
Wacker-Lehrstuhl für Makromolekulare Chemie  
Technische Universität München  
Lichtenbergstrasse 4, 85747 Garching bei München  
Germany  
E-mail: rieger@tum.de

A. Lyuleeva, Prof. P. Lugli  
Institute for Nanoelectronics  
Technische Universität München  
Arcisstrasse 21, 80333 Munich, Germany

L. M. Scherf, Prof. T. F. Fässler  
Lehrstuhl für Anorganische Chemie mit Schwerpunkt  
Neue Materialien  
Technische Universität München  
Lichtenbergstrasse 4, 85747 Garching bei München, Germany



DOI: 10.1002/adfm.201602137

exhibits the properties of both materials and is stabilized against external influences. We demonstrate that different workup procedures allow the isolation of the nanocomposite or the functionalized SiNSs, demonstrating the covalent character of the nanocomposite. Both materials were subsequently characterized by Fourier transform infrared spectroscopy (FTIR), nuclear magnetic resonance (NMR) spectroscopy, photoluminescence (PL) spectroscopy, energy-dispersive X-ray (EDX) spectroscopy, and gel-permeation chromatography (GPC).

## 2. Results and Discussion

### 2.1. Synthesis of Hydride-Terminated Silicon Nanosheets

The hydrogenated silicon nanosheets were synthesized from  $\text{CaSi}_2$ <sup>[27]</sup> via chemical exfoliation with aqueous HCl. In this heterogeneous reaction, puckered, 2D, hydride-terminated SiNSs are liberated through deintercalation of the  $\text{Ca}^{2+}$  ions. (Scheme 1).<sup>[11]</sup>

$\text{CaSi}_2$  was added to concentrated HCl (aq.) under argon at  $-25\text{ }^\circ\text{C}$ , and the reaction mixture was stirred for 5 d.<sup>[14]</sup> The exfoliated SiNSs were then treated with ultrasound (3 min) to break up large agglomerates and subsequently etched with diluted hydrofluoric acid to remove potential oxides. In the next step, the hydride-terminated SiNSs were extracted with dichloromethane. The FTIR spectra of the freshly etched SiNSs show Si–H bands (Si–H  $\approx 2100$ ,  $\approx 900$ ,  $\approx 860\text{ cm}^{-1}$ ), with slight traces of Si–O ( $\approx 1100\text{ cm}^{-1}$ ) (Figure 1a).

### 2.2. Silicon-Nanosheet-Based Composites

Si–H bonds are prone to oxidation under ambient conditions because of the strong oxophilicity of silicon. Si–C bonds, by contrast, are stable against oxidation and hydrolysis. Hence, hydrosilylation reactions are used to functionalize and stabilize sensitive silicon-based nanomaterials.<sup>[28]</sup> The surface modification not only influences the stability and dispersibility properties, but also enables easier handling and opens various fields of application because of the different functional surface groups.<sup>[28]</sup>

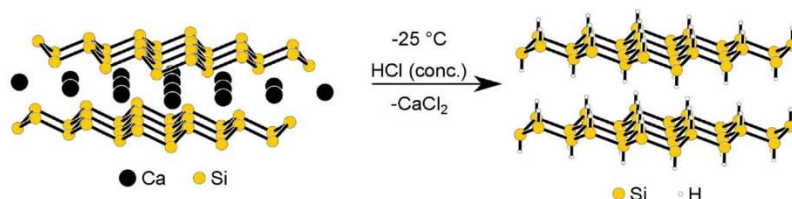
In previous studies, Grignard reagents,<sup>[10,29]</sup> amines,<sup>[30,31]</sup> and unsaturated compounds were used to functionalize SiNSs with organic monolayers.<sup>[27,32]</sup> Although functionalized, SiNSs are still prone to decomposition via external influences such as UV light and basic conditions. Silicon-based materials, in general, are known to dissolve in basic media via the formation of water-soluble forms of silicic acid (e.g.,  $[\text{SiO}_2(\text{OH})_2]^{2-}$ ).<sup>[33]</sup> This instability might limit the potential applications of SiNSs. In

the case of other silicon-based nanomaterials (e.g., silicon nanocrystals), stabilization against basic conditions has been achieved via the embedment of the nanomaterial in a polymer matrix.<sup>[1,34]</sup> The synthesis of nanocomposites from polymers and inorganic nanomaterials enables the combination of the advantageous properties of both classes of materials and additionally stabilizes the nanomaterials against agglomeration and aggregation.<sup>[35]</sup>

For the synthesis of a polystyrene (PS)-based SiNS hybrid nanocomposite (SiNS-PS@PS) the exfoliated SiNSs (88 mg) were etched with HF, extracted, and dispersed in a mixture of styrene (3.30 g) in toluene (12 mL). After this mixture was degassed, AIBN (20 mg) was added under Schlenk conditions and the reaction mixture was stirred at  $70\text{ }^\circ\text{C}$ . After 16 h, the reaction mixture was precipitated in methanol and freeze dried from benzene (Scheme 2).<sup>[36]</sup>

The hybrid material was characterized by FTIR (Figure 1a); its spectrum shows the same signals as radically polymerized styrene. The Si–H band ( $\approx 2100\text{ cm}^{-1}$ ) vanishes because of the radically induced hydrosilylation with styrene and the excess of polymeric material formed around the SiNSs. Instead,  $\text{C}_{\text{sp}^3}\text{--H}$  ( $\approx 2900\text{ cm}^{-1}$ ),  $\text{C}_{\text{sp}^2}\text{--H}$  ( $\approx 3100\text{ cm}^{-1}$ ), and  $\text{C}=\text{C}$  ( $\approx 1650\text{ cm}^{-1}$ ) bands, as well as aromatic overtones ( $\approx 1700\text{--}2000\text{ cm}^{-1}$ ), appear in the FTIR spectra. The corresponding NMR spectra show aromatic signals at  $6.5 \leq \delta \leq 6.7$  and  $6.9 \leq \delta \leq 7.2$  ppm and aliphatic signals at  $1.2 \leq \delta \leq 1.9$  ppm, which match the signals of polystyrene (Figure 1b). EDX analysis confirms the presence of Si, and in Raman spectra (Figures S3 and S4, Supporting Information) the characteristic Si–Si band ( $496\text{ cm}^{-1}$ ) can still be found, proving that SiNSs are retained in the nanocomposite. The resulting hybrid material also still exhibits the photoluminescence properties of the SiNSs (Figure 1c). The thermal properties of the polymer are not changed by the SiNSs presence. The glass transition temperature of the nanocomposite as well as of a polystyrene sample, prepared under the same conditions in absence of SiNSs, was found to lie at around  $103\text{ }^\circ\text{C}$  (Figure S5, Supporting Information). Thermogravimetric analysis (TGA) measurements under air showed that the nanomaterial does not influence the thermo-oxidative stability of the polymer (Figure S6, Supporting Information).

To demonstrate that this straightforward one-step synthesis of SiNS nanocomposites is broadly applicable, we also used methyl methacrylate (MMA) and acrylic acid (AA) to synthesize the polymeric hybrid materials SiNS-PMMA@PMMA and SiNS-PAA@PAA. Again, FTIR (Figures S7 and S8, Supporting Information) and NMR measurements (Figures S9 and S10, Supporting Information) confirm the successful reaction and the presence of Si is indicated by EDX measurements. All hybrid materials exhibit the processability properties of the surrounding polymer but still show the photoluminescence properties of the embedded inorganic SiNSs (Figure S14, Supporting Information).



Scheme 1. Synthesis of 2D layered polysilanes via chemical exfoliation from  $\text{CaSi}_2$ .

### 2.3. Demonstration of the Covalent Character of the Nanocomposite

Because we observed that radical-induced hydrosilylation successfully functionalized

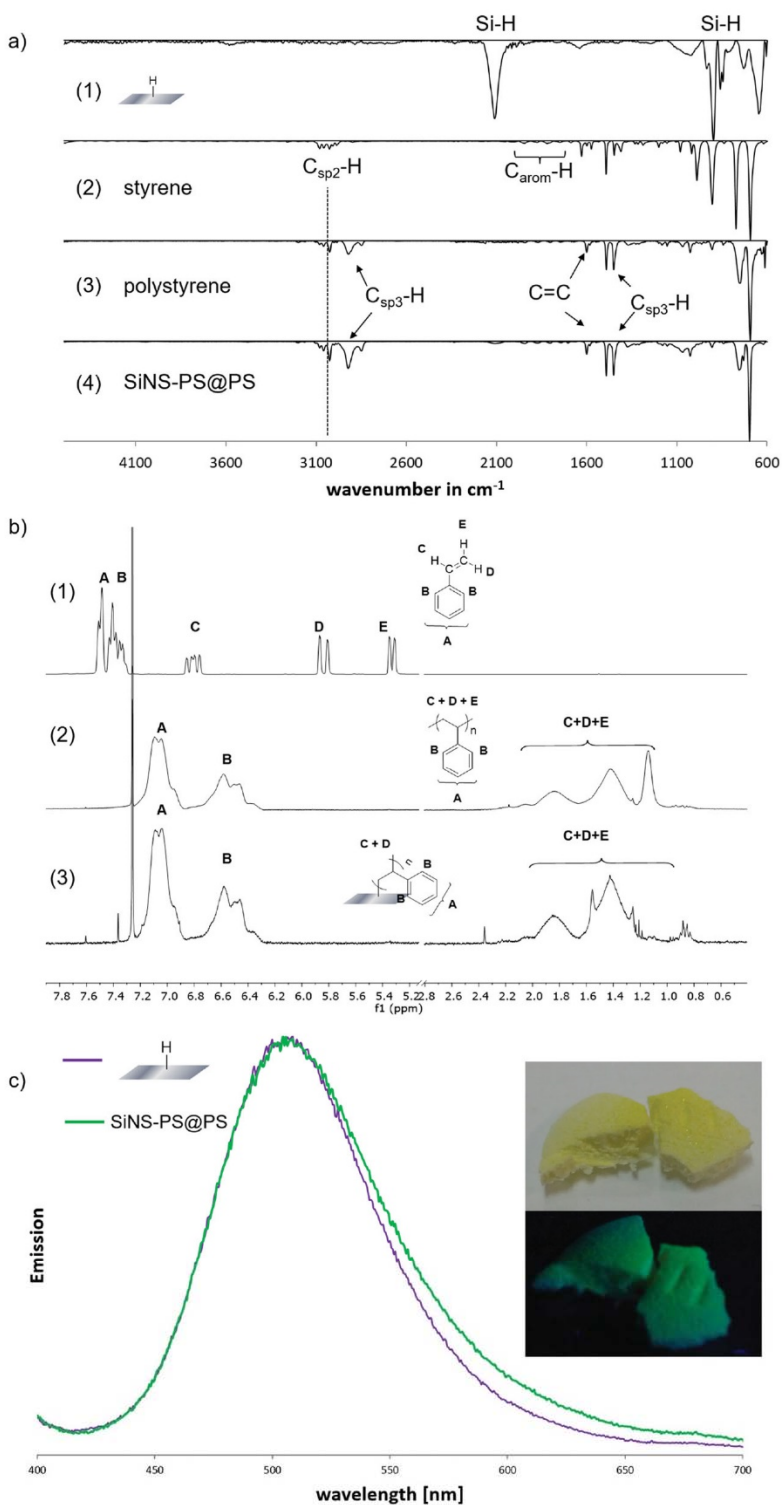


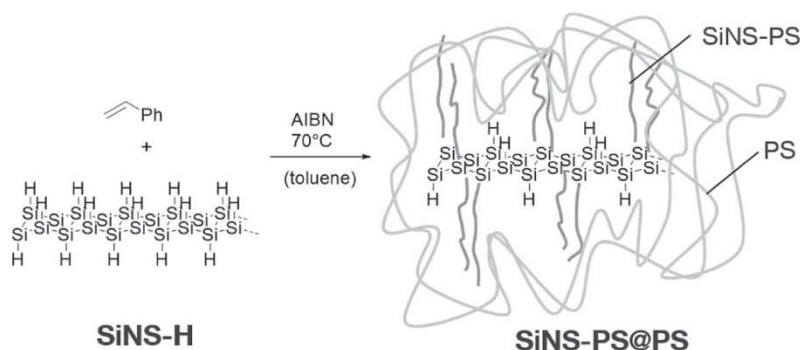
**Figure 1.** a) FTIR spectra of freshly etched SiNSs (1), styrene (2), PS (3), and SiNS-PS@PS (4); b) <sup>1</sup>H NMR spectra of styrene (1), PS (2), and SiNS-PS@PS (3); c) pictures of freeze-dried SiNSs-PS@PS under normal light (top) and under UV light (bottom) and the respective normalized PL spectra of the material and hydride-terminated SiNS dispersed in toluene.

hydride-terminated SiNSs, we used a different workup procedure to remove the excess polymer and thus examine the SiNSs in the absence of the surrounding matrix. This approach allowed us to determine whether the nanocomposite is merely a blend of the unfunctionalized SiNSs in the polymer matrix or if surface functionalization occurs simultaneously in one reaction step. Thus, instead of precipitation, the reaction mixture was diluted, centrifuged, and subsequently washed with a suitable polymer-dissolving solvent.

We performed GPC measurements to demonstrate the successful separation of the polymer matrix from the functionalized SiNSs. The polymer, synthesized under the same conditions in the absence of SiNSs (e.g., PS), the nanocomposite (e.g., SiNS-PS@PS), and the functionalized SiNSs (e.g., SiNS-PS) were dispersed in the appropriate solvent, allowed to dissolve overnight, filtered, and then analyzed by GPC. The dispersion of the hybrid materials (SiNS-PS and SiNS-PS@PS) exhibited the expected PL emission<sup>[27]</sup> at  $\approx 510$  nm and the characteristic yellow color of the SiNSs (Figure 2). After filtration, the clear, colorless filtrate no longer exhibited these properties. This result and the absence of any silicon signal in the EDX spectra of the filtrate after the removal of the solvent demonstrate the successful separation of the SiNSs. Because of their high surface area, the nanosheets tend to agglomerate in concentrated dispersions and can thus be separated via filtration (pore size 0.20  $\mu\text{m}$ ).

Whereas the GPC chromatogram of the filtrate of the nanocomposite SiNS-PS@PS dispersion still shows free polymer, no such signal was detected in the chromatogram of the SiNS-PS filtrate (Figure 2; for PMMA- and PAA-based systems, see Figures S16 and S17, Supporting Information). These results demonstrate that the polymer matrix can be separated from the SiNSs via washing with the appropriate solvent.

After removal of the polymer matrix, the remaining SiNSs were analyzed. FTIR (Figure 3) and NMR (Figures S9–S11, Supporting Information) spectra of the SiNSs indicate successful functionalization. The expected FTIR bands, such as C<sub>sp3</sub>-H ( $\approx 2900$   $\text{cm}^{-1}$ ), C=C ( $\approx 1640$   $\text{cm}^{-1}$ ), C-O ( $\approx 1150$   $\text{cm}^{-1}$ ), and C=O ( $\approx 1700$   $\text{cm}^{-1}$ ) arise from the organic functionalization, whereas the absence of C<sub>sp</sub>-H ( $\approx 3300$   $\text{cm}^{-1}$ ) and C<sub>sp2</sub>-H ( $\approx 3100$   $\text{cm}^{-1}$ ) bands demonstrates the removal of the excess substrate. In addition, 1-dodecene and 1-dodecyne were used as model substrates for the functionalization with AIBN because unsaturated substrates with long alkyl chains do not



**Scheme 2.** Radical polymerization of styrene in the presence of hydride-terminated SiNSs led to the SiNS-PS@PS nanocomposite. The hydrosilylation of the hydride-terminated nanosheets (SiNS-H) led to styrene-functionalized SiNSs (SiNS-PS). Simultaneously, the PS matrix is formed radically.

polymerize as efficiently as styrene and other small molecules. The use of such model substrates enables easier removal of the excess non-reacted alkene or potentially formed small oligomers. Here no polymer matrix is formed during the reaction. Also, in this case, FTIR (Figure 3) and NMR spectra (Figures S12 and S13, Supporting Information) show the successful functionalization, demonstrating that AIBN can indeed be used to initiate surface hydrosilylation reactions on SiNSs with alkenes and alkynes.

The same reactivity toward AIBN has been observed for silicon nanocrystals (SiNCs).<sup>[37]</sup> Because SiNSs in many ways behave differently from seemingly comparable materials (e.g., bulk silicon, silanes, SiNCs),<sup>[27]</sup> confirming the feasibility of functionalizing SiNSs with AIBN was critical in this study.

The GPC measurements, in combination with the NMR and FTIR results, confirm the covalent character of the nanocomposite.

#### 2.4. Characterization of the Functionalized Silicon Nanosheets

In addition to analyzing the differently functionalized SiNSs by FTIR (Figure 3) and NMR (Figures S9–S13, Supporting Information), we further analyzed them by TGA (Figure S18, Supporting Information). The measurements show that more molecules of the small polymerizable substrates styrene, acrylic acid, and methyl methacrylic acid are attached on the surface than are molecules of the long-chain dodecene/dodecyne, indicating a preferred grafting mechanism from the surface.

Atomic force microscopy (AFM) measurements of 1-dodecene-functionalized SiNSs demonstrate that AIBN-induced functionalization leads to freestanding monolayers with a thickness of  $\approx 4.0$  nm (Figure 4).

Neither the polymer matrix nor the functionalization of the SiNSs substantially alters the emission maxima of the SiNSs in the nanocomposites significantly, as evident from PL spectra of the nonfunctionalized and functionalized SiNSs (Figures S14 and S15, Supporting Information).

#### 2.5. Properties of the Nanocomposite: Processing and Stability

To demonstrate the feasibility of standard processing techniques, we subsequently compounded the synthesized

#### Polystyrene (PS)

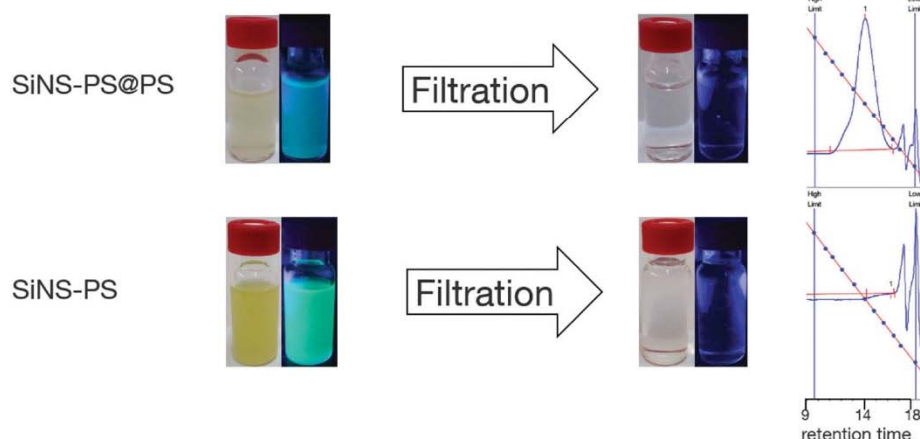


**Figure 2.** Pictures of the dispersions of the hybrid material SiNS-PS@PS in THF before and after filtration under normal (left) and UV light (right) and the corresponding GPC results.

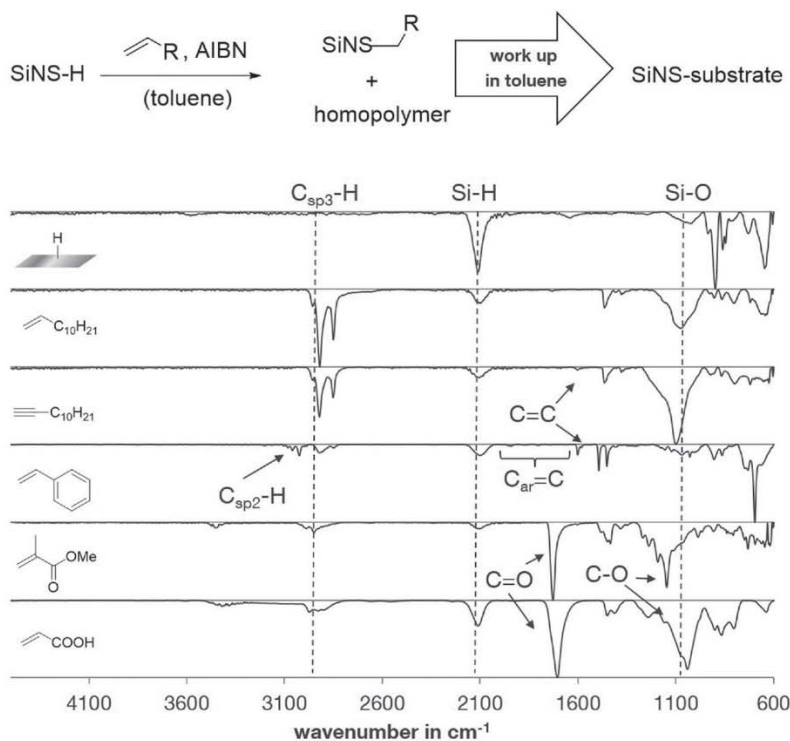


**Figure 3.** FTIR spectra of functionalized SiNSs (corresponding substrates listed on the left) synthesized via radical-induced hydrosilylation with AIBN and subsequent separation of the polymer matrix.

nanocomposite SiNS-PS@PS at 220 °C. The processing conditions maintained the properties of the SiNSs, and the excess of the dense polymer matrix embedded the SiNSs.

Silicon-based nanomaterials, including SiNSs, are sensitive to basic conditions.<sup>[1,34]</sup> When bases were added to dispersions of the nonfunctionalized and functionalized SiNSs, they lost their characteristic yellow color as the SiNSs dissolved. In contrast to this behavior, the dense polymer matrix of the compounded nanocomposite was observed to shield the SiNSs from

10 wt% NaOH (aq) for several days, maintaining the PL properties of the nanomaterial (Figure S19, Supporting Information).

The functionalization of bulk silicon and SiNCs via radical-induced hydrosilylation can also be initiated by UV light<sup>[38]</sup> because Si–H bonds (318 kJ mol<sup>-1</sup>) are known to be homolytically cleaved by UV light (365 nm: 328 kJ mol<sup>-1</sup>). As the bond enthalpy of Si–Si bonds (222 kJ mol<sup>-1</sup>) is smaller than that of Si–H bonds, UV light can also cleave these bonds. For other silicon-based materials (e.g., SiNC, wafers, etc.), the cleavage of the surface Si–Si bonds does not induce a substantial effect because of the fixation of the surface Si radicals by the 3D Si network. In the case of SiNSs, no such stabilization is possible because of their monolayered structure, leading to decomposition of the SiNSs (Scheme 3).

To examine the influence of UV light on SiNSs, we attempted to functionalize hydride-terminated SiNSs with 1-dodecene as a model substrate. After being degassed, the dispersion was irradiated with UV light. During the reaction, the mixture lost its characteristic yellow color and turned clear. After the workup, we observed functionalized silicon-based materials; however, the 2D character of the SiNSs, and with it the PL properties were destroyed (Figures S20 and S21, Supporting Information). This instability of SiNSs against UV light has not been reported before, but is in accordance with their molecular counterparts, polysilanes,<sup>[39]</sup> which also do not possess a stabilizing 3D network and can be decomposed by Si–Si bond cleavage.

To examine the decomposition process further, we irradiated nonfunctionalized and functionalized SiNS (SiNS-PS and SiNS–C<sub>12</sub>H<sub>25</sub>) dispersions with UV light and analyzed the resulting materials (Figure 5a,b). The FTIR spectra of the

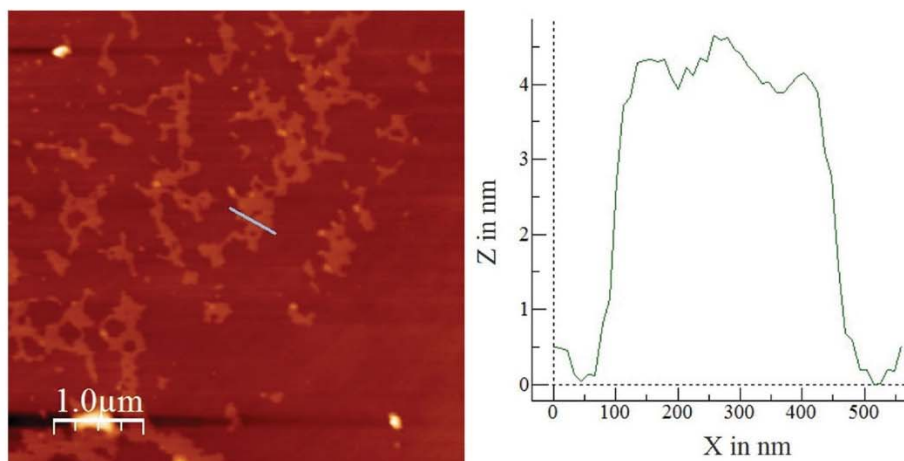
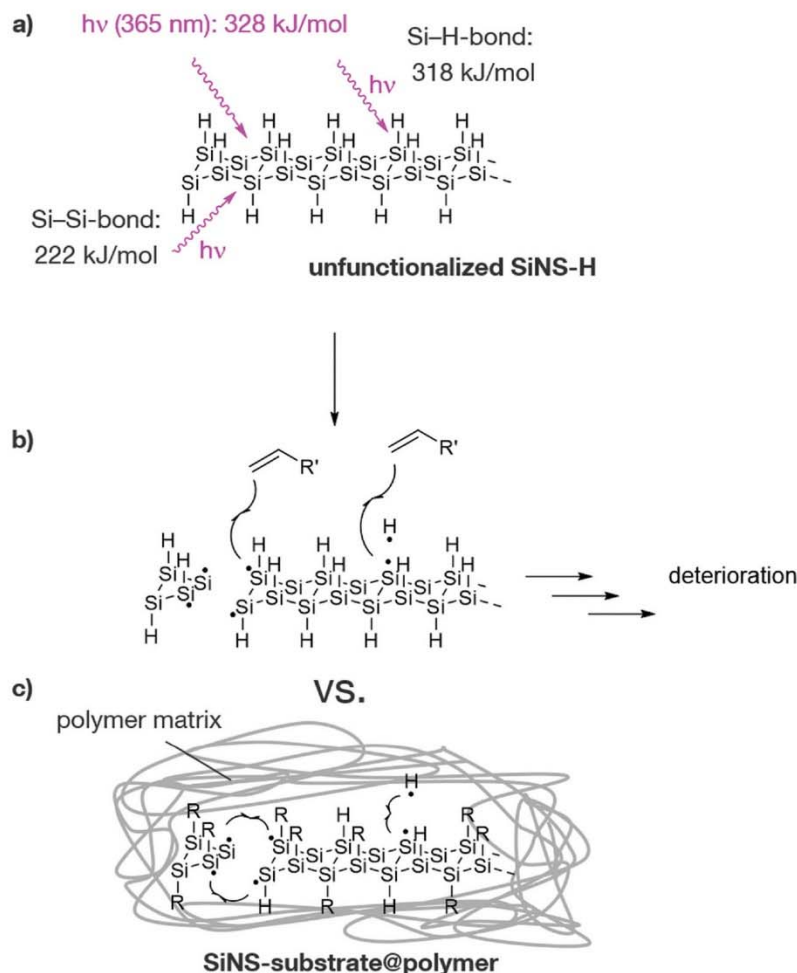


**Figure 4.** Non-contact mode AFM image (5 × 5 μm<sup>2</sup>) of the functionalized SiNSs (left) and the corresponding line profile (right).



**Scheme 3.** a) Schematic of the irradiation of SiNSs with UV light during functionalization. b) The cleavage of the Si-Si bonds leads to decomposition of the SiNSs. c) The fixation of the layered polysilanes within a polymer matrix favors the recombination of the Si radicals.

products demonstrate that, after irradiation, the nonfunctionalized SiNSs are activated and easily oxidized (Si-O band  $\approx 1100\text{ cm}^{-1}$ ) during workup. The C-H ( $\approx 2900\text{ cm}^{-1}$ ) bands of the irradiated, functionalized SiNSs are present in the spectra collected both before and after irradiation and indicate that the functionalization of the deteriorated material is still in place. In addition, stronger Si-O bands arise after irradiation and subsequent workup. These results are consistent with the proposed decomposition via Si-Si cleavage. Nonfunctionalized as well as functionalized SiNSs lose their unique 2D structure and their optoelectronic properties after irradiation.

The compounded nanocomposite exhibits much stronger stability against UV irradiation than the material without the polymer matrix. As such, instead of remaining intact for minutes, the PL properties are still intact after several hours (Figure 5c), demonstrating the stabilization of the SiNSs within the polymer matrix. This enhanced stability might arise from the combination of three different effects. On the one hand, the polymer matrix partially absorbs UV light and prevents the diffusion of the diradical oxygen to the SiNSs. At the same

time, the fixation of the SiNSs within the tight matrix should favor the recombination of the Si-radicals formed by irradiation relative to the reaction with other molecules (Scheme 3c). As a result, the nanocomposite exhibits a substantial improvement in stability against the aforementioned discussed factors, increasing the lifetime of the embedded nanosheets. This stabilization opens the possibility of this new nanomaterial being used in various applications.

### 3. Conclusion

In summary, we reported a straightforward method for the synthesis of a SiNS-based nanocomposite in a single reaction step. The method is applicable to radically polymerizable monomers with different functionalities. The obtained hybrid material exhibits the properties of both the layered polysilanes and the matrix and can be processed via well-established methods such as compounding. In addition, on the basis of the combination of different workup procedures and analytical methods, we demonstrated that the synthesis led to a nanocomposite in which the inorganic nanomaterial was covalently functionalized and stabilized with organic molecules. Thus, AIBN can not only be used for the synthesis of the covalent nanocomposite but also for the preparation of functionalized SiNSs without a polymer matrix. The successful functionalization of the nanomaterial was confirmed by TGA, AFM, and PL-, FTIR-, and NMR spectroscopy.

Furthermore, we demonstrated that SiNSs are unstable against UV light because of their monolayered structure. Irradiation most likely leads to cleavage of Si-Si bonds and, in turn, to the decomposition of the layered polysilanes. The processed nanocomposite SiNS-substrate@polymer, in contrast, leads to improved stabilities not only against UV light but also against other external influences such as basic conditions, paving the way for the implementation of SiNSs in various applications.

### 4. Experimental Section

**General Information:** The reagents were purchased from Sigma-Aldrich, Wacker, and Alfa Aesar; unless stated otherwise, they were used without further purification. Styrene, MMA, and AA were distilled under reduced pressure and stored under argon at  $7\text{ }^{\circ}\text{C}$ . AIBN was recrystallized from methanol. Prior to use, toluene was dried with an MBraun MB SPS-800 solvent purification system; argon 5.0 (99.9990%, Westfalen AG) was used as the inert gas. Acetone was distilled, dried over molecular sieves, degassed, and stored under argon. The exfoliated SiNSs were stored under argon 4.8 (99.998%, Westfalen AG) in a LABmaster 130 (MBraun) glove box. Air- or water-sensitive reactions were executed using standard Schlenk techniques.

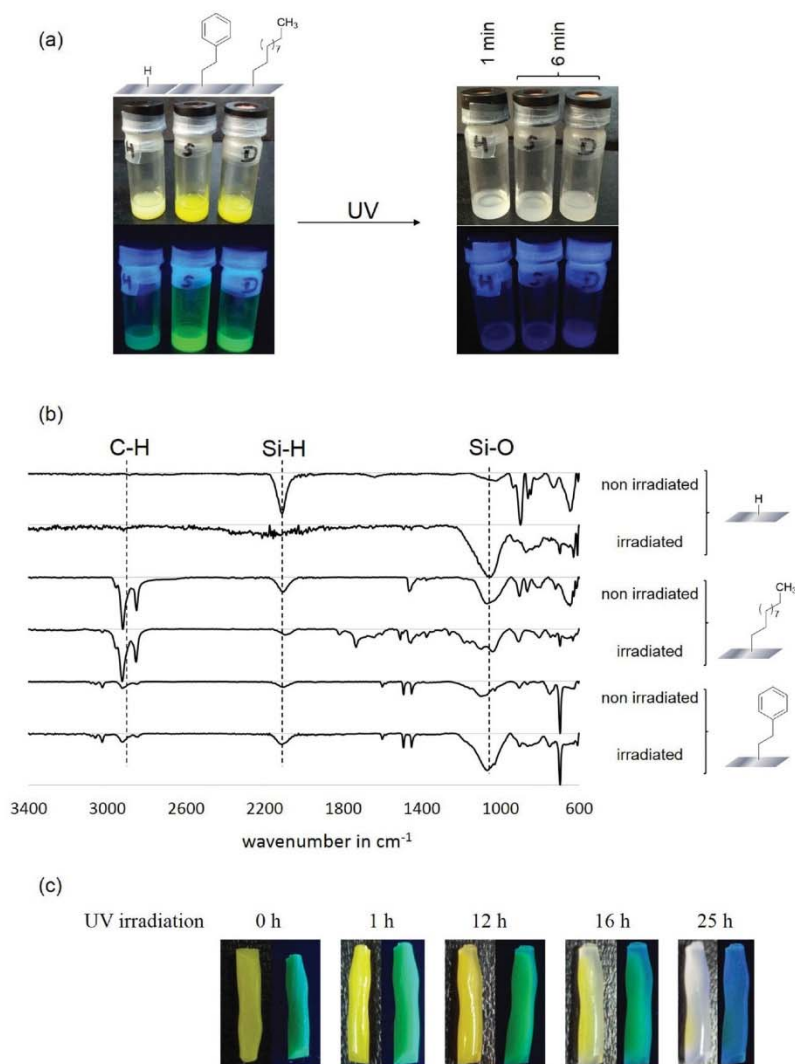


**Figure 5.** a) Irradiation of nonfunctionalized and functionalized SiNS dispersions leads to the decomposition of the SiNSs and to the loss of their PL properties within minutes; b) FTIR spectra of the material before and after irradiation; c) when irradiated with UV light for the given time, the SiNS-based nanocomposite shows high stability, as evident in the pictures. After the given irradiation time, it still exhibits its characteristic yellow color (left: picture under daylight) and the PL properties of the SiNSs (right: picture under UV light).

**NMR:** For NMR measurements, the functionalized SiNSs were freeze-dried from benzene or water. The spectra were collected at 300 K on a Bruker ARX-300. The chemical shifts ( $\delta$ ) are given in ppm and are calibrated to the rest proton signal of the deuterated solvent.

**FTIR:** FTIR spectra were measured with a Bruker Vertex 70 FTIR using a platinum attenuated total reflectance (ATR) apparatus from Bruker.

**PL:** PL spectra were collected with an AVA-Spec 2048 from Avantes using a Prizmatrix (LED current controller) as a light source in toluene or ethanol.

**TGA:** TGA measurements of the freeze-dried samples were conducted under argon 4.8 (99.998%, Westfalen AG) on a Netzsch TG 209 F 1 Libra with heating rates of  $10 \text{ K min}^{-1}$  and argon flow rates of  $20 \text{ mL min}^{-1}$ . TGA measurements under air were performed in a Mettler Toledo Star system with a heating rate of  $10 \text{ K min}^{-1}$ .

**DSC:** DSC measurements were performed on a TA instruments Q2000 DSC with a heating rate of  $10 \text{ K min}^{-1}$  and a constant helium flow of  $50 \text{ mL min}^{-1}$ .

**GPC:** GPC measurements were performed at  $30 \text{ }^\circ\text{C}$  on a Varian PL-GPC 50 Plus; a constant flow rate of  $1 \text{ mL min}^{-1}$  with THF with  $6 \text{ g L}^{-1}$  tetrabutylammonium bromide (TBAB) for PS and PMMA were used. In the case of PAA, a Varian LC-920 equipped with two PL Polargel columns was used, and the eluent was  $0.05 \text{ M NaN}_3$  (aq).

**AFM:** For AFM measurements (contact mode, Asylum Research MFP-3D AFM with an ARC controller), thin films of SiNS- $\text{C}_{12}\text{H}_{25}$  (15 mg of exfoliated sheets in 2 mL of toluene) were spin-coated (90 s, 1000 rpm) onto polished Si/SiO<sub>2</sub> substrates.

**Powder X-Ray Diffraction (PXRD):** Powder X-ray diffraction patterns were recorded using a Stoe STADI P diffractometer equipped with a Ge(111) monochromator, a Cu K $\alpha$  radiation source ( $\lambda = 1.54056 \text{ \AA}$ ), and a Dectris MYTHEN DCS 1K solid-state detector. Samples were ground in an agate mortar and filled into 0.5 mm glass capillaries, which were then sealed. The samples were measured over the  $2\theta$  range from  $5^\circ$  to  $89^\circ$  (position sensitive detector (PSD) steps,  $0.075^\circ$ ; time/step, 41 s).

**Compounding:** Compounding of the nanocomposites was performed in a MicroCompounder (DACA Instruments) by mixing at 100 rpm and at  $220 \text{ }^\circ\text{C}$  under a nitrogen atmosphere.

**IPL:** IPL sintering with a Sinteron 2010 (xenon 4.2, ozone-free, Germacil, USA) was performed for a silicon wafer spin-coated (1500 rpm, 90 s) with SiNS- $\text{C}_{12}\text{H}_{25}$  (in 1,2-dichlorobenzene). The sintering was performed with 30 pulses at 2.5 kV and a period of 3 s; the pulse lengths were 2 ms.

**Raman Spectroscopy:** Samples for Raman spectroscopy were sealed in 0.5 mm glass capillaries. Measurements were performed at 10 mW laser power and  $5 \times 30 \text{ s}$  exposure time using a Senterra Raman spectrometer (Bruker) equipped with a laser diode ( $\lambda = 785 \text{ nm}$ ), an objective lens for 50-fold magnification and a 1200 $\alpha$  grid.

**Synthesis of  $\text{CaSi}_2$ :** According to a known procedure reported in the literature,<sup>[27]</sup> calcium (Alfa Aesar, 99.5%) and silicon (Wacker, 99.99%) in stoichiometric amounts were melted together in an arc furnace inside an argon-filled glove box. Phase-pure  $\text{CaSi}_2$  was obtained, as demonstrated by PXRD (Figure S1, Supporting Information).

**Synthesis of SiNSs via Chemical Exfoliation:** 1.00 g of  $\text{CaSi}_2$  was added to a Schlenk flask containing 100 mL HCl (conc.) at  $-25 \text{ }^\circ\text{C}$  under argon. After stirring for 5 d at  $-25 \text{ }^\circ\text{C}$ , the reaction mixture was filtered; the yellow exfoliated  $(\text{Si}_6\text{H}_6)_n$  was washed with dry, degassed acetone under an argon atmosphere, dried under vacuum, and stored in a glove box until further use.<sup>[27]</sup>

**Etching of SiNSs:** 88.0 mg of the exfoliated  $(\text{Si}_6\text{H}_6)_n$  sheets were dispersed in 2 mL of ethanol and ultrasonicated for 3 min. 2 mL of water and 0.25 mL of HF (48%) were added; the suspension was mixed, immediately extracted with  $6 \times 5 \text{ mL}$  dichloromethane, and transferred into polytetrafluoroethylene centrifuge tubes. The dispersion was then mixed with 60 mL of toluene, and the SiNSs were isolated by centrifugation (9000 rpm/2 min). After removal of the centrifugate, the yellow residue was redispersed in 0.5 mL of dry, degassed acetone. After centrifugation, the SiNSs were redispersed in 12 mL of the appropriate solvent and transferred into a dry Schlenk tube under argon.

**AIBN-Based Radical-Induced Functionalization and Polymerization:** In the Schlenk tube, 12 mL of the dispersion of hydride-terminated SiNSs (corresponds to 88 mg exfoliated  $(\text{Si}_6\text{H}_6)_n$ ) in dry, degassed toluene (or ethanol for acrylic acid) were mixed with 3.30 g (3 wt% of exfoliated  $(\text{Si}_6\text{H}_6)_n$ ) monomer. After the mixture was degassed via three freeze–thaw–pump cycles, 20 mg of AIBN was added and the reaction mixture was stirred at 70 °C for 16 h.

**Isolation of SiNS-Substrate@Polymer:** To isolate the SiNS-substrate@polymer nanocomposites, the reaction mixture was precipitated from methanol (or toluene for PAA) and centrifuged (9000 rpm for 2 min). To remove residual monomer, the hybrid material was twice redispersed, precipitated, and isolated by freeze drying from benzene (or water for SiNS-PAA@PAA).

**Isolation of Functionalized SiNSs (SiNS-Substrate):** To isolate the functionalized material SiNS-substrate and to remove the free homopolymer, the reaction mixture was diluted and subsequently centrifuged (9000 rpm/2 min), 3× redispersed in 0.5 mL of the reaction solvent, centrifuged, and at last freeze-dried from benzene (or water for SiNS-PAA).

**AIBN-Based Radical Induced Functionalization with Non-Polymerizable Substrates:** In the Schlenk tube, 2 mL of the dispersion of hydride-terminated SiNSs (corresponding to 15 mg exfoliated  $(\text{Si}_6\text{H}_6)_n$ ) in dry, degassed toluene were mixed with 3.00 mmol 1-dodecene/1-dodecylene. After the mixture was degassed via three freeze–thaw–pump cycles, 5 mg of AIBN was added, and the reaction mixture was stirred at 70 °C for 16 h. The reaction mixture was then mixed with 4 mL of a methanol/ethanol mixture (1:3) and centrifuged (9000 rpm/2 min). This process was repeated three times before the product was freeze-dried from benzene.

## Supporting Information

Supporting Information is available from the Wiley Online Library or from the author.

## Acknowledgements

The authors thank M. G. M. Knaus for his help with GPC measurements and S. Geier for performing Raman measurements. J. Veinot is thanked for facilitating TGA measurements under air at University of Alberta. The financial support of Alberta/Technische Universität München Graduate School for Functional Hybrid Materials ATUMS (IRTG2022) by Deutsche Forschungsgemeinschaft (DFG) and Natural Science and Engineering Research Council of Canada (NSERC) is greatly appreciated. T.H. and L.M.S. are thankful for their fellowship from Studienstiftung des deutschen Volkes. L.M.S. gratefully acknowledges the funding from Fonds der Chemischen Industrie.

Received: April 28, 2016

Revised: June 22, 2016

Published online: July 28, 2016

- [1] Z. Yang, M. Dasog, A. R. Dobbie, R. Lockwood, Y. Zhi, A. Meldrum, J. G. C. Veinot, *Adv. Funct. Mater.* **2014**, *24*, 1345.
- [2] G. Kickelbick, *Introduction to Hybrid Materials*, Wiley-VCH, Weinheim, Germany **2007**.
- [3] G. Eda, M. Chhowalla, *Nano Lett.* **2009**, *9*, 814.
- [4] G. Eda, H. E. Unalan, N. Rupasinghe, G. A. J. Amaratunga, M. Chhowalla, *Appl. Phys. Lett.* **2008**, *93*, 233502.
- [5] D. R. Paul, L. M. Robeson, *Polymer* **2008**, *49*, 3187.
- [6] S. Stankovich, D. A. Dikin, G. H. B. Dommett, K. M. Kohlhaas, E. J. Zimney, E. A. Stach, R. D. Piner, S. T. Nguyen, R. S. Ruoff, *Nature* **2006**, *442*, 282.

- [7] T. Ramanathan, A. A. Abdala, S. Stankovich, D. A. Dikin, M. Herrera-Alonso, R. D. Piner, D. H. Adamson, H. C. Schniepp, X. Chen, R. S. Ruoff, S. T. Nguyen, I. A. Aksay, R. K. Prud'Homme, L. C. Brinson, *Nat. Nanotechnol.* **2008**, *3*, 327.
- [8] H. Okamoto, Y. Sugiyama, H. Nakano, *Chem. - A Eur. J.* **2011**, *17*, 9864.
- [9] L. B. Drissi, K. Sadki, F. El Yahyaoui, E. H. Saidi, M. Bousmina, O. Fassi-Fehri, *Comput. Mater. Sci.* **2015**, *96*, 165.
- [10] Y. Sugiyama, H. Okamoto, T. Mitsuoka, T. Morikawa, K. Nakanishi, T. Ohta, H. Nakano, *J. Am. Chem. Soc.* **2010**, *132*, 5946.
- [11] H. Nakano, T. Mitsuoka, M. Harada, K. Horibuchi, H. Nozaki, N. Takahashi, T. Nonaka, Y. Seno, H. Nakamura, *Angew. Chem. Int. Ed.* **2006**, *45*, 6303.
- [12] Q. Wu, X. Wang, T. A. Niehaus, R. Zhang, *Phys. Chem. C* **2014**, *118*, 20070.
- [13] F. Zheng, C. Zhang, *Nanoscale Res. Lett.* **2012**, *7*, 422.
- [14] S. Yamanaka, H. Matsu-ura, M. Ishikawa, *Mater. Res. Bull.* **1996**, *31*, 307.
- [15] F. Li, R. Lu, Q. Yao, E. Kan, Y. Liu, H. Wu, Y. Yuan, C. Xiao, K. Deng, *J. Phys. Chem. C* **2013**, *117*, 13283.
- [16] Z. Ni, H. Zhong, X. Jiang, R. Quhe, G. Luo, Y. Wang, M. Ye, J. Yang, J. Shi, J. Lu, *Nanoscale* **2014**, *6*, 7609.
- [17] M. Niu, D. Cheng, D. Cao, *Sci. Rep.* **2014**, *4*, 4810.
- [18] T. H. Osborn, A. a. Farajian, O. V. Pupyshcheva, R. S. Aga, L. C. L. Y. Voon, *Chem. Phys. Lett.* **2011**, *511*, 101.
- [19] N. Gao, W. T. Zheng, Q. Jiang, *Phys. Chem. Chem. Phys.* **2012**, *14*, 257.
- [20] Y. Ding, Y. Wang, *Appl. Phys. Lett.* **2012**, *100*, 083102.
- [21] O. D. Restrepo, R. Mishra, J. E. Goldberger, W. Windl, *J. Appl. Phys.* **2014**, *115*, 033711.
- [22] K. J. Koski, Y. Cui, *ACS Nano* **2013**, *7*, 3739.
- [23] Y. Kumai, S. Shirai, E. Sudo, J. Seki, H. Okamoto, Y. Sugiyama, H. Nakano, *J. Power Sources* **2011**, *196*, 1503.
- [24] Y. Kumai, H. Kadoura, E. Sudo, M. Iwaki, H. Okamoto, Y. Sugiyama, H. Nakano, *J. Mater. Chem.* **2011**, *21*, 11941.
- [25] Y. Kumai, H. Nakano, *Jpn. J. Appl. Phys.* **2015**, *54*, 035201.
- [26] C. K. Chan, H. Peng, G. Liu, K. McIlwrath, X. F. Zhang, R. a. Huggins, Y. Cui, *Nat. Nanotechnol.* **2008**, *3*, 31.
- [27] T. Helbich, A. Lyuleeva, I. M. D. Höhle, L. Scherf, J. Kehrle, T. F. Fässler, P. Lugli, **2016**, *22*, 6194.
- [28] M. Dasog, J. Kehrle, B. Rieger, J. G. C. Veinot, *Angew. Chem. Int. Ed.* **2015**, *54*, 2.
- [29] L. Aslanov, I. Kudryavtsev, V. Zakharov, E. Kulatov, Y. Uspenskii, *Solid State Phenom.* **2015**, *233*, 575.
- [30] H. Okamoto, Y. Kumai, Y. Sugiyama, T. Mitsuoka, K. Nakanishi, T. Ohta, H. Nozaki, S. Yamaguchi, S. Shirai, H. Nakano, *J. Am. Chem. Soc.* **2010**, *132*, 2710.
- [31] H. Okamoto, Y. Sugiyama, K. Nakanishi, T. Ohta, T. Mitsuoka, H. Nakano, *Chem. Mater.* **2015**, *27*, 1292.
- [32] H. Nakano, M. Nakano, K. Nakanishi, D. Tanaka, Y. Sugiyama, T. Ikuno, H. Okamoto, T. Ohta, *J. Am. Chem. Soc.* **2012**, *134*, 5452.
- [33] M. J. Sailor, *Porous Silicon in Practice: Preparation, Characterization and Applications*, Wiley-VCH, Weinheim, Germany **2011**.
- [34] I. M. D. Höhle, P. D. L. Werz, J. G. C. Veinot, B. Rieger, *Nanoscale* **2015**, *7*, 7811.
- [35] A. D. Pomogailo, V. N. Kestelman, *Metallopolymer Nanocomposites*, Vol. 53, Springer-Verlag, Berlin **2005**.
- [36] We refer to functionalized SiNSs as SiNS-substrate (e.g., SiNS-PS for polystyrene functionalized SiNSs) and to the polymer nanocomposite as SiNS-substrate@polymer (e.g., SiNS-PS@PS for the polystyrene based nanocomposite) as indicated in Scheme 2.
- [37] Z. Yang, C. M. Gonzalez, T. K. Purkait, M. Iqbal, A. Meldrum, J. G. C. Veinot, *Langmuir* **2015**, *31*, 10540.
- [38] J. M. Buriak, *Chem. Rev.* **2002**, *102*, 1271.
- [39] E. Hengge, *Top. Curr. Chem.* **2005**, *51*, 1.

Copyright WILEY-VCH Verlag GmbH & Co. KGaA, 69469 Weinheim, Germany, 2016.



## Supporting Information

for *Adv. Funct. Mater.*, DOI: 10.1002/adfm.201602137

### One-Step Synthesis of Photoluminescent Covalent Polymeric Nanocomposites from 2D Silicon Nanosheets

*Tobias Helbich, Alina Lyuleeva, Theresa Ludwig, Lavinia M. Scherf, Thomas F. Fässler, Paolo Lugli, and Bernhard Rieger\**

## Supporting Information

### **One-Step Synthesis of Photoluminescent Polymeric Nanocomposites from Two-Dimensional Silicon Nanosheets**

*Tobias Helbich, Alina Lyuleeva, Theresa Ludwig, Lavinia M. Scherf, Thomas F. Fässler, Paolo Lugli and Bernhard Rieger*

#### **Contents**

XRD Spectra .....	2
Raman Spectra .....	3
DSC Measurements of the Nanocomposite .....	4
TGA Measurements of the Nanocomposite .....	4
IR Spectra of Nano Composite SiNS-Substrate@Polymer .....	5
NMR Spectra of Nano Hybrid Materials .....	6
PL Spectra .....	9
GPC Measurements .....	10
TGA Measurements .....	12
NaOH Stability .....	13
UV Stability of SiNSs .....	13

### XRD Spectra

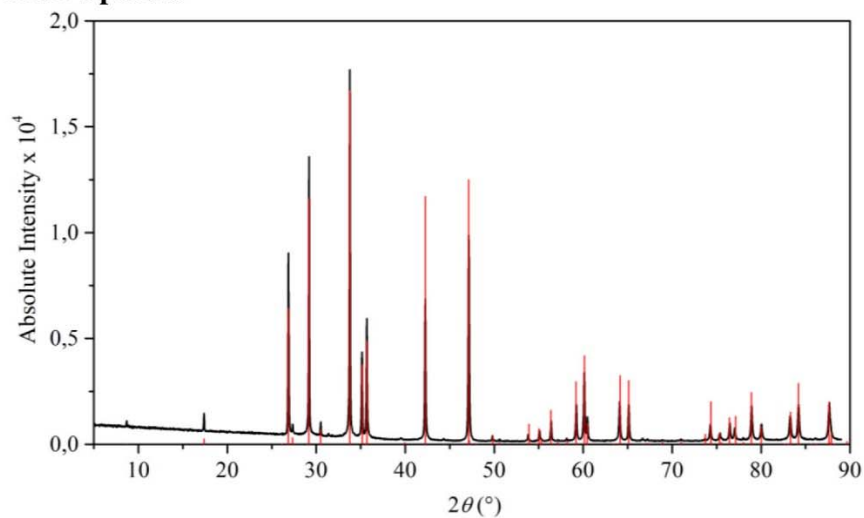


**Figure S1.** Experimental (black) and theoretical (red) powder diffraction patterns of CaSi<sub>2</sub>.

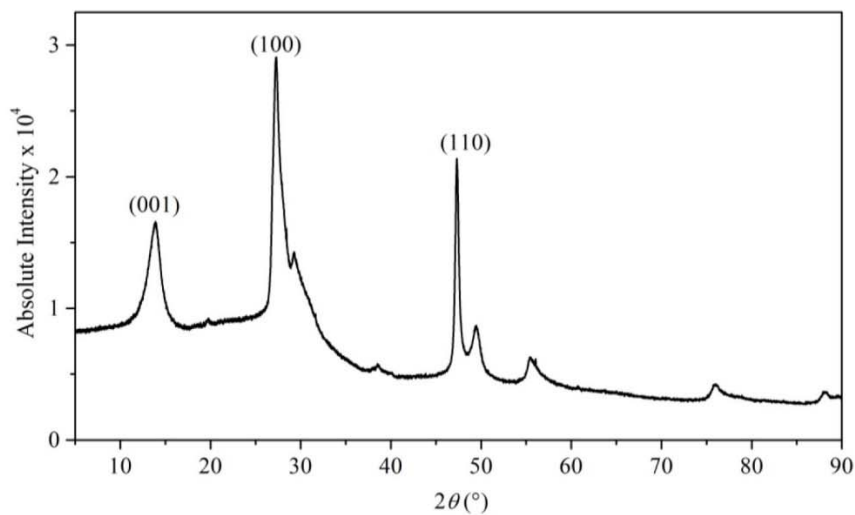


**Figure S2.** Powder diffraction patterns of as-synthesized SiNSs.

## Raman Spectra

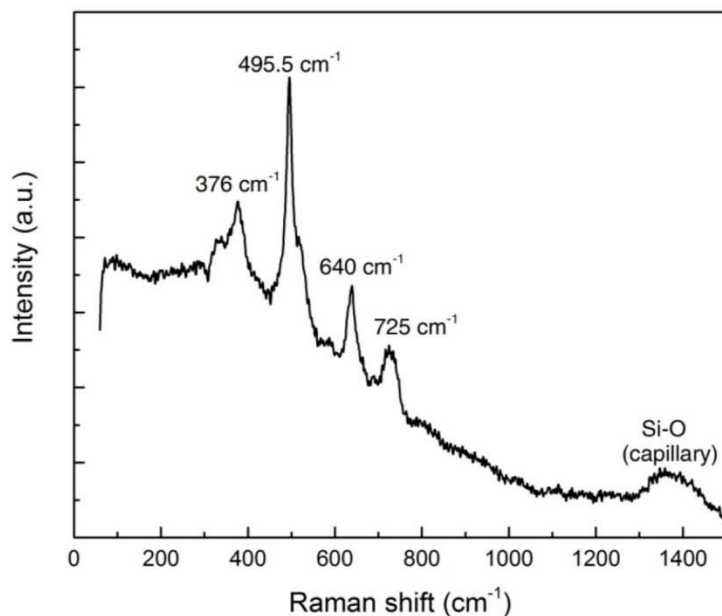


**Figure S3.** Raman spectrum of as-synthesized SiNS-H. The bands at 376 and 495.5  $\text{cm}^{-1}$  are Si-Si modes and the band at 640  $\text{cm}^{-1}$  matches typical Si-H wagging modes.<sup>[1]</sup> We have not yet found an explanation for the band at 725  $\text{cm}^{-1}$ .

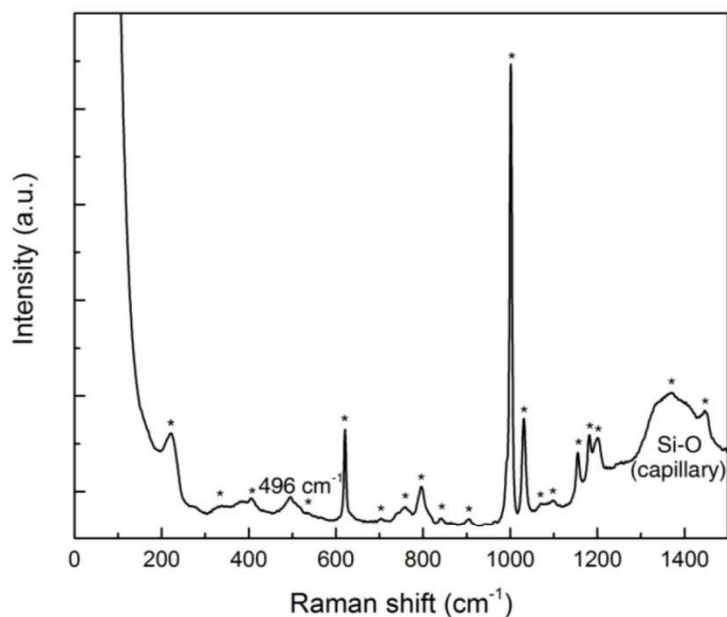


**Figure S4.** Raman spectrum of SiNS-PS@PS (13 wt% SiNS). All bands except for the one at 496  $\text{cm}^{-1}$  can be clearly assigned to polystyrene.<sup>[2]</sup> The presence of the main Si-Si band at 496  $\text{cm}^{-1}$  additionally proves that SiNS are retained in SiNS-PS@PS.

### DSC Measurements of Nanocomposite

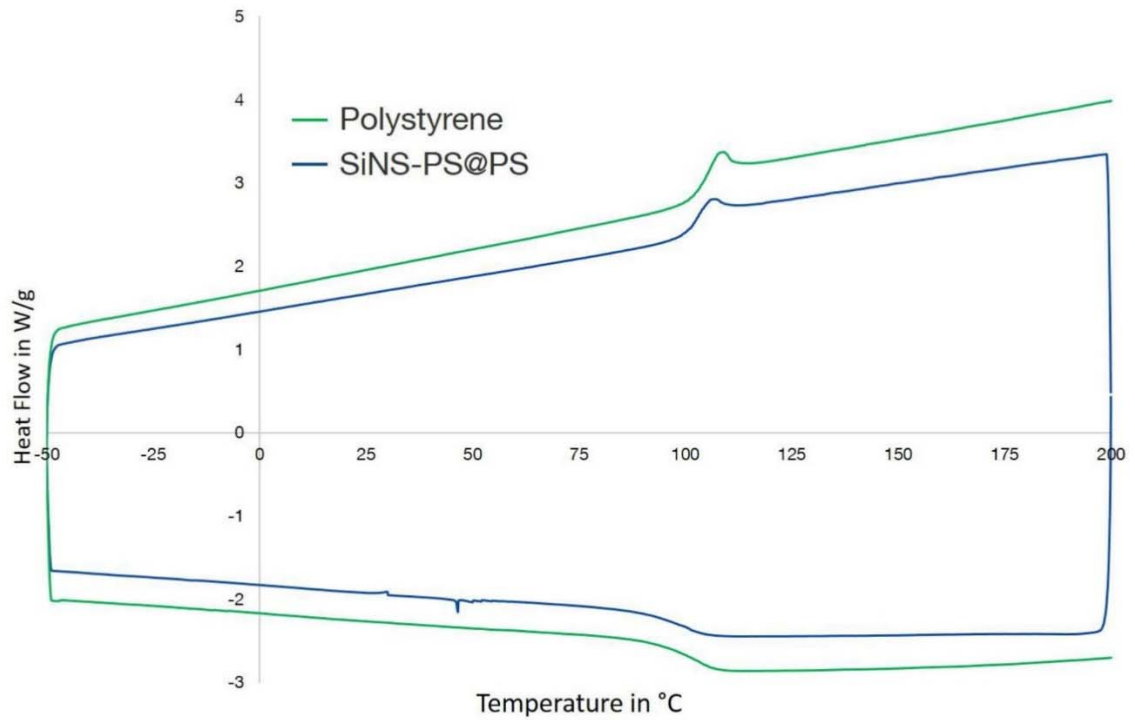


**Figure S5.** DSC measurement of synthesized polystyrene and SiNS-PS@PS nanocomposite show no significant influence of the nanomaterial on the glass transition temperature ( $T_g \sim 104^\circ\text{C}$ ).

### TGA Measurements of Nanocomposite

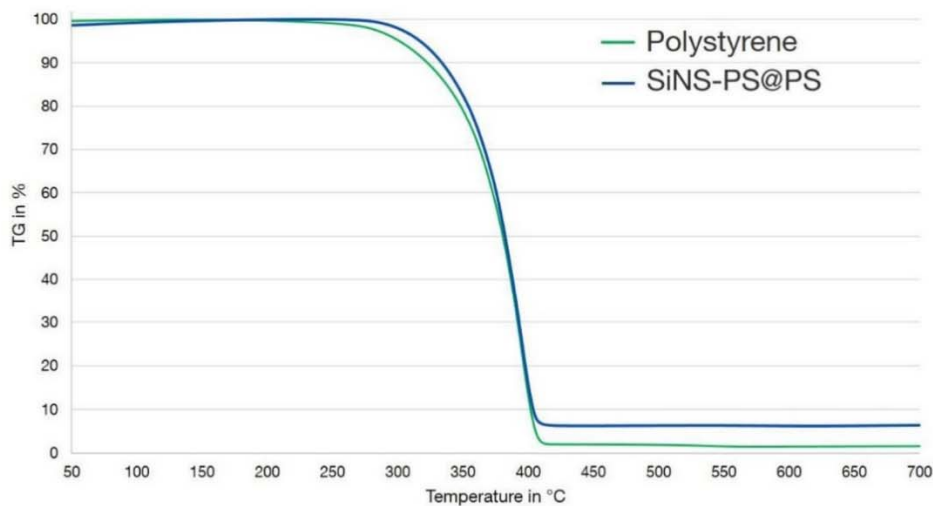


**Figure S6.** TGA measurement of polystyrene as well as SiNS-PS@PS nanocomposite under air show no significant influence of the nanomaterial on the thermos-oxidative properties of the polymer.

### IR Spectra of Nanocomposite SiNS-Substrate@Polymer

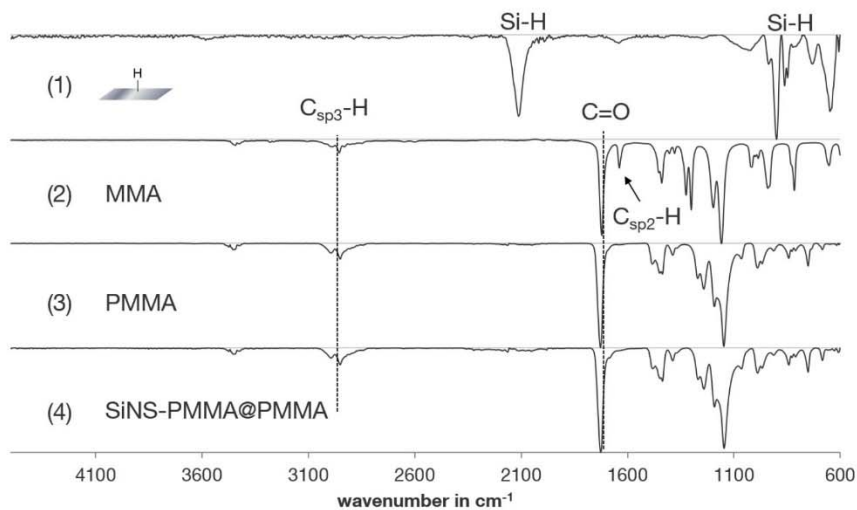


**Figure S7.** FTIR spectra of (1) nonfunctionalized SiNS-H; (2) methyl methacrylate; (3) poly(methyl methacrylate), and (4) nanocomposite SiNS-PMMA@PMMA.

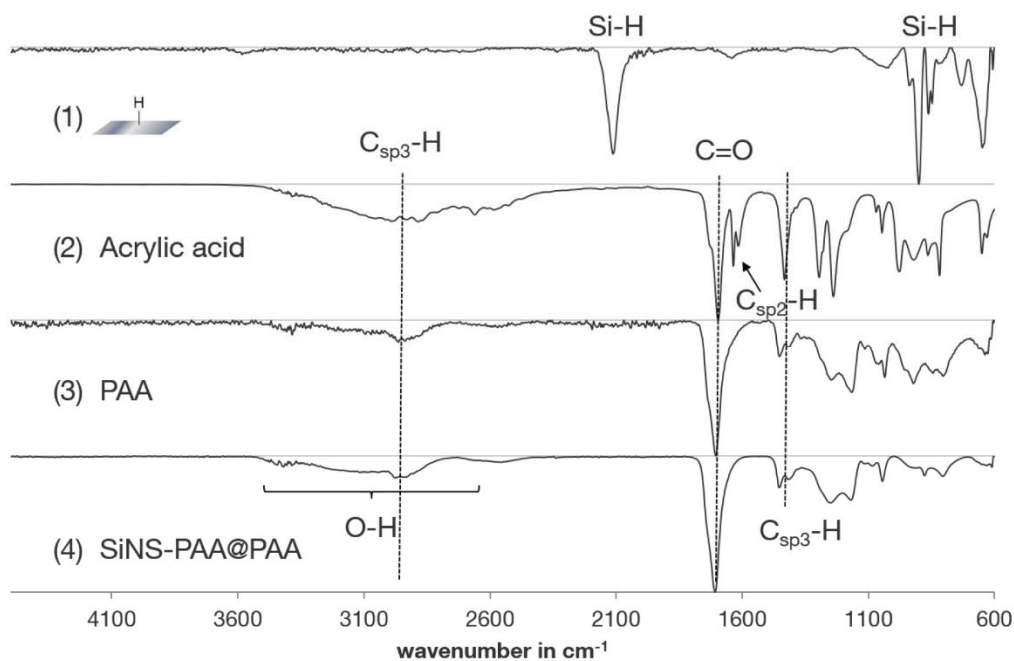


**Figure S8.** FTIR spectra of (1) nonfunctionalized SiNS-H; (2) acrylic acid; (3) poly(acrylic acid); and (4) nanocomposite SiNS-PAA@PAA.

### NMR Spectra of Nano Hybrid Materials

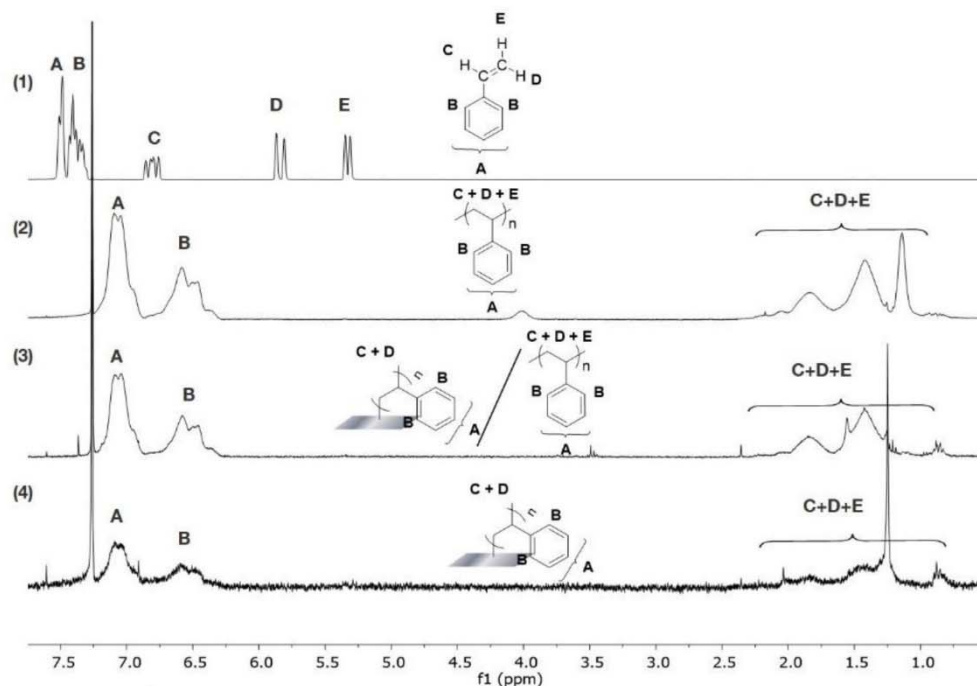


**Figure S9.**  $^1\text{H-NMR}$  spectra of (1) styrene, (2) PS, (3) SiNS-PS@PS, and (4) SiNS-PS in  $\text{CDCl}_3$ .

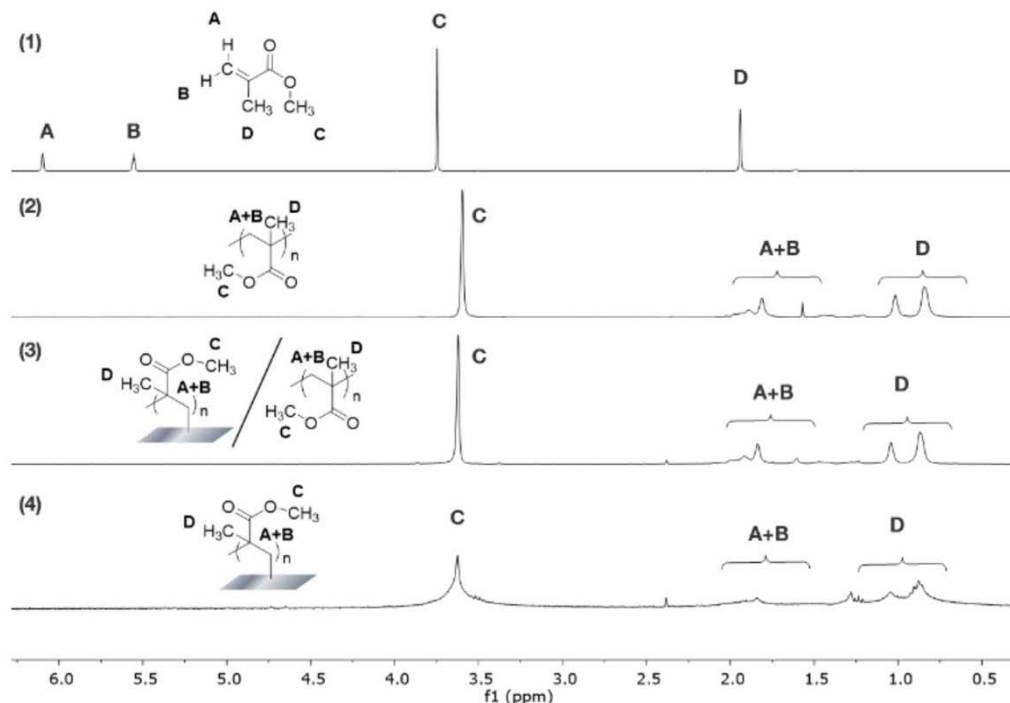


**Figure S10.**  $^1\text{H-NMR}$  spectra of (1) MMA, (2) PMMA, (3) SiNS-PMMA@PMMA and (4) SiNS-PMMA in  $\text{CDCl}_3$ .

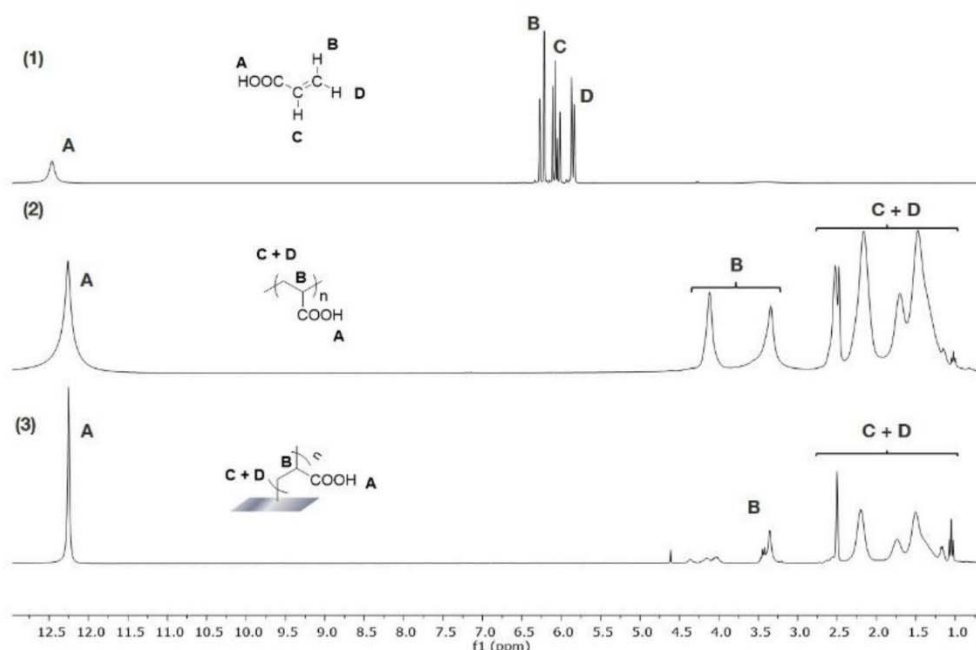


**Figure S11.**  $^1\text{H-NMR}$  spectra of (1) acrylic acid, (2) PAA, and (3) SiNS-PAA@PAA in  $\text{DMSO-d}_6$ .

No useful NMR spectra were obtained from the functionalized SiNS-PAA, possibly because of the small organic content of the functionalized SiNSs (Table S1). In addition, SiNSs were observed to be unstable in DMSO. This instability might arise because of oxidation, as has already been shown for porous silicon.<sup>[3]</sup>

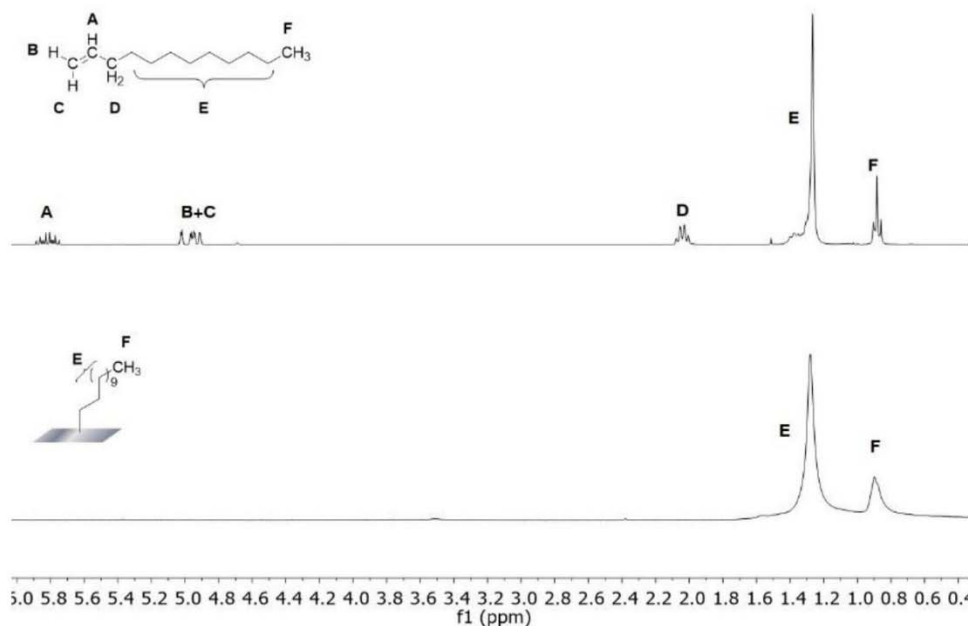


**Figure S12.**  $^1\text{H-NMR}$  spectra of 1-dodecene (top) and SiNS- $\text{C}_{12}\text{H}_{25}$  (bottom) in  $\text{CDCl}_3$ .

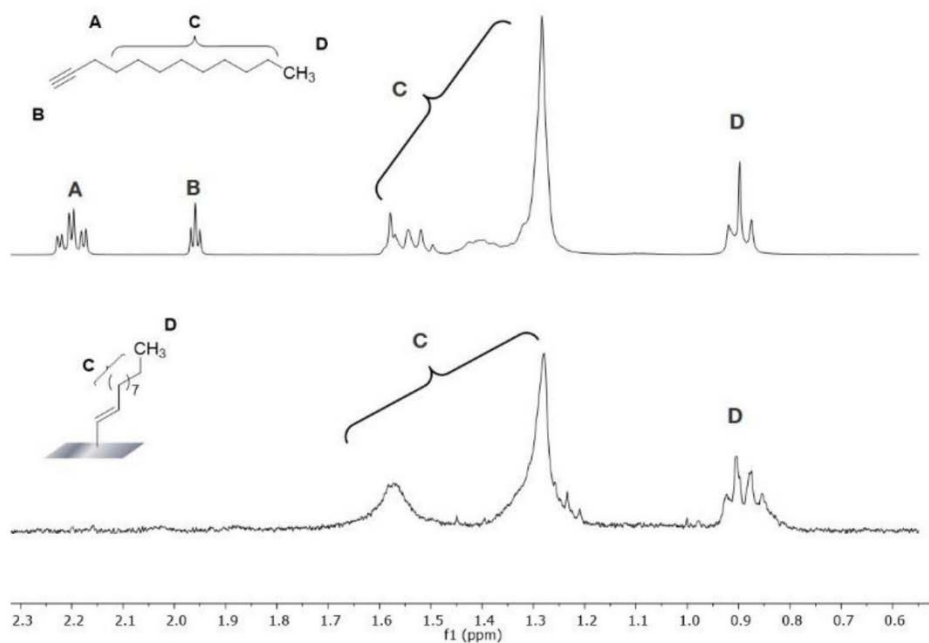


**Figure S13.** <sup>1</sup>H-NMR spectra of 1-dodecyne (top) and SiNS-CHCHC<sub>10</sub>H<sub>21</sub> (bottom) in CDCl<sub>3</sub>.

## PL Spectra

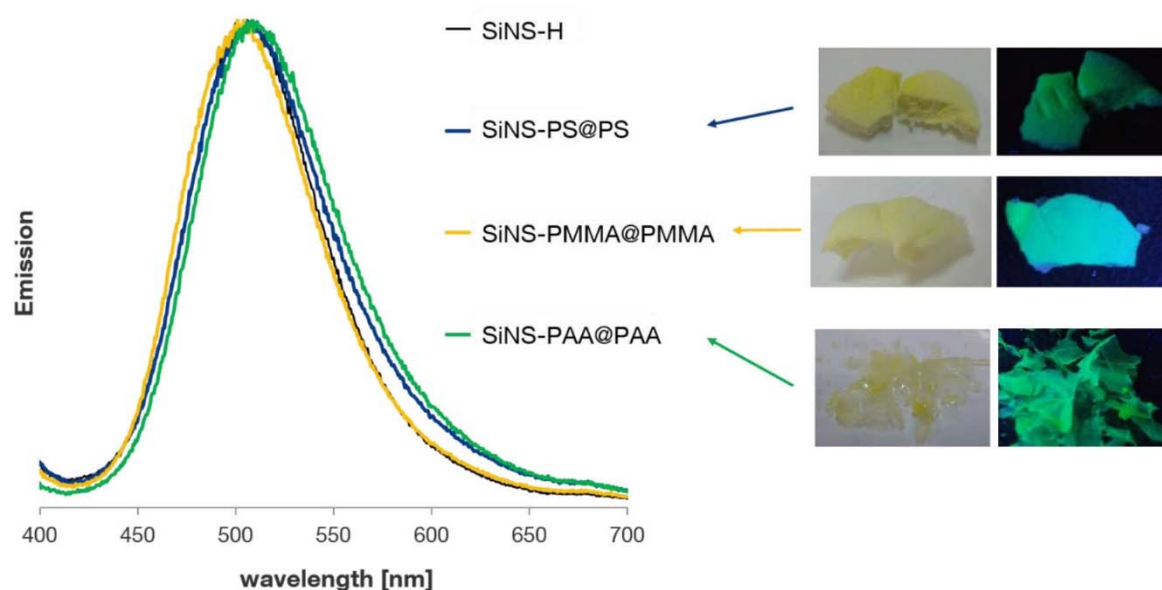


**Figure S14.** Normalized PL spectra of nonfunctionalized dispersions of SiNS-H, SiNS-PS@PS, and SiNS-PMMA@PMMA in toluene and SiNS-PAA@PAA in ethanol; pictures of the freeze-dried nanocomposite under daylight (left) and UV light (right) are included.

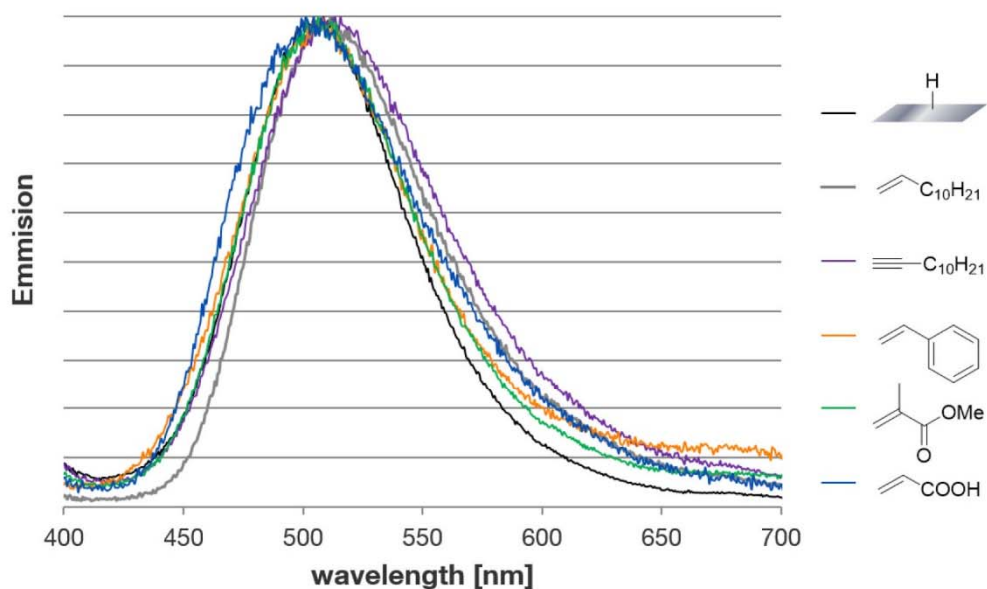


**Figure S15.** PL spectra of the nonfunctionalized SiNS-H and functionalized SiNS-substrate.

## GPC Measurements

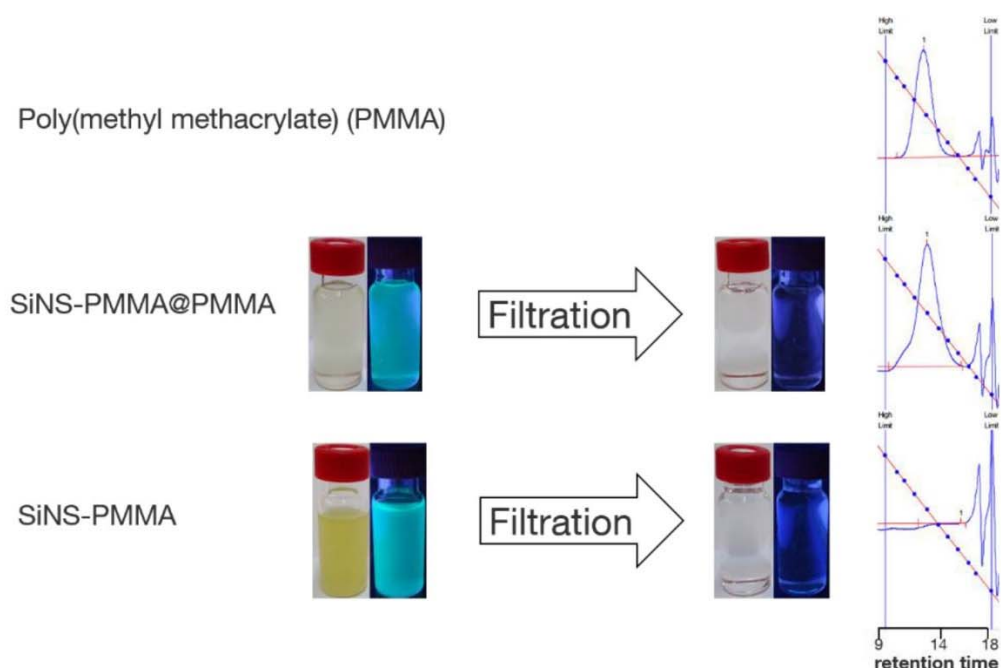


**Figure S16.** Dispersions of the hybrid material in THF under visible (left) and UV light (right) before and after filtration, demonstrating the removal of the silicon nanomaterial. The GPC measurements of the filtrates of SiNS-PMMA@PMMA show an excess of matrix polymer, whereas no free polymer is detected for the merely functionalized SiNSs-PMMA.

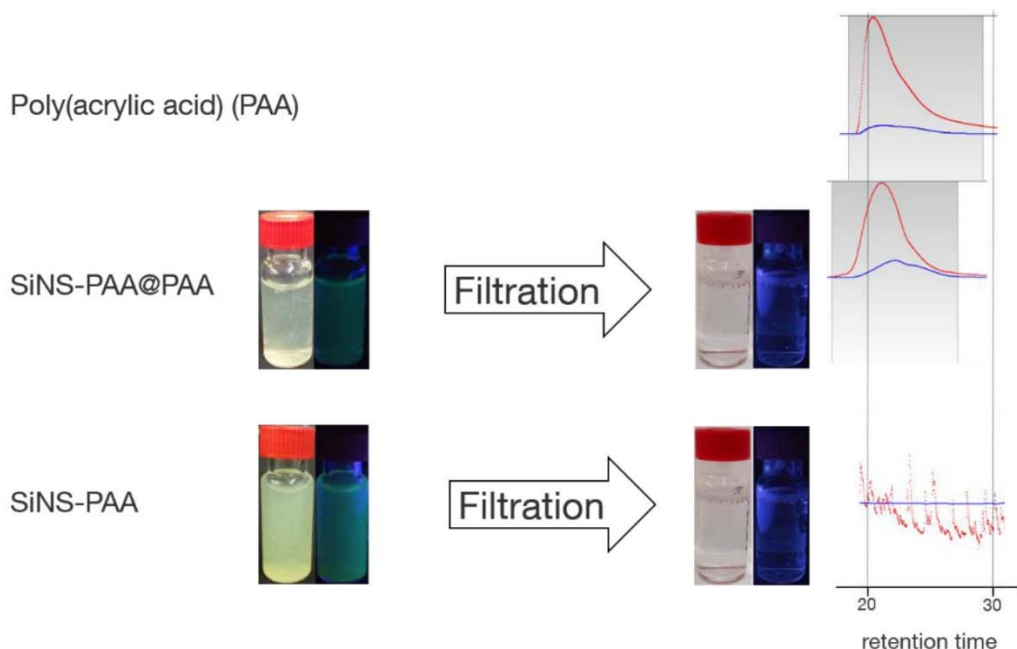


**Figure S17.** Dispersions of the hybrid material in H<sub>2</sub>O under visible (left) and UV light (right) before and after filtration demonstrate the removal of the silicon nanomaterial. The GPC analyses of the filtrates of SiNS-PAA@PAA show an excess of matrix polymer, whereas no free polymer is detected in the case of the merely functionalized SiNSs-PAA.

### GPC data of Polymer and Nanocomposites

**Table S1.** Summary of GPC results.

Sample	Eluent	$M_w$ in $\text{g mol}^{-1}$	PDI
PS		32000	1.83
SiNS-PS@PS	THF	33000	2.31
PMMA		103000	1.76
SINS-PMMA@PMMA		100000	2.73
PAA	$\text{NaN}_3$ aq (0.05 M)	39500	1,18
SiNS-PAA@PAA		32000	1,5

### TGA Measurements of Functionalized SiNSs

The TGA results demonstrate a substantial organic content on the SiNSs. In addition, the nonfunctionalized SiNSs lose some weight as well, which might arise from the pyrolysis of Si–Si bonds in the monolayers and is different from other silicon-based nanomaterials.<sup>[4]</sup> The thermal stability of the functionalized materials depends on the different substrates.

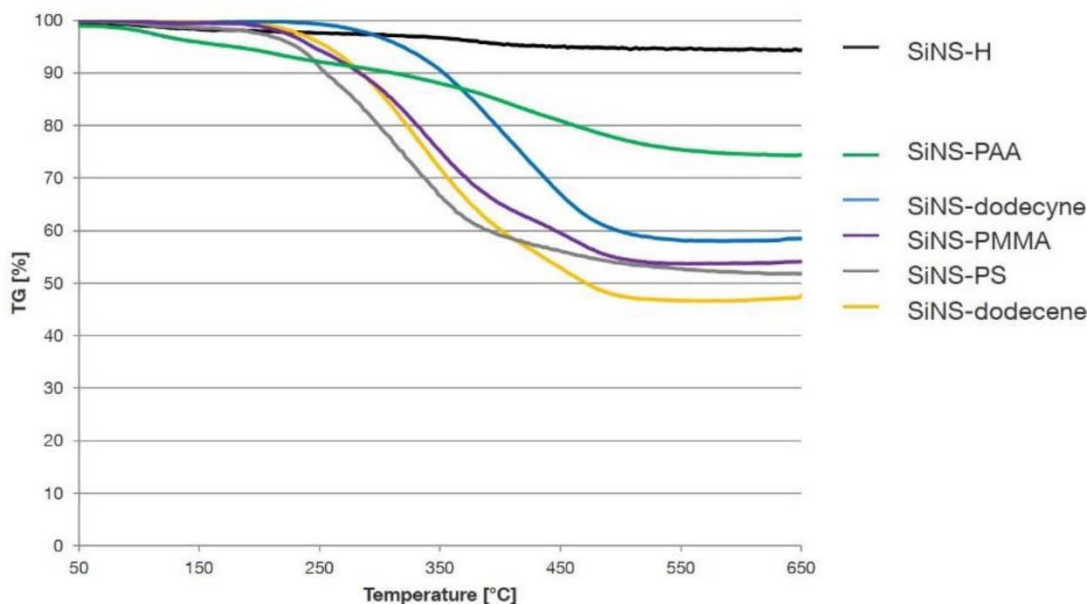


**Figure S18.** TGA measurements of nonfunctionalized and functionalized SiNSs.

**Table S2.** TG data from functionalized SiNSs.

Reagent	Weightloss in %	$M_w$ in $\text{g mol}^{-1}$	Weightloss/molecular weight	Content of SiNS	Organic content in %
1-dodecene	51.6	168.32	0.31	54.3	45.7
1-dodecyne	41.3	166.31	0.25	65.8	34.3
styrene	47.9	104.15	0.46	58.4	41.6
MMA	45.6	100.12	0.46	61.0	39.0
acrylic acid	25.5	72.06	0.35	83.5	16.5

Table S1 shows the ratio of weight loss/molecular weight of the attached organic substrates to obtain comparable values for the number of molecules on the surface. As evident in this table, the small, polymerizable substrates are more reactive towards the functionalization than the long dodecene/dodecyne molecules.

### NaOH Stability

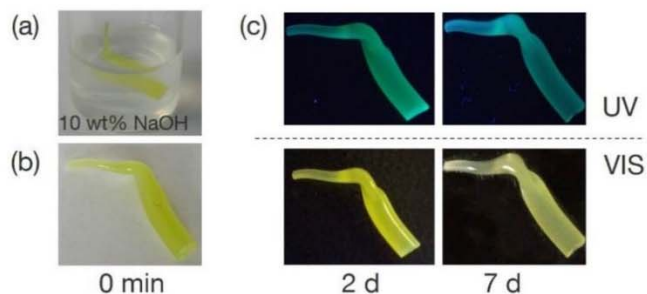


**Figure S19.** (a) Experimental setup: SiNS-PS@PS in 10 wt% NaOH; (b) a picture of compounded nanocomposite before exposure to basic conditions; and (c) pictures of the compounded strand after the mentioned time in aqueous NaOH under UV (top) and visible light (bottom).

### UV Stability of SiNSs

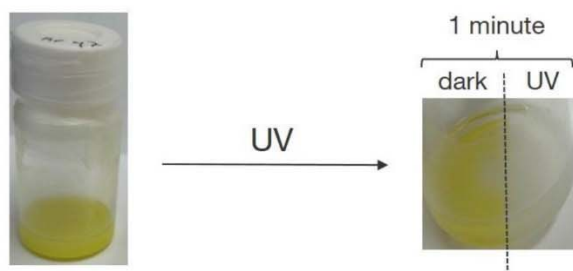


**Figure S20.** Irradiation of SiNSs in toluene with UV light. The dispersion was not stirred, and half of the vial was covered with aluminum foil. After irradiation with UV light, the irradiated SiNSs were destroyed.

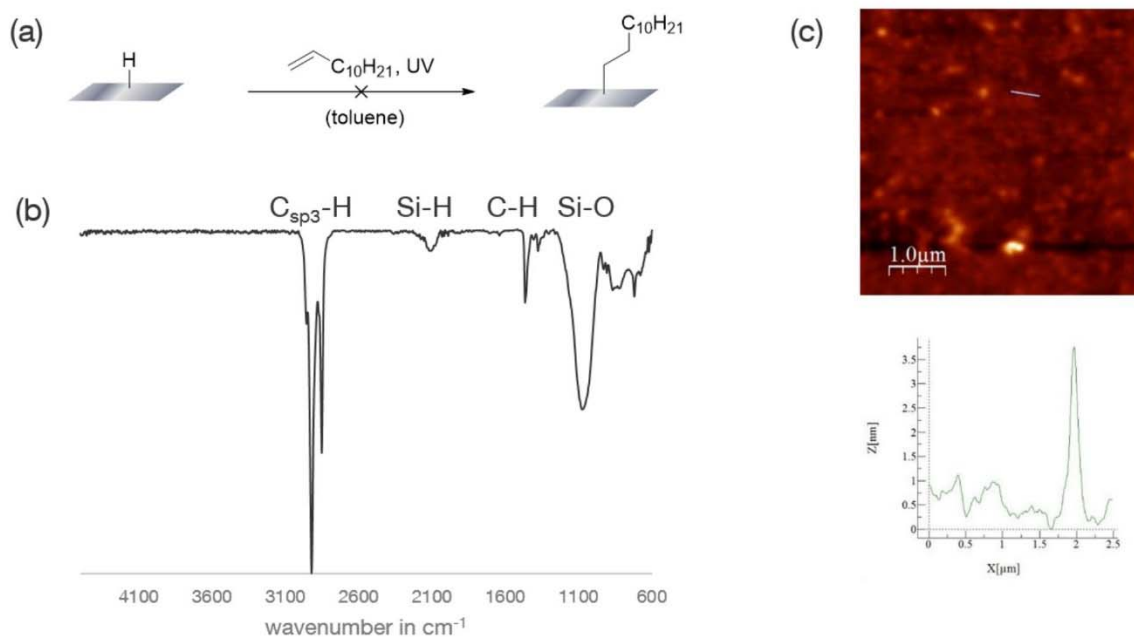


**Figure S21.** (a) Schematic of the functionalization of SiNS-H with 1-dodecene *via* UV-induced hydrosilylation; (b) the FTIR spectrum demonstrates functionalization of the silicon-based material; (c) AFM image (top) of the reaction and profile line (bottom) product demonstrating the deterioration of the material.

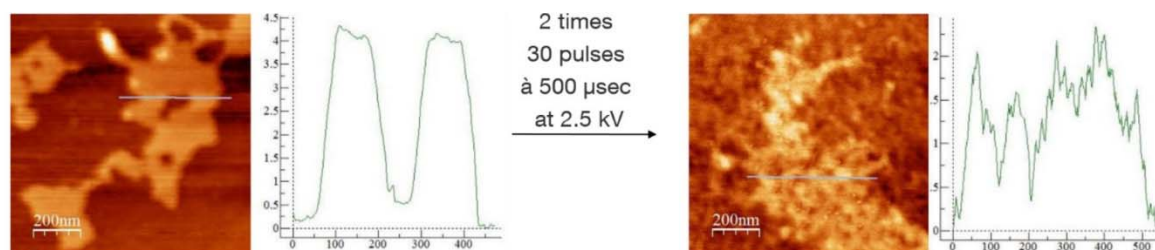


**Figure S22.** AFM pictures (left) and corresponding line profile (right) of the SiNSs-C<sub>12</sub>H<sub>25</sub> before and after photosintering shows the deterioration of SiNSs by light.

- [1] P. Vora, S. A. Solin, P. John, *Phys. Rev. B* **1984**, 29, 3423-3429,
- [2] W. M. Sears, J. L. Hunt, J. R. Stevens, *The Journal of Chemical Physics* **1981**, 75, 1589-1598.
- [3] J. H. Song, M. J. Sailor, *Inorg. Chem.* **1998**, 37, 3355 – 3360.
- [4] Kehrle, J.; Yang, Z.; Jochem, A.; Helbich, T.; Kraus, T.; Veinot, J. G. C.; Rieger, B. **2014**, 12494.

## 6. *Lewis* Acid Induced Functionalization of Photoluminescent Two-Dimensional Silicon Nanosheets for Enhanced P3HT Based Solution Gated Field Effect Transistor Fabrication

<b>Status</b>	Published online
<b>Journal</b>	Advanced Functional Materials
<b>Publisher</b>	Wiley-VCH
<b>DOI</b>	10.1002/adfm.201606764
<b>Authors</b>	Tobias Helbich <sup>‡</sup> , Alina Lyuleeva <sup>‡</sup> , Philip Marx, Lavinia M. Scherf, Tapas Purkait, Jonathan G. C. Veinot, Thomas F. Fässler, Paolo Lugli, Bernhard Rieger <sup>f</sup>

<sup>‡</sup>these authors contributed equally.

Reproduced by permission of John Wiley and Sons (license number 4105290308991).

### **Content:**

Due to the large surface of nanomaterials, their surface character is of decisive importance for the material properties (e.g., stability, dispersibility) and applications (e.g., biological, electronic). Different methods of surface modification exhibit their own advantages and disadvantages. It is therefore important to examine different conditions of introducing surface groups to being able to choose from a bigger repertoire depending on e.g., sensitivity of substrates, intended application, etc.

In our work we functionalized hydride terminated SiNSs *via* Lewis acid catalyzed hydrosilylations to induce reactions with alkenes and alkynes. In contrast to other silicon based nanomaterials, different aluminum and borane based *Lewis* acids can be used for the reaction, demonstrating a higher reactivity of the SiNSs. The method can be applied on a variety of functional alkenes and alkynes. The different reactivity of the substrates gives information about the potential reaction mechanism which is different from other silicon based nanomaterials (e.g., SiNCs, pSi).

The functionalized materials show improved dispersibility of the SiNSs while still maintaining their electronic features. As such we could use the hybrid nanomaterials to, for the first time, fabricate Field Effect Transistors (FET) based on P3HT/SiNS composites. The combination of the two materials enabled us to enhance the sensitivity of the solution-gated FETs and increase the transconductance  $g_m$ .

© 2016 WILEY-VCH Verlag GmbH & Co. KGaA, Weinheim

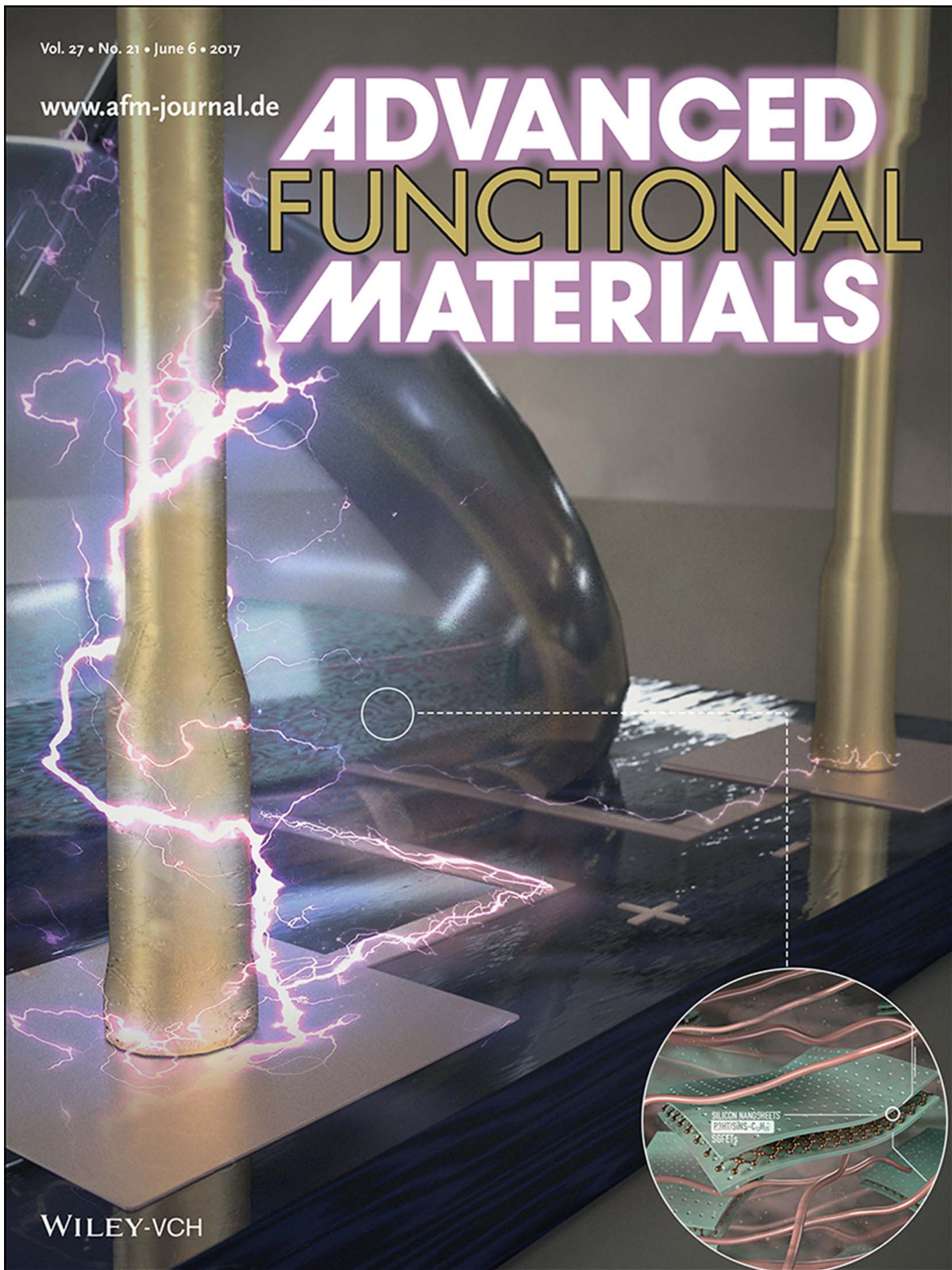
---

<sup>f</sup> T. Helbich planned and executed all experiments concerning the functionalization, characterization and mechanical investigation, with contribution of P. Marx and wrote most of the manuscript; A. Lyuleeva contributed with AFM measurements and FET fabrication as well as characterization and wrote about this work in the manuscript; T. Purkait helped with XPS measurements; L. Scherf synthesized the starting material CaSi<sub>2</sub>. J. Veinot contributed with fruitful mental input and helped writing the manuscript. All work of was performed under the supervision of J. Veinot, T. Fässler, P. Lugli and B. Rieger.

Vol. 27 • No. 21 • June 6 • 2017

[www.afm-journal.de](http://www.afm-journal.de)

# ADVANCED FUNCTIONAL MATERIALS



WILEY-VCH

# Lewis Acid Induced Functionalization of Photoluminescent 2D Silicon Nanosheets for the Fabrication of Functional Hybrid Films

Tobias Helbich, Alina Lyuleeva, Philipp Marx, Lavinia M. Scherf, Tapas K. Purkait, Thomas F. Fässler, Paolo Lugli, Jonathan G. C. Veinot,\* and Bernhard Rieger\*

Various Lewis acids are found to efficiently catalyze hydrosilylation reactions of hydride-terminated 2D silicon nanosheets at room temperature. The hydride-terminated nanosheets can be functionalized with a variety of unsaturated functional substrates and still possess their unique characteristic (opto)electronic properties (e.g., photoluminescence). This is demonstrated by successfully implementing the readily functionalized materials into new silicon/semiconducting polymer-based field-effect transistors (FETs). Surface modification of the freestanding silicon nanosheets opens new possibilities to form highly homogeneous blends with the already broadly used conventional polymers poly(3-hexylthiophene-2,5-diyl). The consequential combination of the different properties of the materials enables the enhancement of the sensitivity of the solution-gated FETs and increases the transconductance of the operating device.

and is finding applications in electronics and photonics.<sup>[8]</sup> In contrast, reports of nanosheets of carbon's heavier Group 14 congener (i.e., Si) are far less common;<sup>[9]</sup> however, the potential of silicon nanosheets (SiNSs) remains vast.

The bonding within the SiNSs and by extension their properties depend upon the preparation method. In general, SiNSs take on one of the two general forms. The graphene analog (i.e., silicene<sup>[1,10–13]</sup>) possesses nearly planar, sp<sup>2</sup> hybridized silicon centers.<sup>[11]</sup> The electronic structure and band gap tailoring of silicenes can be achieved using physical (e.g., introduction of strain<sup>[14,15]</sup>) or chemical (e.g., hydrogenation<sup>[16]</sup> and halogen functionalization<sup>[16]</sup>) approaches. Silicenes are air sensitive and,

to date, have only been prepared in small quantities on supports such as Ag,<sup>[17,18]</sup> zirconium diboride,<sup>[19]</sup> and iridium.<sup>[20]</sup> Despite obvious material challenges, these materials exhibit ultrahigh carrier mobilities that may prove useful in a variety of electronic devices (e.g., transistors).<sup>[9,21–23]</sup>

Fully hydrogenated SiNSs (SiNS-H)<sup>[24]</sup> represent a second bonding motif for 2D SiNSs; these materials are commonly referred to as silicanes or, when stacked, layered polysilanes. They appear as puckered sheets in which silicon atoms are sp<sup>3</sup>-hybridized and form a  $\sigma$ -conjugated network.<sup>[25]</sup> They are readily prepared in gram quantities via straightforward chemical exfoliation from CaSi<sub>2</sub>.<sup>[26,27]</sup> In this procedure, Ca<sup>2+</sup> ions are deintercalated using concentrated hydrochloric acid yielding calcium chloride and sheets of interconnected Si<sub>6</sub> rings (Scheme 1).

SiNS-H are photoluminescent,<sup>[28]</sup> predicted to have highly localized excitons,<sup>[29]</sup> and expected to exhibit nonmagnetic semiconducting behavior.<sup>[30]</sup> In addition, they have been examined as a potential anode material for lithium ion batteries.<sup>[31–34]</sup> It is reasonable that both forms of SiNSs will play important roles in future nano- and microelectronic as well as biomedical device applications.<sup>[21,25,35,36]</sup>

As prepared SiNS-H do not form stable dispersions in common organic solvents and quickly precipitate; this limits the application of solution-based processing methods. Surface modification improves solvent compatibility/dispersibility while concomitantly minimizing the impact of unwanted deleterious reactions (e.g., oxidation).<sup>[37,38]</sup> Tailoring SiNS-H surface chemistry is crucially important if SiNSs are to be rendered

## 1. Introduction

Nanosheets are intriguing “2D” nanomaterials whose properties arise as a result from their unique structure—they possess nanometer (even atomic)–scale thicknesses and lateral dimensions that can reach into the macroscopic regime.<sup>[1–4]</sup> As a result a variety of prototype applications (e.g., sensing, energy harvesting, and catalysis) have been demonstrated.<sup>[5–7]</sup> Graphene is the prototypical nanosheet; it is widely studied

T. Helbich, P. Marx, Prof. B. Rieger  
Catalysis Research Center/Wacker-Lehrstuhl  
für Makromolekulare Chemie  
Technische Universität München  
Lichtenbergstrasse 4  
85747 Garching bei München, Germany  
E-mail: rieger@tum.de

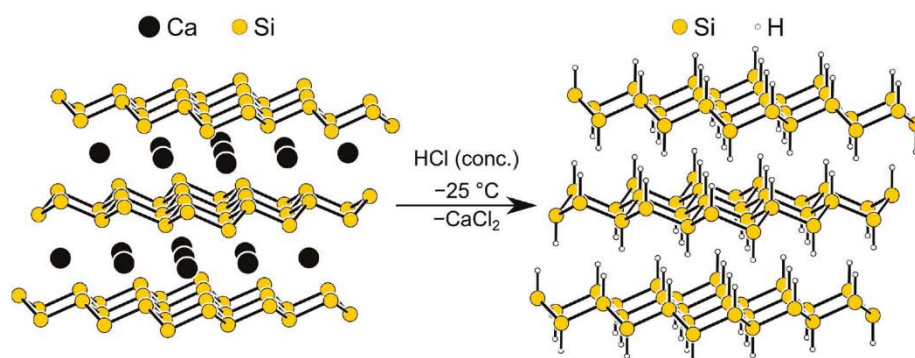
A. Lyuleeva, Prof. P. Lugli  
Institute for Nanoelectronics  
Technische Universität München  
Arcisstrasse 21, 80333 Munich, Germany

L. M. Scherf, Prof. T. F. Fässler  
Lehrstuhl für Anorganische Chemie mit Schwerpunkt Neue Materialien  
Technische Universität München  
Lichtenbergstrasse 4, 85747 Garching bei München, Germany

Dr. T. K. Purkait, Prof. J. G. C. Veinot  
Department of Chemistry  
University of Alberta  
11227 Saskatchewan Drive, Edmonton, T6G 2G2 Alberta, Canada  
E-mail: jveinot@ualberta.ca



DOI: 10.1002/adfm.201606764



**Scheme 1.** Preparation of SiNS via chemical exfoliation from CaSi<sub>2</sub>.

colloidally stable and solution processed. Furthermore, surface functionalization of other silicon-based nanomaterials is known to influence material (opto)electronic properties and tailoring the surface chemistry of SiNSs could dramatically expand the scope of their practical applications.<sup>[39–42]</sup>

Designing the surface chemistry of silicon nanomaterials (e.g., porous silicon, silicon nanocrystals, and SiNSs) draw on established molecular silicon chemistry and pioneering work related bulk silicon surfaces.<sup>[38,43–45]</sup> Despite some similarities, numerous examples of material differences have been reported when standard methods have been applied to “nano” silicon<sup>[46–49]</sup> and it is essential to explore the reactivity of SiNSs if their full potential is to be realized. Already SiNS-H have been derivatized upon direct reaction with amines; these reactions reportedly provided surface functionalities tethered through Si–N linkages.<sup>[50,51]</sup> Similarly, SiNS-H were modified upon reaction with phenylmagnesium bromide (i.e., PhMgBr) to yield sheets bearing phenyl moieties<sup>[52]</sup> or by employing widely utilized hydrosilylation reactions<sup>[49,53]</sup> that are well established for other silicon nanomaterials<sup>[37,48,54–60]</sup> and bulk silicon.<sup>[38,43,45,55,61]</sup> Each of these functionalization approaches has advantages and disadvantages. Thermally induced hydrosilylation is broadly applicable on substrates;<sup>[49]</sup> however, high temperatures associated with these reactions can induce formation of surface-bonded oligomers on the surfaces of other Si nanomaterials.<sup>[47]</sup> SiNSs are sensitive to UV light exposure precluding the effective application of photoinitiated reactions,<sup>[62]</sup> and transition metal catalyzed reactions can lead to unwanted impurities that have previously compromised the desirable properties of other silicon-based nanomaterials<sup>[63]</sup> and can render the material toxic.<sup>[64]</sup>

Lewis acids are commonly used to catalyze molecular hydrosilylation reactions.<sup>[65–68]</sup> This general approach has been effectively extended to a variety of silicon-based nanomaterials (e.g., porous-Si and Si nanocrystals) while maintaining desired material properties (e.g., high surface area and photoluminescence (PL)).<sup>[37,57,69]</sup> Lewis acid mediated reactions are also appealing because they exhibit wide functional group tolerance,<sup>[37,69]</sup> proceed at room temperature, are straightforward, cost-effective, and residual catalyst can be readily removed<sup>[70]</sup> and/or is biocompatible.<sup>[70]</sup> Herein, we present the first investigation of room temperature Lewis acid catalyzed hydrosilylations of hydride-terminated SiNSs-H leading to the covalent modification of SiNSs.

## 2. Lewis Acid Catalyzed Functionalization of Silicon Nanosheets

A series of common Lewis acids (i.e., *tris*(pentafluorophenyl)alane (ACF), *tris*(penta-fluorophenyl)borane (BCF), trifluoroborane (BF<sub>3</sub>), and borane dimethylsulfide (BH<sub>3</sub>:SMe<sub>2</sub>; see Table S1 in the Supporting Information for further discussion of Lewis acidity) were evaluated as candidate catalysts in promoting the hydrosilylation of SiNSs-H with the model substrate 1-dodecene. Having established catalytic activity, the present study was extended to evaluate substrate group tolerance of reactions with 1-decyne, vinyltrimethylsilane, *tert*-butyl methacrylate, and ethyl-10-undecenoate promoted by BH<sub>3</sub>:SMe<sub>2</sub>. The resulting materials were characterized using Fourier transform infrared (FTIR) and PL spectroscopy, atomic force microscopy (AFM), thermal gravimetric analysis (TGA), and X-ray photoelectron spectroscopy (XPS). Finally, a polymer/functionalized nanosheet blend was evaluated as an active material in a prototype solution-gated field-effect transistor (FET).<sup>[71–73]</sup>

For the present study we examined the reactivity of SiNSs toward Lewis acid mediated hydrosilylations of 1-dodecene (**Figure 1**). Exfoliated SiNSs were etched using hydrofluoric acid (HF) and extracted into dry toluene. After addition of 1-dodecene (3.00 mmol) and removal of air by standard degassing procedures, the Lewis acid of choice (0.02 mmol, 0.1 M in toluene) was added and the reaction mixture stirred for 4 h at room temperature. Functionalized SiNSs were isolated by precipitation/centrifugation cycles.

FTIR spectra of the resulting functionalized SiNSs with all the Lewis acids investigated here (**Figure 2** and **Figure S1** (Supporting Information)) show spectral features consistent with successful hydrosilylation with 1-dodecene. In all cases the intensity of Si–H feature ( $\approx 2100\text{ cm}^{-1}$ ) diminishes substantially and some Si–O ( $\approx 1100\text{ cm}^{-1}$ ) bands appear that likely result from limited surface (or edge) oxidation. The spectra are dominated by strong C<sub>sp3</sub>–H stretching ( $\approx 2900\text{ cm}^{-1}$ ) and deformation bands ( $\approx 1460\text{ cm}^{-1}$ ) consistent with covalently bonded dodecyl moieties. Of important note, no C<sub>sp2</sub>–H stretching ( $\approx 3100\text{ cm}^{-1}$ ), deformation bands ( $\approx 1650\text{ cm}^{-1}$ ), or features related to C=C (e.g.,  $1640\text{ cm}^{-1}$ ) are observed at the sensitivity of the FTIR method.

In all cases, TGA (see **Figure S2** in the Supporting Information) shows weight losses between 250 and 500 °C in agreement with previous observations involving SiNCs;<sup>[57]</sup> this

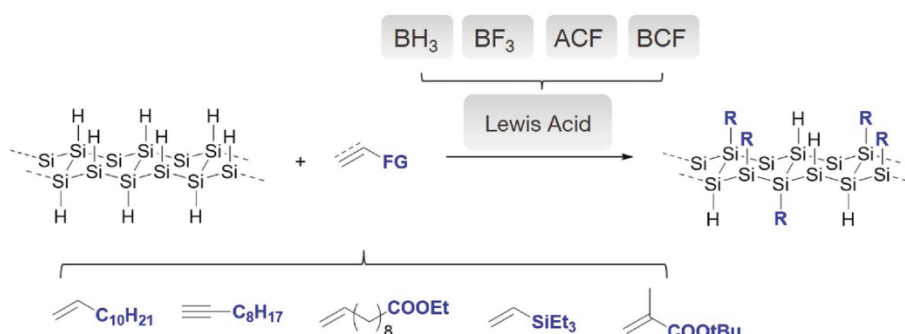


**Figure 1.** Schematic representation of Lewis acid induced SiNS functionalization. The different Lewis acids ACF (*tris*(pentafluorophenyl)alane), BCF (*tris*(penta-fluorophenyl)borane),  $\text{BF}_3$  (Trifluoroborane), and  $\text{BH}_3\cdot\text{SMe}_2$  (borane dimethylsulfide) successfully catalyze surface functionalization of SiNSs. Additionally a variety of different unsaturated functional substrates can be used.

weight loss is attributed to the loss of surface organic functionalities resulting from successful functionalization of the SiNSs with all Lewis acids tested. The present TGA data suggest that strongly Lewis acidic, bulky ACF, and BCF are slightly less reactive (i.e., lead to less functionalization) than small Lewis acids (i.e.,  $\text{BH}_3$  and  $\text{BF}_3$ ; see Figure S2 in the Supporting Information for TGA and Table S1 in the Supporting Information for further discussion of Lewis acidity) consistent with Lewis acid steric demand limiting reactivity. These results further emphasize the differing reactivity of SiNSs compared to other silicon-based nanomaterials—BCF proved ineffective in promoting any functionalization of SiNCs<sup>[57]</sup> and porous silicon (i.e., p-Si).<sup>[37]</sup> Thus Si-H moieties on the present SiNSs seem to be more hydridic than those on the surfaces of SiNCs or p-Si, which explains why lower quantities of Lewis acid can be used in this work as compared to p-Si<sup>[37]</sup> and SiNCs.<sup>[57]</sup> TGA weight loss also indicates the differing Lewis acidities of  $\text{BH}_3$  and  $\text{BF}_3$  (see Table S1, Supporting Information) do not substantially impact on the degree of functionalization and that both are sufficient to activate the hydridic surface. Identifying  $\text{BH}_3$  as the Lewis acid catalyst of choice for promoting hydrosilylation of the present SiNS, we focused in the remainder of the present study on its reactivity. AFM images of SiNSs- $\text{C}_{12}\text{H}_{25}$  prepared

via  $\text{BH}_3$  catalyzed reactions exhibit thicknesses of  $\approx 4.0$  nm (Figure 3) consistent with previous reports.<sup>[53,62]</sup>

Functional group tolerance of  $\text{BH}_3$  catalyzed hydrosilylation was evaluated upon reaction of *tert*-butylmethacrylate, vinyltrimethylsilane, 1-decyne, and 10-ethylundecenoate. As expected, FTIR spectra of the resulting functionalized materials exhibit  $\text{C}_{\text{sp}^3}\text{-H}$  ( $\approx 2920$   $\text{cm}^{-1}$ ),  $\text{C}_{\text{sp}^2}\text{-H}$  ( $\approx 1600$   $\text{cm}^{-1}$ ),  $\text{C}=\text{O}$  ( $\approx 1700$   $\text{cm}^{-1}$ ), and  $\text{C}-\text{O}$  ( $\approx 1150$   $\text{cm}^{-1}$ ) bands, consistent with effective functionalization (Figure 4). Additionally Si-H ( $\approx 2100$   $\text{cm}^{-1}$ ) remained and is reasonably attributed to residual hydride groups. As is the case with other Si nanomaterials, work-up procedures performed under ambient conditions lead to limited oxidation that is manifested in Si-O features at  $\approx 1100$   $\text{cm}^{-1}$ .

Interestingly, the intensity of the Si-O band is inversely related to the established hydrosilylation reactivity of the substrate (i.e., the more reactive the substrate is toward borane catalyzed hydrosilylation, the smaller is the Si-O band). This observation is further manifested in the TGA analysis in which the molecular mass normalized weight loss follows the trend: vinyltrimethylsilane > 1-dodecene > *t*BuMA > 10-ethylundecenoate > 1-decyne (Figure S3, Supporting Information).

To better understand the mechanism of the present reactions we compared them with published Lewis acid catalyzed hydrosilylation reactions of model molecular systems that follow established mechanisms.<sup>[66,67,74,75]</sup> Reflecting the differing hydridic character of Si-H moieties on SiNSs and SiNCs, the presented SiNS reactivity is in accordance with the mechanism proposed

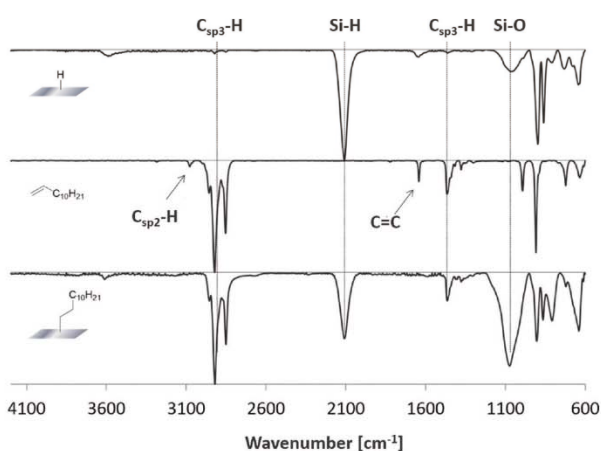


**Figure 2.** FTIR spectra of freshly etched SiNS-H (top), 1-dodecene (middle), and dodecene functionalized SiNS- $\text{C}_{12}\text{H}_{25}$  (bottom) obtained from  $\text{BH}_3\cdot\text{SMe}_2$  catalyzed hydrosilylation reactions.

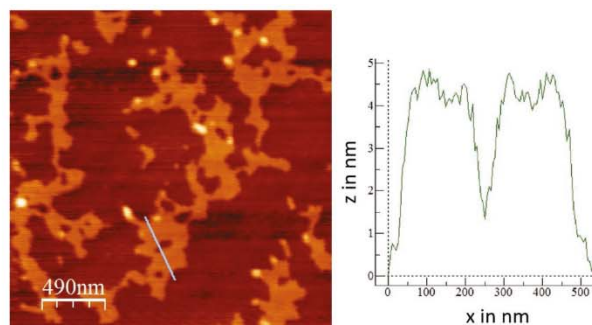


**Figure 3.** Noncontact mode AFM image of SiNSs- $\text{C}_{12}\text{H}_{25}$  (left) and their line profile (right) taken along the line in the left image.

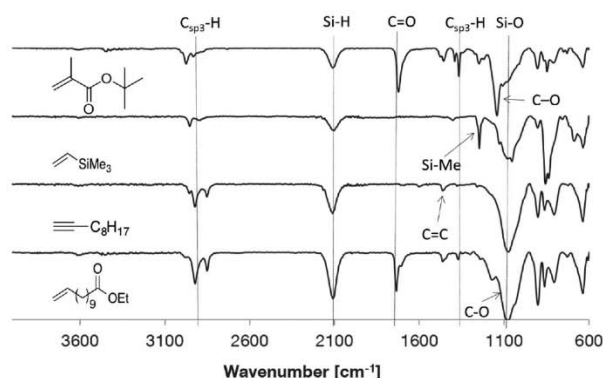


**Figure 4.** FTIR spectra of functionalized SiNSs by  $\text{BH}_3$  catalyzed hydrosilylation.

by Lambert et al. for  $\text{B}(\text{C}_6\text{F}_6)$  catalyzed hydrosilylation.<sup>[76]</sup> This is in direct contrast to the SiNC established mechanism that proceeds via hydroboration of the substrate, followed by addition to the NC surface.<sup>[57]</sup> Lambert et al. proposed hydrosilylation proceeds via the activation of the silicon species and formation of a silylium ion (Figure 5a)<sup>[76]</sup> that reacts directly with the unsaturated substrate (Figure 5b).<sup>[66,75]</sup> The resulting carbenium ion is stabilized by the  $[\text{H-LA}]^-$  adduct and the hydride subsequently reacts with the silylium ion to render the hydrosilylated product (Figure 5c).

The reactivity of the different substrates (based upon TGA weight loss derived degree of functionalization) investigated herein coincides with the Lambert mechanism—the comparatively small trimethylvinylsilane shows the highest reactivity presumably because of steric effects and the trimethylsilyl group stabilizes a positive charge in the beta position due to hyperconjugation effects (Figure 5d).<sup>[77]</sup>

When considering 1-dodecene no such stabilizing effect occurs. When ester groups are present, the carbonyl can coordinate to the Lewis acid reducing their effective concentration/reactivity (Figure 5e). The greater reactivity of <sup>t</sup>BuMA compared to 10-ethylundecenoate may result from inductive and hyperconjugation effects of the methyl group attached to the double

bond.<sup>[78]</sup> Additionally, for surface reactions, sterically accessible molecules are often favored over sterically demanding ones.

FTIR and TGA results of the 1-decyne functionalized SiNSs indicate less efficient functionalization than for its alkene counterpart 1-dodecene. SiNCs<sup>[57]</sup> and p-Si<sup>[37]</sup> are more reactive toward alkynes than alkenes, but surface coverage in both cases is smaller for alkynes. A possible explanation for this observation may lie in the steric demand of the alkene on the surface and its implications on the packing behavior of the surface groups (Figure 5f); however, a detailed discussion is beyond the scope of the present contribution.<sup>[63]</sup>

To further explore the mechanism of SiNS hydrosilylation we performed XPS measurements for freshly etched systems and found that the spectra are dominated by an intense feature at 99.8 eV (as well as a high energy shoulder) arising from Si-based surface species (e.g., Si-H and trace surface oxide; Figure S4, Supporting Information). Similar binding energies have been noted in other reports investigating SiNSs.<sup>[53]</sup> After stirring for 4 h with  $\text{BF}_3$  in a glove box and subsequent work-up under argon, the fluorine content rises drastically (Figures S5 and S6, Supporting Information) and signals arise from more highly oxidized Si species (Figure S7, Supporting Information). These observations are reasonably attributed to the formation of silylium ion-based surface species that are stabilized by  $[\text{HBF}_3]^-$  (Figure 5a).

The differently functionalized SiNSs exhibit a photoluminescence maximum of  $\approx 510$  nm (Figure 6), which is in accordance with previously published results of our group.<sup>[49]</sup> The origin of this PL response is unclear and is the subject of ongoing investigation.

### 3. Silicon Nanosheet Based Functional Hybrid Films

Incorporation of inorganic nanomaterials (e.g., carbon nanotubes (CNTs)<sup>[79]</sup> or graphene<sup>[80]</sup>) into the active area of solution-gated FETs (SGFETs) has led to significant improvement of their sensitivity. In this context, and to demonstrate the potential of SiNS, the dodecyl functionalized SiNSs were blended

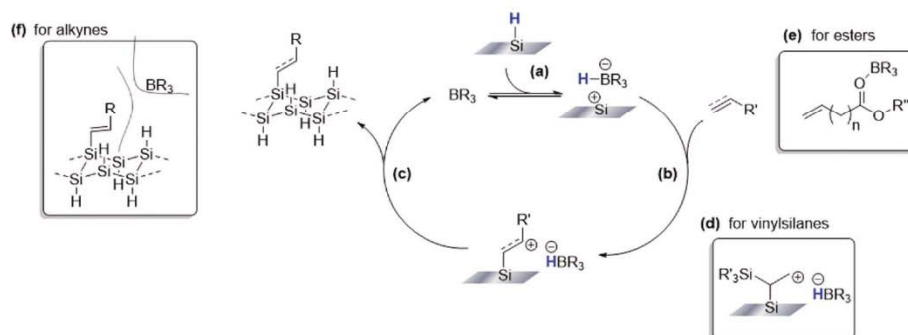


**Figure 5.** Proposed mechanism exemplified for borane catalyzed hydrosilylation of hydride terminated SiNSs and unsaturated substrates: a) Preactivation of the Si surface by the formation of a silylium type surface species. b) Subsequent direct addition of the unsaturated substrate to the silylium ion and trapping of the carbenium species by the boron based hydride. c) Reaction of the carbenium ion with the hydride regenerates the catalyst and renders functionalized surface. d) Silicon atoms stabilize the positive charge in beta position and addition therefore induces a higher reactivity. e) The carbonyl group of esters coordinates to the Lewis acid diminishing its catalytic reactivity. f) Alkynes render alkene functionalized surfaces that exhibit a higher steric demand and thus prevent further surface functionalization.

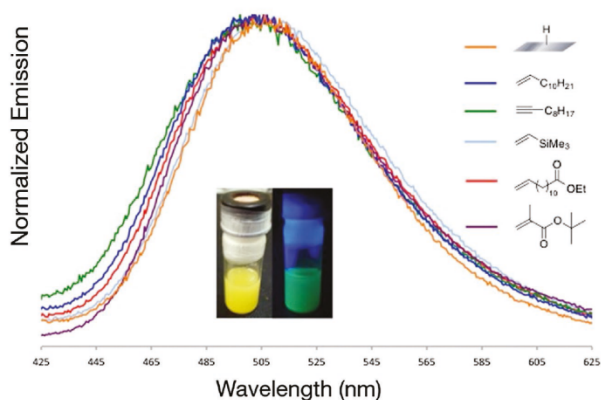


**Figure 6.** Normalized PL spectra of dispersions of freshly etched and by  $\text{BH}_3$  catalyzed hydrosilylation functionalized SiNSs. Inset: Pictures of the dispersion of  $\text{SiNS-C}_{12}\text{H}_{25}$  in toluene under daylight (left) and UV light (right).

with the workhorse semiconducting polymer poly-3-hexylthiophene (P3HT) and used in the fabrication of a SGFET (Figure 7, inset).

In this structure, it is reasonable to expect that the p-type semiconducting behavior of P3HT polymer enables the device operation as FET, which can be switched on and off with an applied gate voltage ( $V_G$ ).<sup>[79,81]</sup> Upon blending with P3HT, the conducting properties of the functionalized SiNS increase the drain current of the device in operating conditions (see Figure 8). This observation may result from improved connection between the crystalline regions in the P3HT/ $\text{SiNS-C}_{12}\text{H}_{25}$

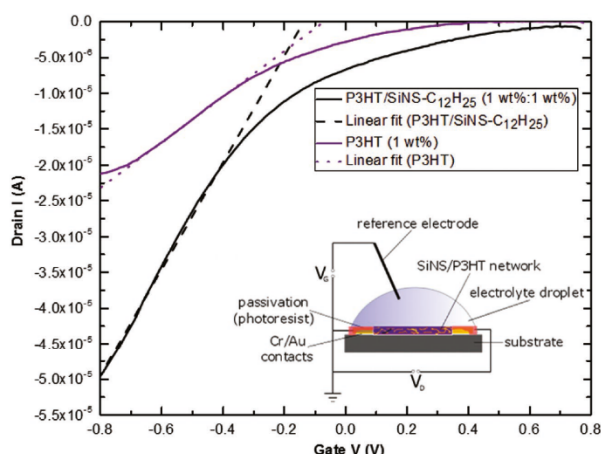


**Figure 7.** Transfer curves for P3HT and P3HT/ $\text{SiNS-C}_{12}\text{H}_{25}$  based SGFETs operating at room temperature (drain voltage  $V_D = -0.1$  V). Transconductances ( $g_m$ ) of the operating devices are  $3.18 \times 10^{-5}$  S and  $7.45 \times 10^{-5}$  S, respectively. The threshold voltages ( $V_{th}$ ) are  $-0.07$  V for P3HT and  $-0.13$  V for the P3HT/ $\text{SiNS-C}_{12}\text{H}_{25}$  blend. The ON/OFF ratios are decreased from  $10^4$  to  $10^2$  while changing the active film from neat polymer to P3HT/ $\text{SiNS-C}_{12}\text{H}_{25}$  blend. The ON current is defined as the maximum drain current and the OFF current as the minimum drain current while sweeping the gate voltage from 0.8 to  $-0.8$  V. The inset presents a schematic of the device structure used during the SGFET characterization. A platinum wire acted as the operating reference electrode.

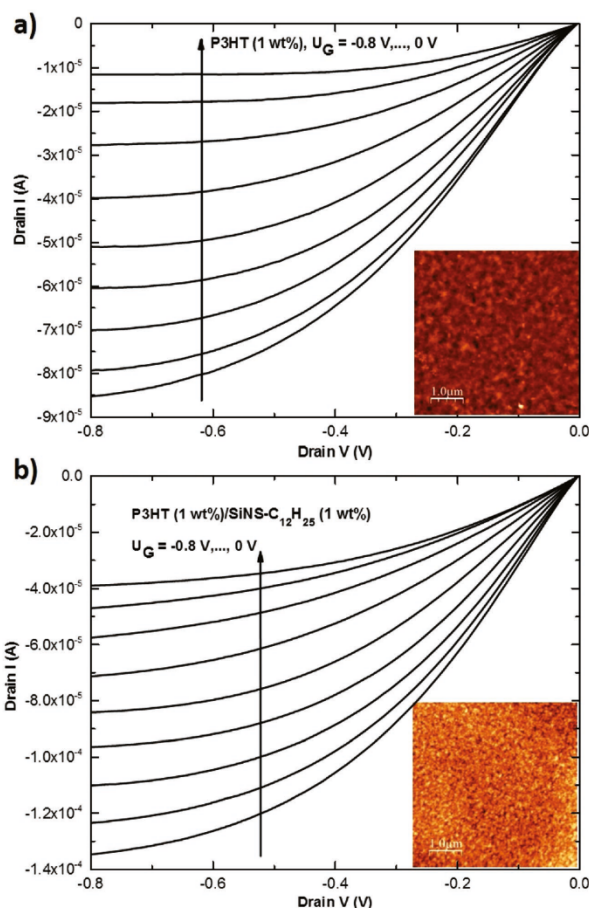


**Figure 8.** a,b) Output curves of P3HT based SGFET (left) and P3HT/ $\text{SiNS-C}_{12}\text{H}_{25}$  based SGFET (right). Drain current ( $I_D$ ) versus drain voltage ( $V_D$ ) measurements were carried out at constant gate voltages ( $V_G$ ), ranging from 0 to  $-0.8$  V. A DI water droplet was used as the electrolyte. The insets show the corresponding AFM images ( $5 \mu\text{m}^2$  scale) of semiconducting films.

blend.<sup>[80]</sup> The enhanced charge carrier mobility within the blend leads to higher currents. The present observations are comparable with those demonstrated by Bo et al. for their “pickup stick” transistors, in which metallic single-wall CNTs were used to reduce the effective source drain distance.<sup>[82]</sup>

The present SGFET was characterized in a deionized water (DI water) electrolyte. Current–voltage curves were measured at room temperature under ambient conditions. Figure 7 shows transfer curves of both P3HT and P3HT/ $\text{SiNS-C}_{12}\text{H}_{25}$  based SGFETs with transconductances ( $g_m$ ) of  $3.18 \times 10^{-5}$  S and  $7.45 \times 10^{-5}$  S, respectively. This parameter provides valuable information regarding the sensitivity of the devices during operation, because it specifies the current response to a gate voltage modulation.<sup>[83]</sup>

Fitting of the transfer curves allows the definition of the operating device threshold voltages. The present P3HT-SGFET shows a  $V_{th}$  of  $-0.07$  V at a drain voltage  $V_D = -0.1$  V and highest drain current  $I_{D,max} = -2.13 \times 10^{-5}$  A at  $V_G = -0.8$  V. Under identical conditions, the equivalent device based upon the SiNS

hybrid (i.e., P3HT/SiNS-C<sub>12</sub>H<sub>25</sub>) sees a small  $V_{th}$  shift up toward  $-0.13$  V and reaches highest currents  $I_{D,max} = -4.97 \times 10^{-5}$  A. In general, a noticeable increase in the  $I_{D,max}$  and the transconductance  $g_m$ , which provides some “tradeoff,” could be achieved. The output characteristics at fixed gate voltages ( $V_G = -0.8 - 0$  V) for both devices are shown in Figure 8.

As already mentioned a comparison of the present devices with those prepared using graphene and CNTs based hybrid films provides useful context; e.g., Huang et al. demonstrated enhanced mobilities in P3HT/graphene-FETs while maintaining favorable ON/OFF ratios.<sup>[80]</sup>

Nevertheless, if the concentrations are too high, nanomaterial stacking and eventual movement during the measurement lead to increased disorder of the blend within the channel, which would lead to lower crystallinity and therefore lower mobility.<sup>[80]</sup> The outcome of this is finding a good agreement between the highest reachable mobility, good ON/OFF ratios, and lowest distracting disorder within the blend film.

The surface modification of the herein used SiNSs enhances the homogeneity (Figure 8) and with it the dispersibility of the hybrid material. Furthermore, due to interactions with the polymer matrix, functional groups are able to “fix” the SiNS-C<sub>12</sub>H<sub>25</sub> within the semiconducting blends. This could suppress aggregation and precipitation within the film.<sup>[80]</sup>

The homogeneity is essential for the reproducibility and good ON/OFF ratios, as it leads to the enhancement of the device sensitivity.

Overall, the role of surface functionalization on the SiNSs can address the remaining challenges and is the subject of ongoing studies. Different functional groups can be introduced to the hybrid material to tune their physical properties. Thus, the interaction between the polymer and the inorganic content of the blend may be further enhanced.

#### 4. Conclusion

2D silicon nanosheets exhibit substantial potential for various nanoelectronic applications. After the straightforward synthesis via deintercalation from CaSi<sub>2</sub> the hydride terminated SiNSs must be functionalized to render them solution processable and stable toward deleterious reactions (e.g., oxidation) that can degrade their properties.

We present here the first example of Lewis acid catalyzed hydrosilylation of SiNS-H with various unsaturated compounds.

BH<sub>3</sub>, BF<sub>3</sub>, BCF, and ACF were all successfully used to promote hydrosilylation reactions. This demonstrates a different reactivity compared to other silicon nanomaterials (i.e., SiNCs and porous Si), for which, e.g., BCF was found ineffective. The unique reactivity is accompanied by a mechanism differing from the one postulated for SiNCs and porous silicon, for which the first mechanistic step involves the hydroboration of the alkene. For SiNSs on the other hand, the mechanism seems to proceed via the formation of a silylium ion, demonstrating once again the difference in reactivity of materials when nanoscales are reached.

With the synthesized hybrid material we built a functional silicane-based nanoelectronic device: a P3HT/SiNS-C<sub>12</sub>H<sub>25</sub> SGFET. The use of the nanocomposite enhanced the sensitivity

of the device while increasing the transconductance by more than 100%.

#### 5. Experimental Section

**General Information:** All reagents were purchased from Sigma-Aldrich, Alfa-Aesar, VWR, or Wacker Chemie and used without further purification unless stated otherwise. *Tert*-butyl methacrylate was distilled under reduced pressure (90 mbar, 65 °C) and stored over molecular sieve. Toluene was dried prior to use with an MBraun solvent purification system MB SPS-800 equipped with argon 5.0 (99.9990%, Westfalen AG) working atmosphere. Acetone was dried, degassed via three freeze-pump-thaw cycles and stored under argon. Exfoliated SiNSs were stored in an argon 4.8 (99.998%, Westfalen AG) filled LABmaster 130 (MBraun) glove box. All air/water sensitive reactions were executed using standard Schlenk techniques.

FTIR spectra were measured using a Bruker Vertex 70 FTIR with a Platinum ATR from Bruker. PL spectra of toluene or ethanol suspensions were acquired using an AVA-Spec 2048 from Avantes using a Prizmatix (LED current controller) light source.

TGA was performed using a Netzsch TG 209 F 1 Libra with heating rates of 10 K min<sup>-1</sup> and argon flow rates of 20 mL min<sup>-1</sup> under argon 4.8 (99.998%, Westfalen AG).

For AFM (contact mode, Asylum Research MFP-3D AFM with an ARC controller) thin films of SiNS-C<sub>12</sub>H<sub>25</sub> (15 mg of exfoliated sheets in 2 mL of toluene) were spin coated (90 s, 1000 rpm) onto Si/SiO<sub>2</sub> substrates.

XPS analyses were performed using a Kratos Axis Ultra instrument operating in energy spectrum mode at 210 W. Samples were prepared as films drop-cast from solution onto a copper foil substrate. The base and operating chamber pressure were maintained at 10<sup>-7</sup> Pa. A monochromatic Al K $\alpha$  source ( $\lambda = 8.34$  Å) was used to irradiate the samples, and the spectra were obtained with an electron takeoff angle of 90°. Survey spectra were collected using an elliptical spot with major and minor axis lengths of 2 and 1 mm, respectively, and 160 eV pass energy with a step of 0.33 eV. CasaXPS software (VAMAS) was used to interpret high-resolution spectra. All spectra were internally calibrated to the C 1s emission (284.8 eV). After calibration, a Shirley-type background was applied to remove most of the extrinsic loss structure.

For transistor characterization transfer curves ( $I_{SD}$  vs  $V_G$ ,  $V_D = -0.8$  V) were recorded by sweeping the gate voltage, applied to the gate-electrode immersed in deionized water, between 0.8 and  $-0.8$  V with a sweep rate of 0.001 V s<sup>-1</sup>, using a Keithley source meter (System 2636A). Output curves ( $I_{SD}$  vs  $V_D$ ) were recorded by sweeping the drain voltage from 0 to  $-0.8$  V at constant gate voltage values ( $V_G = 0$  to  $-0.8$  V).

**Syntheses and Procedures:** Synthesis of calcium silicide (CaSi<sub>2</sub>) was achieved using a modified literature procedure.<sup>[49]</sup> Briefly, a stoichiometric mixture of calcium (Alfa Aesar, 99.5%) and silicon (Wacker, 99.99%) metals was pressed into a pellet and subsequently melted using an arc furnace housed within an argon-filled glove box. To ensure homogenization, the resulting silver, metallic regulus was melted from both sides, ground thoroughly in an agate mortar, pressed into a pellet, melted from both sides in the arc furnace, and ground to a coarse powder again.

Synthesis of layered polysilanes via chemical exfoliation was performed as described previously.<sup>[49]</sup> Concentrated aqueous HCl (100 mL) was cooled to  $-25$  °C in a Schlenk flask. Subsequently 1.00 g of CaSi<sub>2</sub> was added under argon and the mixture was stirred at  $-25$  °C for 7 d. The reaction mixture was then transferred to another Schlenk flask via cannula and subsequently filtered through a Schlenk-frit. The yellow filter cake was washed with dry, degassed acetone, and dried under vacuum (10<sup>-2</sup> mbar). The resulting exfoliated layered polysilanes (Si<sub>6</sub>H<sub>6</sub>)<sub>n</sub> were stored under argon in a glove box.

**Etching of Silicon Nanosheets:** 30.0 mg of the yellow (Si<sub>6</sub>H<sub>6</sub>)<sub>n</sub> sheets was dispersed in ethanol and placed into an ultrasonic bath for 1 min. Then 2 mL of water followed by 0.25 mL of aqueous HF (48%) (Caution: HF is highly dangerous and must be handled with extreme care) was added;

the mixture was immediately extracted with  $3 \times 5$  mL dichloromethane and the crude product mixture was placed in polytetrafluoroethylene (PTFE) centrifuge tubes. Toluene (40 mL) was added to the suspension and the SiNSs were isolated by centrifugation (9000 rpm per 5 min). The supernatant was discarded and the SiNSs were redispersed in 2 mL of dry acetone. After centrifugation the SiNSs (15 mg) were dispersed in 2 mL of dry toluene for use in further reactions.

Functionalization of SiNSs with alkenes and alkynes was achieved by transferring 2 mL of the dispersion of hydrogen-terminated SiNSs in dry, degassed toluene (15 mg exfoliated  $(\text{Si}_6\text{H}_6)_n$ ) into a baked out ( $\approx 300$  °C) Schlenk tube and 3.00 mmol of the substrate in question was added. The reaction mixture was degassed via three freeze-pump-thaw cycles and 0.02 mmol of the corresponding Lewis acid (0.1 M in toluene) was added under argon. After stirring for 4 h at room temperature the mixture was transferred to a centrifuge tube, mixed with 3 mL of ethanol, and centrifuged (9000 rpm for 4 min). After discarding the transparent colorless supernatant, the yellow residue was twice redispersed in a minimal amount of toluene and precipitated with 2 mL of methanol. The functionalized SiNSs were then redispersed in toluene or freeze dried from benzene.

**SiNS-C<sub>12</sub>H<sub>25</sub>/P3HT Blend Preparation:** A 1 wt% poly(3-hexylthiophene-2,5-diyl) (P3HT, Rieke Metals) solution was prepared in anhydrous 1,2-dichlorobenzene (1,2-DCB, VWR) and stirred at 60 °C for 10 min and then at room temperature for an additional 12 h. For comparison, a blend was prepared by adding P3HT (50–70 kg mol<sup>-1</sup>, 1 wt%) to a dispersion of SiNS-C<sub>12</sub>H<sub>25</sub> in 1,2-DCB (1 wt%) under argon, aiming for a resulting blend of 1:1 ratio.

**Device Fabrication:** Prior to the deposition of the P3HT and P3HT/SiNS-C<sub>12</sub>H<sub>25</sub> blend films, substrates with bearing predefined interdigitated electrode (IDE) structures (5 nm chromium, 40 nm gold, channel length 50 mm, W/L  $\frac{1}{4}$  900) were exposed to an argon plasma (0.4 bar, 70%, 5 min) and then oxygen plasma (0.3 bar, 50%, 60 s). The prepared solutions were spin-coated (1500 rpm, 90 s) onto the substrate (Si<sup>++</sup>/SiO<sub>2</sub>) in a glove box and dried at 125 °C for 10 min. The resulting polymer film was  $\approx 50$ –70 nm thick. The potential (0.464 V) of the Pt quasireference electrode was measured against an Ag/AgCl (sat. KCl) reference electrode in DI water (18.2 MΩ cm). The resistance between the reference and Pt electrode was 2650 Ω.

## Supporting Information

Supporting Information is available from the Wiley Online Library or from the author.

## Acknowledgements

T.H. and A.L. contributed equally to this work. The authors thank J. Schwämmlein for his help with electrochemical measurements. M. Knaus, A. Angi, V. Bhatt, and K. Melzer are thanked for their help and fruitful discussions. R. Csiki's help with XPS measurements is greatly appreciated. The authors thank the DFG and the NSERC for financial support of the Alberta/Technische Universität München Graduate School for Functional Hybrid Materials ATUMS (IRTG2022, NSERC CREATE) as well as the TUM Graduate School and IGSE. T.H. and L.M.S. are thankful for their fellowship from Studienstiftung des deutschen Volkes. L.M.S. gratefully acknowledges the funding from the Fonds der Chemischen Industrie.

Received: December 22, 2016

Revised: February 8, 2017

Published online:

- [1] M. Ezawa, G. Le Lay, *New J. Phys.* **2015**, *17*, 90201.
- [2] G. Fiori, F. Bonaccorso, G. Iannaccone, T. Palacios, D. Neumaier, A. Seabaugh, S. K. Banerjee, L. Colombo, *Nat. Nanotechnol.* **2014**, *9*, 768.
- [3] N. J. Roome, J. D. Carey, *ACS Appl. Mater. Interfaces* **2014**, *6*, 7743.
- [4] R. W. Zhang, C. W. Zhang, W. X. Ji, S. J. Hu, S. S. Yan, S. S. Li, P. Li, P. J. Wang, Y. S. Liu, *J. Phys. Chem. C* **2014**, *118*, 25278.
- [5] B. L. Li, J. Wang, H. L. Zou, S. Garaj, C. T. Lim, J. Xie, N. B. Li, D. T. Leong, *Adv. Funct. Mater.* **2016**, *26*, 7034.
- [6] S. Ida, *Bull. Chem. Soc. Jpn.* **2015**, *88*, 1619.
- [7] D. Deng, K. S. Novoselov, Q. Fu, N. Zheng, Z. Tian, X. Bao, *Nat. Nanotechnol.* **2016**, *11*, 218.
- [8] P. Avouris, F. Xia, *MRS Bull.* **2012**, *37*, 1225.
- [9] G. Le Lay, *Nat. Nanotechnol.* **2015**, *10*, 1.
- [10] C. Grazianetti, E. Cinquanta, A. Molle, *2D Mater.* **2016**, *3*, 12001.
- [11] A. Kara, H. Enriquez, A. P. Seitsonen, L. C. Lew Yan Voon, S. Vizzini, B. Aufray, H. Oughaddou, *Surf. Sci. Rep.* **2012**, *67*, 1.
- [12] M. Houssa, A. Dimoulas, A. Molle, *J. Phys.: Condens. Matter* **2015**, *27*, 253002.
- [13] J. Zhuang, X. Xu, H. Feng, Z. Li, X. Wang, Y. Du, *Sci. Bull.* **2015**, *60*, 1551.
- [14] X. Lin, J. Ni, *J. Appl. Phys.* **2015**, *117*, 164305.
- [15] C. Zhang, A. De Sarkar, R. Q. Zhang, *J. Phys. Chem. C* **2011**, *115*, 23682.
- [16] N. Gao, W. T. Zheng, Q. Jiang, *Phys. Chem. Chem. Phys.* **2012**, *14*, 257.
- [17] P. Vogt, P. De Padova, C. Quaresima, J. Avila, E. Frantzeskakis, M. C. Asensio, A. Resta, B. Ealet, G. Le Lay, *Phys. Rev. Lett.* **2012**, *108*, 155501.
- [18] C. L. Lin, R. Arafune, K. Kawahara, N. Tsukahara, E. Minamitani, Y. Kim, N. Takagi, M. Kawai, *Appl. Phys. Express* **2012**, *5*, 45802.
- [19] A. Fleurence, R. Friedlein, T. Ozaki, H. Kawai, Y. Wang, Y. Yamada-Takamura, *Phys. Rev. Lett.* **2012**, *108*, 245501.
- [20] L. Meng, Y. Wang, L. Zhang, S. Du, R. Wu, L. Li, Y. Zhang, G. Li, H. Zhou, W. a. Hofer, H.-J. Gao, *Nano Lett.* **2013**, *13*, 685.
- [21] Z. Ni, H. Zhong, X. Jiang, R. Quhe, G. Luo, Y. Wang, M. Ye, J. Yang, J. Shi, J. Lu, *Nanoscale* **2014**, *6*, 7609.
- [22] L. Tao, E. Cinquanta, D. Chiappe, C. Grazianetti, M. Fanciulli, M. Dubey, A. Molle, D. Akinwande, *Nat. Nanotechnol.* **2015**, *10*, 227.
- [23] E. Scalise, E. Cinquanta, M. Houssa, B. Van Den Broek, D. Chiappe, C. Grazianetti, G. Pourtois, B. Ealet, A. Molle, M. Fanciulli, V. V. Afanas'Ev, A. Stesmans, *Appl. Surf. Sci.* **2014**, *291*, 113.
- [24] H. Nakano, T. Ikuno, *Appl. Phys. Rev.* **2016**, *3*, 40803.
- [25] H. Okamoto, Y. Sugiyama, H. Nakano, *Chem.-Eur. J.* **2011**, *17*, 9864.
- [26] O. Böhm, J. Hassel, *Z. Anorg. Allg. Chem.* **1927**, *160*, 152.
- [27] S. Yamanaka, H. Matsu-ura, M. Ishikawa, *Mater. Res. Bull.* **1996**, *31*, 307.
- [28] H. Nakano, T. Mitsuoka, M. Harada, K. Horibuchi, H. Nozaki, N. Takahashi, T. Nonaka, Y. Seno, H. Nakamura, *Angew. Chem.* **2006**, *118*, 6451.
- [29] Q. Wu, X. Wang, T. A. Niehaus, R. Zhang, *Phys. Chem. C* **2014**, *118*, 20070.
- [30] F. Zheng, C. Zhang, *Nanoscale Res. Lett.* **2012**, *7*, 422.
- [31] Y. Kumai, S. Shirai, E. Sudo, J. Seki, H. Okamoto, Y. Sugiyama, H. Nakano, *J. Power Sources* **2011**, *196*, 1503.
- [32] Y. Kumai, H. Kadoura, E. Sudo, M. Iwaki, H. Okamoto, Y. Sugiyama, H. Nakano, *J. Mater. Chem.* **2011**, *21*, 11941.
- [33] Y. Kumai, H. Nakano, *Jpn. J. Appl. Phys.* **2015**, *54*, 35201.
- [34] H. Nakano, Y. Sugiyama, T. Morishita, M. J. S. Spencer, I. K. Snook, Y. Kumai, H. Okamoto, *J. Mater. Chem. A* **2014**, *2*, 7588.
- [35] S. Jiang, M. Q. Arguilla, N. D. Cultrara, J. E. Goldberger, *Acc. Chem. Res.* **2015**, *48*, 144.
- [36] S. W. Kim, J. Lee, J. H. Sung, D. Seo, I. Kim, M.-H. Jo, B. W. Kwon, W. K. Choi, H.-J. Choi, *ACS Nano* **2014**, *8*, 6556.
- [37] J. M. Buriak, M. P. Stewart, T. W. Geders, M. J. Allen, H. C. Choi, J. Smith, D. Raftery, L. T. Canham, *J. Am. Chem. Soc.* **1999**, *121*, 11491.

- [38] M. R. Linford, C. E. D. Chidsey, *J. Am. Chem. Soc.* **1993**, *115*, 12631.
- [39] J. Buriak, *J. Assoc. Lab. Autom.* **1999**, *4*, 36.
- [40] J. Zou, R. K. Baldwin, K. a. Pettigrew, S. M. Kauzlarich, *Nano Lett.* **2004**, *4*, 1181.
- [41] M. Dasog, G. B. De los Reyes, L. V. Titova, F. A. Hegmann, J. G. C. Veinot, *ACS Nano* **2014**, *8*, 9636.
- [42] M. Dasog, G. B. De, L. V. Titova, F. A. Hegmann, J. G. C. Veinot, G. B. De Los Reyes, L. V. Titova, F. A. Hegmann, J. G. C. Veinot, *ACS Nano* **2014**, *8*, 9636.
- [43] M. R. Linford, P. Fenter, P. M. Eisenberger, C. E. D. Chidsey, *J. Am. Chem. Soc.* **1995**, *117*, 3145.
- [44] R. L. Cicero, M. R. Linford, C. E. D. Chidsey, *Langmuir* **2000**, *16*, 5688.
- [45] J. M. Buriak, *Chem. Rev.* **2002**, *102*, 1271.
- [46] J. a Kelly, A. M. Shukaliak, M. D. Fleischauer, J. G. C. Veinot, *J. Am. Chem. Soc.* **2011**, *133*, 9564.
- [47] Z. Yang, M. Iqbal, A. R. Dobbie, J. G. C. Veinot, *J. Am. Chem. Soc.* **2013**, *135*, 17595.
- [48] I. M. D. Höhle, J. Kehrle, T. Helbich, Z. Yang, J. G. C. Veinot, B. Rieger, *Chem.-Eur. J.* **2014**, *20*, 4212.
- [49] T. Helbich, A. Lyuleeva, I. M. D. Höhle, P. Marx, L. M. Scherf, J. Kehrle, T. F. Fässler, P. Lugli, B. Rieger, *Chem.-Eur. J.* **2016**, *22*, 6194.
- [50] H. Okamoto, Y. Kumai, Y. Sugiyama, T. Mitsuoka, K. Nakanishi, T. Ohta, H. Nozaki, S. Yamaguchi, S. Shirai, H. Nakano, *J. Am. Chem. Soc.* **2010**, *132*, 2710.
- [51] H. Okamoto, Y. Sugiyama, K. Nakanishi, T. Ohta, T. Mitsuoka, H. Nakano, *Chem. Mater.* **2015**, *27*, 1292.
- [52] Y. Sugiyama, H. Okamoto, T. Mitsuoka, T. Morikawa, K. Nakanishi, T. Ohta, H. Nakano, *J. Am. Chem. Soc.* **2010**, *132*, 5946.
- [53] H. Nakano, M. Nakano, K. Nakanishi, D. Tanaka, Y. Sugiyama, T. Ikuno, H. Okamoto, T. Ohta, *J. Am. Chem. Soc.* **2012**, *134*, 5452.
- [54] L. C. P. M. De Smet, H. Zuilhof, E. J. R. Sudhölter, L. H. Lie, A. Houlton, B. R. Horrocks, *J. Phys. Chem. B* **2005**, *109*, 12020.
- [55] J. M. Buriak, *Chem. Mater.* **2014**, *26*, 763.
- [56] Z. Yang, C. M. Gonzalez, T. K. Purkait, M. Iqbal, A. Meldrum, J. G. C. Veinot, *Langmuir* **2015**, *31*, 10540.
- [57] T. K. Purkait, M. Iqbal, M. H. Wahl, K. Gottschling, C. M. Gonzalez, M. A. Islam, J. G. C. Veinot, *J. Am. Chem. Soc.* **2014**, *136*, 17914.
- [58] M. P. Stewart, J. M. Buriak, *J. Am. Chem. Soc.* **2001**, *123*, 7821.
- [59] L. A. Huck, J. M. Buriak, *J. Am. Chem. Soc.* **2012**, *134*, 489.
- [60] J. M. Schmeltzer, L. a. Porter, M. P. Stewart, J. M. Buriak, *Langmuir* **2002**, *18*, 2971.
- [61] Q.-Y. Sun, L. C. P. M. de Smet, B. van Lagen, M. Giesbers, P. C. Thüne, J. van Engelenburg, F. A. de Wolf, H. Zuilhof, E. J. R. Sudhölter, *J. Am. Chem. Soc.* **2005**, *127*, 2514.
- [62] T. Helbich, A. Lyuleeva, T. Ludwig, L. M. Scherf, T. F. Fässler, P. Lugli, B. Rieger, *Adv. Funct. Mater.* **2016**, *26*, 6711.
- [63] J. M. Holland, M. P. Stewart, M. J. Allen, J. M. Buriak, *J. Solid State Chem.* **1999**, *147*, 251.
- [64] J. M. Lambert, *J. Biomed. Mater. Res., Part B* **2006**, *78B*, 167.
- [65] T. Sudo, N. Asao, *J. Org. Chem.* **1999**, *8*, 2494.
- [66] M. Rubin, T. Schwier, V. Gevorgyan, *J. Org. Chem.* **2002**, *67*, 1936.
- [67] K. Oertle, H. Wetter, *Tetrahedron Lett.* **1985**, *26*, 5511.
- [68] M. Pérez, L. J. Hounjet, C. B. Caputo, R. Dobrovetsky, D. W. Stephan, *J. Am. Chem. Soc.* **2013**, *135*, 18308.
- [69] J. M. Buriak, M. J. Allen, *J. Am. Chem. Soc.* **1998**, *120*, 1339.
- [70] Z. J. Lesnikowski, in *Boron Science: New Technologies and Applications* (Ed: N. S. Hosmane), CRC Press, Boca Raton, FL **2012**.
- [71] K. Melzer, A. M. Münzer, E. Jaworska, K. Maksymiuk, A. Michalska, G. Scarpa, *Org. Electron.* **2014**, *15*, 595.
- [72] K. Melzer, M. Brändlein, B. Popescu, D. Popescu, P. Lugli, G. Scarpa, *Faraday Discuss.* **2014**, *174*, 399.
- [73] K. Melzer, V. D. Bhatt, T. Schuster, E. Jaworska, K. Maksymiuk, A. Michalska, P. Lugli, G. Scarpa, *IEEE Sens. J.* **2015**, *15*, 3127.
- [74] J. B. Lambert, Y. Zhao, H. Wu, *J. Org. Chem.* **1999**, *64*, 2729.
- [75] N. Asao, T. Sudo, Y. Yamamoto, *J. Org. Chem.* **1996**, *61*, 7654.
- [76] J. B. Lambert, Y. Zhao, H. Wu, *J. Org. Chem.* **1999**, *64*, 2729.
- [77] I. Fleming, J. Dunoguès, R. Smithers, *Organic Reactions*, WILEY-VCH, Weinheim **2004**, pp. 57–575.
- [78] C. N. Pillai, *Textbook of Organic Chemistry*, CRC Press, Hyderabad, India **2012**.
- [79] A. M. Münzer, K. Melzer, M. Heimgreiter, G. Scarpa, *Biochim. Biophys. Acta, Gen. Subj.* **2013**, *1830*, 4353.
- [80] J. Huang, D. R. Hines, B. J. Jung, M. S. Bronsgeest, A. Tunnell, V. Ballarotto, H. E. Katz, M. S. Fuhrer, E. D. Williams, J. Cumings, *Org. Electron.* **2011**, *12*, 1471.
- [81] L. Kergoat, N. Battaglini, L. Miozzo, B. Piro, M. C. Pham, A. Yassar, G. Horowitz, *Org. Electron. Phys., Mater. Appl.* **2011**, *12*, 1253.
- [82] X. Z. Bo, C. Y. Lee, M. S. Strano, M. Goldfinger, C. Nuckolls, G. B. Blanchet, *Appl. Phys. Lett.* **2005**, *86*, 182102.
- [83] L. H. Hess, M. V. Hauf, M. Seifert, F. Speck, T. Seyller, M. Stutzmann, I. D. Sharp, J. A. Garrido, *Appl. Phys. Lett.* **2011**, *99*, 33503.

Copyright WILEY-VCH Verlag GmbH & Co. KGaA, 69469 Weinheim, Germany, 2017.

# ADVANCED FUNCTIONAL MATERIALS

## Supporting Information

for *Adv. Funct. Mater.*, DOI: 10.1002/adfm.201606764

Lewis Acid Induced Functionalization of Photoluminescent  
2D Silicon Nanosheets for the Fabrication of Functional  
Hybrid Films

*Tobias Helbich, Alina Lyuleeva, Philipp Marx, Lavinia M.  
Scherf, Tapas K. Purkait, Thomas F. Fässler, Paolo Lugli,  
Jonathan G. C. Veinot,\* and Bernhard Rieger\**

Copyright WILEY-VCH Verlag GmbH & Co. KGaA, 69469 Weinheim, Germany, 2016.

## Supporting Information

### **Lewis Acid Induced Functionalization of Photoluminescent Two-Dimensional Silicon Nanosheets**

*Tobias Helbich,<sup>□</sup> Alina Lyuleeva,<sup>□</sup> Philipp Marx, Lavinia M. Scherf, Tapas K. Purkait  
Thomas F. Fässler, Jonathan G. C. Veinôt, Paolo Lugli and Bernhard Rieger\**

#### **Contents**

IR Measurements.....	2
Lewis Acidity Considerations.....	3
TGA Measurements .....	4
XPS Measurements .....	6
References .....	8

## IR Measurements

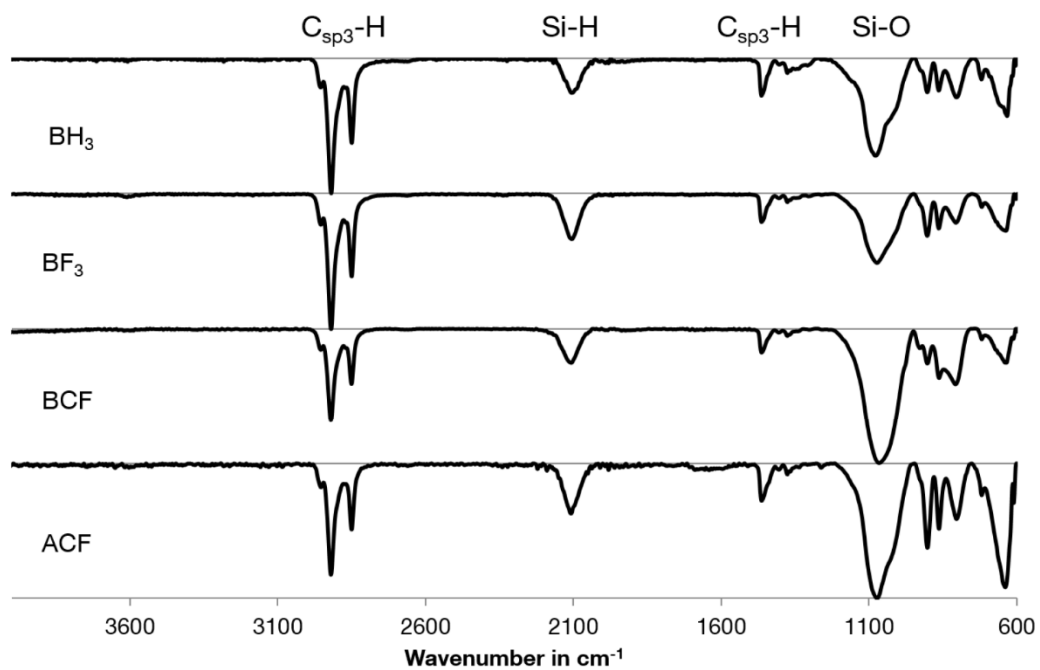


**Figure S1.** IR Spectra of dodecene functionalized SiNSs catalyzed by different *Lewis* acids (reaction time 4 h).

## Lewis Acidity Considerations

Several approaches have been used to quantify the relative acidity of *Lewis* acids. Amongst them is the length of the C=O bond in carbonyl-*Lewis* acid adducts, equilibrium constants of reactions of weak with strong *Lewis* acids, as well as dissociation enthalpies of donor-acceptor complexes.<sup>[1-3]</sup>

Another concept deals with the fluoride ion affinity (FIA), which combines the released energy upon binding of F<sup>-</sup> and the strength of a *Lewis* acid<sup>[4,5]</sup> and is now seen as a reliable measure. Krossing and Co-workers did not determine the FIA values for the borane based system, but ab different initio calculations show that BH<sub>3</sub> is a stronger *Lewis* acid than BF<sub>3</sub>.<sup>[6]</sup>

In another approach NMR measurements of *Lewis* acid-base adducts are used to determine the relative acidity.<sup>[7]</sup> As such the Gutmann-Beckett method is based on the change in chemical shift of the <sup>31</sup>P signal of the Et<sub>3</sub>PO-LA adduct.<sup>[8-10]</sup>

**Table S1.** Used *Lewis* acids and their corresponding fluoride complexes with their FIA<sup>[5]</sup> values and acceptor number.<sup>[7]</sup>

<i>Lewis</i> acid/anion	FIA [kJ/mol]	<i>Lewis</i> acid	AN*
BF <sub>3</sub> /[BF <sub>4</sub> ] <sup>-</sup>	338	BF <sub>3</sub>	84.0
BH <sub>3</sub> /[FBH <sub>3</sub> ] <sup>-</sup>	n/a	BH <sub>3</sub>	93.0
B(C <sub>6</sub> F <sub>5</sub> ) <sub>3</sub> /[FB(C <sub>6</sub> F <sub>5</sub> ) <sub>3</sub> ] <sup>-</sup>	444	B(C <sub>6</sub> F <sub>5</sub> ) <sub>3</sub>	78.1
Al(C <sub>6</sub> F <sub>5</sub> ) <sub>3</sub> /[FAl(C <sub>6</sub> F <sub>5</sub> ) <sub>3</sub> ] <sup>-</sup>	530	Al(C <sub>6</sub> F <sub>5</sub> ) <sub>3</sub>	n/a

Gutmann-Beckett method: \*AN = 2.21 × (δ<sup>31</sup> LA·Et<sub>3</sub>PO - 41)

For many *Lewis* acids compared by NMR spectroscopy it can clearly be seen, that the electron withdrawing character and the steric demand of the ligands around the metal center play a crucial role for the *Lewis* acidity.<sup>[6]</sup>

As can be seen in **Table S1**, the acidity scale based on FIA values results in the following order: BF<sub>3</sub> < B(C<sub>6</sub>F<sub>5</sub>)<sub>3</sub> < Al(C<sub>6</sub>F<sub>5</sub>)<sub>3</sub>. BF<sub>3</sub> relative to the other boranes exhibits a smaller acidity due to the charge donation from the fluorine lone pairs into the empty boron p-orbital.<sup>[6]</sup> The coordinating F<sup>-</sup> ion is very small and thus not as susceptible to the steric demand of the *Lewis* acid. Thus the bigger steric demand of the pentafluorophenyl groups on the FIA scale does not influence the acidity as much as in the Gutmann-Beckett scale. In case of the adduct of Et<sub>3</sub>PO-BR<sub>3</sub>, the steric demand plays a much bigger role, leading to a changed acidity: B(C<sub>6</sub>F<sub>5</sub>)<sub>3</sub> < BF<sub>3</sub> < BH<sub>3</sub>.

Functionalization reactions of silicon (nano)materials are executed at the surface and thus very prone to the steric demand of the *Lewis* acid. As such, besides the stronger acidity of ACF and BCF (according to the FIA scale), the smaller *Lewis* acids BF<sub>3</sub> and BH<sub>3</sub> lead to more efficient surface coverages (in accordance with the Gutmann-Beckett scale; see **Table S2**).

## TGA Measurements

To study the influence of the *Lewis* acid, TGA measurements were executed with the dodecene functionalized SiNSs. The weight loss enables the comparison of the organic content of the hybrid materials. The tables show the ratio of weight loss/molecular weight of the attached organic substrates to get comparable values of how many molecules are on the surface.

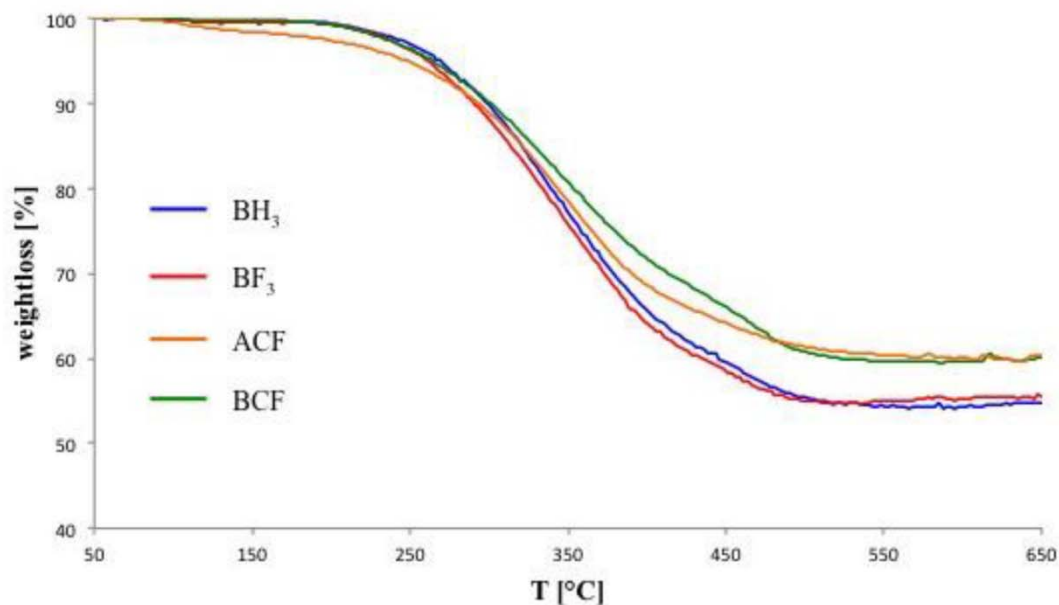


**Figure S2.** TGA measurements of 1-dodecene functionalized SiNSs with different Lewis acids as catalyst.

**Table S2.** TG data from 1-dodecene functionalized SiNSs with different *Lewis* acids as catalyst and normalized weight loss.

<i>Lewis Acid</i>	Weight loss [%]	weight loss/molecular weight (1-dodecene)
BH <sub>3</sub>	47.32	0.28
BF <sub>3</sub>	47.04	0.28
BCF	41.46	0.25
ACF	42.98	0.26

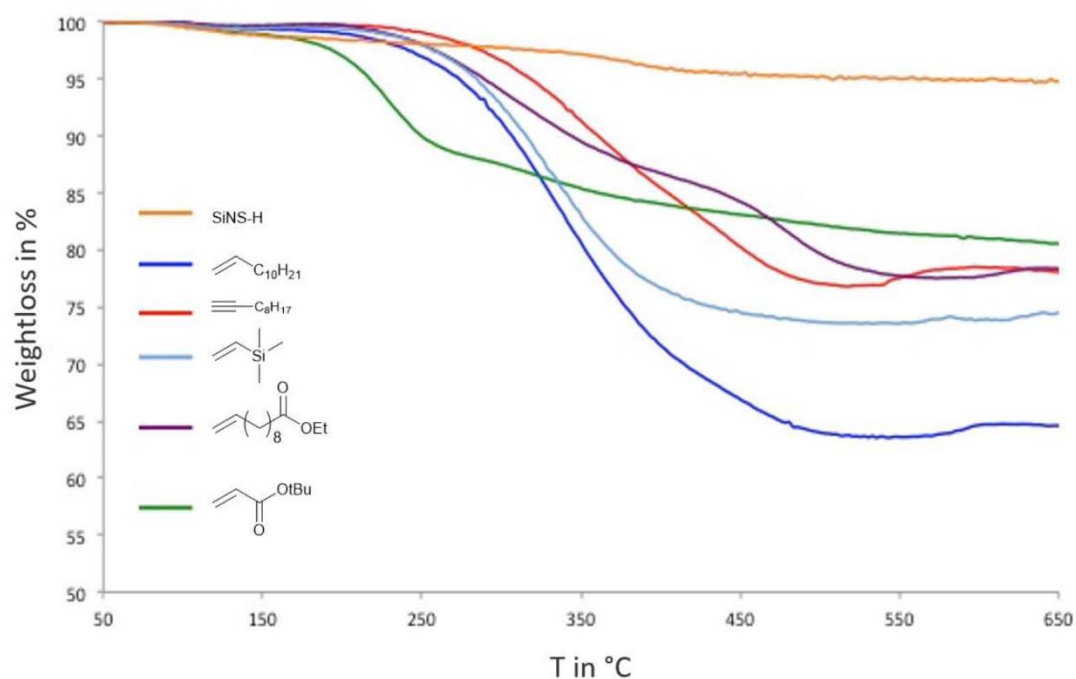


**Figure S3.** TGA measurements of unfunctionalized and functionalized SiNSs.

**Table S3.** TGA data from functionalized SiNSs.

Reagent	Weightloss [%]	Molecular weight [g/mol]	Weightloss/molecular weight
1-Dodecene	42.22	169.32	0.25
1-Decyne	20.05	139.25	0.14
Trimethylvinylsilane	29.94	101.23	0.30
Ethyl-10-undecenoate	36.06	213.33	0.17
tBuMA	27.63	143.20	0.19

## XPS Measurements

### Hydride terminated SiNSs-H

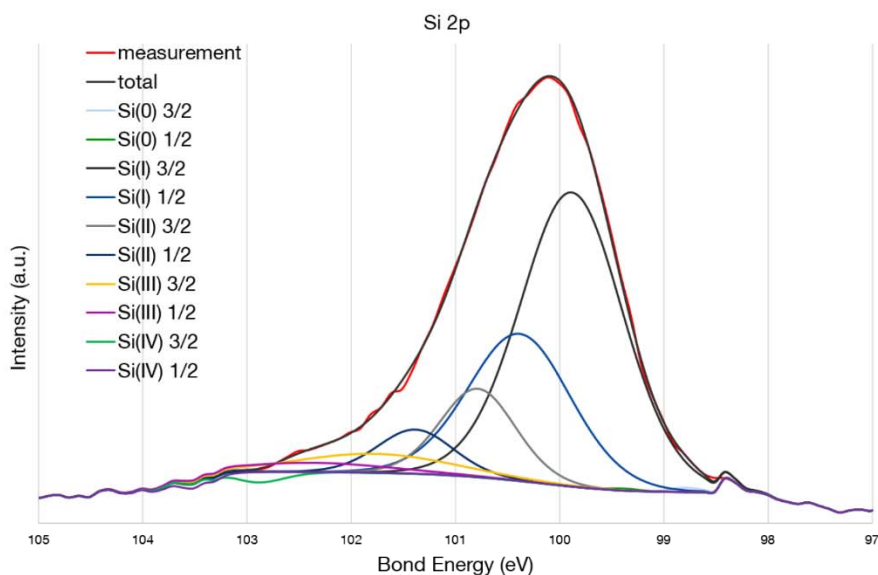
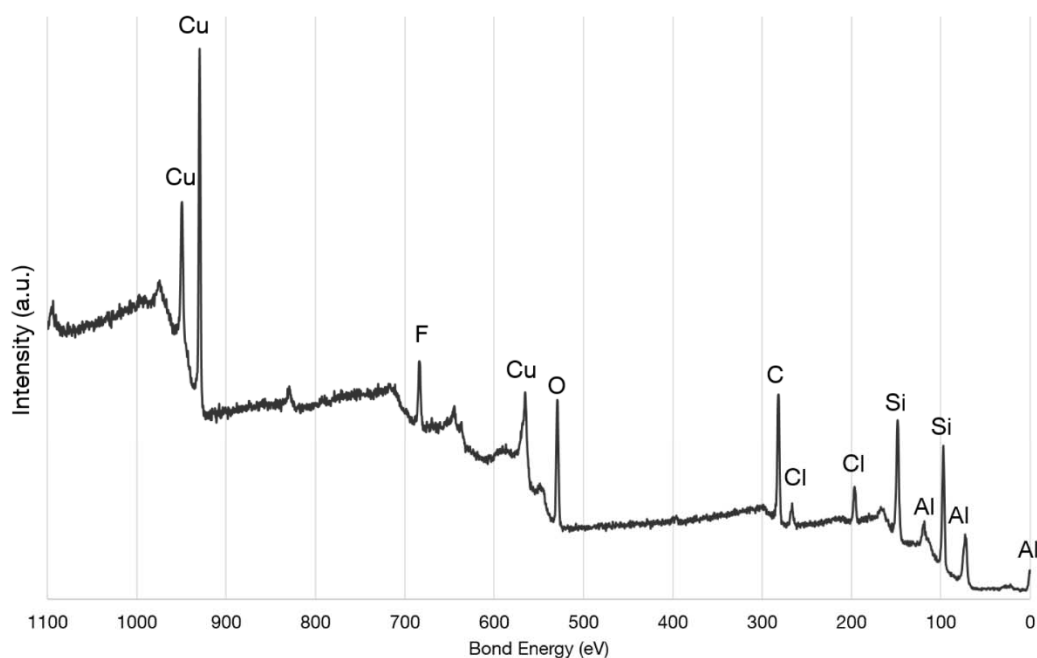


**Figure S4.** High resolution XP spectrum of 2p region of freshly etched SiNSs-H and fitted peaks show mostly Si(I).



29

**Figure S5.** Survey XP spectrum of hydride terminated SiNSs-H. Cu and Al arise from the sample substrate and holder. Cl and C can be solvent residues or minor impurities from the synthesis. Minor F residues are mostly found in XP spectra of HF treated nanocrystalline silicon samples. Si:F = 10.38.

### SiNS-H after $\text{BF}_3$ Treatment

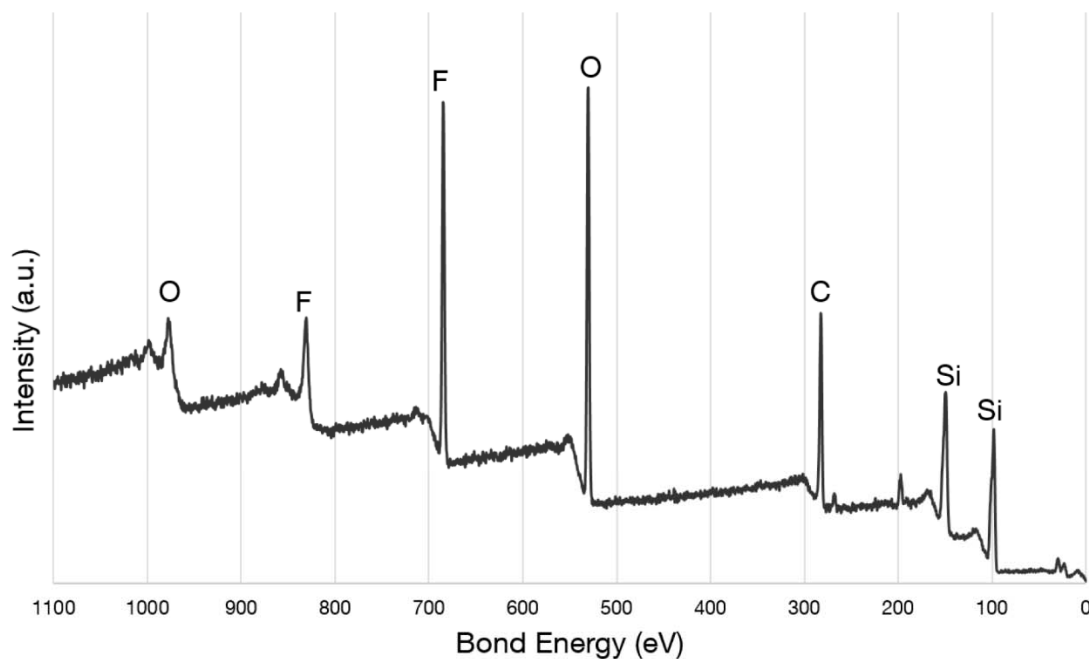


**Figure S6.** Survey XP spectrum of hydride terminated after treating with excess of  $\text{BF}_3$ . C residues arise from adsorption of organic compounds; O might arise from oxidation due to the higher reactivity of the Si-F surface. Si:F = 3.21.

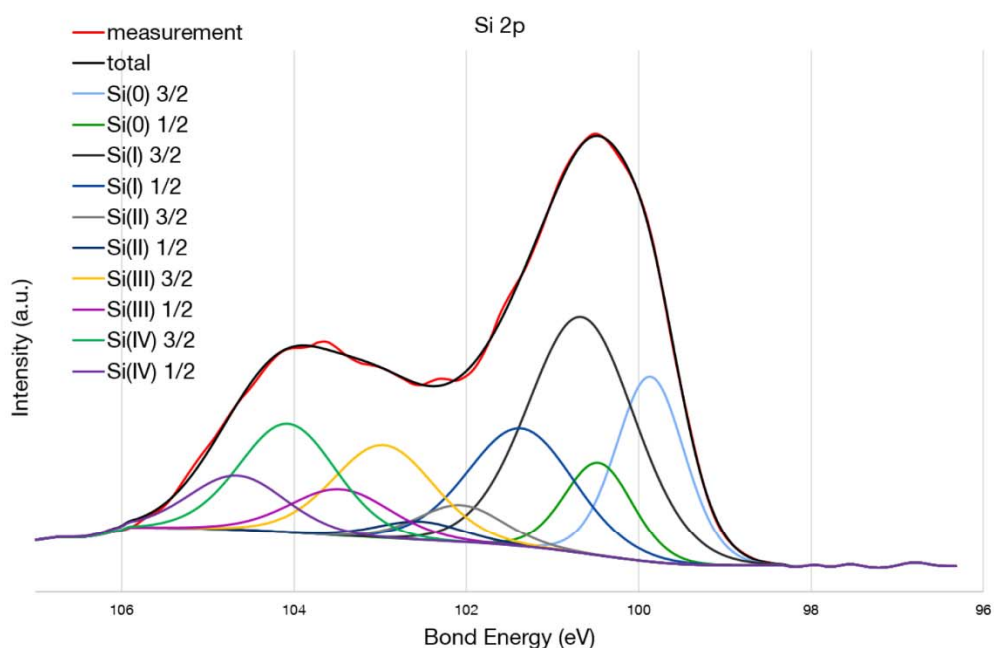


**Figure S7.** High resolution XP spectrum of 2p region of SiNS-H after stirring with excess of  $\text{BF}_3$  for 4 h under inert gas and fitted peaks. Compared to the freshly etched sample higher oxidized Si species appear due to the formation of the silylium species.

## References

- [1] A. Corma, H. García, *Chem. Rev.*, **2003**, *103*, 4307 – 4365.
- [2] I. Wharf; D. F. Shriver, *J. Inorg. Nucl. Chem.* **1970**, *32*, 1831.
- [3] A. Haaland, *Angew. Chem.* **1989**, *101*, 1017-1032.
- [4] T. E. Mallouk, G. L. Rosenthal, G. Mueller, R. Brusasco, N. Barlett, *Inorg. Chem.* **1984**, *23*, 3167-3173.
- [5] L. O. Müller, D. Himmerl, J. Stauffer, G. Steinfeld, J. Slattery, G. Santiso-Quiñones, V. Brecht, I. Krossing, *Angew. Chem. Int. Ed.* **2008**, *47*, 7659 –7663.
- [6] I. B. Sivaev, V. I. Bregadze, *Coordination Chemistry Reviews* **2014**, *270–271*, 75–88.
- [7] N. J. Fitzpatrick, M. O. Fanning, *Journal of Molecular Structure* **1978**, *50*, 127 – 132.
- [8] V. Gutmann, *Coord. Chem. Rev.* **1976**, *18*, 225–255.
- [9] M. A. Beckett, G. C. Strickland, J. R. Holland, K. S. Varma, *Polym. Commun.* **1996** *37*, 4629–4631.
- [10] M. Jakubczyk, A. Adamczyk-Wozniak, A. Sporzynski, *Molecular Receptors*, East Publisher House, Donetsk, **2011**, pp. 53-68.

## 7. Diaryl Iodonium Salts as Hydrosilylation Initiators for the Surface Functionalization of Silicon Nanomaterials and their Collaborative Effect as Ring Opening Polymerization Initiator

<b>Status</b>	Accepted Manuscript on 18 May 2017
<b>Journal</b>	Nanoscale
<b>Publisher</b>	RSC Publishing
<b>DOI</b>	10.1039/C7NR01559C
<b>Authors</b>	Tobias Helbich <sup>‡</sup> , Marc J. Kloberg <sup>‡</sup> , Regina Sinelnikov, Alina Lyuleeva, Jonathan G. C. Veinot, Bernhard Rieger <sup>§</sup>

<sup>‡</sup>these authors contributed equally.

T. Helbich, M. J. Kloberg, R. Sinelnikov, A. Lyuleeva, J. Veinot and B. Rieger, *Nanoscale*, **2017**, Accepted Manuscript - Reproduced by permission from the Royal Chemical Society.

### Content:

Since diazonium salts were found to initiate hydrosilylation on SiNCs, the method became one of the most important surface modification methods in our group. The chemical similarity of iodonium salts and their use in grafting experiments on silicon wafers hence motivated us to look into their properties as initiators for silicon nanomaterial surface functionalization.

In this work, the potential of diaryliodonium salts in hydrosilylation reactions on the surface of silicon nanosheets as well as silicon nanocrystals of different sizes is examined. A variety of different functional substrates can be used to stabilize the surface of the photoluminescent materials. Additionally, the combination of hydride terminated silicon nanomaterials with diaryliodonium salts was found to initiate cationic ring opening polymerization, demonstrating the potential of silicon based nanomaterials as coinitiators and enabling a mild, straight forward reaction method.

© 2016 RSC Publishing, Cambridge.

---

<sup>§</sup> T. Helbich defined the project, executed the necessary experiments to do so and wrote the manuscript; M. Kloberg, with the support of T. Helbich planned and executed the majority of experiments; A. Lyuleeva contributed with AFM measurements; all work was performed under the supervision of J. Veinot and B. Rieger.



Cite this: DOI: 10.1039/c7nr01559c

Received 3rd March 2017,  
Accepted 16th May 2017

DOI: 10.1039/c7nr01559c  
rsc.li/nanoscale

## Diaryliodonium salts as hydrosilylation initiators for the surface functionalization of silicon nanomaterials and their collaborative effect as ring opening polymerization initiators†

T. Helbich,<sup>‡a</sup> M. J. Kloberg,<sup>‡a</sup> R. Sinelnikov,<sup>b</sup> A. Lyuleeva,<sup>c</sup> J. G. C. Veinot<sup>b</sup> and B. Rieger<sup>†a</sup>

**Diaryliodonium salts were found to initiate hydrosilylation reactions on the surface of silicon nanosheets as well as silicon nanocrystals of different sizes. A variety of different functional substrates can be used to stabilize the surface of the photoluminescent materials. Additionally, the combination of hydride terminated silicon nanomaterials with diaryliodonium salts was found to initiate cationic ring opening polymerization, demonstrating the potential of silicon based nanomaterials as coinitiators and enabling a mild, straightforward reaction method.**

Nanomaterials exhibit some very different properties compared to their bulk or molecular counterparts. For example they show different reactivities,<sup>1,2</sup> a size dependent photoluminescence (PL) and band gap,<sup>3–5</sup> as well as tunable absorption properties.<sup>6</sup> These characteristics open up a vast field of applications in sensing,<sup>7–9</sup> photovoltaic,<sup>10–13</sup> light emitting diodes (LED),<sup>14,15</sup> lithium ion batteries,<sup>16</sup> bioimaging<sup>17–21</sup> and catalysis.<sup>22,23</sup>

Especially for electronic applications, silicon based nanomaterials (SiNMs) are the material of choice and central to nanotechnology research, as current information technology is based on silicon. Additionally, silicon is abundant, biocompatible and exhibits a purported low toxicity, especially when compared to conventional nanodots such as CdSe and CdS.<sup>24</sup>

In this context, silicon nanocrystals (SiNCs) are among the most widely-explored materials.<sup>24,25</sup> Most syntheses render hydride terminated SiNCs, which are known to oxidize under

ambient conditions due to the strong oxophilicity of silicon.<sup>5,26,27</sup> But the reactive Si–H bond can be used to functionalize the SiNC surface *via* hydrosilylation with unsaturated (functional) organic compounds. This leads to the stabilization of the SiNCs due to the formation of Si–C-bonds. The functionalized SiNCs are readily dispersible in various solvents and render stable, clear dispersions.<sup>1,24,25</sup>

A new and less well-examined nanostructured silicon-based material with a thickness in the nano regime and lateral sizes on the microscale are two-dimensional (2D) silicon nanosheets (SiNSs).<sup>27,28</sup> Two different SiNS types are known in literature. Silicene exhibits sp<sup>2</sup>-hybridized Si atoms and is as such the silicon analogue of graphene. It can be synthesized *via* the deposition of a silicon monolayer on substrates such as Ag (111),<sup>29,30</sup> ZrBr<sub>2</sub> (0001)<sup>31</sup> and Ir (111).<sup>32</sup> They exhibit ultra-high carrier mobilities<sup>33,34</sup> and have already found first applications in field effect transistor (FET) technology.<sup>35</sup> The hydrogenated and thus puckered, sp<sup>3</sup>-hybridized SiNSs-H are called silicenes (or layered polysilanes) and can be synthesized in a straight forward and scalable manner by deintercalation of Ca<sup>2+</sup> from CaSi<sub>2</sub>.<sup>27</sup> They are predicted to exhibit a (tunable) bandgap,<sup>36,37</sup> show green PL<sup>2,27</sup> and have already been investigated in applications such as lithium ion batteries,<sup>38–40</sup> photonic sensors<sup>9</sup> and FETs.<sup>41</sup> Like SiNCs, SiNSs-H surfaces can be functionalized with organic substrates. This surface modification improves their stability and dispersibility properties and enables further applications, as shown for sensing devices<sup>24</sup> with SiNSs, functionalized *via* hydrosilylation.<sup>2,42</sup>

Aryl diazonium salts were found to efficiently functionalize the surface of hydride terminated silicon wafers,<sup>43</sup> porous silicon,<sup>44</sup> SiNCs-H<sup>1</sup> and SiNSs-H<sup>2</sup> with different functional groups. For bulk silicon, electrochemical activation is necessary to directly graft the aryl groups of the diazonium compound on the surface,<sup>43</sup> while for nanostructured silicon, diazonium salts act as radical initiators for hydrosilylation reactions without any further activation.<sup>1,44</sup> For surface modification purposes, iodonium salts are by far less well-examined than diazonium salts, but can be used for surface grafting

<sup>a</sup>Catalysis Research Center/Wacker-Lehrstuhl für Makromolekulare Chemie, Technische Universität München, Lichtenbergstrasse 4, 85747 Garching, Germany. E-mail: rieger@tum.de

<sup>b</sup>Department of Chemistry, University of Alberta, 11227 Saskatchewan Drive, Edmonton, Alberta T6G 2G2, Canada

<sup>c</sup>Institute for Nanoelectronics, Technische Universität München, Arcisstrasse 21, 80333 Munich, Germany

†Electronic supplementary information (ESI) available: Experimental details, FTIR, NMR, EDX, DLS, GPC and TGA measurements. See DOI: 10.1039/c7nr01559c

‡These authors contributed equally.

## Communication

reactions on carbon<sup>45–50</sup> and gold.<sup>51,52</sup> Additionally, Dirk *et al.* successfully expanded this electrochemical grafting procedure to functionalize silicon hydride terminated surfaces.<sup>53</sup>

Apart from their use as grafting agents for surface modification, aryl iodonium salts are used in cationic (ring opening) polymerizations. After (mostly light induced) initiation, a cationic radical  $\text{ArI}^{+\cdot}$  is generated, which can subsequently initiate cationic as well as radical polymerization reactions.<sup>54,55</sup> Thus, a broad variety of monomers<sup>56</sup> (*e.g.* THF,<sup>55</sup> cyclohexene oxide, trioxane, epichlorohydrin, oxetane,  $\epsilon$ -caprolactone,<sup>56</sup> *etc.*) can be polymerized. For the polymerization to start, initiation is needed that leads to the formation of the cationic radicals. In general this formation is induced by UV light.

In this work we examine the diaryliodonium salt induced functionalization of hydride terminated SiNMs (3 and 5 nm SiNCs and SiNSs) towards different functional, unsaturated compounds (Fig. 1). Unfunctionalized, hydride terminated SiNCs are hydrophobic, but render turbid dispersions in organic solvents due to the formation of agglomerates. Once they are functionalized to a certain extent, the dispersions turn clear, so that a qualitative reaction control is easily feasible with SiNCs.<sup>1</sup> Due to their large surface area, SiNSs, even when functionalized, tend to agglomerate in concentrated dispersions. For this reason we first focus the following discussion on SiNCs and afterwards address SiNSs.

SiNCs were synthesized *via* the disproportionation of polymeric hydrogen silsesquioxane (HSQ) and the subsequent liberation of the hydride terminated SiNCs by etching with ethanolic HF solution. The functionalization reactions were executed in chloroform due to the solubility properties of the here used initiator; the commercially available bis(4-*tert*-butylphenyl)iodonium hexafluorophosphate (BIP).

Within minutes after the addition, the turbid reaction mixture turned clear, indicating that the surface of 3 nm SiNCs can successfully be functionalized. The hydrosilylation reaction initiated with BIP was found to proceed faster and more efficiently than the reaction initiated with the established diazonium compound 4-decylbenzene diazonium tetrafluoroborate (DDB)<sup>1</sup> (Fig. S1†). After 16 h, the excess substrate was removed *via* three precipitation/centrifugation steps and the product was analysed by Fourier transform infrared spectroscopy (FTIR). The unfunctionalized hydride terminated

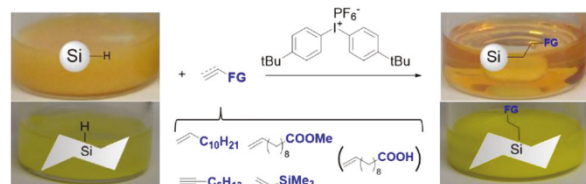


**Fig. 1** Schematic overview of the executed iodonium salt induced surface functionalization on hydride terminated SiNCs (top) and SiNSs (bottom) by hydrosilylation. Different functional unsaturated compounds can be used to stabilize the nanomaterial. Undecenoic acid is only applicable for SiNSs.

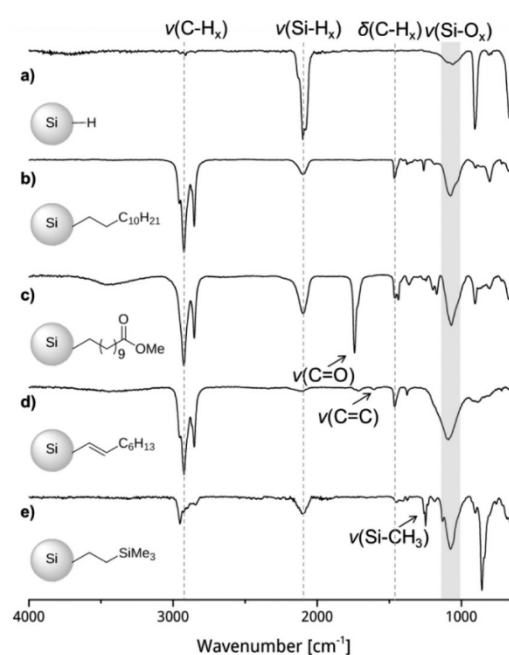


**Fig. 2** FTIR spectra of 3 nm SiNCs (a) freshly etched SiNC-H, (b) dodecene functionalized SiNC-C<sub>12</sub>H<sub>25</sub> (c) methyl 10-undecenoate functionalized SiNC-C<sub>10</sub>H<sub>20</sub>COOMe, (d) octyne functionalized SiNC-CH=CHC<sub>6</sub>H<sub>13</sub>, (e) vinyltrimethylsilane functionalized SiNC-C<sub>2</sub>H<sub>2</sub>SiMe<sub>2</sub>.

SiNCs (Fig. 2a) exhibit strong bands arising from Si-H vibrations ( $\sim 860\text{ cm}^{-1}$ ,  $\sim 900\text{ cm}^{-1}$ ,  $\sim 2100\text{ cm}^{-1}$ ). After functionalization these bands decrease drastically and the FTIR bands of the organic molecules on the surface dominate the spectrum (Fig. 2b).  $\text{C}_{\text{sp}^3}\text{-H}$  stretching ( $\sim 2900\text{ cm}^{-1}$ ) and deformation bands ( $\sim 1460\text{ cm}^{-1}$ ) show the attached dodecyl moieties on the surface and the absence of  $\text{C}_{\text{sp}^2}\text{-H}$  stretching ( $\sim 3100\text{ cm}^{-1}$ ) or deformation bands ( $\sim 1650\text{ cm}^{-1}$ ) demonstrate the successful removal of the substrate, which was also confirmed by NMR spectroscopy (Fig. S2†). During handling and workup minor oxidation can occur, leading to small Si-O bands ( $\sim 1100\text{ cm}^{-1}$ ). As confirmed by transmission electron microscopy (TEM) (Fig. 3a), the size of the SiNCs is not influenced by the initiation method.

Due to the very high surface area of nanomaterials, surface modification plays a crucial role for their applications. Thus, the introduction of different functional groups on the surface is a desirable goal. As such we used 1-octyne to demonstrate the feasibility with alkynes and methyl 10-undecenoate to show the functional group tolerance and to demonstrate a broader applicability of BIP. Again, IR spectra confirm the successful functionalization by the presence of C=O ( $\sim 1740\text{ cm}^{-1}$ ) bands (Fig. 2c) arising from the ester functionality and C=C bands ( $\sim 1640\text{ cm}^{-1}$ ) (Fig. 2d) for alkyne functionalization, as well as the Si-Me bands ( $\sim 1250\text{ cm}^{-1}$ ) (Fig. 2e) caused by the trimethylsilyl group. DLS measurements show that independent of the different functionalities, the SiNCs are stabilized against agglomeration (Fig. S3†).

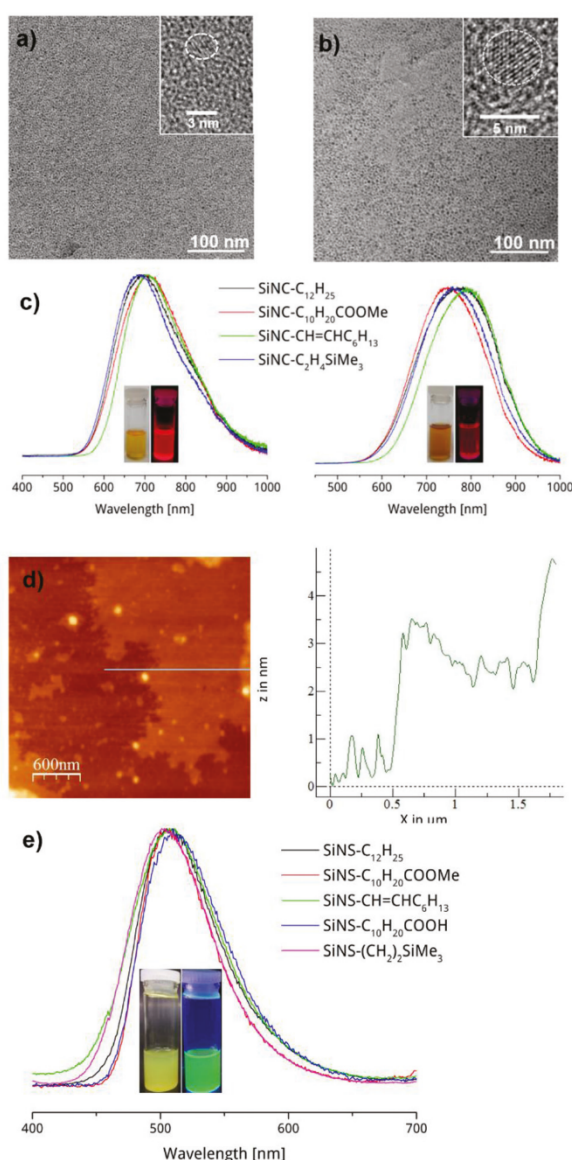


**Fig. 3** TEM and HR-TEM (inset in TEM) images of SiNC-C<sub>12</sub>H<sub>25</sub> with (a) 3 nm and (b) 5 nm diameter. (c) Corresponding PL spectra of functionalized SiNCs excited at  $\lambda_{\text{ex}} = 365$  nm. (d) Left: AFM picture of SiNS-C<sub>12</sub>H<sub>25</sub>; right: line profile taken along the line of the AFM image. (e) PL spectra of functionalized silicon nanosheets excited at  $\lambda_{\text{ex}} = 365$  nm.

Since the size of nanomaterials strongly influences their properties,<sup>3</sup> we additionally demonstrate the applicability of the described method to 5 nm SiNCs. FTIR spectra (Fig. S5†) confirm the successful reactions with different substrates, while TEM images (Fig. 3b) and DLS measurements (Fig. S4†) verify the colloidal stabilization of the SiNCs.

Next, we extended the herein described concept to hydride terminated SiNSs, which, due to their anisotropic character, exhibit outstanding (opto)electronic properties,<sup>27</sup> are by far

less explored than SiNCs and were found to show in part different reactivity than SiNCs.<sup>2,41,57</sup>

Prior to functionalization with a substrate in ethyl acetate, SiNSs were synthesized from CaSi<sub>2</sub> via chemical exfoliation with HCl (aq) at -25 °C.

Similar to their 0D counterparts, the 2D SiNSs can be successfully functionalized with the above discussed substrates, as confirmed by FTIR (Fig. S6†). When compared to SiNCs, a difference in reactivity was found for SiNSs. For the latter carboxylic acids can be successfully used as substrate (Fig. S6f†), which is not the case for SiNCs. Similar observations could be made when diazonium salts were used to induce surface functionalization.<sup>1,2</sup> This is yet another example of a difference in reactivity when looking at seemingly similar materials.

Due to their large surface area, SiNSs tend to agglomerate visibly and hence much more than SiNCs, even when functionalized. Thus, the turbid reaction mixtures only render clear dispersions when diluted further (Fig. S7†). The presence of the SiNSs was found to lead to the occurrence of the Tyndall effect.

We performed AFM measurements to confirm that the 2D character of the SiNSs is preserved during the functionalization (Fig. 3d) and obtained images which are in accordance with previously reported data of our groups.<sup>2,57</sup>

Thermogravimetric analysis (TGA) measurements of the described SiNMs showed weight loss corresponding to organic groups on the surface, demonstrating the successful functionalization (Fig. S8†). It can also be seen, that independent of the material (*i.e.*, different SiNCs or SiNSs), the substrate related reactivity of BIP follows the trend vinyltrimethylsilane > 1-dodecene > 1-octyne > methyl 10-undecenoate (see ESI Table S3†). As can be seen in PL measurements (Fig. 3c and d), after functionalization the SiNMs still exhibit their size and material dependent emission maximum.

Iodonium salts are thus very efficient initiators that can be applied for the surface functionalization of SiNMs with unsaturated substrates. Based on the accepted mechanisms of the iodonium initiated, UV induced polymerization<sup>56,58</sup> and the decomposition of diazonium salts in the presence of SiNMs,<sup>1,2,44</sup> we believe that the functionalization mechanism starts with a single electron transfer from the SiNM to the iodonium salt. Subsequently, the formed diaryliodonium radical decomposes to iodobenzene and a reactive phenyl radical. The cationic surface proton is abstracted by the counter ion X<sup>-</sup> of the iodonium salt, forming the silyl radical which undergoes hydrosilylation with unsaturated substrates (see Scheme S1 and ESI† for more detailed mechanistic considerations).

During our studies, we found that the combination of hydride terminated SiNMs with diaryliodonium salts efficiently initiates the cationic ring opening polymerization of THF, leading to a SiNS/poly(tetrahydrofuran) (pTHF) composite (Fig. 4). The polymerization reaction takes place even in the absence of light and cannot be initiated with the seemingly similar 4-decylbenzene diazonium tetrafluoroborate, which can be used as a functionalization reagent.<sup>1,2</sup>

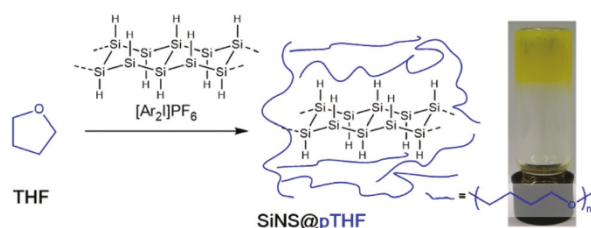


Fig. 4 Schematic of the SiNS/BIP initiated cationic ring opening polymerization of THF leading to the SiNS@pTHF nanocomposite.

To examine this observation further, we dispersed freeze dried, hydride terminated SiNSs in dry, degassed THF under inert atmosphere, added diphenyl iodonium hexafluorophosphate (PIP) and stirred the dispersion. After *ca.* 2 h the reaction mixture was solid. The formed poly(tetrahydrofuran) (pTHF) based nanocomposite SiNS@pTHF was purified by precipitation.

We subsequently analysed the as synthesized photoluminescent nanocomposites (Fig. S9†) and found that IR and NMR showed the expected signals of the pTHF matrix (Fig. S10 and S11†). The presence of the SiNSs was confirmed by the characteristic yellow color (Fig. 4) and electrodispersive X-ray spectroscopy (EDX; Fig. S12†).

To determine if the SiNSs are functionalized within the polymer matrix or if the nanocomposite consists of a blend of non-functionalized SiNSs in pTHF, we removed the excess polymer matrix by centrifuging a concentrated solution of the nanocomposite in THF.<sup>57</sup> The removal of the free polymer was confirmed by gel permeation chromatography (Fig. S13†). The residual SiNSs were then analysed by FTIR spectroscopy and TGA (Fig. S14 and S15†). FTIR spectra show no corresponding bands of the organic layer, but merely oxidized silicon material. Additionally the TGA measurements do not show any substantial weight loss, which indicates that the SiNSs are not functionalized.

This finding is in accordance with the SiNC/[Ar<sub>2</sub>I]PF<sub>6</sub> initiated polymerization, which resulted in a turbid SiNC@pTHF nanocomposite (Fig. S16†), indicating that no surface functionalization took place.

Since their presence is necessary for the polymerization to occur, SiNMs seem to play a crucial role in the initiation, but do not take part in the reaction itself, unlike in the case of radical induced polymerization reactions.<sup>57</sup> To the best of our knowledge, such a collaborative effect with SiNMs has never been observed before, but exhibits a high potential for cationic ring opening polymerizations due to the mild reaction conditions (*i.e.*, no UV light) and is currently under further investigation in our groups.

## Conclusions

In conclusion, we introduce diaryliodonium salts as new, efficient initiators for hydrosilylation reactions on the surface

of hydride terminated SiNMs. A variety of functional unsaturated substrates could be used to stabilize silicon nanocrystals of different sizes (3 and 5 nm). The resulting hybrid materials render clear dispersions in organic solvents and were shown to still possess the desirable optical properties. We fully characterized this zero-dimensional nanomaterial and expanded the reaction scope to the anisotropic 2D silicon nanosheets. The iodonium salt was shown to be very effective in initiating hydrosilylations with different functional alkenes and alkynes.

Next, we report a never before observed reactivity of the nanomaterials in combination with diaryliodonium salts. The hydride terminated SiNMs initiate the decomposition of diaryliodonium salts (which is generally fulfilled by UV irradiation), which subsequently initiates cationic ring opening polymerization. We show that the SiNSs do not take part in the polymerization reactions, but rather, together with the diaryliodonium salt, act as cocatalyst. Such a collaborative effect has not been reported before, but exhibits high potential for a variety of new composite materials accessible through mild reaction conditions.

## Acknowledgements

We gratefully acknowledge the help of Lavinia Scherf and Prof. Thomas Fässler for providing the starting material CaSi<sub>2</sub>. The authors thank DFG (IRTG 2022) and NSERC (CREATE) for financial support of Alberta/Technische Universität München Graduate School for Functional Hybrid Materials ATUMS as well as TUM Graduate School and IGSSSE. T. H. gratefully acknowledges the funding from Studienstiftung des deutschen Volkes. R. S. acknowledges the financial support from AITF. Kai Cui is thanked for assistance with HR-TEM measurements.

## Notes and references

- I. M. D. Höhle, J. Kehrle, T. Helbich, Z. Yang, J. G. C. Veinot and B. Rieger, *Chem. – Eur. J.*, 2014, **20**, 4212–4216.
- T. Helbich, A. Lyuleeva, I. M. D. Höhle, P. Marx, L. M. Scherf, J. Kehrle, T. F. Fässler, P. Lugli and B. Rieger, *Chem. – Eur. J.*, 2016, **22**, 6194–6198.
- A. P. Alivisatos, *Science*, 1996, **271**, 933–937.
- I. Moreels, K. Lambert, D. De Muynck, F. Vanhaecke, D. Poelman, J. C. Martins, G. Allan and Z. Hens, *ACS Nano*, 2009, **3**, 3023–3030.
- J. G. C. Veinot, *Chem. Commun.*, 2006, 4160–4168.
- Y. Q. He, S. P. Liu, L. Kong and Z. F. Liu, *Spectrochim. Acta, Part A*, 2005, **61**, 2861–2866.
- I. N. Germanenko, S. Li and M. S. El-Shall, *J. Phys. Chem. B*, 2001, **105**, 59–66.
- C. M. Gonzalez, M. Iqbal, M. Dasog, D. G. Piercey, R. Lockwood, T. M. Klapötke and J. G. C. Veinot, *Nanoscale*, 2014, **6**, 2608–2612.

- 9 A. Lyuleeva, T. Helbich, B. Rieger and P. Lugli, *J. Phys. D: Appl. Phys.*, 2017, **50**, 135106.
- 10 F. Deubel, M. Steenackers, J. A. Garrido, M. Stutzmann and R. Jordan, *Macromol. Mater. Eng.*, 2013, **289**, 1160–1165.
- 11 S. Niesar, R. Dietmueller, H. Nesswetter, H. Wiggers and M. Stutzmann, *Phys. Status Solidi A*, 2009, **206**, 2775–2781.
- 12 G. Conibeer, *Silicon Nanocrystals: Fundamentals, Synthesis and Applications - Applications of Si Nanocrystals in Photovoltaic Solar Cells*, Wiley-VCH Verlag GmbH & Co. KGaA, Weinheim, Germany, 2010.
- 13 G. Conibeer, M. Green, R. Corkish, Y. Cho, E. C. Cho, C. W. Jiang, T. Fangsuwannarak, E. Pink, Y. Huang, T. Puzzer, T. Trupke, B. Richards, A. Shalav and K. Lung Lin, *Thin Solid Films*, 2006, **511–512**, 654–662.
- 14 F. Maier-Flaig, J. Rinck, M. Stephan, T. Bocksrocker, M. Bruns, C. Kübel, A. K. Powell, G. A. Ozin and U. Lemmer, *Nano Lett.*, 2013, **13**, 475–480.
- 15 F. Maier-Flaig, C. Kübel, J. Rinck, T. Bocksrocker, T. Scherer, R. Prang, A. K. Powell, G. A. Ozin and U. Lemmer, *Nano Lett.*, 2013, **13**, 3539–3545.
- 16 N. Delpuech, D. Mazouzi, N. Dupré, P. Moreau, M. Cerbelaud, J. S. Bridel, J. C. Badot, E. De Vito, D. Guyomard, B. Lestriez and B. Humbert, *J. Phys. Chem. C*, 2014, **118**, 17318–17331.
- 17 B. A. Kairdolf, A. M. Smith, T. H. Stokes, M. D. Wang, A. N. Young and S. Nie, *Annu. Rev. Anal. Chem.*, 2013, **6**, 143–162.
- 18 B. F. P. McVey and R. D. Tilley, *Acc. Chem. Res.*, 2014, **47**, 3045–3051.
- 19 Z. F. Li and E. Ruckenstein, *Nano Lett.*, 2004, **4**, 1463–1467.
- 20 F. Erogbogbo, C.-A. Tien, C.-W. Chang, K.-T. Yong, W.-C. Law, H. Ding, I. Roy, M. T. Swihart and P. N. Prasad, *Bioconjugate Chem.*, 2011, **22**, 1081–1088.
- 21 J.-H. Park, L. Gu, G. von Maltzahn, E. Ruoslahti, S. N. Bhatia and M. J. Sailor, *Nat. Mater.*, 2009, **8**, 331–336.
- 22 Z. Kang, C. H. A. Tsang, N. B. Wong, Z. Zhang and S. T. Lee, *J. Am. Chem. Soc.*, 2007, **129**, 12090–12091.
- 23 D. Kovalev and M. Fujii, *Adv. Mater.*, 2005, **17**, 2531–2544.
- 24 M. Dasog, J. Kehrle, B. Rieger and J. G. C. Veinot, *Angew. Chem., Int. Ed.*, 2016, **55**, 2322–2339.
- 25 L. Pavesi and R. Turan, *Silicon Nanocrystals*, Wiley-VCH Verlag GmbH & Co. KGaA, Weinheim, Germany, 2010.
- 26 J. M. Buriak, *Chem. Commun.*, 1999, 1051–1060.
- 27 H. Okamoto, Y. Sugiyama and H. Nakano, *Chem. – Eur. J.*, 2011, **17**, 9864–9887.
- 28 A. Kara, H. Enriquez, A. P. Seitsonen, L. C. Lew Yan Voon, S. Vizzini, B. Aufray and H. Oughaddou, *Surf. Sci. Rep.*, 2012, **67**, 1–18.
- 29 P. Vogt, P. De Padova, C. Quaresima, J. Avila, E. Frantzeskakis, M. C. Asensio, A. Resta, B. Ealet and G. Le Lay, *Phys. Rev. Lett.*, 2012, **108**, 155501.
- 30 C. L. Lin, R. Arafune, K. Kawahara, N. Tsukahara, E. Minamitani, Y. Kim, N. Takagi and M. Kawai, *Appl. Phys. Express*, 2012, **5**, 45802.
- 31 A. Fleurence, R. Friedlein, T. Ozaki, H. Kawai, Y. Wang and Y. Yamada-Takamura, *Phys. Rev. Lett.*, 2012, **108**, 245501.
- 32 L. Meng, Y. Wang, L. Zhang, S. Du, R. Wu, L. Li, Y. Zhang, G. Li, H. Zhou, W. A. Hofer and H.-J. Gao, *Nano Lett.*, 2013, **13**, 685–690.
- 33 Z. Ni, H. Zhong, X. Jiang, R. Quhe, G. Luo, Y. Wang, M. Ye, J. Yang, J. Shi and J. Lu, *Nanoscale*, 2014, **6**, 7609–7618.
- 34 G. Le Lay, *Nat. Nanotechnol.*, 2015, **10**, 1–2.
- 35 L. Tao, E. Cinquanta, D. Chiappe, C. Grazianetti, M. Fanciulli, M. Dubey, A. Molle and D. Akinwande, *Nat. Nanotechnol.*, 2015, **10**, 227–231.
- 36 F. Li, R. Lu, Q. Yao, E. Kan, Y. Liu, H. Wu, Y. Yuan, C. Xiao and K. Deng, *J. Phys. Chem. C*, 2013, **117**, 13283–13288.
- 37 N. Gao, W. T. Zheng and Q. Jiang, *Phys. Chem. Chem. Phys.*, 2012, **14**, 257.
- 38 Y. Kumai, S. Shirai, E. Sudo, J. Seki, H. Okamoto, Y. Sugiyama and H. Nakano, *J. Power Sources*, 2011, **196**, 1503–1507.
- 39 Y. Kumai, H. Kadoura, E. Sudo, M. Iwaki, H. Okamoto, Y. Sugiyama and H. Nakano, *J. Mater. Chem.*, 2011, **21**, 11941.
- 40 Y. Kumai and H. Nakano, *Jpn. J. Appl. Phys.*, 2015, **54**, 35201.
- 41 T. Helbich, A. Lyuleeva, P. Marx, L. M. Scherf, T. K. Purkait, T. F. Fässler, P. Lugli and B. Rieger, *Adv. Funct. Mater.*, 2017, accepted.
- 42 H. Nakano, M. Nakano, K. Nakanishi, D. Tanaka, Y. Sugiyama, T. Ikuno, H. Okamoto and T. Ohta, *J. Am. Chem. Soc.*, 2012, **134**, 5452–5455.
- 43 *Aryl Diazonium Salts New Coupling Agents in Polymer and Surface Science*, ed. M. M. Chehimi, 2012.
- 44 D. Wang and J. M. Buriak, *Langmuir*, 2006, **22**, 6214–6221.
- 45 K. H. Vase, A. H. Holm, S. U. Pedersen and K. Daasbjerg, *Langmuir*, 2005, **21**, 8085–8089.
- 46 D. M. Hernández, M. A. González, P. D. Astudillo, L. S. Hernández and F. J. González, *Procedia Chem.*, 2014, **12**, 3–8.
- 47 K. J. Stevenson, P. A. Veneman, R. I. Gearba, K. M. Mueller, B. J. Holliday, T. Ohta and C. K. Chan, *Faraday Discuss.*, 2014, **172**, 273–291.
- 48 R. I. Gearba, K. M. Mueller, P. A. Veneman, B. J. Holliday, C. K. Chan and K. J. Stevenson, *J. Electroanal. Chem.*, 2014, **753**, 9–15.
- 49 C. K. Chan, T. E. Beechem, T. Ohta, M. T. Brumbach, D. R. Wheeler and K. J. Stevenson, *J. Phys. Chem. C*, 2013, **117**, 12038–12044.
- 50 M. Weissmann, S. Baranton and C. Coutanceau, *Langmuir*, 2010, **26**, 15002–15009.
- 51 S. Zhang, K. L. Chandra and C. B. Gorman, *J. Am. Chem. Soc.*, 2007, **129**, 4876–4877.
- 52 T. Matrab, C. Combellas and F. Kanoufi, *Electrochem. Commun.*, 2008, **10**, 1230–1234.
- 53 S. M. Dirk, S. Pylypenko, S. W. Howell, J. E. Fulghum and D. R. Wheeler, *Langmuir*, 2005, **21**, 10899–10901.
- 54 J. V. Crivello, in *Initiators – Poly Reactions—Optical Activity*, Springer Berlin Heidelberg, Berlin, Heidelberg, 1984, pp. 1–44.

- 55 J. A. Kampmeier and T. W. Nallit, *J. Org. Chem.*, 1994, **59**, 1381–1388.
- 56 J. V. Crivello and J. H. W. Lam, *Macromolecules*, 1977, **10**, 1307–1315.
- 57 T. Helbich, A. Lyuleeva, T. Ludwig, L. M. Scherf, T. F. Fässler, P. Lugli and B. Rieger, *Adv. Funct. Mater.*, 2016, **26**, 6711–6718.
- 58 J. V. Crivello, *Adv. Polym. Sci.*, 1984, **62**, 1–48.

Electronic Supplementary Material (ESI) for Nanoscale.  
This journal is © The Royal Society of Chemistry 2017

*Electronic Supporting Information*

**Diaryliodonium Salts as Hydrosilylation Initiators for the Surface Functionalization of Silicon Nanomaterials and their United Capability as Ring Opening Polymerization Initiators**

T. Helbich,<sup>a\*</sup> M. J. Kloberg,<sup>a\*</sup> S. Sinelnikov,<sup>b</sup> A. Lyuleeva,<sup>c</sup> J. G. C. Veinot,<sup>b</sup> and B. Rieger<sup>a</sup>

<sup>a</sup> Wacker-Lehrstuhl für Makromolekulare Chemie, Technische Universität München, Lichtenbergstrasse 4, 85747 Garching (Germany), Email: rieger@tum.de.

<sup>b</sup> Department of Chemistry, University of Alberta, 11227 Saskatchewan Drive, Edmonton, Alberta T6G 2G2 (Canada).

<sup>c</sup> Institute for Nanoelectronics, Technische Universität München, Arcisstrasse 21, 80333 Munich (Germany).

**Contents**

General Information .....	2
Syntheses and Procedures .....	2
Iodonium Salts as Functionalization Initiators for Silicon Nanocrystals (SiNCs) .....	4
Time Dependence of SiNC Functionalization with Iodonium Salts .....	4
NMR of SiNC-C <sub>12</sub> H <sub>25</sub> .....	5
Dynamic Light Scattering Data of functionalized SiNCs .....	5
IR Spectra of Functionalized 5 nm SiNCs .....	7
Iodonium Salts as Functionalization Initiators for Silicon Nanosheets (SiNSs) .....	8
FTIR Measurements of functionalized SiNSs .....	8
Visualization of SiNSs Dilution .....	8
Material Dependent Comparison of Reactivity .....	9
TGA Measurements of Functionalized SiNMs .....	9
Mechanistic Considerations .....	11
Cationic Ring Opening Polymerizations Induced by Si Nanomaterial/Diaryliodonium Salt Initiators ..	12
PL Spectrum of SiNS@pTHF Composite .....	12
IR Spectra of SiNS@pTHF Composite .....	12
NMR Spectra of SiNS@pTHF Composite .....	13
EDX Spectrum of SiNS@pTHF Composite .....	13
GPC Measurements of SiNS@pTHF Composite .....	14
Analytics of Residual SiNSs after Removal of pTHF Matrix .....	15
SiNC@pTHF Nanocomposites .....	16
References .....	16

## General Information

All experiments were performed under Schlenk conditions. Reactants and reagents were purchased from *Sigma-Aldrich* and used without further purification if not stated otherwise. 1-dodecene, methyl 10-undecenoate, 1-octyne, trimethylvinylsilane, acetone, chloroform and ethyl acetate were dried over molecular sieves and stored under argon prior to use. THF was dried with an *MBraun* solvent purification system, *MB SPS-800*, whereby argon 5.0 (99.999%, *Westfalen AG*) was used as inert gas. For polymerization reactions and storage of exfoliated SiNSs, a *LABmaster 130 (MBraun)* glove box was used with nitrogen 4.8 (99.998%, *Westfalen AG*).

Fourier transform infrared spectroscopy (**FTIR**) samples were prepared as a thin film by drop-casting the sample on a silicon wafer from a suitable solvent and the FTIR spectra were obtained using a *Nicolet 8700 FTIR* in combination with a *Nicolet Continuum* FTIR microscope. Nuclear magnetic resonance (**NMR**) spectra were recorded on an *ARX-300* from *Bruker* at 300 K. Chemical shifts ( $\delta$ ) are calibrated to the residual proton signal of the deuterated solvent and given in ppm. For functionalized SiNC samples, a concentrated solution (5 mg/mL) in benzene- $d_6$  was used to obtain the spectrum. **PL** spectra were measured in toluene on an *AVA-Spec 2048* from *Avantes* using a *Prizmatix* (LED current controller) as a light source. Thermogravimetric analysis (**TGA**) was performed on a *Mettler Toledo STARe* TGA/DSC system by heating the freeze-dried SiNC sample to 600 °C at a heating rate of 10 K/min. Dynamic light scattering (**DLS**) data was collected on a *Dyna Pro NanoStar* from *Wyatt* with toluene as the solvent. Gel permeation chromatography (**GPC**) measurements were conducted on a *Varian PL-GPC 50 Plus* at 30 °C with a constant flow rate of 1 mL/min THF, stabilized with 220 mg/L BHT. Transmission electron microscopy (**TEM**) was performed on a JEOL-2012 electron microscope equipped with LaB<sub>6</sub> filament and operated at an accelerating voltage of 200 kV. For contact mode atomic force microscopy (**AFM**) measurements, a Veeco Dimension V instrument equipped with a Veeco Nanoscope V controller in tapping mode with Si cantilever probes (Veeco OTESPA) was used. Thin films of SiNS-C<sub>12</sub>H<sub>25</sub> (15 mg of exfoliated sheets in 2 mL of toluene) were dip coated on Si/SiO<sub>2</sub> substrates and dried with a nitrogen gas flow. Energy dispersive x-ray (**EDX**) spectra were taken on a HITACHI TM-1000 table microscope with SwiftED-TM detector.

## Syntheses and Procedures

**Synthesis of oxide embedded silicon nanocrystals** was achieved through a known method.<sup>1</sup> 7.00 g polymeric hydrogen silsesquioxane (HSQ) synthesized according to a published method<sup>2</sup> was placed in a quartz reaction boat, transferred in a furnace and heated under a slightly reducing atmosphere (H<sub>2</sub>/N<sub>2</sub> = 5/95). As such the HSQ was heated to 1100 °C over 1 h and then kept at that temperature for 1 hour. Upon cooling to room temperature, the resulting solid was ground to a fine powder.<sup>3</sup>

**Liberation of silicon nanocrystals:** In a polytetrafluoroethylene (PTFE) beaker, 200 mg of ground SiNC/SiO<sub>2</sub> composite are suspended in 2 mL ethanol and 2 mL water. 2 mL HF (48%) is added and the mixture stirred for 45 minutes. The liberated SiNCs are extracted with toluene (3 × 10 mL) and isolated *via* centrifugation (3000 rpm for 5 min). After subsequent washing with dry toluene and centrifugation, the hydride-terminated SiNCs are dispersed in 2 mL dry chloroform for use in further reactions.

**Iodonium induced functionalization of silicon nanocrystals with alkenes and alkynes:** The hydride-terminated SiNCs obtained from the previously described procedure are dispersed in 2 mL dry chloroform and transferred to a heat-dried Schlenk tube. 2.50 mmol of alkene/alkyne are added and the reaction mixture is degassed via three freeze-pump-thaw cycles. After addition of 22.2  $\mu$ mol of bis(4-*tert*-butylphenyl)iodonium hexafluorophosphate (BIP), the reaction mixture was stirred for 16 hours. The clear orange dispersion is precipitated into a 3:1 ethanol/methanol mixture (for methyl 10-undecenoate and trimethylvinylsilane only methanol is used) and centrifuged (9000 rpm/5 min). Washing is performed three times by redispersing the residue in a minimal amount of toluene, adding the anti-solvent methanol and centrifuging the suspension (9000 rpm/5 min). The thus obtained functionalized SiNCs can be dispersed in organic solvents (e.g., toluene) or freeze-dried from benzene.

**Synthesis of CaSi<sub>2</sub>** was performed as previously published.<sup>4,5</sup> Stoichiometric amounts of calcium (Alfa Aesar, 99.5 %) and silicon (Wacker, 99.99 %) are mixed and pressed to a pellet. The resulting pellet is then melted in an arc-furnace set up in an argon-filled glovebox. Homogenization is achieved by twice-repeated grinding in an agate-mortar of the obtained metallic regulus and melting from both sides. Final grinding yields CaSi<sub>2</sub> that can be used in the synthesis of SiNSs.

**Synthesis of layered polysilanes via chemical exfoliation** was performed as published earlier.<sup>4,5</sup> Under inert-gas conditions, 1.00 g of  $\text{CaSi}_2$  is exfoliated in 100 mL HCl (conc.) at  $-25\text{ }^\circ\text{C}$  for seven days. The resulting SiNSs are then filtered off, washed with acetone (dry and degassed) and dried under vacuum before storage under argon in a glove box.

**Etching of silicon nanosheets:** Under argon, a given amount of exfoliated SiNSs are dispersed in 2 mL ethanol and sonicated for 5 minutes. The dispersion is transferred to a PTFE container and 2 mL water and 0.25 mL HF (48%) are added. The etched SiNSs are immediately extracted into PTFE centrifuge tubes with dichloromethane ( $3 \times 5\text{ mL}$ ) and 40 mL of toluene is added. The dispersion is centrifuged (9000 rpm for 4 min), the supernatant discarded and the obtained SiNSs are washed with dry acetone and centrifuged to remove any residual water. Per 15 mg of etched SiNSs, 2 mL of dry ethyl acetate (EtOAc) is used to disperse the hydride-terminated SiNSs.

**Iodonium induced functionalization of silicon nanosheets with alkenes and alkynes:** 2 mL of the hydride-terminated SiNS-dispersion are transferred to a heat-dried Schlenk-tube and 2.50 mmol of substrate is added. The mixture is degassed via three freeze-pump-thaw cycles and stirred for 16 hours after addition of  $9\text{ }\mu\text{mol}$  BIP. The reaction mixture is precipitated in a solution of ethanol and methanol (2:1) and subsequently centrifuged. The supernatant is discarded, the residue redispersed in toluene and centrifuged with methanol. The cycle is repeated twice to obtain the functionalized SiNSs, which can be dispersed in toluene or freeze-dried from benzene.

**SiNS/iodonium initiated ring opening polymerization:** After etching, extraction, washing with dry toluene and centrifugation, the hydride-terminated SiNSs are freeze-dried from benzene and transferred to a glove box. There, they are dispersed in 1 mL of dried and degassed THF. 15 mg of BIP are added and the mixture is stirred until polymerization was completed. Work-up of the nanocomposite SiNS@pTHF is conducted by dissolving it in 2 mL THF and precipitating in 20 mL methanol. The composite is then dried under vacuum or freeze-dried from benzene.

### Iodonium Salts as Functionalization Initiators for Silicon Nanocrystals (SiNCs)

#### Time Dependence of SiNC Functionalization with Iodonium Salts

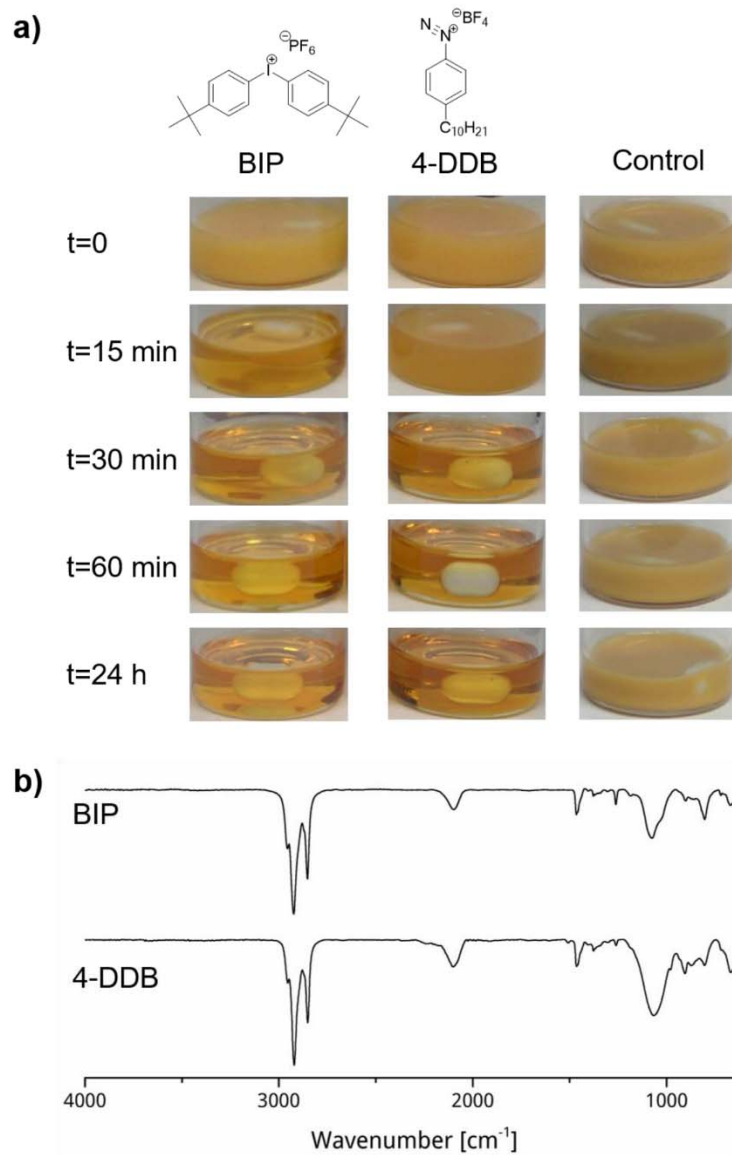


**Fig. S1** a) Time and initiator dependent functionalization of SiNCs with 1-dodecene. Left: BIP initiated hydrosilylation in chloroform. Middle: DDB initiated reaction in toluene. Right: Control reaction in chloroform without any initiator. b) IR spectra of SiNCs-C<sub>10</sub>H<sub>25</sub> initiated with BIP and DDB respectively show smaller Si-H bands as well as Si-O bands.

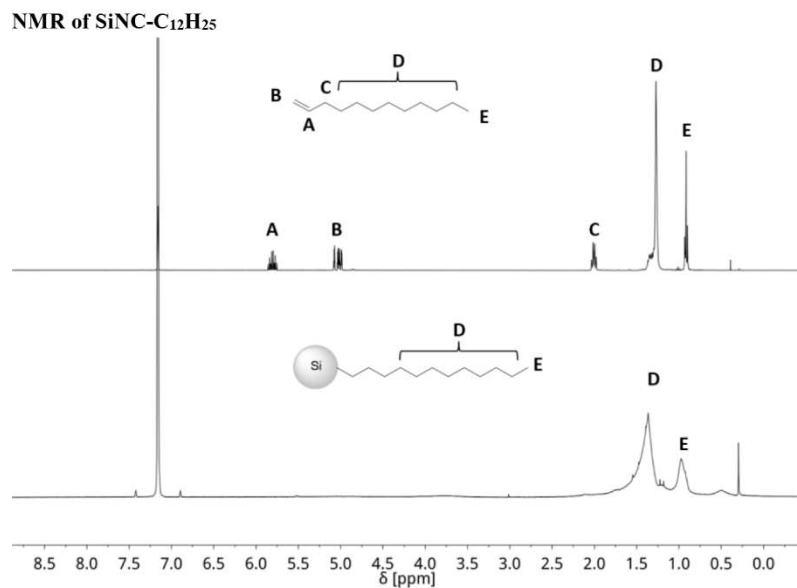


Fig. S2 NMR spectrum (CDCl<sub>3</sub>, 300 K) of 1-dodecene (top) and SiNC-C<sub>12</sub>H<sub>25</sub> (bottom).

#### Dynamic Light Scattering Data of functionalized SiNCs

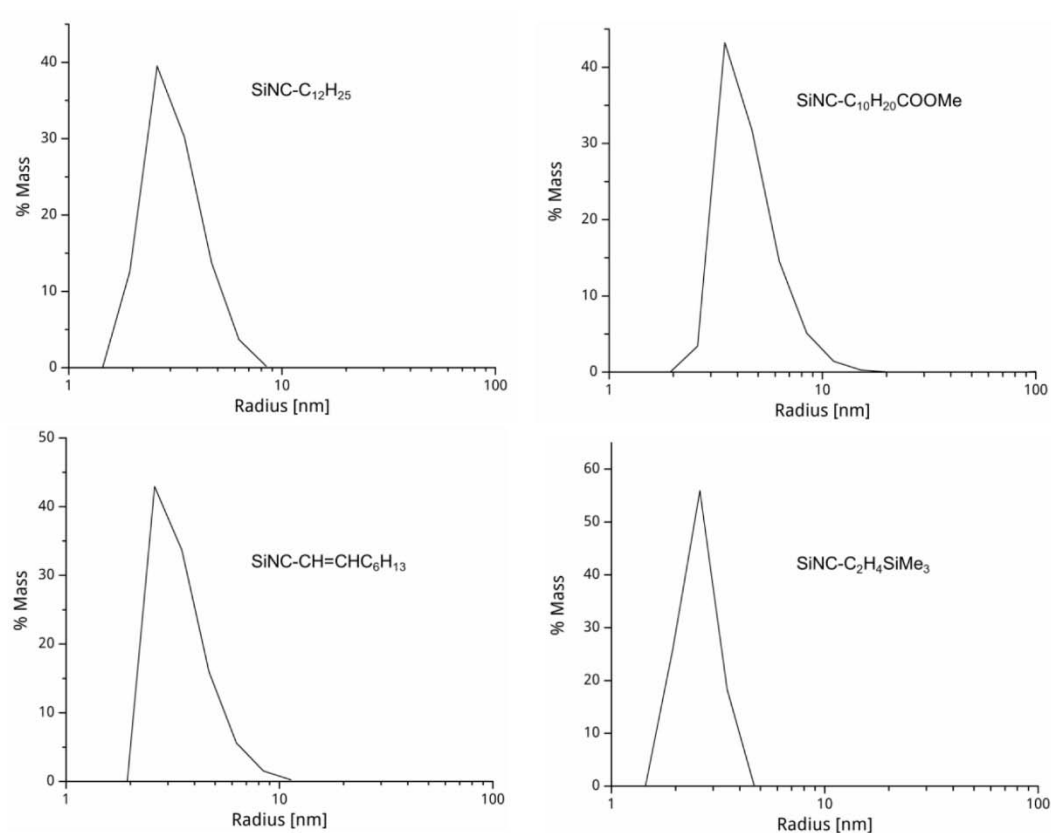
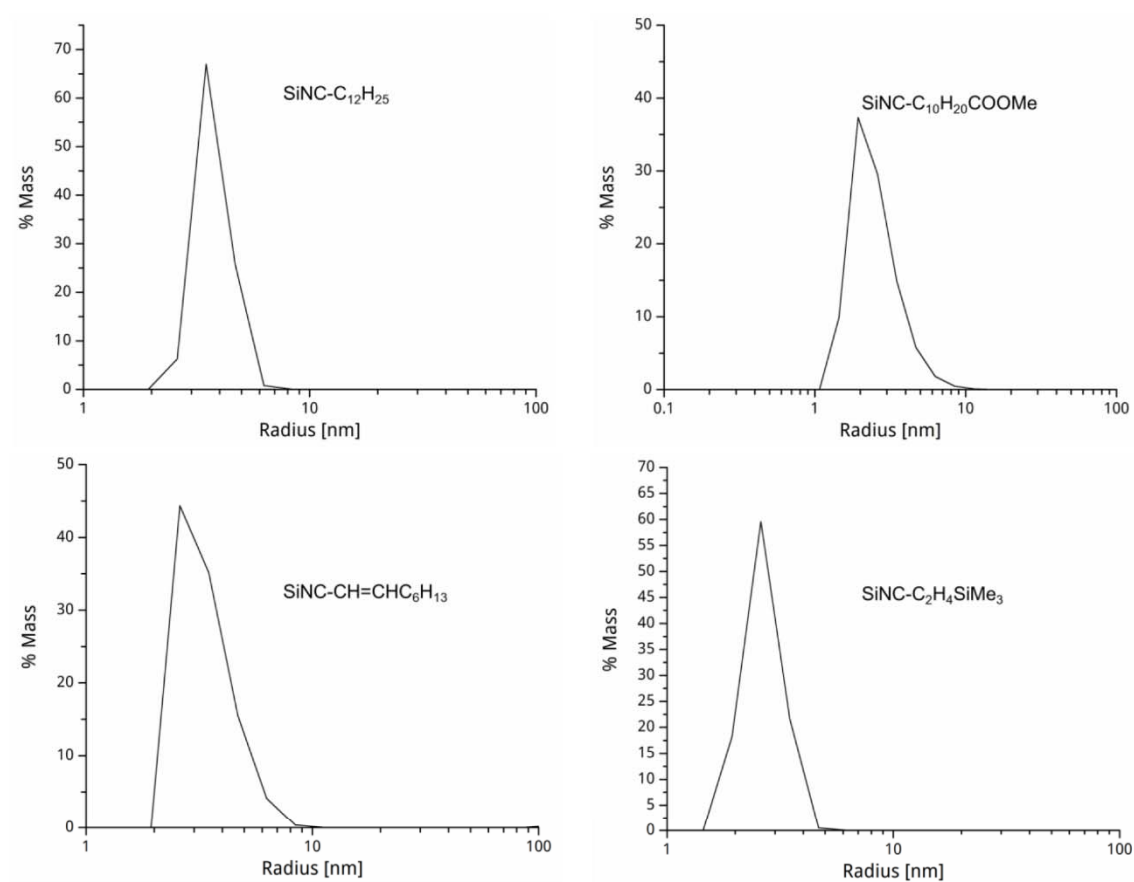


Fig. S3 DLS data of functionalized 3 nm SiNCs.

**Table S1** Hydrodynamic radii with polydispersities of the different functionalized SiNCs ( $d = 3$  nm) by diaryliodonium induced hydrosilylation determined with DLS measurement.

Substrate	Hydrodynamic radius [nm]	Polydispersity [%]
dodecene	3.1	32.1
methyl 10-undecenoate	4.3	35.6
octyne	3.9	28.4
trimethylvinylsilane	2.3	32.9



**Fig. S4** DLS data of functionalized 5 nm SiNCs.

**Table S2** Hydrodynamic radii with polydispersities of the different functionalized SiNCs ( $d = 5$  nm) by diaryliodonium induced hydrosilylation determined with DLS measurement.

Substrate	Hydrodynamic radius [nm]	Polydispersity [%]
dodecene	3.5	22.3
methyl 10-undecenoate	2.3	51.5
octyne	3.5	22.3
trimethylvinylsilane	2.5	26.7

IR Spectra of Functionalized 5 nm SiNCs

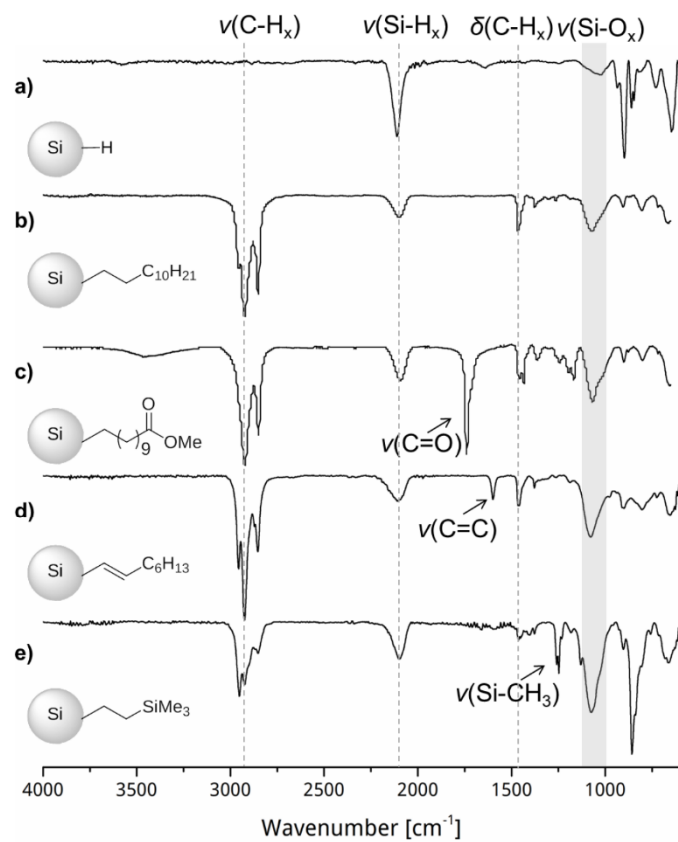
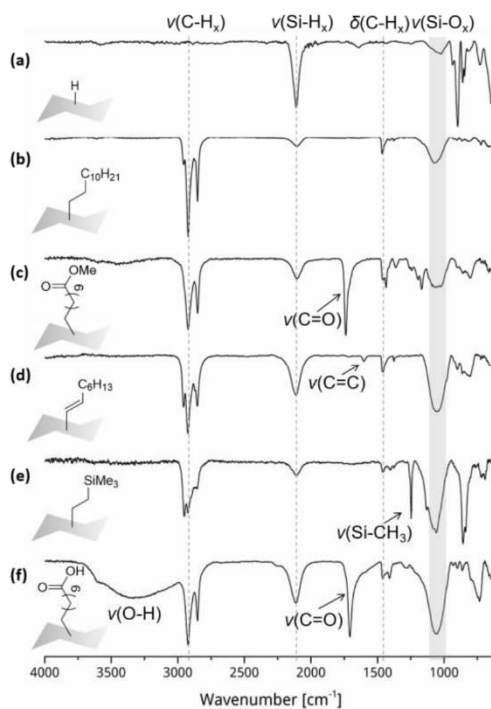


Fig. S5 IR spectra of SiNCs (5nm): a) hydride terminated, b) SiNC-C<sub>12</sub>H<sub>25</sub>, c) SiNC-C<sub>10</sub>H<sub>20</sub>COOMe, d) SiNC-CHCH-C<sub>6</sub>H<sub>13</sub>, e) SiNC-C<sub>2</sub>H<sub>4</sub>SiMe<sub>3</sub>.

## Iodonium Salts as Functionalization Initiators for Silicon Nanosheets (SiNSs)

### FTIR Measurements of functionalized SiNSs



**Fig. S6** FTIR spectra of freshly etched SiNSs (a) freshly etched, (b) dodecene functionalized SiNS-C<sub>12</sub>H<sub>25</sub>, (c) methyl 10-undecenoate functionalized SiNS-C<sub>10</sub>H<sub>20</sub>COOMe, (d) octyne functionalized SiNS-CH=CHC<sub>6</sub>H<sub>13</sub>, (e) vinyltrimethylsilane functionalized SiNS-C<sub>2</sub>H<sub>2</sub>SiMe<sub>3</sub> and (f) undecenoic acid functionalized SiNSs-C<sub>10</sub>H<sub>20</sub>-COOH.

### Visualization of SiNSs Dilution

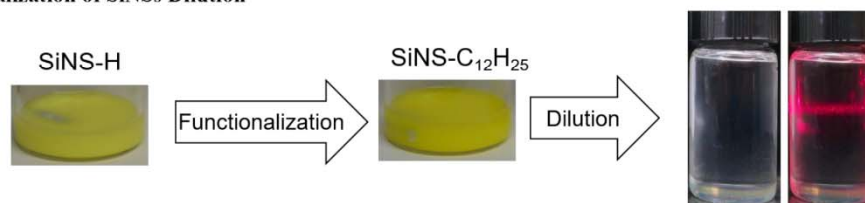


**Fig. S7** Functionalization of SiNSs with 1-dodecene in concentrated dispersions only leads to clear dispersions when the reaction mixture is further diluted. When irradiated with a laser (here: red laser pointer), a Tyndall effect is visible due to the presence of the SiNSs.

## Material Dependent Comparison of Reactivity

### TGA Measurements of Functionalized SiNMs

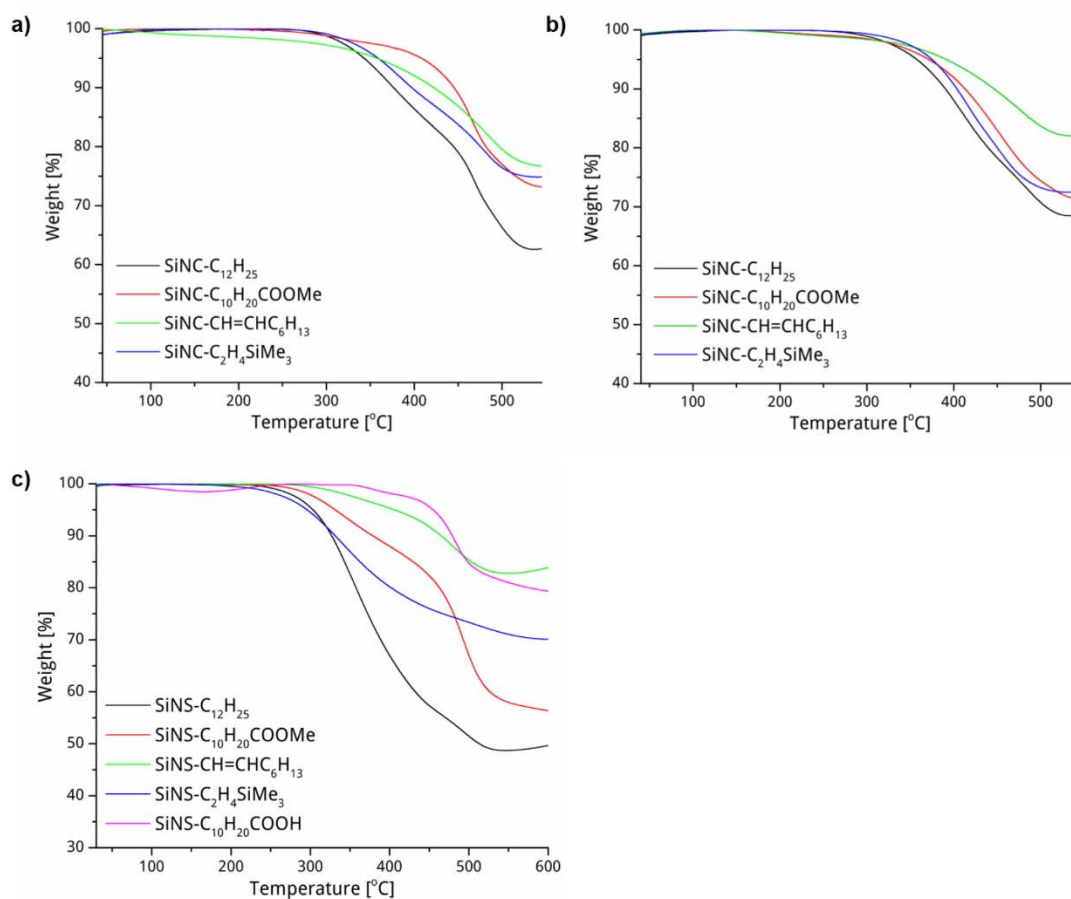


Fig. S8 TGA data of functionalized SiNCs with diameters of a) 3 nm and b) 5 nm and c) SiNSs.

**Table S3** TGA data from functionalized SiNCs and SiNSs.

SiNM	Substrate	Molecular Weight	Weight loss [%]	Weightloss/ molecular weight
SiNC 3 nm	Dodecene	168.3	36.3	0.22
SiNC 3 nm	Methyl 10-undecenoate	198.3	26.4	0.13
SiNC 3 nm	Octyne	110.2	23.3	0.21
SiNC 3 nm	Trimethylvinylsilane	100.2	25.1	0.25
SiNC 5 nm	Dodecene	168.3	30.6	0.18
SiNC 5 nm	Methyl 10-undecenoate	198.3	28.6	0.14
SiNC 5 nm	Octyne	110.2	17.9	0.16
SiNC 5 nm	Trimethylvinylsilane	100.2	26.3	0.26
SiNS	Dodecene	168.3	51	0.30
SiNS	Methyl 10-undecenoate	198.3	45.1	0.23
SiNS	Octyne	110.2	17.2	0.16
SiNS	Trimethylvinylsilane	100.2	29.9	0.30
SiNS	Undecenoic acid	184.3	22.7	0.12

To get comparable values of how many molecules are on the surface, Table S1 shows the ratio of weight loss/molecular weight of the attached organic substrates. The substrates seem to have the same reactivity towards SiNCs of different sizes as can be seen by the same trend in weight loss (trimethylvinylsilane < dodecene < octyne methyl < 10-undecenoate).

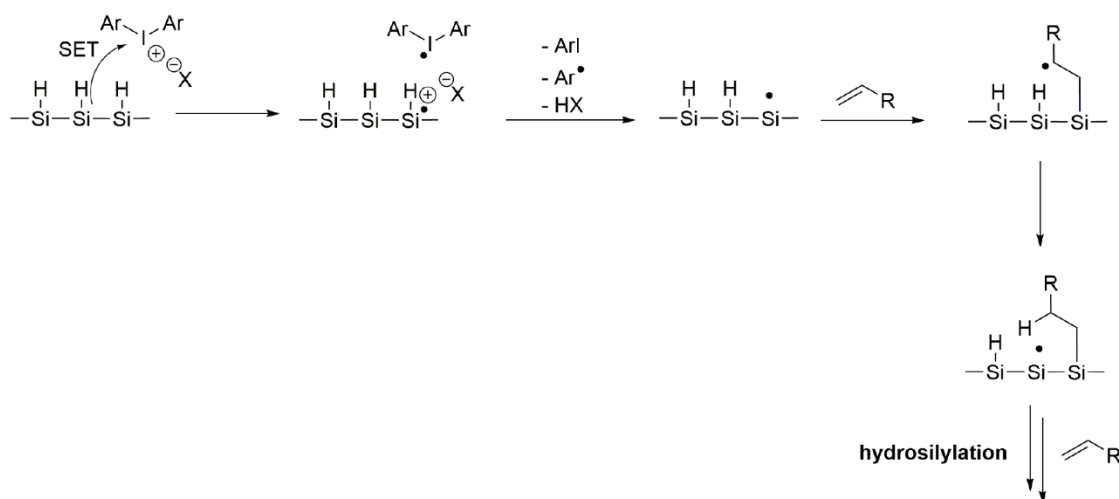
## Mechanistic Considerations

As a potential mechanism for the diaryliodonium salt initiated hydrosilylation, we suggest a reaction scheme similar to the decomposition of diazonium salts induced by a single-electron transfer (SET). This concept is based on the accepted mechanisms of the molecular iodonium initiated polymerization<sup>6,7</sup> and the decomposition of diazonium salts in the presence of SiNMs<sup>3,4,8</sup>:

**Diazonium salts** can be electrochemically grafted on flat bulk silicon. The power source provides electrons that reduce the diazonium compound and lead to surface grafting.<sup>9</sup> For silicon nanomaterials, no further bias is necessary to activate the diazonium salt. A spontaneous SET from the nanomaterial to the diazonium compound leads to the cleavage of nitrogen and the generation of an aryl radical.<sup>3,4,8</sup> The SET additionally leaves the silicon surface activated (*i.e.*, hole). In the presence of unsaturated substrates these activated species then react *via* radical induced hydrosilylation, leading to the surface functionalization of the SiNMs.

**Diaryliodonium salt initiated (molecular) polymerization reactions** are generally induced by UV light and the subsequent decomposition of the iodonium salt to free aryl radicals and cation-radicals. The cation-radicals further decompose to generate an acidic proton, which initiates the cationic polymerization.<sup>6,7</sup> Additionally, Crivello *et al.* could show that a reducing agent, such as ascorbic acid or triethylsilane, in combination with a catalyst, Cu(II) or Pt, reduces the diaryliodonium salt in redox initiated cationic polymerizations with diaryliodonium compounds, resulting in the formation of a strong acid, HMTX<sub>n</sub>, which subsequently initiates cationic polymerizations.<sup>10,11</sup>

For **diaryliodonium salt induced surface functionalizations** of silicon nanomaterials a combination of these two mechanism might explain the proceeding reaction. An electron is transferred from the nanomaterial to the iodonium salt *via* SET. Subsequently the diaryliodine radical decomposes to iodobenzene and a phenyl radical. Both compounds can be detected in NMR measurements, underlining the proposed mechanism. The cationic surface proton is abstracted by the counter ion X<sup>-</sup> of the iodonium salt. In the next step, the thus formed surface silyl radical undergoes hydrosilylation with unsaturated substrates as generally accepted for radical induced surface functionalizations of silicon (nano)materials.<sup>3,4,8</sup>



**Scheme S1** Schematic of the potential mechanism for the diaryliodonium salt initiated hydrosilylation: An electron is transferred from the nanomaterial to the iodonium salt *via* a single-electron transfer (SET). Subsequently the diaryliodine radical decomposes to iodobenzene and a phenyl radical (as known for UV induced iodonium salt decompositions), while the cationic surface proton is abstracted from the counter ion X<sup>-</sup> of the iodonium salt. In the next step, the silyl radical undergoes hydrosilylation with unsaturated substrates as generally accepted for radical induced surface functionalizations of silicon (nano)materials.

### Cationic Ring Opening Polymerizations Induced by Si Nanomaterial/Diarylodonium Salt Initiators

#### PL Spectrum of SiNS@pTHF Composite

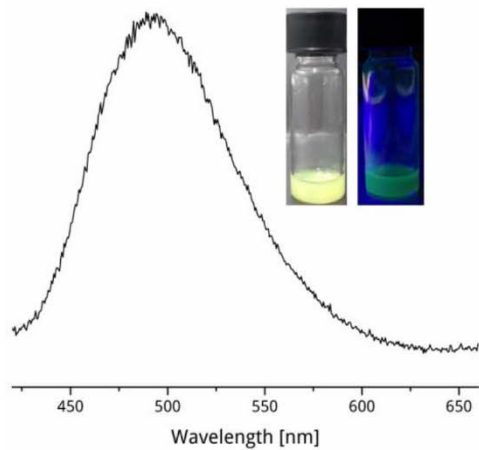


Fig. S9 PL spectrum of SiNS@pTHF and pictures taken under visible (left) and UV light (right).

#### IR Spectra of SiNS@pTHF Composite

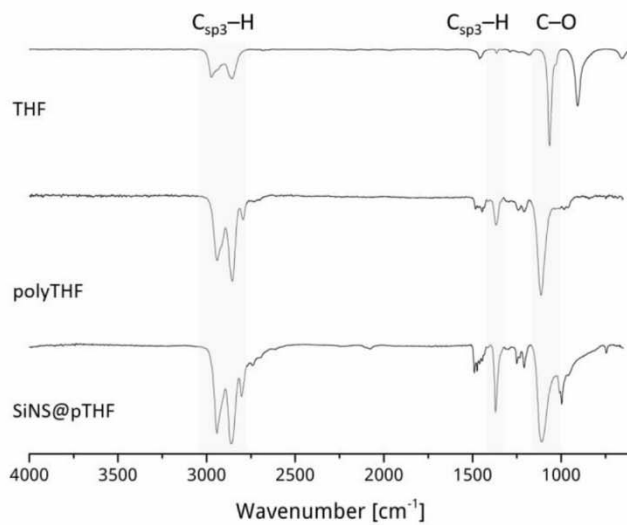


Fig. S10 FTIR spectra of (a) the monomer THF, (b) pTHF, (c) SiNS@pTHF.

NMR Spectra of SiNS@pTHF Composite

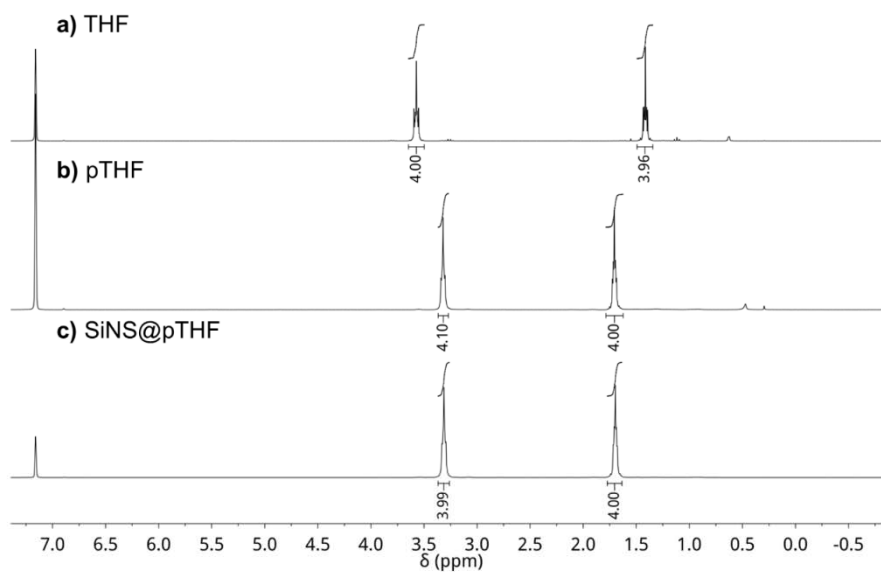


Fig. S11 NMR spectra of (a) the monomer THF, (b) pTHF, (c) SiNS@pTHF in  $\text{CDCl}_3$ .

EDX Spectrum of SiNS@pTHF Composite

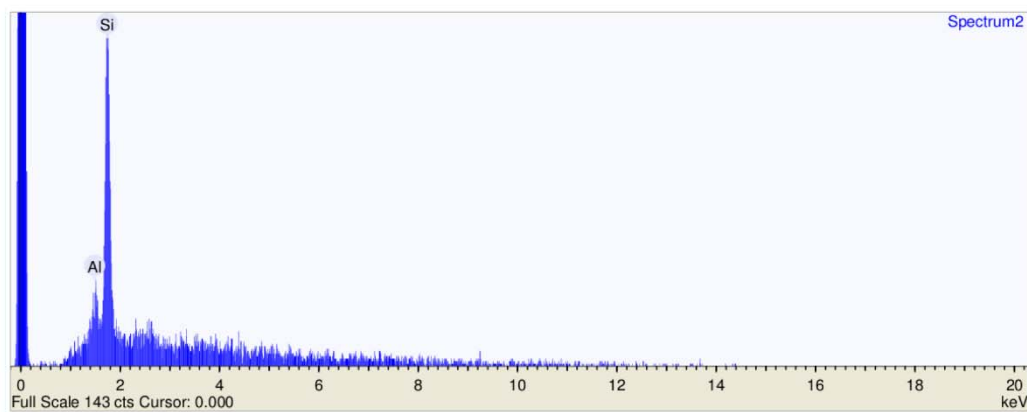
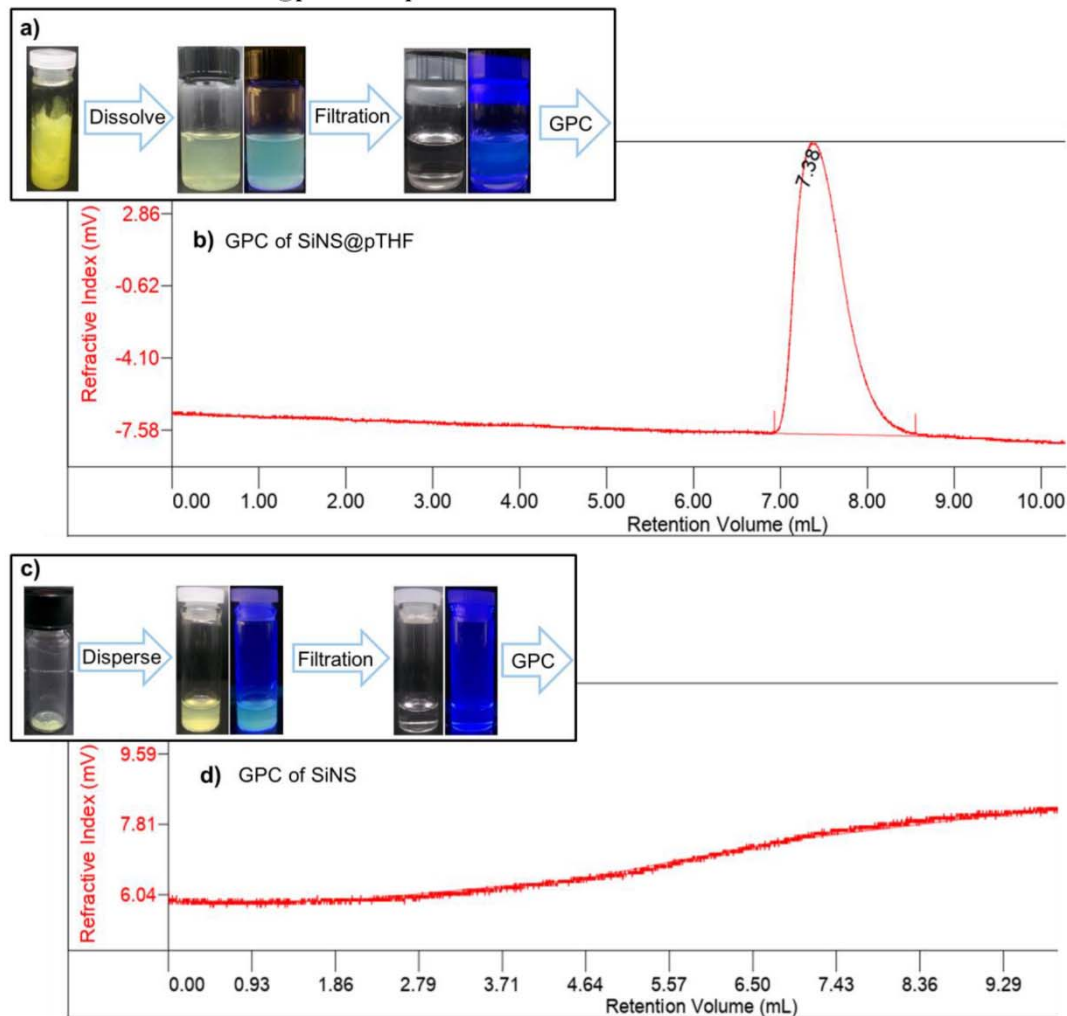


Fig. S12 EDX spectrum of SiNS@pTHF. \*elements starting with Na can be detected with the instrument. Aluminum is present from the sample holder.

GPC Measurements of SiNS@pTHF Composite



**Fig. S13** GPC was performed to confirm successful separation of the polymer matrix and SiNSs. a) The solid SiNS@pTHF is dissolved in THF to render slightly yellow dispersions (left) which show PL under UV light (right). Before GPC measurements, the SiNSs (agglomerates) are removed by filtration with a 450 nm PTFE syringe filter, confirmed by loss of the characteristic yellow color (left) and absence of PL (right). b) GPC data of the filtered nanocomposite shows the signal of the polymer matrix surrounding the inorganic SiNSs. c) After removal of the pTHF matrix by centrifugation in THF, the residual SiNSs are dispersed in THF rendering yellow dispersions (left) which still exhibit PL under UV light (right). After filtration of the SiNSs (agglomerates), the clear solvent shows no characteristic yellow color anymore (left) and without the SiNSs, no PL can be detected under UV light (right). d) GPC data of the filtered nanosheet dispersion in THF shows the successful separation of the polymer matrix by the workup procedure as no signal is detected.

**Analytics of Residual SiNSs after Removal of pTHF Matrix**

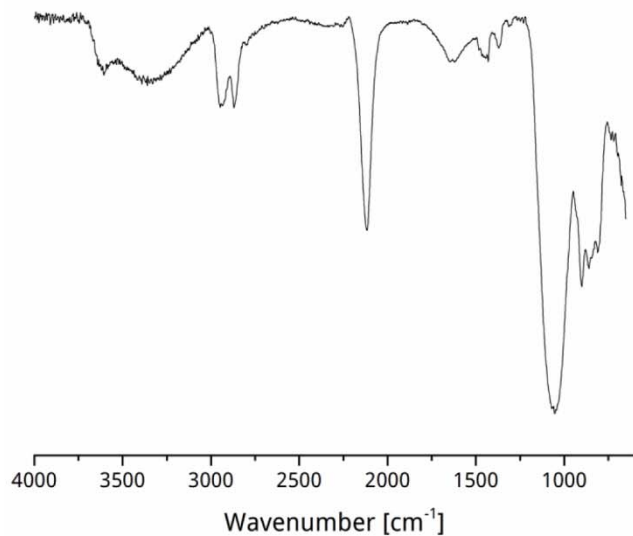


**Fig. S14** FTIR spectrum of the residual SiNSs from the nanocomposite SiNS@pTHF after removal of pTHF by centrifugation show no functionalization.

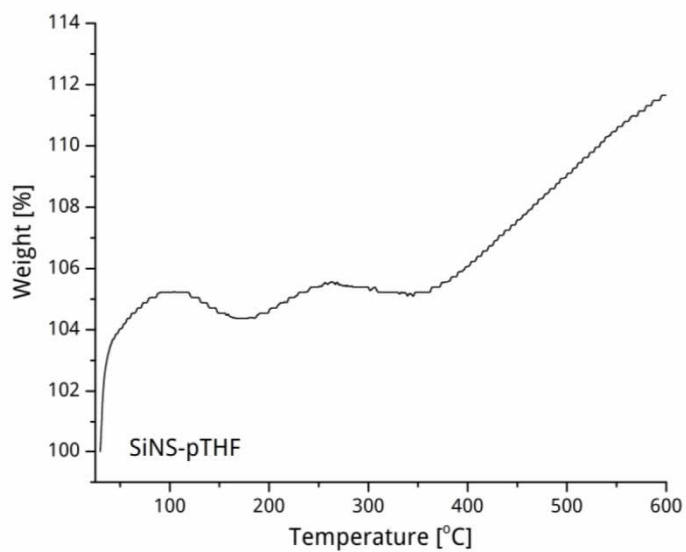


**Fig. S15** TGA of the residual SiNSs after removal of pTHF by centrifugation show no weight loss corresponding to no functionalization. Most likely the gain in weight arises from minor oxidations by oxygen impurities in the carrier gas.

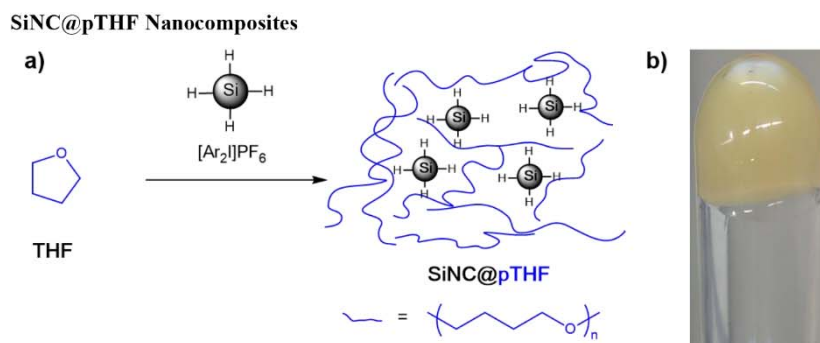


**Fig. S16** a) Schematic of the SiNC/BIP initiated cationic ring opening polymerization of THF leading to the SiNC@pTHF nanocomposite. b) Picture of the turbid SiNC@pTHF nanocomposite after the reaction. Functionalized SiNCs render clear dispersions, especially when covered with long polymer chains. The consistency therefore suggests that the SiNCs are not functionalized, but merely initiate the polymerization.

## References

- 1 C. M. Hessel, E. J. Henderson and J. G. C. Veinot, *Chem. Mater.*, 2006, **18**, 6139–6146.
- 2 H. M. Bank, M. E. Cifuentes and E. M. Theresa, *United States Pat*, 1991, 5.010.159.
- 3 I. M. D. Höhle, J. Kehrle, T. Helbich, Z. Yang, J. G. C. Veinot and B. Rieger, *Chem. - A Eur. J.*, 2014, **20**, 4212–4216.
- 4 T. Helbich, A. Lyuleeva, I. M. D. Höhle, P. Marx, L. M. Scherf, J. Kehrle, T. F. Fässler, P. Lugli and B. Rieger, *Chem. - A Eur. J.*, 2016, **22**, 6194–6198.
- 5 T. Helbich, A. Lyuleeva, T. Ludwig, L. M. M. Scherf, T. F. Fässler, P. Lugli, P. B. Rieger and B. Rieger, *Adv. Funct. Mater.*, 2016, **26**, 6711–6718.
- 6 J. V. Crivello, *Adv. Polym. Sci.*, 1984, **62**, 1–48.
- 7 J. V. Crivello and J. H. W. Lam, *Macromolecules*, 1977, **10**, 1307–1315.
- 8 D. Wang and J. M. Buriak, *Langmuir*, 2006, **22**, 6214–6221.
- 9 J. Pinson, *Aryl Diazonium Salts New Coupling Agents Polym. Surf. Sci.*, 2012, 1–35.
- 10 J. V. Crivello, *J. Polym. Sci. Part A Polym. Chem.*, 2009, **47**, 5639–5651.
- 11 J. V. Crivello and J. L. Lee, *J. Polym. Sci. Part A Polym. Chem.*, 2010, **48**, 4484–4495.

## 8. Silicon Nanosheets as Initiators for Diaryliodonium Induced Radical and Cationic Polymerization

Based on the findings of our previous works on iodonium salt initiated hydrosilylations and the therein made observation of poly(THF) formation, the system of SiNS/diaryliodonium salt was investigated further. The polymerization seems to rely on a collaborative effect between the silicon nanomaterial and the diaryliodonium salt. The silicon nanomaterial acts as co-initiator, inducing the decomposition of the diaryliodonium salt, thereby enabling the mild and straightforward polymerization of a variety of cationically and radically polymerizable monomers. This work emphasizes the potential role of silicon nanomaterials as an activator or in catalytic applications and is further described in the appendix (see chapter 13.1).

## 9. Summary and Outlook

At the beginning of this PhD thesis, the synthesis of SiNSs from  $\text{CaSi}_2$  (**Figure 5**) was implemented based on the work of Okamoto *et al.*<sup>[108]</sup> The developed etching/extracting procedure allowed to produce photoluminescent, reactive, hydride terminated SiNSs in large amounts.

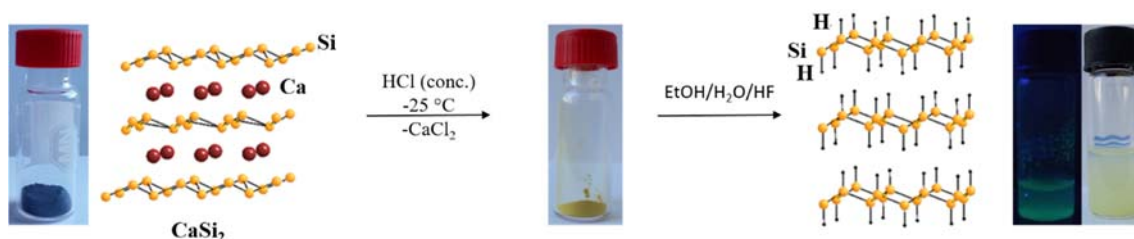


**Figure 5.** Schematic of SiNS-H synthesis by chemical exfoliation from the *Zintl* salt  $\text{CaSi}_2$  and a subsequent etching step with aqueous HF.

As the first project of the PhD thesis, high temperatures and diazonium salts were explored as new reaction procedures to induce hydrosilylation on the surface of hydride terminated SiNSs. These conditions were proven to be applicable to a broad variety of functional substrates and render the photoluminescent material, which is dispersible in organic solvents (**Figure 6**).

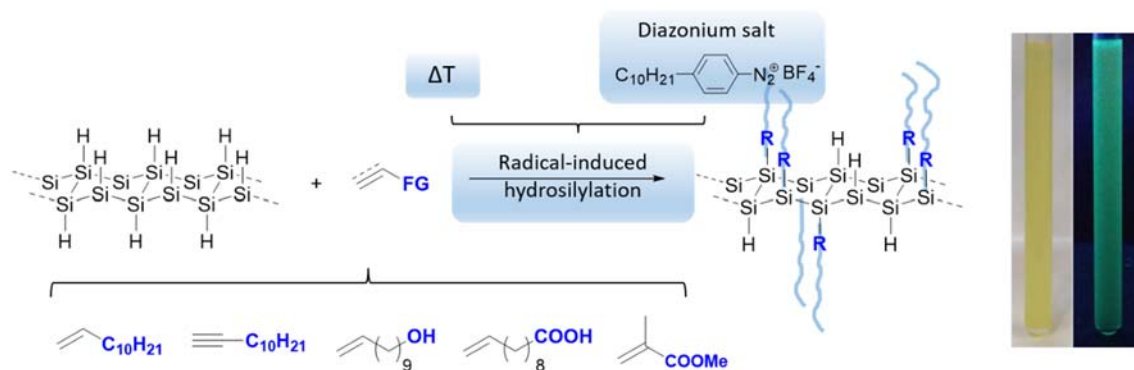


**Figure 6.** Schematic of the radical induced surface functionalization of SiNSs with a broad variety of substrates and pictures of the resulting SiNS- $\text{C}_{12}\text{H}_{25}$  dispersion under visible (left) and UV light (right).<sup>[222]</sup>

The next project extended the concept of radical induced functionalization through the use of classical radical polymerization initiators and illuminated some fundamental properties of SiNSs. As such, we examined the UV induced decomposition of SiNSs. To stabilize them, we suggested the encapsulation of the material in a polymer matrix. In a single reaction step, the SiNSs were functionalized and a polymer matrix was formed (**Figure 7**), as shown by the combination of different work up methods with GPC and FTIR measurements. The synthesized nanocomposite exhibits the processing properties of the organic polymer matrix and the (opto)electronic properties of the inorganic SiNSs. Additionally, the SiNSs are stabilized against external influences such as bases and UV light.

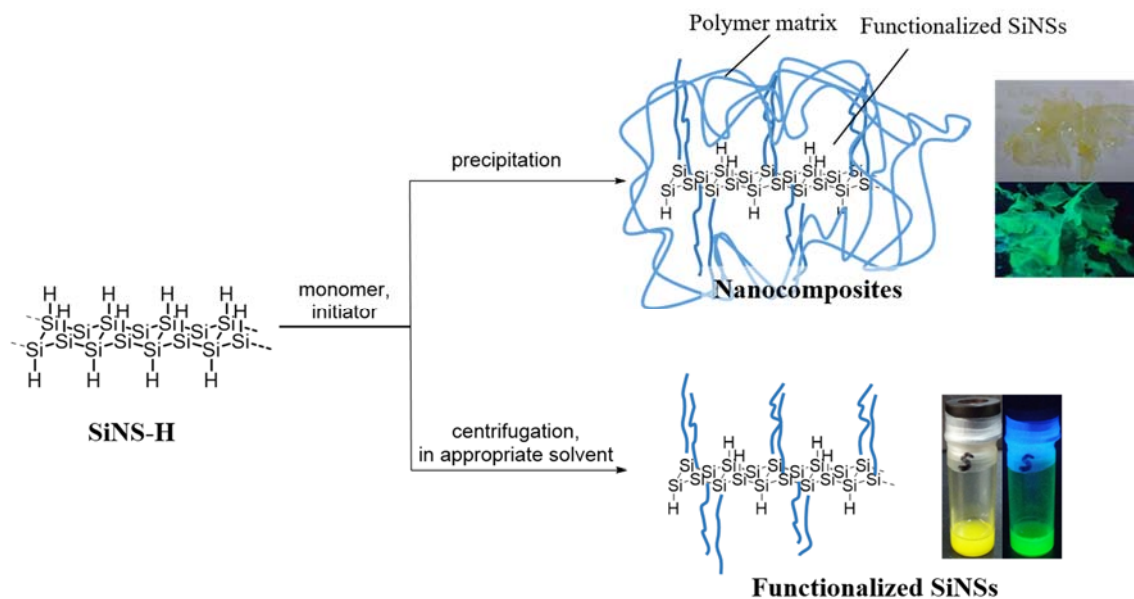


**Figure 7.** Schematic of different work-up procedures leading to either SiNS based nanocomposites or functionalized SiNSs. Pictures top: SiNS-PAA@PAA composite under visible (top) and UV light (bottom); pictures bottom: Dispersion of SiNS-C<sub>12</sub>H<sub>25</sub> in toluene under visible (left) and UV light (right).<sup>[223]</sup>

The third project of this thesis deals with the *Lewis* acid catalyzed functionalization of SiNSs. Here, different *Lewis* acids were used to catalyze the hydrosilylation on the SiNS surface with different functional substrates (**Figure 8a**). On this basis, the differences of SiNSs and SiNCs towards the hydrosilylation reaction and the corresponding mechanism were elucidated. In the second part of the project, the synthesized hybrid materials were used to fabricate solution gated Field Effect Transistors (FET) based on P3HT/SiNS composites (**Figure 8b**). The combination of the two materials enabled the enhancement of the device's sensitivity and an increase in the transconductance  $g_m$ .

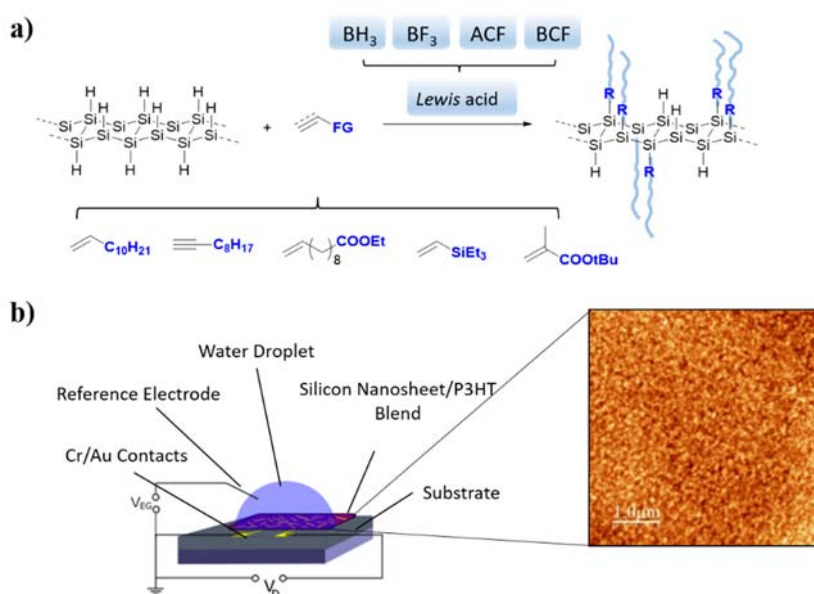


**Figure 8.** a) Schematic of the *Lewis* acid catalyzed functionalization of SiNSs. Different *Lewis* acids and functional substrates could be used to modify the SiNSs surface. b) Schematic of the solution gated FET setup and corresponding AFM picture (inset) of SiNS-C<sub>12</sub>H<sub>25</sub>/P3HT hybrid films show good dispersibility of functionalized SiNSs in the polymer.<sup>[224]</sup>

In another project of this PhD thesis, we use diaryliodonium salts to induce hydrosilylation on SiNSs and SiNCs of different sizes. This new class of initiators was found to be vastly applicable on different functional substrates for the used silicon based nanomaterials. We were additionally able to show an unprecedented collaborative effect of the studied silicon nanomaterials and the diaryliodonium salt. The nanomaterials act as co-catalysts by inducing the decomposition of the iodonium salt, which results in an efficient initiation of ring-opening polymerizations e.g., with THF.

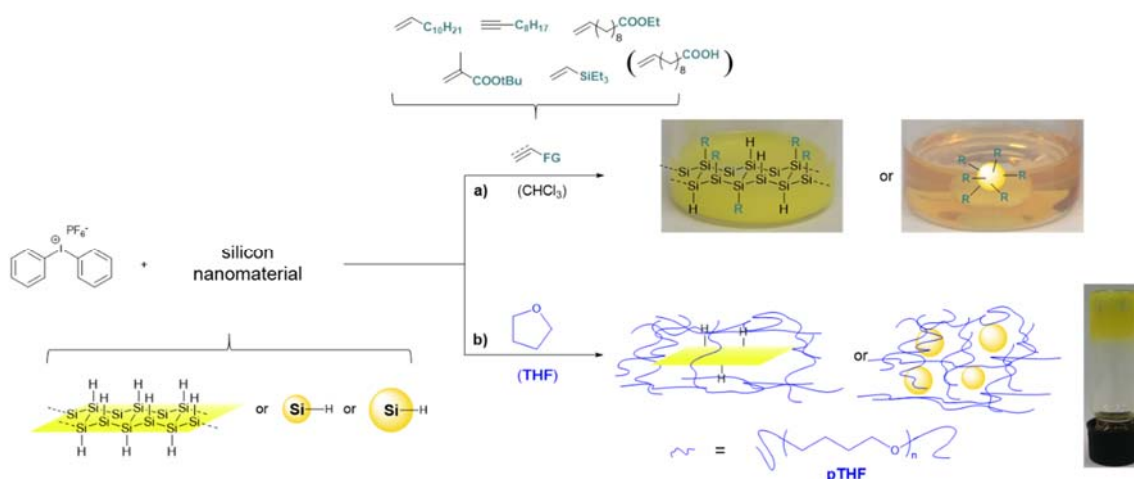


**Figure 9.** Schematic of the explored reaction pathways of SiNMs (i.e., SiNSs, SiNCs with  $d = 3$  nm and 5 nm) with diaryliodonium salts. a) Iodonium salts act as initiators of hydrosilylation reactions when unsaturated substrates are present in the reaction mixture. Hence a variety of different functional substrates could be used for surface functionalizations on SiNSs and SiNCs. b) In the absence of unsaturated reactants, monomers (e.g., THF) can successfully be polymerized by ring opening polymerization.<sup>[225]</sup>

This concept was then extended to different monomers (e.g., cyclohexene oxide, trioxane, cyclohexene sulfide, MMA, <sup>t</sup>BuMA, Vinylacetate) and the underlying mechanism was examined in more detail (**Figure 10**).

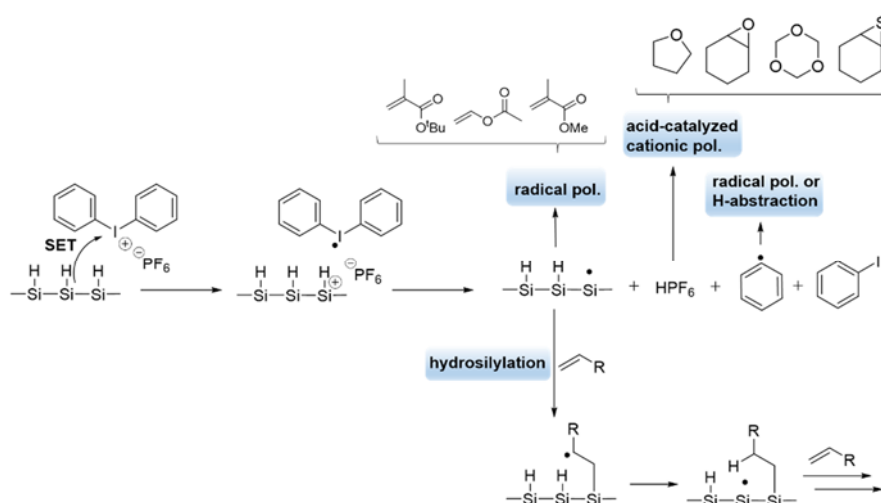


**Figure 10.** Schematic of the SiNM co-catalyzed polymerization of different monomers with iodonium salts and the underlying mechanism *via* a single-electron-transfer (SET) and possible effects of the decomposition products.

The methods and concepts presented in this PhD thesis lay the foundation for further studies and applications. The established surface functionalization method could be extended to other 0D or 2D materials such as germanium nanocrystals and nanosheets.

The SiNS based nanocomposites are promising candidates for applications in Li-ion batteries. The replacement of the presented polymer with an electron and ion conductive polymer (additive blend) could result in a promising anode material for Li-ion batteries. Thus the capacity of the anode is expected to be very high due to the high theoretical lithium storage capacity of silicon. Furthermore, the nature of the nanocomposite might enhance the cycling stability of silicon anode due to its flexibility.

Based on the fabricated nanoelectronic FET, studies on SiNSs with different functional groups could be of high interest. Hence, SiNSs with an organic surface cover of conjugated  $\pi$ -systems (e.g. phenylacetylene functionalized SiNSs) might exhibit different electronic (e.g., band structures) or physical properties (e.g., dispersibility, interaction with matrix material) and thus change the characteristics of the devices. Additionally, it would be appealing to examine the electronic properties of these functionalized SiNSs with scanning tunneling spectroscopy (STS) or conductive AFM and try to understand the underlying mechanism. Here electron spin resonance studies at different conditions might be of use.

Especially SiNSs with functional groups that can interact with molecules in the surrounding environment (e.g., carboxy groups *via* hydrogen bonds), might be useful for the use as gas or humidity sensors.

## 10. Zusammenfassung und Ausblick

Aufbauend auf den Arbeiten von Okamoto *et al.* wurde zunächst die Synthese von SiNSs aus  $\text{CaSi}_2$  etabliert (**Abbildung 1**) und hierbei speziell die Behandlung der SiNSs mit HF und der anschließenden Extraktion verbessert. Damit können reaktive, Hydrid-terminierte SiNSs in großer Menge hergestellt werden.

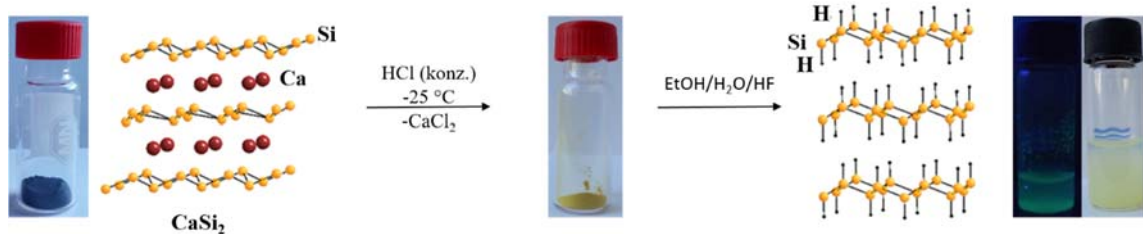


**Abbildung 1.** Schematische Darstellung der SiNSs-H Synthese aus dem Zintl Salz  $\text{CaSi}_2$  und anschließendem Ätzen mit HF (aq.).

Im ersten Teilprojekt der Doktorarbeit wurde die radikalische Initiation von Hydrosilylierungsreaktionen untersucht, welche erfolgreich für die Funktionalisierung der Hydrid-terminierten SiNSs angewendet werden kann (**Abbildung 2**). Hierbei konnten Substrate mit unterschiedlichen funktionellen Gruppen verwendet werden und photolumineszente, dispergierbare SiNSs erhalten werden.

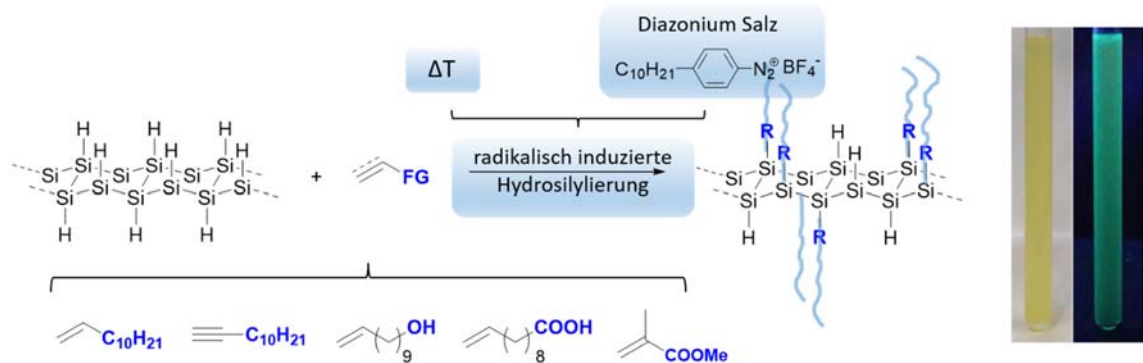


**Abbildung 2.** Schematische Darstellung der radikalisch induzierten Funktionalisierung von SiNSs-H mit unterschiedlichen Substraten und Bildern der resultierenden SiNSs-  $\text{C}_{12}\text{H}_{25}$  Dispersionen unter sichtbarem Licht (links) und UV Licht (rechts).<sup>[222]</sup>

In einem weiteren Projekt wurde das Konzept der radikalisch induzierten Funktionalisierung durch Verwendung von klassischen Radikalinitiatoren für Polymerisationen erweitert und weiterhin einige grundlegende Eigenschaften der SiNSs untersucht. Zum Beispiel die UV Instabilität der SiNSs, welche auf die Spaltung von Si-Si-Bindungen zurückgeführt werden konnte. Weiterhin wurde eine Ein-Topf Synthese von SiNS-basierten Nanokompositen beschrieben, in welcher die SiNSs funktionalisiert werden und gleichzeitig die Polymermatrix gebildet wird (**Abbildung 3**). Im Kompositmaterial bleiben die (opto)elektronischen Eigenschaften der Nanomaterialien erhalten, die

SiNSs werden gegen äußere Einflüsse (z.B. UV Licht, alkalische Bedingungen) stabilisiert und die Komposite können mit herkömmlichen Polymermethoden verarbeitet werden.

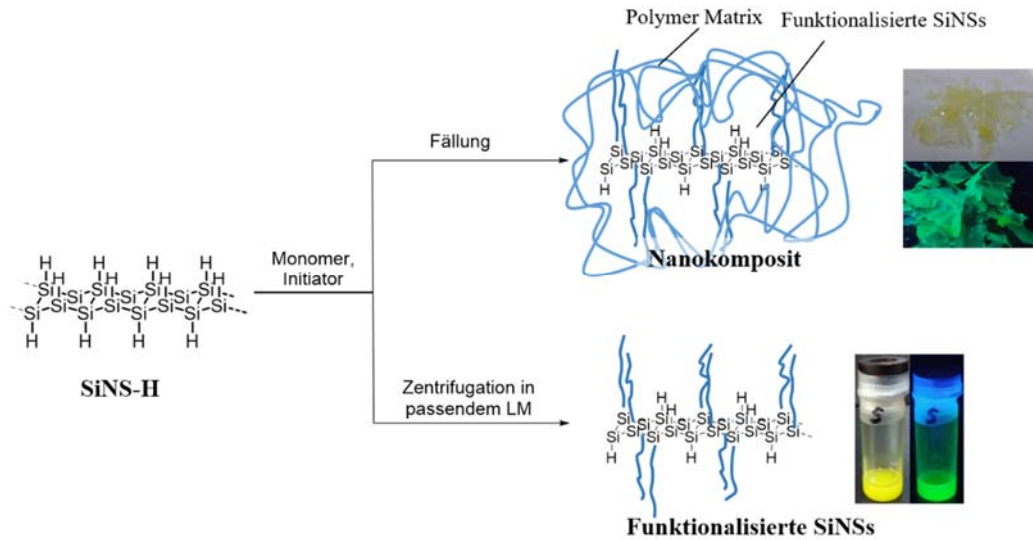


**Abbildung 3.** Schematische Darstellung der SiNS Nanokomposit Synthese und deren Aufarbeitung zum Nachweis des kovalenten Charakters. Bilder oben: SiNS-PAA@PAA Komposit unter sichtbarem (oben) und UV Licht (unten); Bilder unten: SiNS-C<sub>12</sub>H<sub>25</sub> Dispersionen in Toluol unter sichtbarem (links) und UV Licht (rechts). <sup>[223]</sup>

Das dritte Teilprojekt der Arbeit beschäftigt sich mit der *Lewis* Säure katalysierten Funktionalisierung von SiNSs. Hierbei wurden die Unterschiede von Hydrosilylierungsreaktionen auf SiNSs und SiNCs untersucht und der ablaufende Mechanismus beleuchtet. Im zweiten Teil wurden die synthetisierten Hybridmaterialien verwendet, um im Elektrolyt betriebenen Feldeffekttransistoren (SGFET) herzustellen (**Abbildung 4**), welche auf P3HT/SiNS Mischungen basieren. Die Kombination der beiden Materialien ermöglicht die Verbesserung der Sensitivität der FETs und der Transkonduktanz  $g_m$ .

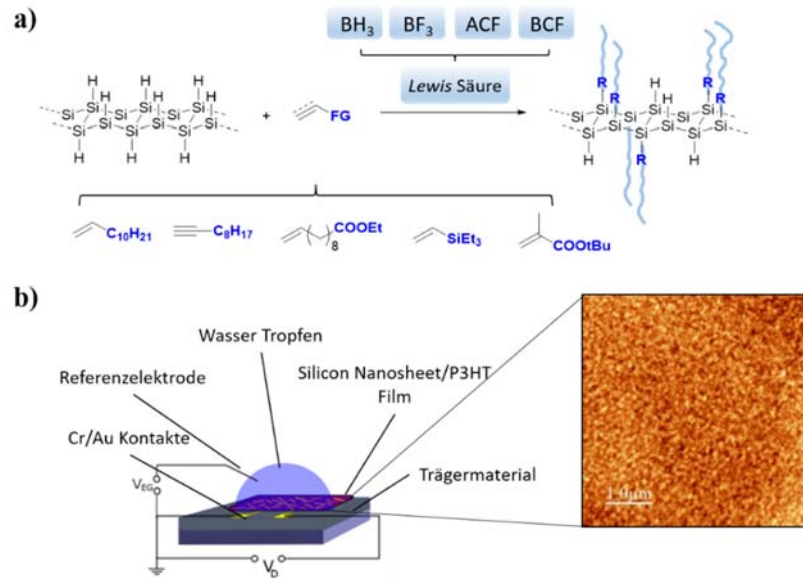


**Abbildung 4.** a) Schematische Darstellung der Lewis Säure katalysierten Funktionalisierung von SiNSs. Verschieden Lewis Säuren und funktionelle Substrate konnten verwendet werden, um die Oberfläche zu modifizieren. b) Schematische Darstellung des FET Aufbau und das zugehörige AFM Bild (rechts) des SiNS-C<sub>12</sub>H<sub>25</sub>/P3HT Films. Gute Dispergierbarkeit der funktionalisierten SiNSs im Polymer ist ersichtlich.<sup>[224]</sup>

In einem weiteren Teilprojekt wurden Diaryliodoniumsalze verwendet, um Hydrosilylierungsreaktionen auf SiNSs und SiNCs unterschiedlicher Größe durchzuführen. Diese neue Klasse an Initiatoren ist für alle SiNMs mit unterschiedlichen Substraten anwendbar und führt unter milden Bedingungen und kurzen Reaktionszeiten zu funktionalisierten Hybridmaterialien (**Abbildung 5**). Weiterhin konnte ein bisher nicht bekannter Effekt zwischen Diaryliodoniumsalz und SiNM beobachtet werden. Die Silicium Materialien induzieren den Zerfall des Iodoniumsalzes, was in der Initiation von Ringöffnungspolymerisationen von z.B. THF resultiert.

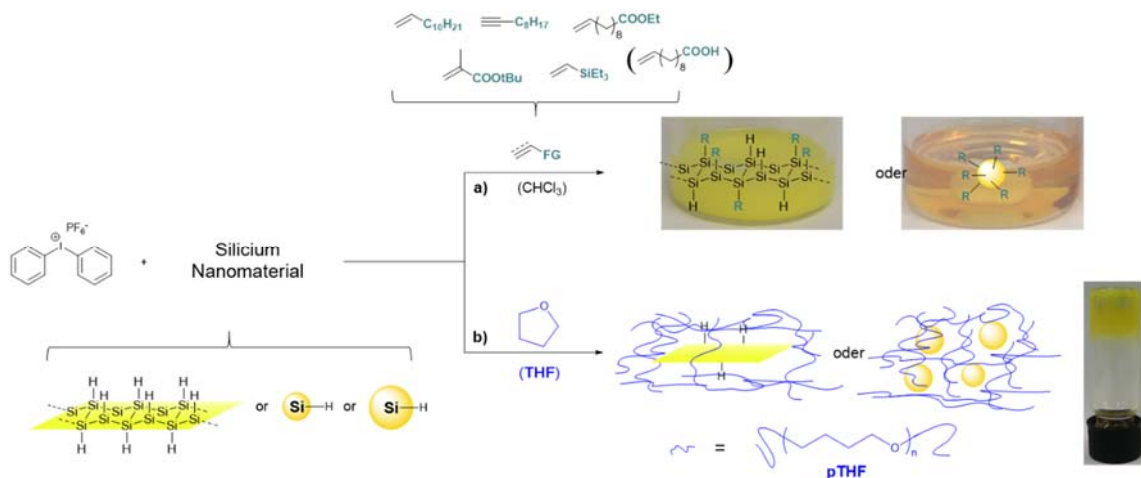


**Abbildung 5.** Schematische Darstellung der untersuchten Reaktionswege der SiNMs (SiNS, SiNC mit  $d = 3$  nm and 5 nm) mit Diaryliodoniumsalzen. a) In der Gegenwart ungesättigter Substrate fungieren Iodoniumsalze als Initiatoren für Hydrosilylierungsreaktionen. Eine Vielzahl an unterschiedlichen, funktionellen Substraten konnte somit genutzt werden, um die Oberfläche der SiNMs zu funktionalisieren. b) In Abwesenheit von ungesättigten Reagenzien tritt ein kollaborativer Effekt durch SiNM/Iodoniumsalz auf, welcher die Ringöffnungspolymerisation von Monomeren (z.B. THF) auslöst.<sup>[225]</sup>

Das Konzept wurde anschließend auf andere Monomere (z.B. Cyclohexenoxid, Trioxan, Cyclohexensulfid, MMA, <sup>t</sup>BuMA, Vinylacetat) erweitert und der zu Grunde liegende Mechanismus wurde genauer untersucht (**Abbildung 6**).

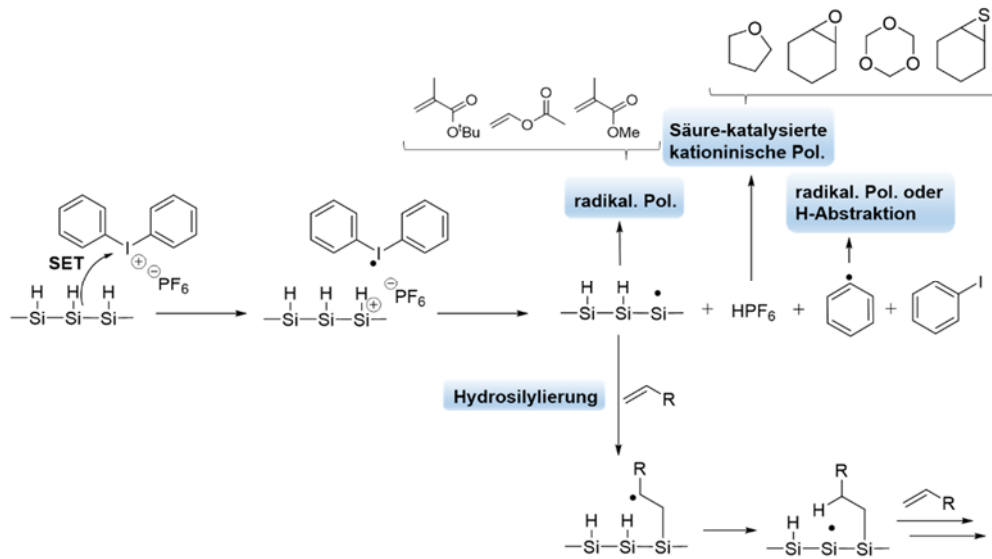


**Abbildung 6.** Schematische Darstellung der SiNM co-katalysierten Polymerisation von unterschiedlichen Monomeren mit Iodoniumsalzen und dem zu Grunde liegenden Mechanismus *via* Einzel-Elektronen-Transfer und die durch die gebildeten Reaktionsprodukte möglichen, eröffneten Reaktionspfade.

Die Methoden und Konzepte, welche in dieser Doktorarbeit beschrieben werden, bilden die Grundlage für weitergehende Studien und Anwendungen. So kann die entwickelte Funktionalisierungsschemie auf weitere 0D oder 2D Materialien wie zum Beispiel Germanium Nanokristalle oder Nanosheets angewendet werden.

Weiterhin können die SiNS basierten Nanokomposite vielversprechende Materialien zur Anwendung in Lithium-Ionen-Batterien sein. Durch Ersatz des verwendeten Polymers durch ein elektrisch und Ionen-leitfähiges Polymer (oder einer Kompositmischung) könnte ein vielversprechendes Anodenmaterial entstehen. Durch die hohe theoretische Li Speicherkapazität sollten diese Materialien die Kapazität der Anode sehr stark erhöhen und die Flexibilität des Nanokomposits sollte zur Zyklusstabilität der Si Anode beitragen.

Basierend auf den hergestellten nanoelektronischen FETs wäre es interessant SiNSs mit unterschiedlichen funktionellen Gruppen zu untersuchen. So könnten SiNSs mit einer organischen Oberflächenfunktionalisierung, basierend auf konjugierten  $\pi$ -Systemen (z.B. Phenylacetylen funktionalisierte SiNSs) andere elektronische (z.B. Bandstruktur) sowie physikalische Eigenschaften (z.B. Dispergierbarkeit, Wechselwirkung mit Matrixmaterial) aufweisen und somit die Eigenschaften der Geräte beeinflussen. Zusätzlich wäre es interessant die elektronischen Eigenschaften der funktionalisierten SiNSs mittels Rastertunnelspektroskopie oder leitfähigem AFM zu untersuchen und

die zugrunde liegenden Mechanismen zu erforschen. Hierfür könnten Elektronspin Resonanz Messungen bei unterschiedlichen Bedingungen verwendet werden.

Speziell modifizierte SiNSs mit unterschiedlichen funktionellen Gruppen, die mit Molekülen in ihrer unmittelbaren Umgebung wechselwirken können (z.B. Carbonylgruppen mittels Wasserstoffbrückenbindungen), könnten sich für Anwendungen in Gas- oder Feuchtigkeitssensoren eignen.

## 11. Publications Beyond the Scope of this Thesis

The publication “*Diazonium Salts as Grafting Agents and Efficient Radical-Hydrosilylation Initiators for Free Standing Photoluminescent Silicon Nanocrystals*” was the first work our group published on the functionalization of silicon based nanomaterials. It expands the use of diazonium salts, which are commonly used for monolayer assembly on silicon wafers, to free standing silicon nanomaterials. This new class of initiators is fast, applicable on a broad scope of substrates and suppresses homogeneous side reactions in the reaction mixture.

In “*Thermoresponsive and Photoluminescent Hybrid Silicon Nanoparticles by Surface Initiated Group Transfer Polymerization of Diethyl Vinylphosphonate*”, we extended earlier works of our group on the surface initiated group transfer polymerization.<sup>[226]</sup> We were thus able to synthesize water-soluble, SiNC based hybrid particles that combine the thermoresponsive behavior of the polymer and the optoelectronic properties of the nanomaterial.

As theoretical works already postulate the many promising properties and potential applications of the new 2D silicon monolayers. Together with Alina Lyuleeva and Prof. Lugli we took the first step to prove and exploit these unique properties. As such, we looked into the electronic properties and were able to build the first silicane based devices in form of photonic sensors in our publication “*Polymer–Silicon Nanosheet Composites: Bridging the Way to Practical (Opto)electronic Applications*”.

In our accepted publication “*In-situ Infrared Spectroscopy as Tool for Monitoring the Radical Hydrosilylation Process on Silicon Nanocrystal Surfaces*”, we could give experimental evidence for the mechanism underlying the radical induced surface functionalization of SiNCs. Our findings could thus prove formerly postulated steps and gave new insights into AIBN induced reactions.

## 11.1 Diazonium Salts as Grafting Agents and Efficient Radical-Hydrosilylation Initiators for Free Standing Photoluminescent Silicon Nanocrystals

<b>Status</b>	Published online September 8, 2014
<b>Journal</b>	Chemistry – A European Journal, 2014, Volume 15, 4212 – 4216.
<b>Publisher</b>	Wiley-VCH
<b>DOI</b>	10.1002/chem.201400114
<b>Authors</b>	Ignaz M. D. Höhle, Julian Kehrle, Tobias Helbich, Zhenyu Yang, Jonathan G. C. Veinot, Bernhard Rieger

Abstract reproduced by permission of John Wiley and Sons (license number 4078170368913).

### Abstract

The reactivity of diazonium salts towards freestanding, photoluminescent silicon nanocrystals (SiNCs) is reported. It was found that SiNCs can be functionalized with aryl groups by direct reductive grafting of the diazonium salts. Furthermore, diazonium salts are efficient radical initiators for SiNC hydrosilylation. For this purpose, novel electron-deficient diazonium salts, highly soluble in nonpolar solvents were synthesized. The SiNCs were functionalized with a variety of alkenes and alkynes at room temperature with short reaction times.

© 2014 Wiley-VCH Verlag GmbH&Co. KGaA, Weinheim

## 11.2 Thermoresponsive and Photoluminescent Hybrid Silicon Nanoparticles by Surface-Initiated Group Transfer Polymerization of Diethyl Vinylphosphonate

<b>Status</b>	Published online March 24, 2014
<b>Journal</b>	Angewandte Chemie International Edition, Volume 53, 12494 - 12497.
<b>Publisher</b>	Wiley-VCH
<b>DOI</b>	10.1002/anie.201405946
<b>Authors</b>	Ignaz M. D. Höhle, Julian Kehrle, Tobias Helbich, Zhenyu Yang, Jonathan G. C. Veinot, Bernhard Rieger

Abstract reproduced by permission of John Wiley and Sons (license number 4078170450409).

### Abstract

We present a method to combine the functional features of poly(diethyl vinylphosphonate) (PDEV) and photoluminescent silicon nanocrystals. The polymer-particle hybrids were synthesized in three steps through surface-initiated group transfer polymerization using  $\text{Cp}^*_2\text{YCH}_2\text{TMS}(\text{thf})$  as a catalyst. This pathway of particle modification renders the nanoparticle surface stable against oxidation. Although SiNC properties are known to be sensitive toward transition metals, the hybrid particles exhibit red photoluminescence in water. The temperature-dependent coiling of PDEV results in a change of the hydrodynamic radius of the hybrid particles in water. To the best of our knowledge, this is the first example of controlled catalytic polymerization reactions on a silicon nanocrystal surface.

© 2014 Wiley-VCH Verlag GmbH&Co. KGaA, Weinheim

## 11.3 Polymer–Silicon Nanosheet Composites: Bridging the Way to Practical (Opto)electronic Applications

<b>Status</b>	Published online March 2, 2017
<b>Journal</b>	Journal of Physics D: Applied Physics, Volume 50, 135106.
<b>Publisher</b>	IOP Publishing
<b>DOI</b>	10.1088/1361-6463/aa5005
<b>Authors</b>	Alina Lyuleeva, Tobias Helbich, Bernhard Rieger, Paolo Lugli

Abstract reproduced by permission of IOP Publishing (license number 4078180811332).

### **Abstract**

The fabrication of electronic devices from sensitive, functional, two-dimensional (2D) nanomaterials with anisotropic structural properties has attracted much attention. Many theoretical and experimental studies have been performed; however, such materials have not been used in applications. In this context, the focus has shifted toward the study and synthesis of new materials. Freestanding hydrogen-terminated silicon nanosheets (SiNSs) are a new class of material with outstanding (opto)electronic properties (e.g. photoluminescence at approximately 510 nm) (Nakano 2014 *J. Ceram. Soc. Japan* 122 748). SiNSs are promising candidates for use in nanoelectronic devices and flexible electronics. Additional reasons for interest in such nanomaterials are their structural anisotropy and the fact that they are made from silicon. Here, we present examples for the application of functionalized SiNS-based composites as active materials for photonic sensors. The implementation of SiNSs in a covalent nanocomposite not only improves their stability but also facilitates subsequent device fabrication. Thus, SiNSs can be used in a straightforward setup preparation procedure. We show that the modification of novel Si-based 2D nanosheets with selected organic components not only opens a new field of photosensitive applications but also improves the processability of these nanosheets (Niu et al 2014 *Sci. Rep.* 4 4810, Chimene et al 2015 *Adv. Mater.* 27 7261).

© IOP Publishing. Reproduced with permission. All rights reserved.

## 11.4 In-situ Infrared Spectroscopy as Tool for Monitoring the Radical Hydrosilylation Process on Silicon Nanocrystal Surfaces

<b>Status</b>	Accepted manuscript
<b>Journal</b>	Nanoscale.
<b>Publisher</b>	RCS Publishing
<b>DOI</b>	10.1039/C7NR02265D
<b>Authors</b>	Julian Kehrle <sup>‡</sup> , Simon J. Kaiser <sup>‡</sup> , Tapas Purkait, Malte Winnacker, Tobias Helbich, Sergei Vagin, Jonathan G. C. Veinot, Bernhard Rieger

<sup>‡</sup>these authors contributed equally.

J. Kehrle, S. J. Kaiser, T. Purkait, M. Winnacker, T. Helbich, S. Vagin, J. G. C. Veinot, B. Rieger, *Nanoscale*, **2017**, Accepted Manuscript – Abstract reproduced by permission from the Royal Chemical Society.

### Abstract

Among the variety of SiNC functionalization methods, radical initiated grafting is very promising due to its straightforward nature and low propensity to form surface oligomers. In the present study, we employed in-situ IR spectroscopy in combination with visible light transmittance measurements to investigate the radical induced grafting process on the welldefined SiNCs. Our findings support the proposed model: Unfunctionalized hydride-terminated SiNCs form agglomerates in organic solvents, which break up during the grafting process. However, clearing of the dispersion is not a valid indicator for complete surface functionalization. Furthermore, radical-initiated grafting reactions in which azobisisobutyronitrile (AIBN) is the initiator are strongly influenced by external factors including initiator concentration, grafting temperature, as well as substrate steric demand. The monomer concentration was proven to have a low impact on the grafting process. Based on these new insights an underlying mechanism could be discussed, offering an unprecedented view on the functionalization of SiNC surfaces *via* radical initiated hydrosilylation.

## 12. Bibliography

- [1] K. S. Novoselov, *Angew. Chem. Int. Ed.* **2011**, *50*, 6986.
- [2] H. Zhang, *ACS Nano* **2015**, *9*, 9451.
- [3] W. S. Yun, S. W. Han, S. C. Hong, I. G. Kim, J. D. Lee, *Phys. Rev. B* **2012**, *85*, 33305.
- [4] M. Osada, T. Sasaki, *J. Mater. Chem.* **2009**, *19*, 2503.
- [5] Q. Wang, D. O. Hare, *Chem. Rev.* **2012**, *112*, 4124.
- [6] C. Zhi, Y. Bando, C. Tang, H. Kuwahara, D. Golberg, *Adv. Mater.* **2009**, *21*, 2889.
- [7] A. Pakdel, Y. Bando, D. Golberg, *Chem. Soc. Rev.* **2014**, *43*, 934.
- [8] Y. Peng, Y. Li, Y. Ban, H. Jin, W. Jiao, X. Liu, W. Yang, *Science* **2014**, *346*, 1356.
- [9] T. Rodenas, I. Luz, G. Prieto, B. Seoane, H. Miro, A. Corma, F. Kapteijn, F. X. Llabrés i Xamena, J. Gascon, *Nat. Mater.* **2015**, *14*, 48.
- [10] M. Zhao, Y. Wang, Q. Ma, Y. Huang, X. Zhang, J. Ping, Z. Zhang, Q. Lu, Y. Yu, H. Xu, Y. Zhao, H. Zhang, *Adv. Mater.* **2015**, *27*, 7372.
- [11] J. W. Colson, A. R. Woll, A. Mukherjee, M. P. Levendorf, E. L. Spitler, V. B. Shields, M. G. Spencer, J. Park, W. R. Dichtel, *Science (80-. )*. **2011**, *332*, 228.
- [12] N. A. A. Zwaneveld, R. Pawlak, M. Abel, D. Catalin, D. Gigmes, D. Bertin, L. Porte, *J. Am. Chem. Soc.* **2008**, *130*, 6678.
- [13] M. Naguib, V. N. Mochalin, M. W. Barsoum, Y. Gogotsi, *Adv. Mater.* **2014**, *26*, 992.
- [14] H. Liu, Y. Du, Y. Deng, P. D. Ye, *Chem. Soc. Rev.* **2015**, *44*, 2732.
- [15] Y. Chen, C. Tan, H. Zhang, L. Wang, *Chem. Soc. Rev.* **2015**, *44*, 2681.
- [16] X. Duan, C. Wang, A. Pan, R. Yu, X. Duan, *Chem. Soc. Rev.* **2015**, *44*, 8859.
- [17] K. S. K. S. Kim, Y. Zhao, H. Jang, S. Y. Lee, J. M. Kim, K. S. K. S. Kim, J.-H. Ahn, P. Kim, J.-Y. Choi, B. H. Hong, *Nature* **2009**, *457*, 706.
- [18] Y. Zhang, T.-T. Tang, C. Girit, Z. Hao, M. C. Martin, A. Zettl, M. F. Crommie, Y. R. Shen, F. Wang, *Nature* **2009**, *459*, 820.
- [19] Y. Chen, J. Xi, D. O. Dumcenco, Z. Liu, K. Suenaga, D. Wang, Z. Shuai, Y. S. Huang, L. Xie, *ACS Nano* **2013**, *7*, 4610.
- [20] Y. Shi, H. Li, L.-J. Li, *Chem. Soc. Rev.* **2015**, *44*, 2744.
- [21] B. Marinho, M. Ghislandi, E. Tkalya, C. E. Koning, G. de With, *Powder Technol.* **2012**, *221*, 351.
- [22] M. J. Allen, V. C. Tung, R. B. Kaner, *Chem. Rev.* **2010**, *110*, 132.
- [23] M. Ghorbani-Asl, S. Borini, A. Kuc, T. Heine, *Phys. Rev. B - Condens. Matter Mater. Phys.* **2013**, *87*, 235434.
- [24] C. R. Ryder, J. D. Wood, S. A. Wells, M. C. Hersam, *ACS Nano* **2016**, *10*, 3900.
- [25] S. Stankovich, D. A. Dikin, G. H. B. Dommett, K. M. Kohlhaas, E. J. Zimney, E. A. Stach, R. D. Piner, S. T. Nguyen, R. S. Ruoff, *Nature* **2006**, *442*, 282.
- [26] J. J. Park, W. J. Hyun, S. C. Mun, Y. T. Park, O. O. Park, *ACS Appl. Mater. Interfaces* **2015**, *7*, 6317.
- [27] Y. Huang, J. Guo, Y. Kang, Y. Ai, C. M. Li, *Nanoscale* **2015**, *7*, 19358.
- [28] L. H. Hess, A. Lyuleeva, B. M. Blaschke, M. Sachsenhauser, M. Seifert, J. a. Garrido, F. Deubel, *ACS Appl. Mater. Interfaces* **2014**, *6*, 9705.

- [29] J. Liu, Z. Liu, C. J. Barrow, W. Yang, *Anal. Chim. Acta* **2015**, *859*, 1.
- [30] J. Zhou, M. M. Wu, X. Zhou, Q. Sun, *Appl. Phys. Lett.* **2009**, *95*, 103108.
- [31] X. Chen, A. R. McDonald, *Adv. Mater.* **2016**, *28*, 5738.
- [32] C. R. Ryder, J. D. Wood, S. A. Wells, Y. Yang, D. Jariwala, T. J. Marks, G. C. Schatz, M. C. Hersam, *Nat. Chem.* **2016**, *8*, 597.
- [33] F. Erogbogbo, C.-A. Tien, C.-W. Chang, K.-T. Yong, W.-C. Law, H. Ding, I. Roy, M. T. Swihart, P. N. Prasad, *Bioconjug. Chem.* **2011**, *22*, 1081.
- [34] F. Erogbogbo, K.-T. Yong, I. Roy, G. Xu, P. N. Prasad, M. T. Swihart, *ACS Nano* **2008**, *2*, 873.
- [35] M. J. S. Spencer, T. Morishita, I. K. Snook, *Nanoscale* **2012**, *4*, 2906.
- [36] P. Avouris, F. Xia, *MRS Bull.* **2012**, *37*, 1225.
- [37] D. C. Elias, R. R. Nair, T. M. G. Mohiuddin, S. V. Morozov, P. Blake, M. P. Halsall, A. C. Ferrari, D. W. Boukhvalov, M. I. Katsnelson, A. K. Geim, K. S. Novoselov, *Science (80-. )*. **2009**, *323*, 610.
- [38] H. Okamoto, Y. Sugiyama, H. Nakano, *Chem. - A Eur. J.* **2011**, *17*, 9864.
- [39] Z. Ni, H. Zhong, X. Jiang, R. Quhe, G. Luo, Y. Wang, M. Ye, J. Yang, J. Shi, J. Lu, *Nanoscale* **2014**, *6*, 7609.
- [40] Y. Kumai, H. Nakano, *Jpn. J. Appl. Phys.* **2015**, *54*, 35201.
- [41] Y. Kumai, H. Kadoura, E. Sudo, M. Iwaki, H. Okamoto, Y. Sugiyama, H. Nakano, *J. Mater. Chem.* **2011**, *21*, 11941.
- [42] Y. Kumai, S. Shirai, E. Sudo, J. Seki, H. Okamoto, Y. Sugiyama, H. Nakano, *J. Power Sources* **2011**, *196*, 1503.
- [43] H. Nakano, Y. Sugiyama, T. Morishita, M. J. S. Spencer, I. K. Snook, Y. Kumai, H. Okamoto, *J. Mater. Chem. A* **2014**, *2*, 7588.
- [44] R. Yaokawa, T. Ohsuna, T. Morishita, Y. Hayasaka, M. J. S. Spencer, H. Nakano, *Nat. Commun.* **2016**, *7*, 10657.
- [45] R. Q. Zhang, X. M. Liu, Z. Wen, Q. Jiang, *J. Phys. Chem. C* **2011**, *115*, 3425.
- [46] J. Wang, J. Li, S.-S. Li, Y. Liu, *J. Appl. Phys.* **2013**, *114*, 124309.
- [47] G. Cao, Y. Wang, *Nanostructures and nanomaterials - Synthesis, properties, and applications*; 2nd ed.; World Scientific: Singapore; London, 2011.
- [48] J. G. C. Veinot, *Chem. Commun.* **2006**, *0*, 4160.
- [49] L. Pavesi, R. Turan, *Silicon Nanocrystals*; Pavesi, L.; Turan, R., Eds.; Wiley-VCH Verlag GmbH & Co. KGaA: Weinheim, Germany, 2010.
- [50] G. N. Makarov, *Phys. - Uspekhi* **2013**, *56*, 643.
- [51] X. Yu, F. Xue, H. Huang, C. Liu, J. Yu, Y. Sun, X. Dong, G. Cao, Y. Jung, *Nanoscale* **2014**, *6*, 6860.
- [52] W.-S. Kim, Y. Hwa, J.-H. Shin, M. Yang, H.-J. Sohn, S.-H. Hong, *Nanoscale* **2014**, *6*, 4297.
- [53] Z. Lu, J. Zhu, D. Sim, W. Zhou, W. Shi, H. H. Hng, Q. Yan, *Chem. Mater.* **2011**, *23*, 5293.
- [54] U. Kim, I. Kim, Y. Park, K.-Y. Y. Lee, S.-Y. Y. Yim, J.-G. G. Park, H.-G. G. Ahn, S.-H. H. Park, H.-J. J. Choi, *ACS Nano* **2011**, *5*, 2176.
- [55] S. W. Kim, J. Lee, J. H. Sung, D. Seo, I. Kim, M.-H. Jo, B. W. Kwon, W. K. Choi, H.-J. Choi, *ACS Nano* **2014**, *8*, 6556.
- [56] M. A. Ali, M. R. Tchalala, *J. Phys. Conf. Ser.* **2014**, *491*, 12009.

- [57] K. Takeda, K. Shiraishi, *Phys. Rev. B* **1994**, *50*, 14916.
- [58] C. Leandri, G. Le Lay, B. Aufray, C. Girardeaux, J. Avila, M. E. Dávila, M. C. Asensio, C. Ottaviani, a. Cricenti, *Surf. Sci.* **2005**, *574*, L9.
- [59] B. Aufray, A. Kara, S. Vizzini, H. Oughaddou, C. Landri, B. Ealet, G. Le Lay, S. Vizzini, H. Oughaddou, C. Léandri, B. Ealet, G. Le Lay, *Appl. Phys. Lett.* **2010**, *96*, 183102.
- [60] P. De Padova, C. Quaresima, C. Ottaviani, P. M. Sheverdyeva, P. Moras, C. Carbone, D. Topwal, B. Olivieri, A. Kara, H. Oughaddou, B. Aufray, G. Le Lay, *Appl. Phys. Lett.* **2010**, *96*, 261905.
- [61] S. B. Fagan, R. J. Baierle, R. Mota, A. J. R. da Silva, A. Fazzio, *Phys. Rev. B* **2000**, *61*, 9994.
- [62] S. Lebègue, O. Eriksson, *Phys. Rev. B - Condens. Matter Mater. Phys.* **2009**, *79*, 115409.
- [63] S. Cahangirov, M. Topsakal, E. Aktürk, H. Sahin, S. Ciraci, *Phys. Rev. Lett.* **2009**, *102*, 236804.
- [64] H. Sahaf, L. Masson, C. Léandri, B. Aufray, G. Le Lay, F. Ronci, *Appl. Phys. Lett.* **2007**, *90*, 263110.
- [65] P. De Padova, C. Quaresima, P. Perfetti, B. Olivieri, C. Leandri, B. Aufray, S. Vizzini, G. Le Lay, *Nano Lett.* **2008**, *8*, 271.
- [66] A. Kara, C. Léandri, M. E. Dávila, P. De Padova, B. Ealet, H. Oughaddou, B. Aufray, G. Le Lay, *J. Supercond. Nov. Magn.* **2009**, *22*, 259.
- [67] P. De Padova, C. Quaresima, B. Olivieri, P. Perfetti, G. Le Lay, *Appl. Phys. Lett.* **2011**, *98*, 81909.
- [68] M. R. Tchalala, H. Enriquez, A. J. Mayne, A. Kara, G. Dujardin, M. A. Ali, H. Oughaddou, *J. Phys. Conf. Ser.* **2014**, *491*, 12002.
- [69] S. Colonna, G. Serrano, P. Gori, A. Cricenti, F. Ronci, *J. Phys. Condens. Matter* **2013**, *25*, 315301.
- [70] B. Lalmi, H. Oughaddou, H. Enriquez, A. Kara, S. Vizzini, B. Ealet, B. Aufray, *Appl. Phys. Lett.* **2010**, *97*, 223109.
- [71] P. Vogt, P. De Padova, C. Quaresima, J. Avila, E. Frantzeskakis, M. C. Asensio, A. Resta, B. Ealet, G. Le Lay, *Phys. Rev. Lett.* **2012**, *108*, 155501.
- [72] D. Chiappe, C. Grazianetti, G. Tallarida, M. Fanciulli, A. Molle, *Adv. Mater.* **2012**, *24*, 5088.
- [73] B. Feng, Z. Ding, S. Meng, Y. Yao, X. He, P. Cheng, L. Chen, K. Wu, *Nano Lett.* **2012**, *12*, 3507.
- [74] A. Fleurence, R. Friedlein, T. Ozaki, H. Kawai, Y. Wang, Y. Yamada-Takamura, *Phys. Rev. Lett.* **2012**, *108*, 245501.
- [75] L. Meng, Y. Wang, L. Zhang, S. Du, R. Wu, L. Li, Y. Zhang, G. Li, H. Zhou, W. a. Hofer, H.-J. Gao, *Nano Lett.* **2013**, *13*, 685.
- [76] M. Rachid Tchalala, H. Enriquez, A. J. Mayne, A. Kara, S. Roth, M. G. Silly, A. Bendounan, F. Sirotti, T. Greber, B. Aufray, G. Dujardin, M. Ait Ali, H. Oughaddou, *Appl. Phys. Lett.* **2013**, *102*, 10.
- [77] P. De Padova, O. Kubo, B. Olivieri, C. Quaresima, T. Nakayama, M. Aono, G. Le Lay, *Nano Lett.* **2012**, *12*, 5500.
- [78] M. Kanno, R. Arafune, C. Liang Lin, E. Minamitani, M. Kawai, N. Takagi, *New J. Phys.* **2014**, *16*, 105019.
- [79] S. Sattar, R. Hoffmann, U. Schwingenschlögl, *New J. Phys.* **2014**, *16*, 65001.
- [80] L. Tsetseris, D. Kaltsas, *Phys. Chem. Chem. Phys.* **2014**, *16*, 5183.
- [81] M. Houssa, G. Pourtois, V. V. Afanas'ev, A. Stesmans, *Appl. Phys. Lett.* **2010**, *97*, 112106.
- [82] L. Tao, E. Cinquanta, D. Chiappe, C. Grazianetti, M. Fanciulli, M. Dubey, A. Molle, D.

- Akinwande, *Nat. Nanotechnol.* **2015**, *10*, 227.
- [83] A. Molle, C. Grazianetti, D. Chiappe, E. Cinquanta, E. Cianci, G. Tallarida, M. Fanciulli, *Adv. Funct. Mater.* **2013**, *23*, 4340.
- [84] J. R. Dahn, B. M. Way, E. Fuller, J. S. Tse, *Phys. Rev. B* **1993**, *48*, 17872.
- [85] F. Wöhler, *Ann. der Chemie und Pharm.* **1863**, *127*, 257.
- [86] H. Kautsky, H. Thiele, *Zeitschrift für Anorg. und Allg. Chemie* **1925**, *144*, 197.
- [87] H. Kautsky, *Zeitschrift für Anorg. und Allg. Chemie* **1921**, *117*, 209.
- [88] G. Schott, D. Naumann, *Zeitschrift für Anorg. und Allg. Chemie* **1957**, *291*, 112.
- [89] A. Weiss, G. Beil, H. Meyer, *Z. Naturforsch., B* **1979**, *34b*, 25.
- [90] E. Hengge, G. Scheffler, *Monatshefte für Chemie* **1964**, *95*, 1450.
- [91] S. Yamanaka, H. Matsu-ura, M. Ishikawa, *Mater. Res. Bull.* **1996**, *31*, 307.
- [92] G. Schott, D. Naumann, *Zeitschrift für Anorg. und Allg. Chemie* **1957**, *291*, 103.
- [93] E. Hengge, G. Olbrich, *Monatshefte für Chemie* **1970**, *101*, 1068.
- [94] E. Hengge, G. Scheffler, *Monatshefte für Chemie* **1964**, *95*, 1461.
- [95] H. D. Fuchs, M. Stutzmann, M. S. Brandt, M. Rosenbauer, J. Weber, A. Breitschwerdt, P. Deák, M. Cardona, *Phys. Rev. B* **1993**, *48*, 8172.
- [96] M. Stutzmann, M. S. Brandt, M. Rosenbauer, J. Weber, H. D. Fuchs, *Phys. Rev. B* **1993**, *47*, 4806.
- [97] H. Nakano, T. Mitsuoka, M. Harada, K. Horibuchi, H. Nozaki, N. Takahashi, T. Nonaka, Y. Seno, H. Nakamura, *Angew. Chemie* **2006**, *118*, 6451.
- [98] Y. Sugiyama, H. Okamoto, T. Mitsuoka, T. Morikawa, K. Nakanishi, T. Ohta, H. Nakano, *J. Am. Chem. Soc.* **2010**, *132*, 5946.
- [99] I. M. D. Höhle, New Methods for the Surface Functionalization of Photoluminescent Silicon Nanocrystals, Technische Universität München, 2015.
- [100] J. G. C. Veinot, *Chem. Commun.* **2006**, *0*, 4160.
- [101] J. M. Buriak, *Adv. Mater.* **1999**, *11*, 265.
- [102] I. M. D. Höhle, J. Kehrle, T. Helbich, Z. Yang, J. G. C. Veinot, B. Rieger, *Chem. - A Eur. J.* **2014**, *20*, 4212.
- [103] P. K. Sudeep, Z. Page, T. Emrick, *Chem. Commun.* **2008**, 6126.
- [104] Z. F. Li, E. Ruckenstein, *Nano Lett.* **2004**, *4*, 1463.
- [105] M. Dasog, G. B. De, L. V. Titova, F. A. Hegmann, J. G. C. Veinot, G. B. De Los Reyes, L. V. Titova, F. A. Hegmann, J. G. C. Veinot, *ACS Nano* **2014**, *8*, 9636.
- [106] T. Zhou, R. T. Anderson, H. Li, J. Bell, Y. Yang, B. P. Gorman, S. Pylypenko, M. T. Lusk, A. Sellinger, *Nano Lett.* **2015**, *15*, 3657.
- [107] H. Nakano, T. Ikuno, *Appl. Phys. Rev.* **2016**, *3*, 40803.
- [108] H. Okamoto, Y. Kumai, Y. Sugiyama, T. Mitsuoka, K. Nakanishi, T. Ohta, H. Nozaki, S. Yamaguchi, S. Shirai, H. Nakano, *J. Am. Chem. Soc.* **2010**, *132*, 2710.
- [109] J. Ohshita, K. Yamamoto, D. Tanaka, M. Nakashima, Y. Kunugi, M. Ohashi, H. Nakano, *J. Phys. Chem. C* **2016**, *120*, 10991.
- [110] H. Okamoto, Y. Sugiyama, K. Nakanishi, T. Ohta, T. Mitsuoka, H. Nakano, *Chem. Mater.* **2015**, *27*, 1292.

- [111] H. Nakano, M. Nakano, K. Nakanishi, D. Tanaka, Y. Sugiyama, T. Ikuno, H. Okamoto, T. Ohta, *J. Am. Chem. Soc.* **2012**, *134*, 5452.
- [112] M. Ohashi, H. Nakano, T. Morishita, M. J. S. Spencer, Y. Ikemoto, C. Yogi, T. Ohta, *Chem. Commun.* **2014**, *50*, 9761.
- [113] D. Morachis-Galindo, P. Rubio-Pereda, N. Takeuchi, *Appl. Surf. Sci.* **2017**, *392*, 841.
- [114] B. K. Teo, X. H. Sun, *Chem. Rev.* **2007**, *107*, 1454.
- [115] C. Grazianetti, E. Cinquanta, A. Molle, *2D Mater.* **2016**, *3*, 12001.
- [116] Z. G. Shao, X. S. Ye, L. Yang, C. L. Wang, *J. Appl. Phys.* **2013**, *114*, 2013.
- [117] N. J. Roome, J. D. Carey, *ACS Appl. Mater. Interfaces* **2014**, *6*, 7743.
- [118] C. Xu, G. Luo, Q. Liu, J. Zheng, Z. Zhang, S. Nagase, Z. Gao, J. Lu, *Nanoscale* **2012**, *4*, 3111.
- [119] M. Ezawa, *Phys. Rev. Lett.* **2012**, *109*, 55502.
- [120] C.-C. Liu, W. Feng, Y. Yao, *Phys. Rev. Lett.* **2011**, *107*, 76802.
- [121] Z.-X. Guo, S. Furuya, J. Iwata, A. Oshiyama, *Phys. Rev. B* **2013**, *87*, 235435.
- [122] J. Gao, J. Zhao, *Sci. Rep.* **2012**, *2*, 861.
- [123] S. Cahangirov, M. Audiffred, P. Tang, A. Iacomino, W. Duan, G. Merino, A. Rubio, *Phys. Rev. B* **2013**, *88*, 35432.
- [124] Z.-X. Guo, S. Furuya, J. Iwata, A. Oshiyama, *J. Phys. Soc. Japan* **2013**, *82*, 63714.
- [125] Jiajie Zhu, U. Schwingenschlögl, *2D Mater.* **2015**, *2*, 45004.
- [126] D. Chiappe, E. Scalise, E. Cinquanta, C. Grazianetti, B. van den Broek, M. Fanciulli, M. Houssa, A. Molle, *Adv. Mater.* **2014**, *26*, 2096.
- [127] H. Liu, J. Gao, J. Zhao, *J. Phys. Chem. C* **2013**, *117*, 10353.
- [128] S. Kokott, L. Matthes, F. Bechstedt, *Phys. status solidi - Rapid Res. Lett.* **2013**, *7*, 538.
- [129] G. Li, J. Tan, X. Liu, X. Wang, F. Li, M. Zhao, *Chem. Phys. Lett.* **2014**, *595–596*, 20.
- [130] Y. Li, Z. Chen, *J. Phys. Chem. Lett.* **2013**, *4*, 269.
- [131] R. W. Zhang, C. W. Zhang, W. X. Ji, S. J. Hu, S. S. Yan, S. S. Li, P. Li, P. J. Wang, Y. S. Liu, *J. Phys. Chem. C* **2014**, *118*, 25278.
- [132] A. O'Hare, F. V. Kusmartsev, K. I. Kugel, *Nano Lett.* **2012**, *12*, 1045.
- [133] Z. Ni, Q. Liu, K. Tang, J. Zheng, J. Zhou, R. Qin, Z. Gao, D. Yu, J. Lu, *Nano Lett.* **2012**, *12*, 113.
- [134] S. Li, Y. Wu, Y. Tu, Y. Wang, T. Jiang, W. Liu, Y. Zhao, *Sci. Rep.* **2015**, *5*, 7881.
- [135] J. Gao, J. Zhang, H. Liu, Q. Zhang, J. Zhao, *Nanoscale* **2013**, *5*, 9785.
- [136] H. Liu, H. Feng, Y. Du, J. Chen, K. Wu, J. Zhao, *2D Mater.* **2016**, *3*, 25034.
- [137] N. Gao, W. T. Zheng, Q. Jiang, *Phys. Chem. Chem. Phys.* **2012**, *14*, 257.
- [138] J. C. Garcia, D. B. de Lima, L. V. C. Assali, J. F. Justo, *J. Phys. Chem. C* **2011**, *115*, 13242.
- [139] Q. G. Jiang, J. F. Zhang, Z. M. Ao, Y. P. Wu, *Sci. Rep.* **2015**, *5*, 15734.
- [140] P. Zhang, X. D. Li, C. H. Hu, S. Q. Wu, Z. Z. Zhu, *Phys. Lett. A* **2012**, *376*, 1230.
- [141] W. Wei, T. Jacob, *Phys. Rev. B* **2013**, *88*, 45203.
- [142] T. H. Osborn, A. a. Farajian, O. V. Pupyshva, R. S. Aga, L. C. Lew Yan Voon, *Chem. Phys. Lett.* **2011**, *511*, 101.
- [143] Y. Song, Y. Su, G.-P. Zhang, C.-K. Wang, G. Chen, *Comput. Mater. Sci.* **2017**, *129*, 37.

- [144] A. N. Kholod, S. Ossicini, V. E. Borisenko, F. Arnaud d'Avitaya, *Surf. Sci.* **2003**, 527, 30.
- [145] N. Gao, G. Y. Lu, Z. Wen, Q. Jiang, *J. Mater. Chem. C* **2017**, 5, 627.
- [146] G. García, M. Atilhan, S. Aparicio, *Phys. Chem. Chem. Phys.* **2015**, 17, 16315.
- [147] T. Morishita, K. Nishio, M. Mikami, *Phys. Rev. B* **2008**, 77, 81401.
- [148] J. Bai, H. Tanaka, X. C. Zeng, *Nano Res.* **2010**, 3, 694.
- [149] O. D. Restrepo, R. Mishra, J. E. Goldberger, W. Windl, *J. Appl. Phys.* **2014**, 115, 33711.
- [150] S. Naji, B. Khalil, H. Labrim, M. Bhihi, A. Belhaj, A. Benyoussef, M. Lakhall, a El Kenz, *J. Phys. Conf. Ser.* **2014**, 491, 12006.
- [151] Z.-X. Guo, A. Oshiyama, *Phys. Rev. B* **2014**, 89, 155418.
- [152] P. Pflugradt, L. Matthes, F. Bechstedt, *Phys. Rev. B* **2014**, 89, 205428.
- [153] S. Cahangirov, V. O. Özçelik, L. Xian, J. Avila, S. Cho, M. C. Asensio, S. Ciraci, A. Rubio, *Phys. Rev. B* **2014**, 90, 35448.
- [154] C. Kamal, A. Chakrabarti, A. Banerjee, S. K. Deb, *J. Phys. Condens. Matter* **2013**, 25, 85508.
- [155] N. W. Johnson, P. Vogt, A. Resta, P. De Padova, I. Perez, D. Muir, E. Z. Kurmaev, G. Le Lay, A. Moewes, *Adv. Funct. Mater.* **2014**, 24, 5253.
- [156] P. De Padova, C. Leandri, S. Vizzini, C. Quaresima, P. Perfetti, B. Olivieri, H. Oughaddou, B. Aufray, G. Le Lay, *Nano Lett.* **2008**, 8, 2299.
- [157] Z. Majzik, M. Rachid Tchalala, M. Švec, P. Hapala, H. Enriquez, A. Kara, a J. Mayne, G. Dujardin, P. Jelínek, H. Oughaddou, *J. Phys. Condens. Matter* **2013**, 25, 225301.
- [158] Y. Du, J. Zhuang, J. Wang, Z. Li, H. Liu, J. Zhao, X. Xu, H. Feng, L. Chen, K. Wu, X. Wang, S. X. Dou, *Sci. Adv.* **2016**, 2, e1600067.
- [159] J. Avila, P. De Padova, S. Cho, I. Colambo, S. Lorcy, C. Quaresima, P. Vogt, A. Resta, G. Le Lay, M. C. Asensio, *J. Phys. Condens. Matter* **2013**, 25, 262001.
- [160] S. K. Mahatha, P. Moras, V. Bellini, P. M. Sheverdyeva, C. Struzzi, L. Petaccia, C. Carbone, *Phys. Rev. B* **2014**, 89, 201416.
- [161] C.-L. Lin, R. Arafune, K. Kawahara, M. Kanno, N. Tsukahara, E. Minamitani, Y. Kim, M. Kawai, N. Takagi, *Phys. Rev. Lett.* **2013**, 110, 76801.
- [162] C. Grazianetti, E. Cinquanta, L. Tao, P. De Padova, C. Quaresima, C. Ottaviani, D. Akinwande, A. Molle, *ACS Nano* **2017**, 11, 3376.
- [163] P. De Padova, P. Vogt, A. Resta, J. Avila, I. Razado-Colambo, C. Quaresima, C. Ottaviani, B. Olivieri, T. Bruhn, T. Hirahara, T. Shirai, S. Hasegawa, M. Carmen Asensio, G. Le Lay, *Appl. Phys. Lett.* **2013**, 102, 2013.
- [164] T. Ikuno, H. Okamoto, Y. Sugiyama, H. Nakano, F. Yamada, I. Kamiya, *Appl. Phys. Lett.* **2011**, 99, 23107.
- [165] P. De Padova, P. Perfetti, B. Olivieri, C. Quaresima, C. Ottaviani, G. Le Lay, *J. Phys. Condens. Matter* **2012**, 24, 223001.
- [166] E. Cinquanta, E. Scalise, D. Chiappe, C. Grazianetti, B. van den Broek, M. Houssa, M. Fanciulli, A. Molle, *J. Phys. Chem. C* **2013**, 117, 16719.
- [167] P. Vogt, P. Capiod, M. Berthe, A. Resta, P. De Padova, T. Bruhn, G. Le Lay, B. Grandidier, *Appl. Phys. Lett.* **2014**, 104, 21602.
- [168] P. De Padova, C. Ottaviani, C. Quaresima, B. Olivieri, P. Imperatori, E. Salomon, T. Angot, L. Quagliano, C. Romano, A. Vona, M. Muniz-Miranda, A. Generosi, B. Paci, G. Le Lay, *2D Mater.* **2014**, 1, 21003.
- [169] A. M. Tokmachev, D. V. Averyanov, I. A. Karateev, O. E. Parfenov, A. L. Vasiliev, S. N.

- Yakunin, V. G. Storchak, *Nanoscale* **2016**, *8*, 16229.
- [170] E. Noguchi, K. Sugawara, R. Yaokawa, T. Hitosugi, H. Nakano, T. Takahashi, *Adv. Mater.* **2015**, *27*, 856.
- [171] A. Nourbakhsh, M. Cantoro, T. Vosch, G. Pourtois, F. Clemente, M. H. van der Veen, J. Hofkens, M. M. Heyns, S. De Gendt, B. F. Sels, *Nanotechnology* **2010**, *21*, 435203.
- [172] P. A. Denis, *Chem. Phys. Lett.* **2010**, *492*, 251.
- [173] A. J. Lu, X. B. Yang, R. Q. Zhang, *Solid State Commun.* **2009**, *149*, 153.
- [174] G. G. Guzmán-Verri, L. C. Lew Yan Voon, *J. Phys. Condens. Matter* **2011**, *23*, 145502.
- [175] C. G. Van de Walle, J. E. Northrup, *Phys. Rev. Lett.* **1993**, *70*, 1116.
- [176] M. J. S. Spencer, M. R. Bassett, T. Morishita, I. K. Snook, H. Nakano, *New J. Phys.* **2013**, *15*, 125018.
- [177] Y. Liu, H. Shu, P. Liang, D. Cao, X. Chen, W. Lu, *J. Appl. Phys.* **2013**, *114*, 94308.
- [178] F. Zheng, C. Zhang, *Nanoscale Res. Lett.* **2012**, *7*, 422.
- [179] Q. Wu, X. Wang, T. A. Niehaus, R. Zhang, *Phys. Chem. C* **2014**, *118*, 20070.
- [180] C. Zhang, A. De Sarkar, R. Q. Zhang, *J. Phys. Chem. C* **2011**, *115*, 23682.
- [181] D. Q. Fang, Y. Zhang, S. L. Zhang, *New J. Phys.* **2014**, *16*, 115006.
- [182] M. Montazeri, L. M. Smith, H. E. Jackson, J. M. Yarrison-Rice, Y.-J. Choi, J.-G. Park, *Appl. Phys. Lett.* **2009**, *95*, 83105.
- [183] A. J. Lu, R. Q. Zhang, S. T. Lee, *Appl. Phys. Lett.* **2007**, *91*, 263107.
- [184] C. L. dos Santos, P. Piquini, *Phys. Rev. B* **2010**, *81*, 75408.
- [185] P. M. Fauchet, *Mater. Today* **2005**, *8*, 26.
- [186] Y. Ding, Y. Wang, *Appl. Phys. Lett.* **2012**, *100*, 83102.
- [187] N. Lu, Z. Li, J. Yang, *J. Phys. Chem. C* **2009**, *113*, 16741.
- [188] M. J. S. Spencer, T. Morishita, M. Mikami, I. K. Snook, Y. Sugiyama, H. Nakano, *Phys. Chem. Chem. Phys.* **2011**, *13*, 15418.
- [189] F. Li, R. Lu, Q. Yao, E. Kan, Y. Liu, H. Wu, Y. Yuan, C. Xiao, K. Deng, *J. Phys. Chem. C* **2013**, *117*, 13283.
- [190] J. Požela, In *Physics of High-Speed Transistors*; Springer US: Boston, MA, 1993; pp. 35–47.
- [191] F. Schwierz, *Nat. Nanotechnol.* **2010**, *5*, 487.
- [192] W. Hu, X. Wu, Z. Li, J. Yang, *Nanoscale* **2013**, *5*, 9062.
- [193] W. Hu, X. Wu, Z. Li, J. Yang, *Phys. Chem. Chem. Phys.* **2013**, *15*, 5753.
- [194] J. Zhuang, X. Xu, G. Peleckis, W. Hao, S. X. Dou, Y. Du, *Adv. Mater.* **2017**, 1606716.
- [195] J. Huang, H.-J. Chen, M.-S. Wu, G. Liu, C.-Y. Ouyang, B. Xu, *Chinese Phys. Lett.* **2013**, *30*, 17103.
- [196] Y.-H. Guo, J.-X. Cao, B. Xu, *Chinese Phys. B* **2016**, *25*, 17101.
- [197] J. Setiadi, M. D. Arnold, M. J. Ford, *ACS Appl. Mater. Interfaces* **2013**, *5*, 10690.
- [198] G. A. Tritsarlis, E. Kaxiras, S. Meng, E. Wang, *Nano Lett.* **2013**, *13*, 2258.
- [199] J. K. Deng, J. Z. Liu, N. V Medhekar, *Rsc Adv.* **2013**, *3*, 20338.
- [200] W. Hu, N. Xia, X. Wu, Z. Li, J. Yang, *Phys. Chem. Chem. Phys.* **2014**, *16*, 6957.

- [201] M. Niu, D. Cheng, D. Cao, *Sci. Rep.* **2014**, *4*, 4810.
- [202] V. V Kulish, O. I. Malyi, M.-F. Ng, Z. Chen, S. Manzhos, P. Wu, *Phys. Chem. Chem. Phys.* **2014**, *16*, 4260.
- [203] M. N. Obrovac, L. Christensen, *Electrochem. Solid-State Lett.* **2004**, *7*, A93.
- [204] T. D. Hatchard, J. R. Dahn, *J. Electrochem. Soc.* **2004**, *151*, A838.
- [205] I. M. D. Höhle, J. Kehrle, T. K. Purkait, J. G. C. Veinot, B. Rieger, *Nanoscale* **2015**, *7*, 914.
- [206] I. M. D. Höhle, A. Angl, R. Sinelnikov, J. G. C. Veinot, B. Rieger, *Chem. Eur. J.* **2014**, *21*, 2755.
- [207] A. Angl, R. Sinelnikov, A. Meldrum, J. G. C. Veinot, I. Balberg, D. Azulay, O. Millo, B. Rieger, *Nanoscale* **2016**, *8*, 7849.
- [208] I. M. D. Höhle, P. D. L. Werz, J. G. C. Veinot, B. Rieger, *Nanoscale* **2015**, *7*, 7811.
- [209] J. Kehrle, I. M. D. Höhle, Z. Yang, A. Jochem, T. Helbich, T. Kraus, J. G. C. Veinot, B. Rieger, *Angew. Chemie Int. Ed.* **2014**, *53*, 12494.
- [210] T. K. Purkait, M. Iqbal, M. H. Wahl, K. Gottschling, C. M. Gonzalez, M. A. Islam, J. G. C. Veinot, *J. Am. Chem. Soc.* **2014**, *136*, 17914.
- [211] D. Wang, J. M. Buriak, *Langmuir* **2006**, *22*, 6214.
- [212] *Aryl Diazonium Salts - New Coupling Agents in Polymer and Surface Science*; Mohamed Mehdi Chehimi, Ed.; WILEY-VCH Verlag: Weinheim, Germany, 2012.
- [213] S. M. Dirk, S. Pylypenko, S. W. Howell, J. E. Fulghum, D. R. Wheeler, *Langmuir* **2005**, *21*, 10899.
- [214] Z. Yang, M. Dasog, A. R. Dobbie, R. Lockwood, Y. Zhi, A. Meldrum, J. G. C. Veinot, *Adv. Funct. Mater.* **2014**, *24*, 1345.
- [215] G. Kickelbick, *Introduction to hybrid materials*; WILEY-VCH Verlag: Weinheim, Germany, 2007.
- [216] G. Eda, M. Chhowalla, *Nano Lett.* **2009**, *9*, 814.
- [217] G. Eda, H. Emrah Unalan, N. Rupasinghe, G. A. J. Amaratunga, M. Chhowalla, *Appl. Phys. Lett.* **2008**, *93*, 233502.
- [218] X. Z. Bo, C. Y. Lee, M. S. Strano, M. Goldfinger, C. Nuckolls, G. B. Blanchet, *Appl. Phys. Lett.* **2005**, *86*, 182102.
- [219] J. Vazquez-Arenas, A. Galano, D. U. Lee, D. Higgins, A. Guevara-García, Z. Chen, *J. Mater. Chem. A* **2016**, *4*, 976.
- [220] J. M. Buriak, *Chem. Commun.* **1999**, *0*, 1051.
- [221] J. Kelly, J. G. C. Veinot, *ACS Nano* **2010**, *4*, 4645.
- [222] T. Helbich, A. Lyuleeva, I. M. D. Höhle, P. Marx, L. M. Scherf, J. Kehrle, T. F. Fässler, P. Lugli, B. Rieger, *Chem. - A Eur. J.* **2016**, *22*, 6194.
- [223] T. Helbich, A. Lyuleeva, T. Ludwig, L. M. M. Scherf, T. F. F. Fässler, P. Lugli, P. B. Rieger, B. Rieger, *Adv. Funct. Mater.* **2016**, *26*, 6711.
- [224] T. Helbich, A. Lyuleeva, P. Marx, L. M. Scherf, T. K. Purkait, T. F. Fässler, P. Lugli, J. G. C. Veinot, B. Rieger, *Adv. Funct. Mater.* **2017**, *27*.
- [225] T. Helbich, M. J. Klobberg, R. Sinelnikov, A. Lyuleeva, J. G. C. Veinot, B. Rieger, *Nanoscale* **2017**, *in press*.
- [226] N. Zhang, S. Salzinger, F. Deubel, R. Jordan, B. Rieger, *J. Am. Chem. Soc.* **2012**, *134*, 7333.
- [227] T. Helbich, A. Lyuleeva, T. Ludwig, L. M. Scherf, T. F. Fässler, P. Lugli, P. B. Rieger, *Adv. Funct. Mater.* **2016**, *26*, 6711.

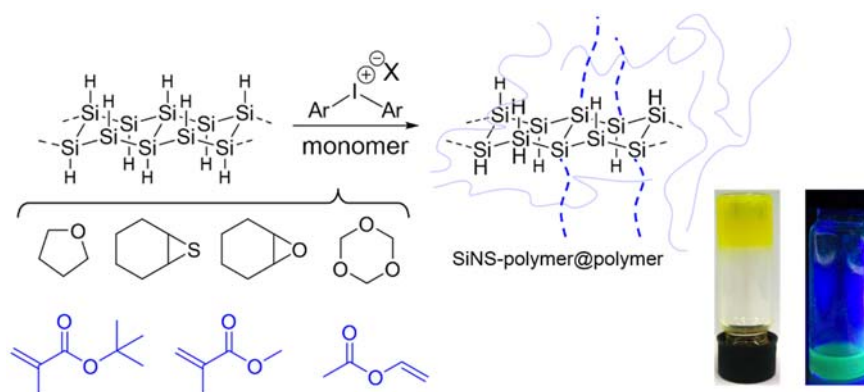
- [228] A. Lyuleeva, T. Helbich, B. Rieger, P. Lugli, *J. Phys. D. Appl. Phys.* **2017**, *50*, 135106.
- [229] J. A. Kampmeier, T. W. Nalli, *J. Org. Chem* **1994**, *59*, 1381.
- [230] J. V Crivello, *J. Polym. Sci. Part A Polym. Chem.* **1999**, *37*, 4241.

## 13. Appendix

### 13.1 Silicon Nanosheets as Initiators for Diaryliodonium Induced Radical and Cationic Polymerization<sup>h</sup>

Based on the findings of our previous works on iodonium salt initiated hydrosilylations and the therein made observation of poly(THF) formation, the system of SiNS/diaryliodonium salt was investigated further.

Hence, a mixture of diphenyliodonium hexafluorophosphate (PIP) and SiNSs was stirred in THF (**Scheme 1**). After 2 hours a yellow, solid composite material was formed. After purification by precipitation, the proton nuclear magnetic resonance spectrum (<sup>1</sup>H-NMR, **Figure 13a**), the Fourier transformed infrared (FTIR) spectrum (**Figure 11a**) and the gel permeation chromatogram (GPC, see chapter 8.1 **Figure S1a**) exhibit the expected signals of the excess of polymer. The solid composite shows hardly any photoluminescence (PL), but when dissolved in THF, PL can clearly be detected (**Scheme 1** right inset and **Figure S2**).



**Scheme 1.** Reaction scheme of the SiNSs/diaryliodonium system and corresponding monomers. Insets show SiNSs@pTHF composite under visible light (left) and dissolved in THF under UV light (right).

Although SiNSs have been shown to participate in radical polymerizations,<sup>[227]</sup> no cationic polymerization in presence of SiNSs has been observed before. This finding thus exhibits the first proof, that besides physical applications (i.e., photonic sensors,<sup>[228]</sup> FETs<sup>[224]</sup>), chemical applications are possible for SiNSs. Hence they might serve as catalyst or activator in chemical reactions. The described polymerization reaction is straight forward and proceeds under mild conditions (i.e., no UV-light, rt), which emphasizes the potential once more.

To better understand the system and its potential in further reactions, the underlying mechanism was studied. Hence, the SiNSs were separated from the polymer matrix by centrifugation, as described previously<sup>[227]</sup> and both components analyzed individually. In contrast to the nanocomposites formed with radical polymerization reactions, the isolated SiNSs were not functionalized, as shown by FTIR

<sup>h</sup> The work described in this chapter was prepared together with Marc J. Kloberg with equal contribution.

spectroscopy: No signal corresponding to the potential surface functionalization could be detected, while the Si–O stretching ( $\sim 1100\text{ cm}^{-1}$ ) and O–H stretching band ( $\sim 3300\text{ cm}^{-1}$ ) are strongly visible (**Figure 11b**) This demonstrates surface oxidation during the work up process. Although SiNSs in this reaction act as activators, they seem not to take part in the reaction themselves.

The lack of surface functionalization after the reaction was furthermore confirmed by  $^1\text{H-NMR}$  spectroscopy and thermogravimetric analysis (TGA, **Figure S3a**), as neither signal corresponding to organic groups nor significant weight-loss could be detected. These results indicate that the species which initiates the cationic ring-opening polymerization of THF is not located on the SiNS surface, but seems to rather be generated in its periphery.

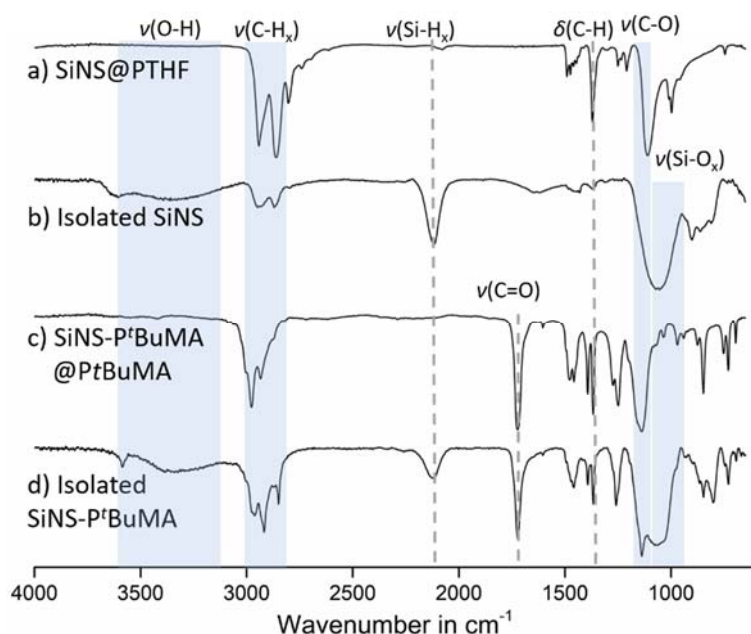


**Figure 11.** FTIR spectra of a) FTIR spectra of a) SiNS@PTHF composite, b) SiNSs separated from the SiNS@PTHF composite, c) SiNS-PtBuMA@PtBuMA composite and d) SiNS-PtBuMA separated from the SiNS-PtBuMA@PtBuMA composite.

Further experiments were conducted to better understand the role of the SiNSs in the polymerization reaction. As such, under otherwise identical reaction conditions, the iodonium salt was replaced with seemingly similar diazonium salt 4-decylbenzene diazonium tetrafluoroborate (4-DDB), but no polymer formation could be observed. Typically iodonium salt initiated polymerization reactions are initiated with UV light. In the presence of SiNSs the reaction could even be started in the complete absence of light. The addition of the radical inhibitor hydroquinone on the other hand lead to the successful inhibition of the polymerization reaction, indicating the involvement of radical pathways during the mechanism. *Nalli* and coworkers stated that in this reaction type, light merely serves as free radical source.<sup>[229]</sup> This agrees with the fact, that the decomposition of diaryliodonium salts can be induced by radical initiators, such as AIBN and dibenzoyl peroxide.<sup>[229]</sup> It is therefore likely that the silicon nanomaterial acts as a source of free radicals.

Different works with SiNMs have suggested, that the materials are capable of a spontaneous single electron transfer (SET).<sup>[102,211,222]</sup> A SET can also explain the here described reactivity, as the electron

transfer from the nanomaterial to the iodonium salt would induce the decomposition to iodobenzene and a phenyl radical. Additionally a Brønsted acid is formed as side product, which can then initiate the cationic polymerization. (**Figure 12a**). Due to the spontaneous SET, no external activation (e.g., light, heat, catalyst) is required.

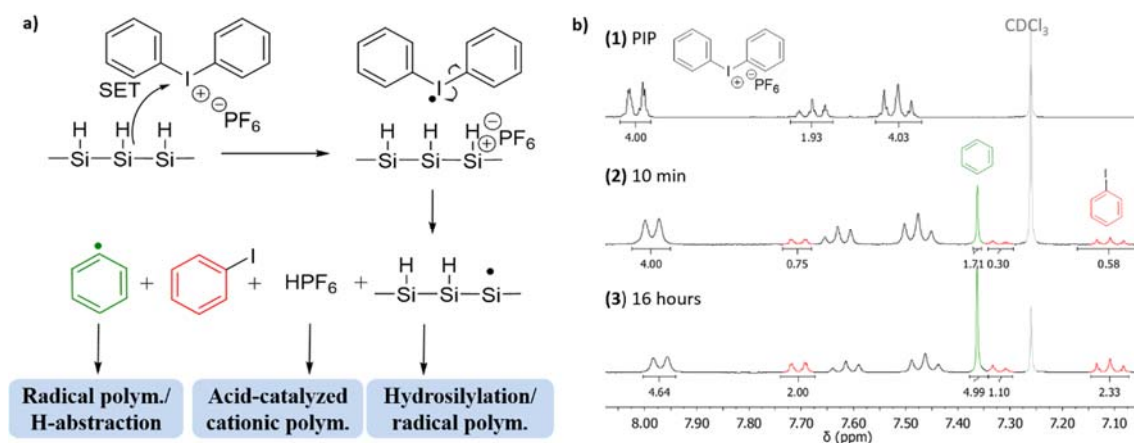


**Figure 12.** a) Proposed mechanism of the SiNM/diaryliodonium initiated polymerization. b) <sup>1</sup>H-NMR spectra in CDCl<sub>3</sub> of PIP without SiNS (1) and after the addition of SiNSs, depending on the time (2-3).

With the postulated SET and the subsequent decomposition of the diaryliodonium salt, its deterioration products should be detectable during the reaction. Hence PIP was dissolved in CDCl<sub>3</sub> in a NMR tube and <sup>1</sup>H-NMR measurements were conducted. In the absence of light, the reagent was shown to be stable (**Figure 12b (1)**). However, when SiNSs were added into the NMR tube, the formation of iodobenzene and benzene could be observed, proving the decomposition of PIP (**Figure 12b (2,3)**).

The postulated mechanism also explains how the SiNS/PIP system can initiate cationic polymerizations while no surface functionalization occurs: The formed super acid HPF<sub>6</sub> can easily initiate the ring opening polymerization of THF in the reaction mixture, but no active SiNSs surface species occurs. The mechanism further explains the role of diaryliodonium salts in SiNSs surface functionalizations by radical induced hydrosilylation: The surface silyl radical reacts with unsaturated substrates, leading to the formation of stable Si-C-bonds. This also suggests a difference in reactivity when, instead of cationically polymerizable monomers, radically polymerizable ones are used. For radically polymerizable monomers, homopolymerization in solution can be initiated by both, the formed free radicals and the SiNS silyl radical. The surface radical should simultaneously lead to the functionalization of the SiNSs. We thus tested the initiation system with the radically polymerizable *tert*-butyl methacrylate (*t*BuMA). After 1 hour reaction time, the monomer was completely polymerized. After dissolution and purification, the <sup>1</sup>H-NMR spectrum of the composite depicts the characteristic signals of *Pt*BuMA (**Figure 13**) and GPC measurements clearly show the presence of polymer (**Figure S1d**).

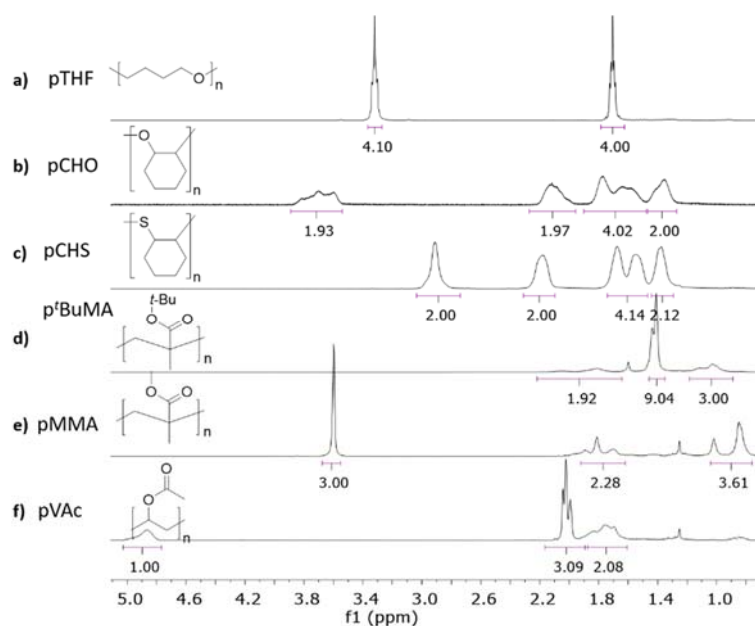


**Figure 13.**  $^1\text{H-NMR}$  spectra of the synthesized polymers. a) PTHF, b) PCHO, c) PCHS, d) PtBuMA, e) PMMA, f) PVAc.

After separation of the nanomaterial from the polymer matrix, both components were analyzed individually. Like for the nanocomposite, FTIR spectra of the isolated SiNSs show bands, such as  $\nu(\text{C-H}_x)$  ( $\sim 2900\text{ cm}^{-1}$ ),  $\delta(\text{C-H}_x)$  ( $1460\text{ cm}^{-1}$ ) and  $\nu(\text{C=O})$  ( $1700\text{ cm}^{-1}$ ), corresponding to those of PtBuMA (**Figure 11d**), demonstrating the successful functionalization of SiNSs. The absence of any  $\nu(\text{H-C}_{sp^2})$  ( $\sim 3050\text{ cm}^{-1}$ ) and  $\nu(\text{C=C})$  ( $1640\text{ cm}^{-1}$ ) bands show, that the double bond of the monomer has been consumed during the reaction and any excess of monomer was removed successfully. TGA measurements of the isolated SiNSs additionally show a significant weight loss and for the *t*BuMA functionalized SiNSs the characteristic step-wise weight loss, demonstrating, that the surface of the SiNSs is functionalized during the polymerization reaction (**Figure S3e**). All these results are in accordance with the proposed mechanism.

To demonstrate the significance of the SiNS/diaryl iodonium system, a broader applicability was shown. Hence we successfully polymerized the cationically polymerizable monomers cyclohexene oxide (CHO), cyclohexene sulfide (CHS) and 1,3,5-trioxane. After separation of the nanomaterial, the resulting polymers were analyzed by  $^1\text{H-NMR}$  (**Figure 13**), FTIR (**Figure S6-8**), GPC (**Figure S1**) and TGA and the isolated SiNSs by TGA (**Figure S3**). As expected, the isolated SiNSs showed no significant mass loss in TGA measurements.

Next, the scope of radically polymerizable monomers was examined. Methyl methacrylate (MMA) and vinyl acetate (VAc) can successfully be used in the reaction. After 1 hour the reaction mixture was completely polymerized and the resulting polymers were analyzed by  $^1\text{H-NMR}$  (**Figure 13**), FTIR (**Figure S9-11**), GPC (**Figure S1**) and TGA (**Figure S3**). In accordance with the observations made before and the mechanisms, the FTIR spectrum and TGA measurement of the isolated SiNSs show evidence for surface functionalization, as characteristic PMMA/PVAc signals occur in the spectra and

weightloss can be detected upon heating. After the polymerization, the composite materials exhibit the characteristic yellow color of the SiNSs which can easily be removed if only the polymer is needed.

As the SiNSs act as co-initiators, they can be used as “heterogeneous” activators for cationic polymerizations reactions, if a solution of diaryliodonium salt and monomer is brought in contact with them. To exemplify this potential, a syringe was charged with SiNSs. A stock solution of PIP in THF is then drawn into the syringe, shaken together with the SiNSs and afterwards pressed through a filter in a reaction flask. The activated reaction mixture will then polymerize completely, even in the absence of SiNSs (**Figure S15**). This simple experiment indicates the potential of SiNSs in heterogeneous catalysis and represents a very mild reaction procedure for performing cationic polymerizations.

The polymerization system was additionally tested with silicon nanocrystals (SiNC,  $d = 3$  nm). Under the same conditions as with SiNSs, freshly etched, hydride terminated SiNCs were dispersed in THF and PIP added. The reaction mixture turned solid after 2 hours, producing a turbid, orange composite. The same results can be observed, when *t*BuMA is used as monomer. As expected, in the case of THF, no surface functionalization of the SiNCs could be observed. For the reaction with *t*BuMA, no isolation of the SiNCs from the surrounding matrix is possible as functionalized SiNCs are well dispersed in organic solvents and cannot be separated by centrifugation. FTIR (**Figure S11, S13**) and <sup>1</sup>H-NMR (**Figure S12, S14**) depict the expected signals for polymer formation for both composites, indicating, that the described system is not restricted to SiNSs only. This observation is in accordance with the expected mechanism as SiNCs are capable of SETs (e.g. diazonium induced surface functionalization)<sup>[102]</sup> as well.

In summary, this chapter describes, that the system consisting of a diaryliodonium salt and a silicon nanomaterial can be used for not only cationic, but also radical polymerizations without further activation by e.g., UV light. A variety of monomers were polymerized and the underlying mechanism investigated. The collaborative effect presents the first proof that SiNSs can be used for activating or catalytic purposes, thus opening up the possibility of using SiNMs not just in physical applications (e.g. photonic sensor, anode material), but also in chemical applications (e.g. initiator, catalysis).

## 13.2 Supplementary Information

### Experimental Procedures

**General Methods** All experiments were performed under Schlenk conditions. Reactants and reagents were purchased from *Sigma-Aldrich* if not stated otherwise and used without further purification. Prior to use tetrahydrofuran, cyclohexene oxide, cyclohexene sulfide, *tert*-butyl methacrylate, methyl methacrylate, vinyl acetate and acetone were dried over molecular sieves and stored under argon. A *MBraun* solvent purification system, *MB SPS-800*, was used to dry THF, whereby argon 5.0 (99.9990%, *Westfalen AG*) was used as inert gas. For polymerization reactions and storage of exfoliated SiNSs, a *LABmaster 130 (MBraun)* glove box was used with argon 4.8 (99.998%, *Westfalen AG*).

**Analytical Methods** A *Bruker Vertex 70 FTIR* using a *Platinum ATR* from *Bruker* was used to measure Fourier transform infrared spectra (FTIR). NMR spectra were measured on an *ARX-300* from *Bruker* at 300 K. Chemical shifts ( $\delta$ ) are calibrated to the rest proton signal of the deuterated solvent and given in ppm. PL spectra were recorded on an *AVA-Spec 2048* from *Avantes* in toluene with the light source *Prizmatix* (LED current controller). TGA was performed on a *Netzsch TG 209 F 1 Libra* by heating the sample to 800 °C at a heating rate of 10 K/min and argon flow of 20 ml/min. A *Varian PL-GPC 50 Plus* was used to perform GPC measurements. The measurements were performed at 30 °C with a constant flow rate of 1 ml/min THF, to which 220 mg/L BHT were added for stabilization.

**Synthesis of CaSi<sub>2</sub>** The synthesis was performed according to procedures described beforehand.

**Synthesis of Silicon Nanosheets** The procedure was performed as previously described.

**Etching of Silicon Nanosheets** The etching process was performed as described in the previous chapters.

**Cationic and Radical Polymerization with SiNSs and PIP** 15 mg SiNSs are etched with dilute HF according to the procedure above. The resulting hydride-terminated SiNSs are dispersed in 2 mL benzene, freeze-dried and transferred to a glove box (freeze-dried SiNSs can be stored for later use). The freeze-dried SiNSs are dispersed in 1 mL dry and degassed monomer and transferred to a vial. 15 mg diphenyliodonium hexafluorophosphate is added and the mixture stirred until completely solid. The resulting composite is dissolved in an appropriate solvent and precipitated in an antisolvent. Centrifugation (9000 rpm/5 min) yields the SiNS/polymer composite, denoted as SiNS@polymer.

**1.7 Polymerization of 1,3,5-Trioxane with SiNSs and PIP** 15 mg SiNSs are etched with dilute HF according to the procedure above. The resulting hydride-terminated SiNSs are dispersed in 2 mL benzene, freeze-dried and transferred to a glove box (freeze-dried SiNSs can be stored for later use). The freeze-dried SiNSs are added to vial charged with 1.00 g 1,3,5-trioxane and 15 mg diphenyliodonium hexafluorophosphate. The vial is placed in an oil bath and heated to 70 °C. After 30 min of stirring, the solidified reaction mixture is cooled to room temperature. The composite is washed with ethanol, yielding SiNSs in a polyoxymethylene (POM) matrix, SiNS@POM. The SiNSs can be removed from the polymer matrix by treating the base stable POM with a slightly alkaline solution (NaOH (aq.), pH = 8).

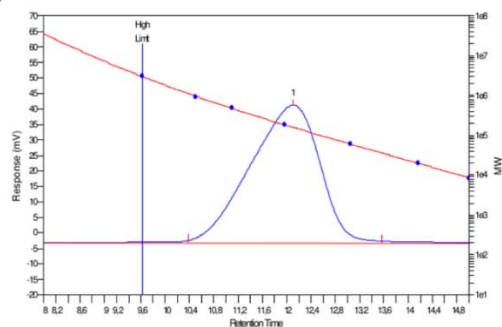
**Isolation of SiNSs from a Polymer Composite** The nanocomposite, SiNS-polymer@polymer, is dissolved in an appropriate solvent and centrifuged at 9000 rpm for 10 minutes. The supernatant contains the polymer and is separated from the SiNS residue. Centrifugation of the supernatant is repeated, to ensure removal of all SiNSs. The homopolymer is then obtained by precipitation in an anti-solvent. The (combined) SiNS residues are washed three times with a polymer dissolving solvent, removing excess homopolymer and resulting in polymer-free SiNSs.

**Synthesis of Silicon Nanocrystals** Silicon nanocrystals were synthesized according to the procedure described in chapter 7.

**<sup>1</sup>H-NMR Study on the Decomposition of Diaryliodonium Salts** In a glove box a heat dried NMR tube with a Young valve is charged with 10 mg diphenyliodonium hexafluorophosphate and dissolved in 0.5 mL CDCl<sub>3</sub>. While shielding the NMR tube from light, <sup>1</sup>H-NMR measurements are performed. The NMR tube is then transferred back into the glove box and 5 mg SiNSs-H are added. <sup>1</sup>H-NMR is then measured in the given time intervals.

## Gel Permeation Chromatography

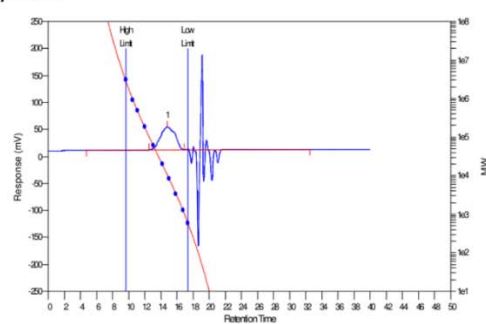
a) PTHF



## MW Averages

Peak No	Mp	Mn	Mw	Mz	Mz+1	Mv	PD
1	158722	166706	227992	321308	439143	216624	1.36763

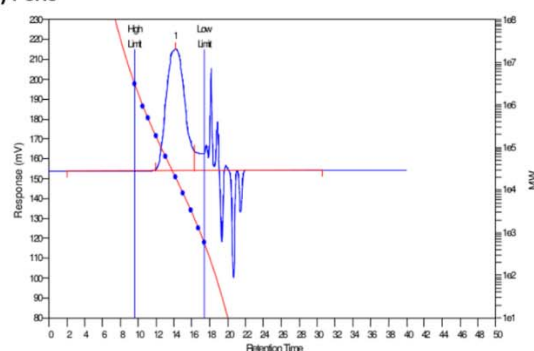
b) PCHO



## MW Averages

Peak No	Mp	Mn	Mw	Mz	Mz+1	Mv	PD
1	10617	7286	13860	24683	37699	12600	1.90228

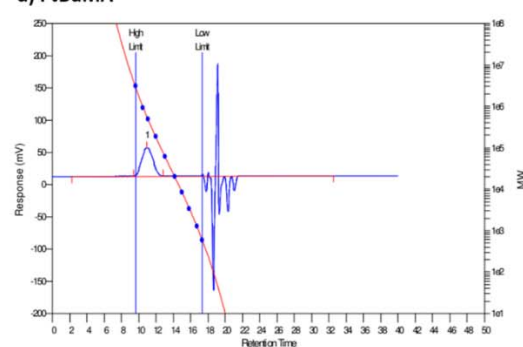
c) PCHS



## MW Averages

Peak No	Mp	Mn	Mw	Mz	Mz+1	Mv	PD
1	20072	13199	27626	49147	72181	24976	2.09304

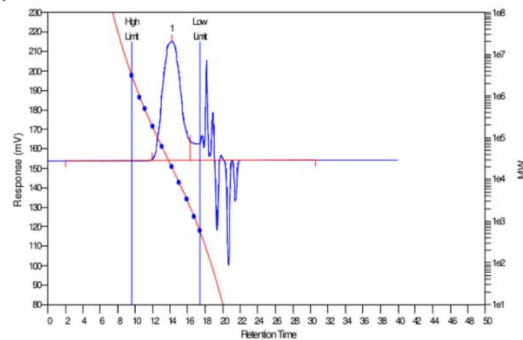
d) PtBuMA



## MW Averages

Peak No	Mp	Mn	Mw	Mz	Mz+1	Mv	PD
1	573951	441219	674326	1004056	1395203	633080	1.52832

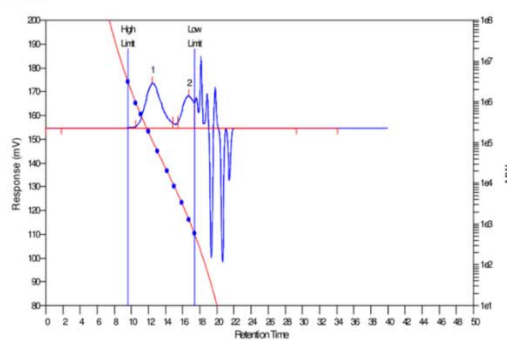
e) PMMA



## MW Averages

Peak No	Mp	Mn	Mw	Mz	Mz+1	Mv	PD
1	20072	13199	27626	49147	72181	24976	2.09304

f) PVAc

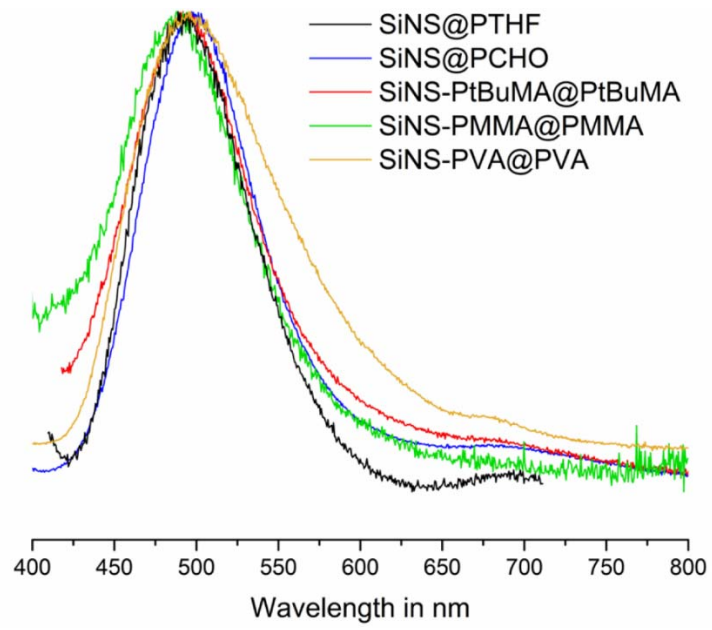


## MW Averages

Peak No	Mp	Mn	Mw	Mz	Mz+1	Mv	PD
1	110323	62618	137998	263224	410830	123612	2.20381
2	1347	1366	1795	2432	3013	1701	1.31406

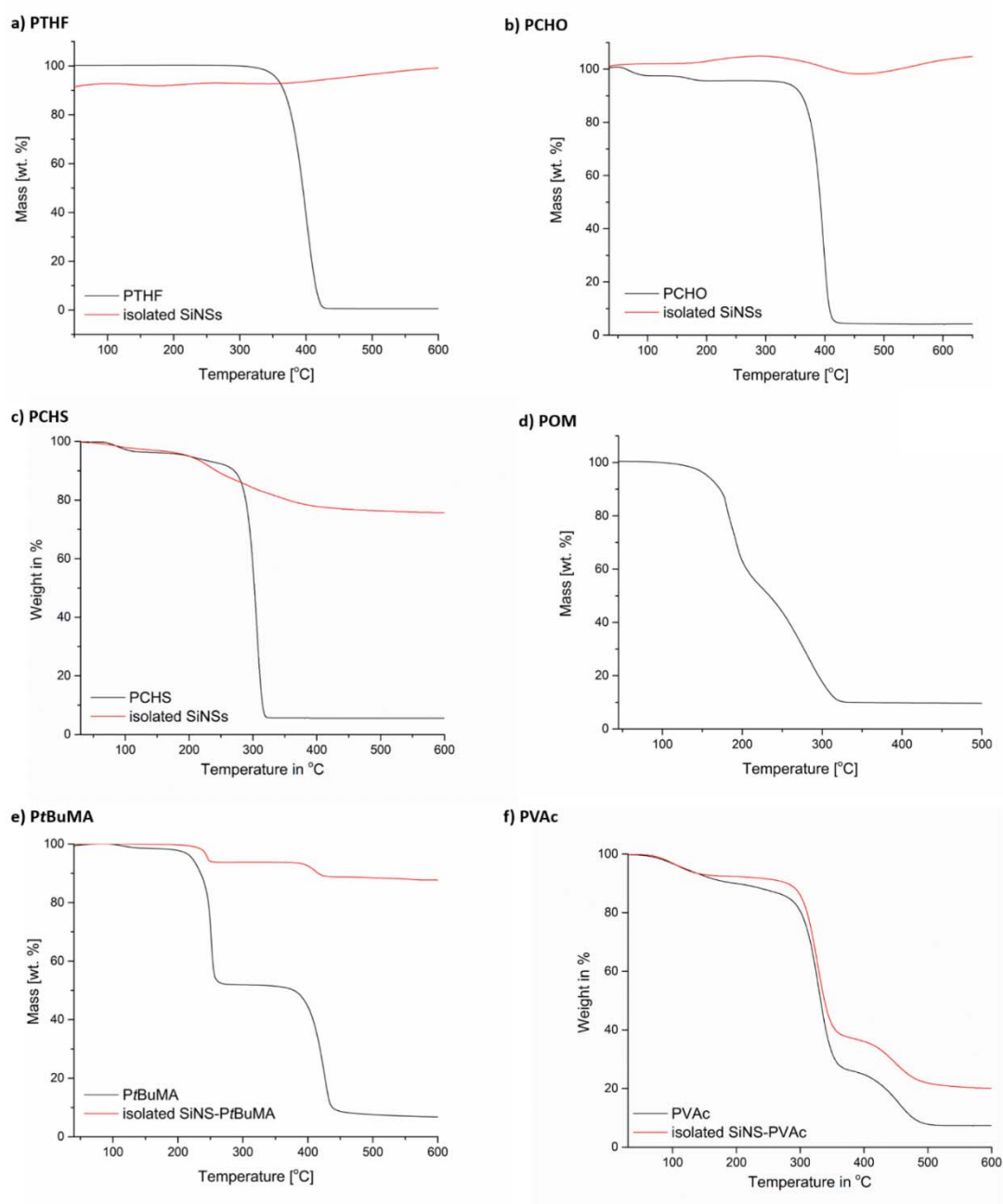
Figure S1. Gel permeation chromatograms of a) PTHF, b) PCHO, c) PCHS, d) PtBuMA, e) PMMA and f) PVAc.

### Photoluminescence



**Figure S2.** Photoluminescence spectra of SiNS/polymer composites directly after synthesis.

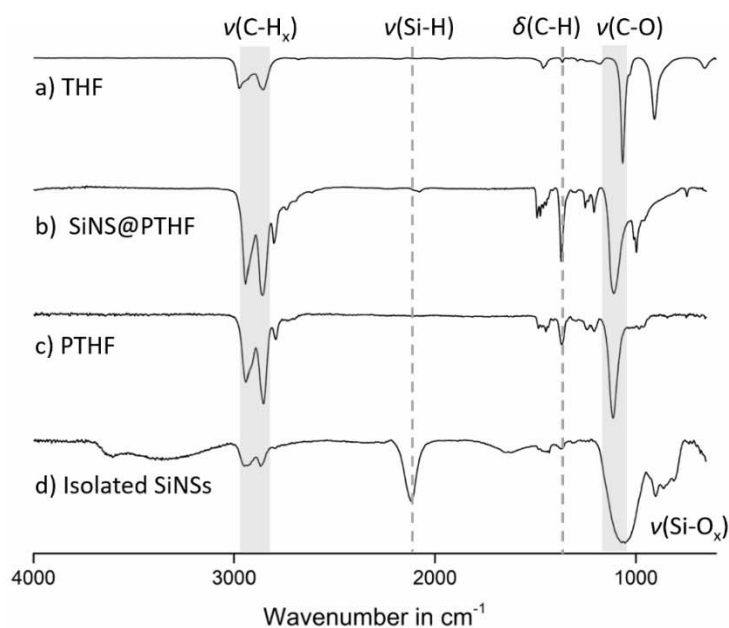
## Thermogravimetric Analysis



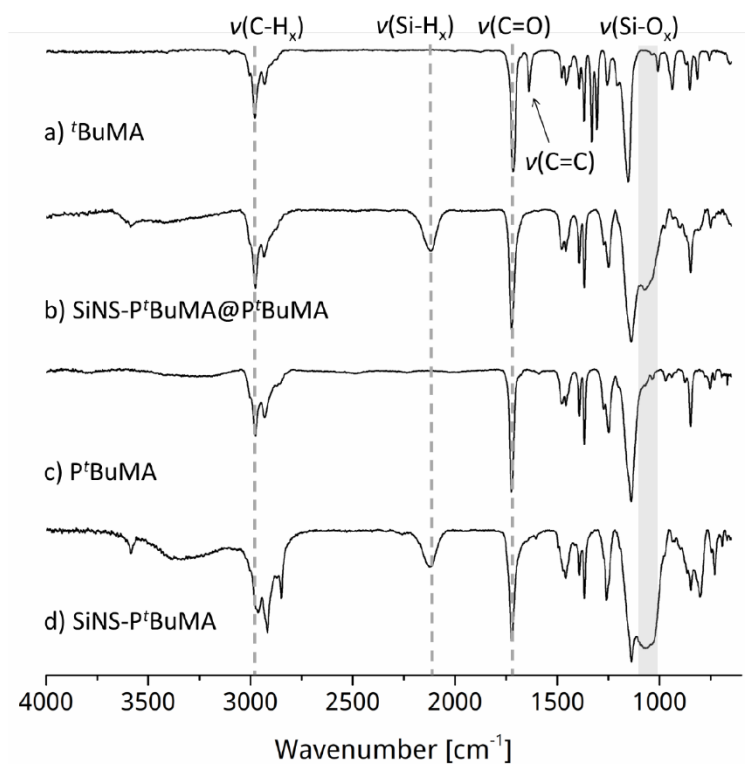
**Figure S3.** TGA measurements of a) PTHF, b) PCHO, c) PCHS, d) POM (isolation of SiNSs not possible due to bad solubility), e) PrBuMA and f) PVAc, as well as isolated SiNSs from the respective composite.

## FTIR Spectra

## THF based Reactions



**Figure S4.** FTIR spectra of a) tetrahydrofuran (THF), b) SiNS/polytetrahydrofuran composite (SiNS@PTHF), c) polytetrahydrofuran (PTHF) and d) SiNSs isolated from the composite.

***t*BuMA based Reactions**

**Figure S5.** FTIR spectra of a) *t*BuMA, b) SiNS-*Pt*BuMA@*Pt*BuMA, c) *Pt*BuMA homopolymer and d) isolated SiNS-*Pt*BuMA.

## CHO based Reactions

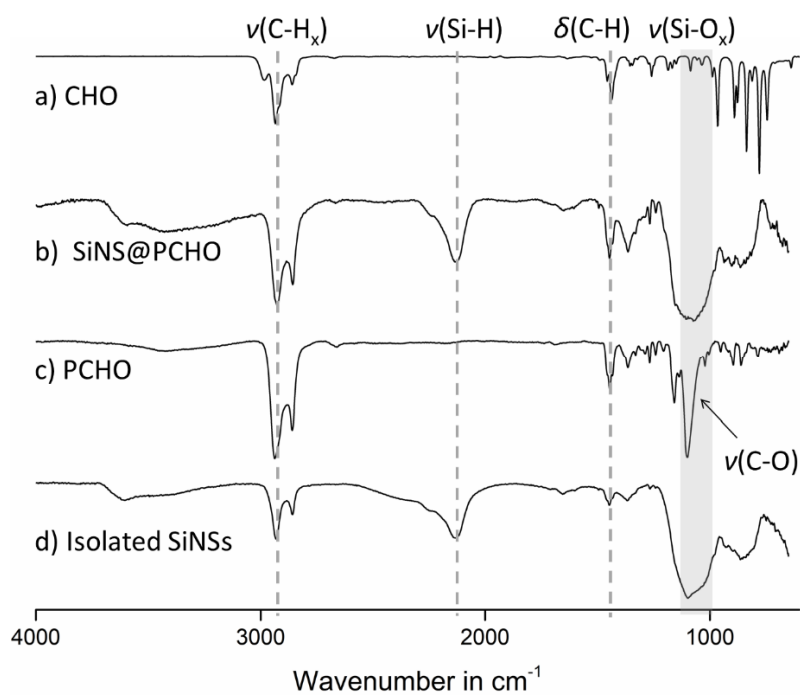


Figure S6. FTIR spectra of a) SiNS@PCHO, b) isolated SiNSs, c) isolated homopolymer PCHO.

## CHS based Reactions

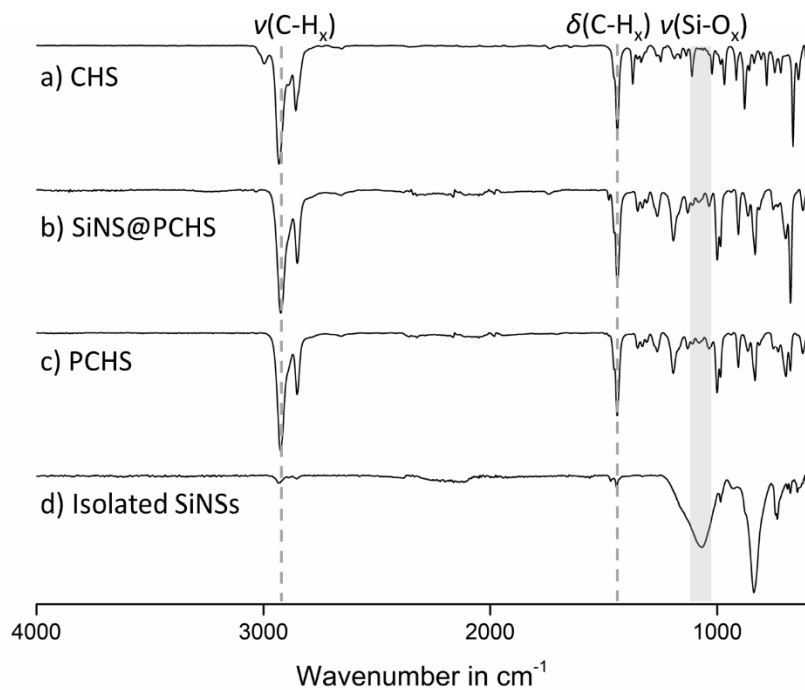


Figure S7. FTIR spectra of a) cyclohexene sulfide (CHS), b) SiNS@PCHS, c) isolated homopolymer PCHS and d) isolated SiNSs.

## Trioxane based Reactions

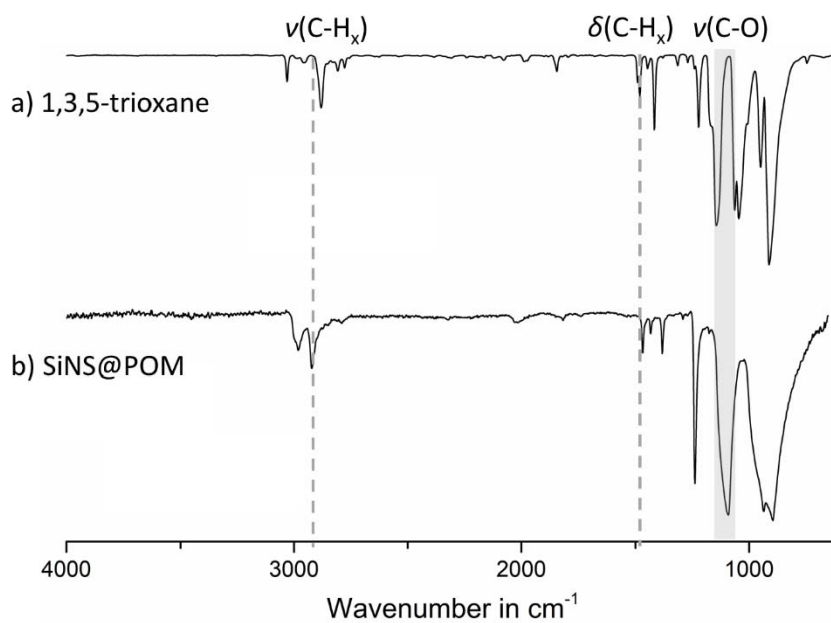


Figure S8. FTIR spectra of a) 1,3,5-trioxane and b) SiNS@POM.

## MMA based Reactions

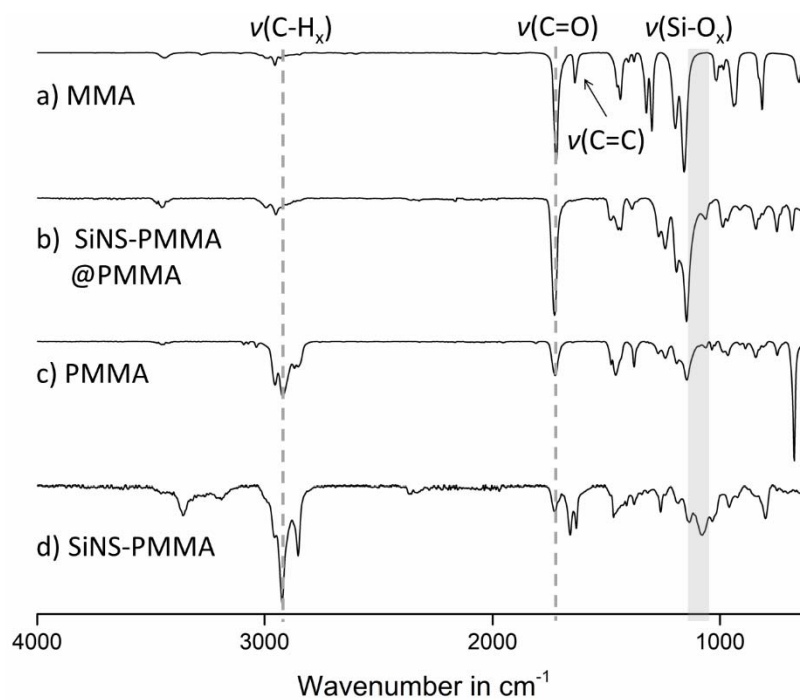
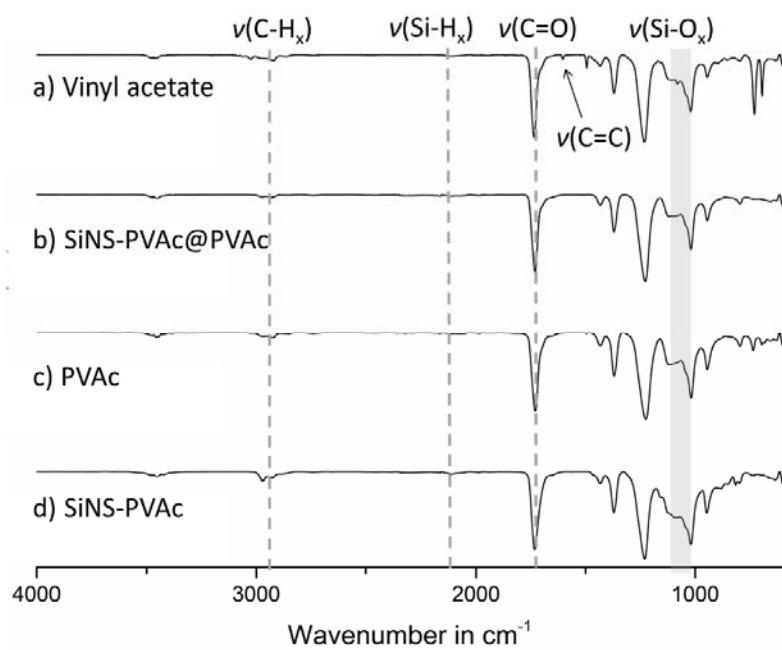


Figure S9. FTIR spectra of a) MMA, b) SiNS-PMMA@PMMA, c) isolated SiNS-PMMA and d) isolated PMMA.

## Vinylacetate based Reactions



**Figure S10.** FTIR spectra of a) vinyl acetate (VAc), b) SiNS-PVAc@PVAc, c) isolated homopolymer PVAc and d) isolated SiNS-PVAc

## SiNC based Reactions

## SiNC@pTHF

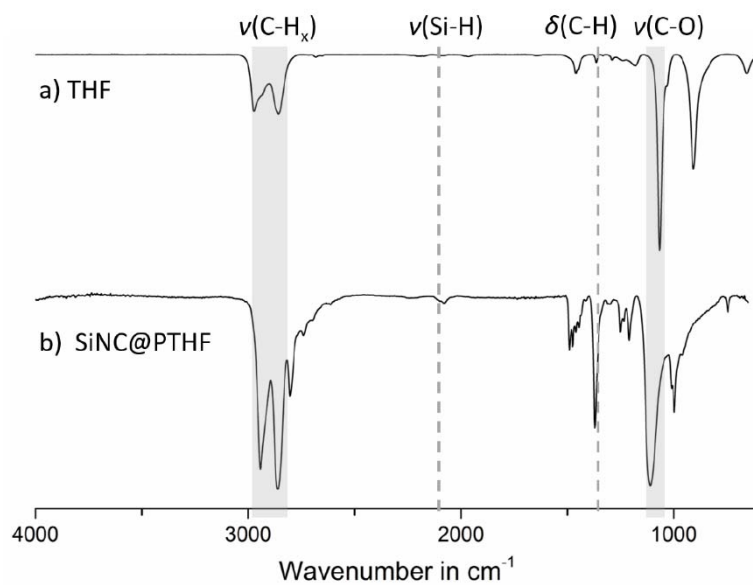


Figure S11. FTIR spectra of a) THF and b) SiNC@PTHF.

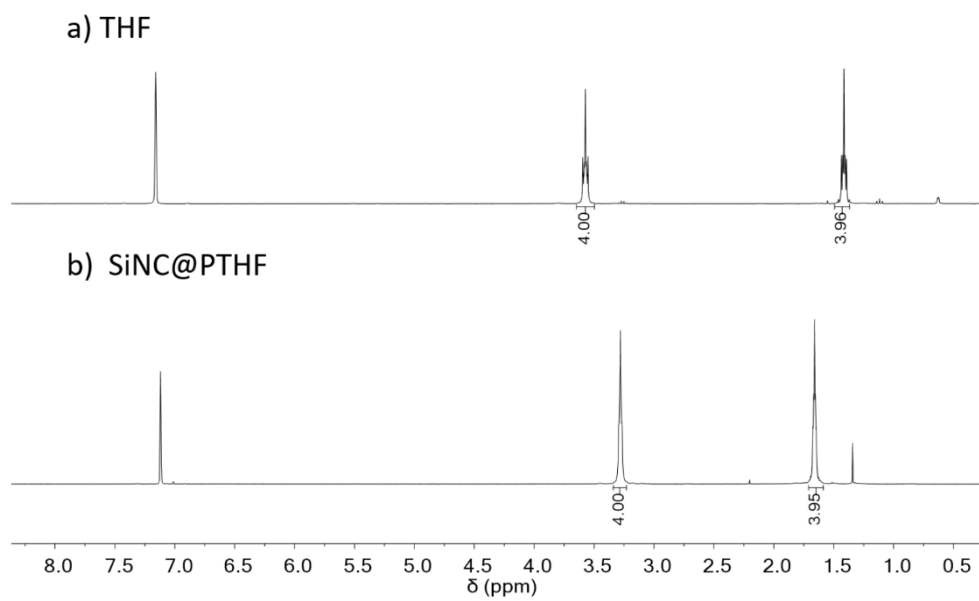


Figure S12.  $^1\text{H-NMR}$  spectra of a) THF and b) SiNC@PTHF.

## SiNC-p'BuMA@p'BuMA

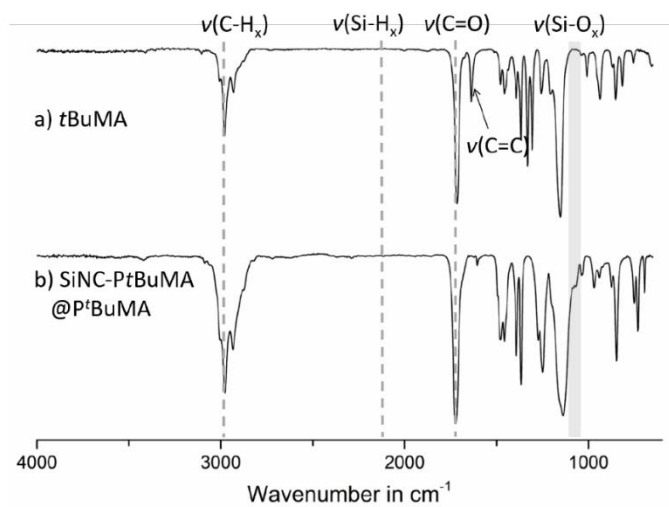


Figure S13. FTIR spectra of a) THF and b) SiNC@PTHF.

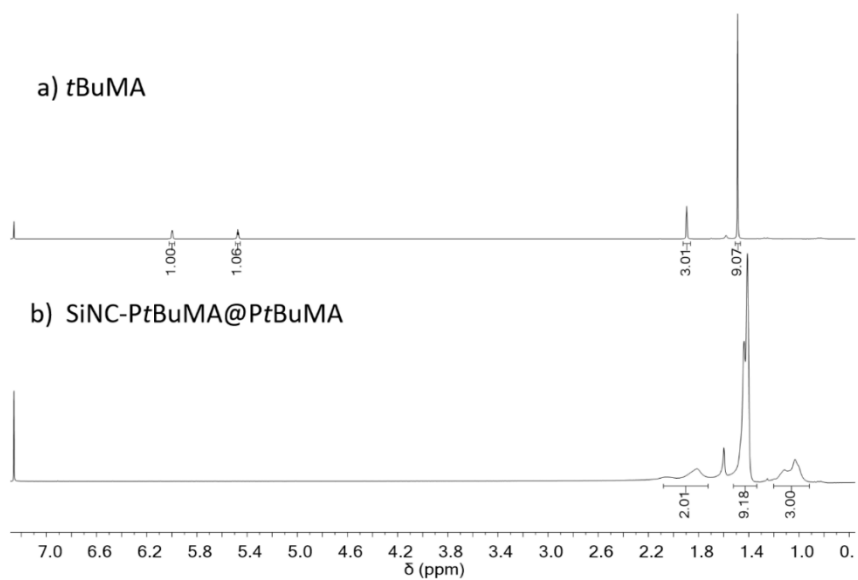
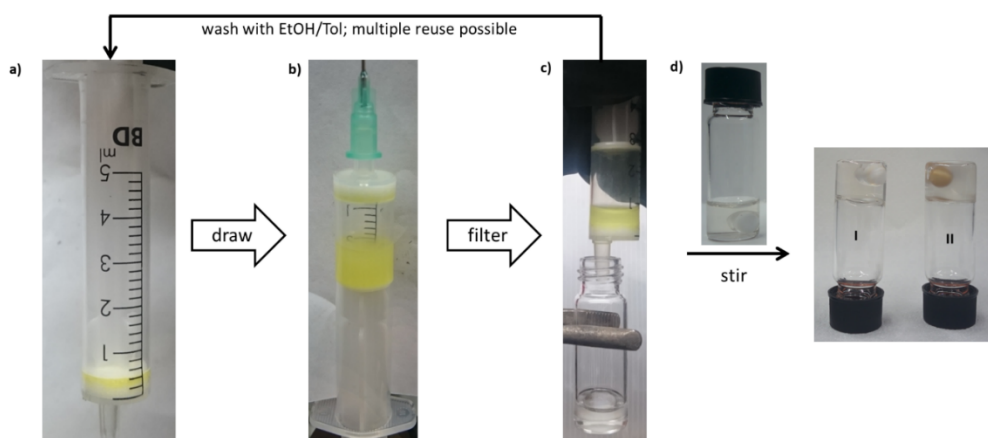


Figure S14.  $^1\text{H-NMR}$  spectra of a) THF and b) SiNC@PTHF.

### Heterogeneous Initiation of Cationic Polymerization

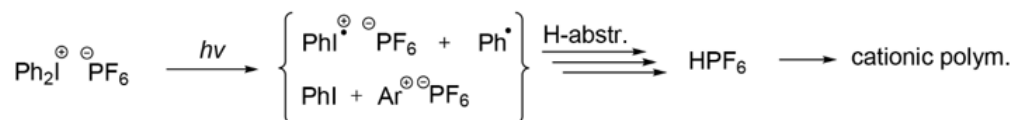


**Figure S15.** a) A syringe filter is charged with H-SiNSs. b) A solution of BIP in THF is drawn into the syringe dispersing the SiNSs. The dispersion is shaken for 5 min. c) The solution is filtered into a vial, resulting in a clear solution with no SiNSs. d) The solution is stirred for ca. 2 hours to obtain polyTHF (Vial I). The syringe reaction vessel can be reused for multiple polymerizations (Vial II).

A stock solution of diphenyliodonium hexafluorophosphate in dry THF (35.2 mmol/L) is prepared in a glove box. A syringe with a cake filter is then filled with 15 mg H-SiNS. 1 L of the stock solution is drawn into the syringe and shaken for 5 min. The solution is then slowly pushed out of the syringe into a vial charged with a stir bar and stirred for 2 hours to obtain polyTHF. To remove the iodonium salt and reaction byproducts, the polymer is dissolved in THF and precipitated in methanol to obtain polyTHF. The syringe is washed with ethanol and subsequently toluene and can be stored for further use.

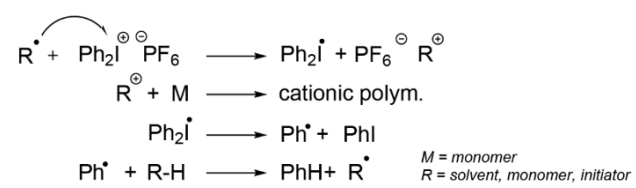
### Mechanism of the Diaryliodonium Induced Cationic Polymerization

Diaryliodonium salts can be activated in various manners to initiate the cationic polymerization. In the UV-induced polymerization the diaryliodonium salt is photoexcited to a singlet state, which subsequently decays with homolytic and heterolytic cleavage of the carbon-iodine bond, resulting in free-radical, cation-radical and cationic fragments (**Scheme S1**). These are highly reactive and react with impurities, solvent or monomer to form a protonic acids, e.g. HPF<sub>6</sub>, which initiates the polymerization.<sup>[230]</sup>



**Scheme S1** Mechanism of the UV induced, diaryliodonium initiated cationic polymerization exemplified with diphenyliodonium hexafluorophosphate (PIP).

In the redox radical-chain mechanism a free radical source, such as AIBN, initiates the fragmentation of the diaryliodonium salt (**Scheme S2**). The cations resulting from the electron transfer and from side reactions initiate the cationic polymerization.<sup>[229]</sup>



**Scheme S2** Mechanism of the redox radical-chain mechanism using the example of PIP.<sup>5</sup>

## 13.3 Licenses for Copyrighted Content

**Figure 2**

RightsLink Printable License

<https://s100.copyright.com/CustomerAdmin/PLF.jsp?ref=3e20f8ba-a0...>

### AMERICAN PHYSICAL SOCIETY LICENSE TERMS AND CONDITIONS

Apr 10, 2017

This Agreement between Tobias Helbich ("You") and American Physical Society ("American Physical Society") consists of your license details and the terms and conditions provided by American Physical Society and Copyright Clearance Center.

License Number	4078190699556
License date	
Licensed Content Publisher	American Physical Society
Licensed Content Publication	Physical Review Letters
Licensed Content Title	Silicene: Compelling Experimental Evidence for Graphenelike Two-Dimensional Silicon
Licensed Content Author	Patrick Vogt et al.
Licensed Content Date	Apr 12, 2012
Licensed Content Volume	108
Type of Use	Thesis/Dissertation
Requestor type	Student
Format	Electronic
Portion	image/photo
Number of images/photos requested	1
Portion description	Figure 4
Rights for	Main product
Duration of use	Life of Current Edition
Creation of copies for the disabled	no
With minor editing privileges	no
For distribution to	Worldwide
In the following language(s)	Original language of publication
With incidental promotional use	no
The lifetime unit quantity of new product	0 to 499
The requesting person/organization is:	Tobias Helbich/Technical University of Munich
Order reference number	
Title of your thesis / dissertation	Two-dimensional Hybrid Nanomaterials: Functionalization and Characterization of Photoluminescent Silicon Nanosheets
Expected completion date	Jul 2017
Expected size (number of pages)	150
Requestor Location	Tobias Helbich Spitzingseestr. 5

## Figure 3

RightsLink Printable License

<https://s100.copyright.com/CustomerAdmin/PLF.jsp?ref=1773f286-a8...>**ROYAL SOCIETY OF CHEMISTRY LICENSE  
TERMS AND CONDITIONS**

Apr 10, 2017

This Agreement between Tobias Helbich ("You") and Royal Society of Chemistry ("Royal Society of Chemistry") consists of your license details and the terms and conditions provided by Royal Society of Chemistry and Copyright Clearance Center.

License Number	4085560179116
License date	
Licensed Content Publisher	Royal Society of Chemistry
Licensed Content Publication	Physical Chemistry Chemical Physics
Licensed Content Title	Density functional theory calculations for two-dimensional silicene with halogen functionalization
Licensed Content Author	Nan Gao,Wei Tao Zheng,Qing Jiang
Licensed Content Date	Nov 14, 2011
Licensed Content Volume	14
Licensed Content Issue	1
Type of Use	Thesis/Dissertation
Requestor type	academic/educational
Portion	figures/tables/images
Number of figures/tables /images	1
Format	electronic
Distribution quantity	500
Will you be translating?	no
Order reference number	
Title of the thesis/dissertation	Two-dimensional Hybrid Nanomaterials: Functionalization and Characterization of Photoluminescent Silicon Nanosheets
Expected completion date	Jul 2017
Estimated size	150
Requestor Location	Tobias Helbich Spitzingseestr. 5  Kolbermoor, Bavaria 83059 Germany Attn: Tobias Helbich
Billing Type	Invoice
Billing Address	Tobias Helbich Spitzingseestr. 5  Kolbermoor, Germany 83059 Attn: Tobias Helbich
Total	0.00 USD
Terms and Conditions	

## Figure 4

11.4.2017

RightsLink Printable License

**NATURE PUBLISHING GROUP LICENSE  
TERMS AND CONDITIONS**

Apr 11, 2017

This Agreement between Tobias Helbich ("You") and Nature Publishing Group ("Nature Publishing Group") consists of your license details and the terms and conditions provided by Nature Publishing Group and Copyright Clearance Center.

License Number	4086000404388
License date	Apr 11, 2017
Licensed Content Publisher	Nature Publishing Group
Licensed Content Publication	Nature Nanotechnology
Licensed Content Title	Silicene field-effect transistors operating at room temperature
Licensed Content Author	Li Tao, Eugenio Cinquanta, Daniele Chiappe, Carlo Grazianetti, Marco Fanciulli, Madan Dubey
Licensed Content Date	Feb 2, 2015
Licensed Content Volume	10
Licensed Content Issue	3
Type of Use	reuse in a dissertation / thesis
Requestor type	academic/educational
Format	electronic
Portion	figures/tables/illustrations
Number of figures/tables/illustrations	1
High-res required	no
Figures	Figure 1, bottom
Author of this NPG article	no
Your reference number	
Title of your thesis / dissertation	Two-dimensional Hybrid Nanomaterials: Functionalization and Characterization of Photoluminescent Silicon Nanosheets
Expected completion date	Jul 2017
Estimated size (number of pages)	150
Requestor Location	Tobias Helbich Spitzingseestr. 5  Kolbermoor, Bavaria 83059 Germany Attn: Tobias Helbich
Billing Type	Invoice
Billing Address	Tobias Helbich Spitzingseestr. 5  Kolbermoor, Germany 83059 Attn: Tobias Helbich
Total	0.00 USD
Terms and Conditions	

## Radical Induced Hydrosilylation Reactions for the Functionalization of Two-Dimensional Hydride Terminated Silicon Nanosheets

RightsLink Printable License

https://s100.copyright.com/CustomerAdmin/PLF.jsp?ref=c4306c10-cc...

### JOHN WILEY AND SONS LICENSE TERMS AND CONDITIONS

Apr 10, 2017

This Agreement between Tobias Helbich ("You") and John Wiley and Sons ("John Wiley and Sons") consists of your license details and the terms and conditions provided by John Wiley and Sons and Copyright Clearance Center.

License Number	4078160391640
License date	
Licensed Content Publisher	John Wiley and Sons
Licensed Content Publication	Chemistry - A European Journal
Licensed Content Title	Radical-Induced Hydrosilylation Reactions for the Functionalization of Two-Dimensional Hydride Terminated Silicon Nanosheets
Licensed Content Author	Tobias Helbich,Alina Lyuleeva,Ignaz M. D. Höhlelein,Philipp Marx,Lavinia M. Scherf,Julian Kehrlie,Thomas F. Fässler,Paolo Lugli,Bernhard Rieger
Licensed Content Date	Mar 15, 2016
Licensed Content Pages	5
Type of use	Dissertation/Thesis
Requestor type	Author of this Wiley article
Format	Electronic
Portion	Full article
Will you be translating?	No
Title of your thesis / dissertation	Two-dimensional Hybrid Nanomaterials: Functionalization and Characterization of Photoluminescent Silicon Nanosheets
Expected completion date	Jul 2017
Expected size (number of pages)	150
Requestor Location	Tobias Helbich Spitzingseestr. 5  Kolbermoor, Bavaria 83059 Germany Attn: Tobias Helbich
Publisher Tax ID	EU826007151
Billing Type	Invoice
Billing Address	Tobias Helbich Spitzingseestr. 5  Kolbermoor, Germany 83059 Attn: Tobias Helbich
Total	0.00 USD
Terms and Conditions	

### TERMS AND CONDITIONS

This copyrighted material is owned by or exclusively licensed to John Wiley & Sons, Inc. or

## One-Step Synthesis of Photoluminescent Covalent Polymeric Nanocomposites from 2D Silicon Nanosheets

RightsLink Printable License

<https://s100.copyright.com/CustomerAdmin/PLF.jsp?ref=3db4a53b-f3...>

### JOHN WILEY AND SONS LICENSE TERMS AND CONDITIONS

Apr 10, 2017

This Agreement between Tobias Helbich ("You") and John Wiley and Sons ("John Wiley and Sons") consists of your license details and the terms and conditions provided by John Wiley and Sons and Copyright Clearance Center.

License Number	4078160049566
License date	
Licensed Content Publisher	John Wiley and Sons
Licensed Content Publication	Advanced Functional Materials
Licensed Content Title	One-Step Synthesis of Photoluminescent Covalent Polymeric Nanocomposites from 2D Silicon Nanosheets
Licensed Content Author	Tobias Helbich,Alina Lyuleeva,Theresa Ludwig,Lavinia M. Scherf,Thomas F. Fässler,Paolo Lugli,Bernhard Rieger
Licensed Content Date	Jul 28, 2016
Licensed Content Pages	8
Type of use	Dissertation/Thesis
Requestor type	Author of this Wiley article
Format	Electronic
Portion	Full article
Will you be translating?	No
Title of your thesis / dissertation	Two-dimensional Hybrid Nanomaterials: Functionalization and Characterization of Photoluminescent Silicon Nanosheets
Expected completion date	Jul 2017
Expected size (number of pages)	150
Requestor Location	Tobias Helbich Spitzingseestr. 5  Kolbermoor, Bavaria 83059 Germany Attn: Tobias Helbich
Publisher Tax ID	EU826007151
Billing Type	Invoice
Billing Address	Tobias Helbich Spitzingseestr. 5  Kolbermoor, Germany 83059 Attn: Tobias Helbich
Total	0.00 USD
Terms and Conditions	

### TERMS AND CONDITIONS

This copyrighted material is owned by or exclusively licensed to John Wiley & Sons, Inc. or one of its group companies (each a "Wiley Company") or handled on behalf of a society with

## Lewis Acid Induced Functionalization of Photoluminescent 2D Silicon Nanosheets for the Fabrication of Functional Hybrid Films

RightsLink Printable License

<https://s100.copyright.com/CustomAdmin/PLF.jsp?ref=356f5bd8-c8...>

### JOHN WILEY AND SONS LICENSE TERMS AND CONDITIONS

Jun 06, 2017

This Agreement between Tobias Helbich ("You") and John Wiley and Sons ("John Wiley and Sons") consists of your license details and the terms and conditions provided by John Wiley and Sons and Copyright Clearance Center.

License Number	4123320789941
License date	Jun 06, 2017
Licensed Content Publisher	John Wiley and Sons
Licensed Content Publication	Advanced Functional Materials
Licensed Content Title	Silicon Nanosheets: Lewis Acid Induced Functionalization of Photoluminescent 2D Silicon Nanosheets for the Fabrication of Functional Hybrid Films (Adv. Funct. Mater. 21/2017)
Licensed Content Author	Tobias Helbich, Alina Lyuleeva, Philipp Marx, Lavinia M. Scherf, Tapas K. Purkait, Thomas F. Fässler, Paolo Lugli, Jonathan G. C. Veinot, Bernhard Rieger
Licensed Content Date	Jun 5, 2017
Licensed Content Pages	1
Type of use	Dissertation/Thesis
Requestor type	Author of this Wiley article
Format	Print and electronic
Portion	Full article
Will you be translating?	No
Title of your thesis / dissertation	Two-dimensional Hybrid Nanomaterials: Functionalization and Characterization of Photoluminescent Silicon Nanosheets
Expected completion date	Jul 2017
Expected size (number of pages)	150
Requestor Location	Tobias Helbich Spitzingseestr. 5  Kolbermoor, Bavaria 83059 Germany Attn: Tobias Helbich
Publisher Tax ID	EU826007151
Billing Type	Invoice
Billing Address	Tobias Helbich Spitzingseestr. 5  Kolbermoor, Germany 83059 Attn: Tobias Helbich
Total	0.00 USD
Terms and Conditions	

## Abstract - Diazonium Salts as Grafting Agents and Efficient RadicalHydrosilylation Initiators for Freestanding Photoluminescent Silicon Nanocrystals

RightsLink Printable License

<https://s100.copyright.com/CustomerAdmin/PLF.jsp?ref=086c07d1-81...>

### JOHN WILEY AND SONS LICENSE TERMS AND CONDITIONS

Apr 10, 2017

This Agreement between Tobias Helbich ("You") and John Wiley and Sons ("John Wiley and Sons") consists of your license details and the terms and conditions provided by John Wiley and Sons and Copyright Clearance Center.

License Number	4078170368913
License date	
Licensed Content Publisher	John Wiley and Sons
Licensed Content Publication	Chemistry - A European Journal
Licensed Content Title	Diazonium Salts as Grafting Agents and Efficient Radical-Hydrosilylation Initiators for Freestanding Photoluminescent Silicon Nanocrystals
Licensed Content Author	Ignaz M. D. Höhle, Julian Kehrle, Tobias Helbich, Zhenyu Yang, Jonathan G. C. Veinot, Bernhard Rieger
Licensed Content Date	Mar 24, 2014
Licensed Content Pages	5
Type of use	Dissertation/Thesis
Requestor type	Author of this Wiley article
Format	Electronic
Portion	Abstract
Will you be translating?	No
Title of your thesis / dissertation	Two-dimensional Hybrid Nanomaterials: Functionalization and Characterization of Photoluminescent Silicon Nanosheets
Expected completion date	Jul 2017
Expected size (number of pages)	150
Requestor Location	Tobias Helbich Spitzingseestr. 5  Kolbermoor, Bavaria 83059 Germany Attn: Tobias Helbich
Publisher Tax ID	EU826007151
Billing Type	Invoice
Billing Address	Tobias Helbich Spitzingseestr. 5  Kolbermoor, Germany 83059 Attn: Tobias Helbich
Total	0.00 USD
Terms and Conditions	

### TERMS AND CONDITIONS

This copyrighted material is owned by or exclusively licensed to John Wiley & Sons, Inc. or

**Abstract - Thermoresponsive and Photoluminescent Hybrid Silicon Nanoparticles by Surface-Initiated Group Transfer Polymerization of Diethyl Vinylphosphonate**

RightsLink Printable License

<https://s100.copyright.com/CustomerAdmin/PLF.jsp?ref=8943d505-d...>**JOHN WILEY AND SONS LICENSE  
TERMS AND CONDITIONS**

Apr 10, 2017

This Agreement between Tobias Helbich ("You") and John Wiley and Sons ("John Wiley and Sons") consists of your license details and the terms and conditions provided by John Wiley and Sons and Copyright Clearance Center.

License Number	4078170450409
License date	
Licensed Content Publisher	John Wiley and Sons
Licensed Content Publication	Angewandte Chemie International Edition
Licensed Content Title	Thermoresponsive and Photoluminescent Hybrid Silicon Nanoparticles by Surface-Initiated Group Transfer Polymerization of Diethyl Vinylphosphonate
Licensed Content Author	Julian Kehrle, Ignaz M. D. Höhle, Zhenyu Yang, Aljosha-Rakim Jochem, Tobias Helbich, Tobias Kraus, Jonathan G. C. Veinot, Bernhard Rieger
Licensed Content Date	Sep 8, 2014
Licensed Content Pages	4
Type of use	Dissertation/Thesis
Requestor type	Author of this Wiley article
Format	Electronic
Portion	Abstract
Will you be translating?	No
Title of your thesis / dissertation	Two-dimensional Hybrid Nanomaterials: Functionalization and Characterization of Photoluminescent Silicon Nanosheets
Expected completion date	Jul 2017
Expected size (number of pages)	150
Requestor Location	Tobias Helbich Spitzingseestr. 5  Kolbermoor, Bavaria 83059 Germany Attn: Tobias Helbich
Publisher Tax ID	EU826007151
Billing Type	Invoice
Billing Address	Tobias Helbich Spitzingseestr. 5  Kolbermoor, Germany 83059 Attn: Tobias Helbich
Total	0.00 USD
Terms and Conditions	

## Abstract - Polymer-silicon nanosheet composites: bridging the way to optoelectronic applications

RightsLink Printable License

<https://s100.copyright.com/CustomerAdmin/PLF.jsp?ref=af926000-c7...>

### Institute of Physics - Journals LICENSE TERMS AND CONDITIONS

Apr 10, 2017

This is a License Agreement between Tobias Helbich ("You") and Institute of Physics - Journals ("Institute of Physics - Journals") provided by Copyright Clearance Center ("CCC"). The license consists of your order details, the terms and conditions provided by Institute of Physics - Journals, and the payment terms and conditions.

**All payments must be made in full to CCC. For payment instructions, please see information listed at the bottom of this form.**

License Number	4078180811332
License date	Mar 29, 2017
Licensed content publisher	Institute of Physics - Journals
Licensed content title	Journal of Physics D : Applied Physics
Licensed content date	Jan 1, 1970
Type of Use	Thesis/Dissertation
Requestor type	Academic institution
Format	Electronic
Portion	abstract
Title or numeric reference of the portion(s)	Abstract
Title of the article or chapter the portion is from	Polymer-silicon nanosheet composites: bridging the way to optoelectronic applications
Editor of portion(s)	N/A
Author of portion(s)	Alina Lyuleeva, Tobias Helbich, Bernhard Rieger and Paolo Lugli
Volume of serial or monograph.	N/A
Issue, if republishing an article from a serial	13
Page range of the portion	Abstract only
Publication date of portion	2 March 2017
Rights for	Main product
Duration of use	Life of current and all future editions
Creation of copies for the disabled	no
With minor editing privileges	no
For distribution to	Worldwide
In the following language(s)	Original language of publication
With incidental promotional use	no
The lifetime unit quantity of new product	Up to 499
Made available in the following markets	the thesis should be accessible on the university library website